Dynamic of root plastids and stromules

Dissertation

zur Erlangung des Doktorgrades

der Naturwissenschaften

vorgelegt beim Fachbereich Biowissenschaften (FB15)

der Johann Wolfgang Goethe-Universität

in Frankfurt am Main

von

Philipp Gebhardt

aus Frankfurt am Main

Frankfurt am Main (2022)

(D30)

Vom Fachbereich Biowissenschaften der

Johann Wolfgang Goethe-Universität als Dissertation angenommen

Dekan: Prof. Dr. S. Kimpel

Erster Gutachter: Prof. Dr. E. Schleiff

Zweite Gutachterin: Prof. Dr. C. Büchel

Datum der Disputation: …….

Table of contents

Movie index

Movies that are referred to in this work are attached on the additional Data-DVD. They comprise maximum intensity projections of light sheet-based microscopic image sets. All movies are shown with 15 frames per second, if not indicated otherwise. All attached files are saved in a .gif format. Besides standard video players, files can be opened in Fiji (ImageJ) for single frame analysis.

Movie number	Description
Movie 1	**Exemplary: Diversity of plastidal movement in control conditions 1.** Plastid movement in control condition imaged over 15 minutes (211 frames). Various movement patterns of plastids are displayed. The dataset displays much movement of plastids in comparison to movie 2. Diverse structures and movement sets of plastids are included. Stromule movement is very dynamic and different stromule induced movement patterns are displayed.
Movie 2	**Exemplary: Diversity of plastidal movement in control conditions 2.** Plastid movement in control condition imaged over 15 minutes (211 frames). Various movement patterns of plastids are displayed. In comparison to Movie 1, the plastids are more lethargic and display less overall movement.
Movie 3	**Exemplary: Diversity of plastidal movement in salt stress conditions 1.** Plastidal movement in 0.1 M NaCl (salt stress) condition imaged over 15 minutes (211 frames). Various movement patterns of plastids are displayed. Dataset displays much movement of plastids compared to movie 4. Resolution of the images is low, but movement of the plastid body and partial movement of stromules could be followed. Movement of plastids using cellular “highways” for fast, directed movement is very prominent. Swollen cells are visible, which are characteristic for the prolonged salt stress conditions.
Movie 4	**Exemplary: Diversity of plastidal movement in salt stress conditions 2.** Plastidal movement in 0.1 M NaCl (salt stress) condition imaged over 15 minutes (211 frames). Various movement patterns of plastids are displayed. Dataset displays low movement of plastids compared to movie 3. Cells are less swollen than cells in Movie 3, but still look affected by the salt treatment in comparison to Movie 1 and 2.
Movie 5	**Exemplary: Diversity of plastidal movement in drought stress conditions 1.** Plastidal movement in 5 % PEG 4000 (drought stress) condition imaged over 15 minutes (211 frames). Various movement patterns of plastids are displayed. Dynamics of plastids is reduced compared to Movie 1-4. Number of stromules is drastically increased compared to Movie 6.
Movie 6	**Exemplary: Diversity of plastidal movement in drought stress conditions 2.** Plastidal movement in 5 % PEG 4000 (drought stress) condition imaged over 15 minutes (211 frames). Various movement patterns of plastids are displayed. Stromule frequency is drastically reduced compared to Movie 5.

Movie 7	**Exemplary: Diversity of plastidal movement in sucrose depletion conditions 1.** Plastidal movement in sucrose depletion condition imaged over 15 minutes (211 frames). Various movement patterns of plastids are displayed. Stromule frequency is drastically enhanced in comparison to most image data of sucrose depletion conditions. Furthermore, the overall dynamic of plastids is above average in comparison to other replicates.
Movie 8	**Exemplary: Diversity of plastidal movement in sucrose depletion conditions 2.** Plastidal movement in sucrose depletion condition imaged over 15 minutes (211 frames). Various movement patterns of plastids are displayed. Stromule frequency and dynamics are drastically reduced compared to Movie 7.
Movie 9	**Longest stromule measured.** Longest stromule detected throughout all image data is shown. The event was observed in control conditions. The stromule is elongating from the plastid in the bottom right corner and is directly retracted again. The maximal length of the stromule is 60 µm. The stromule elongates and retracts across different paths but with comparable speed. Thinning of the stromule can be seen upon stretching of the structure.
Movie 10	**Plastid without stromule shows no motion.** A plastid without stromule is displayed showing no motion for the time of 15 minutes (211 frames).
Movie 11	**Plastids without stromules display directed, stop-and-go, and wiggling motion.** Plastids without stromules that were transported in a directed manner. Directed movements of plastids are interrupted halfway through the movie resulting in stop-and-go motions. During stops, plastids display wiggle motions.
Movie 12	**Fastest movement measured for a plastid.** The plastid showing the fasted movement measured throughout all image data with 8.5 µm/sec is displayed. Framerate is reduced to 5 frames per second to capture the fast movements. Different fast-moving plastids are visible with comparable velocities. The fastest movement was measured at the first plastid showing fast movement crossing the frame from the right to the left.
Movie 13	**Plastid with stromule shows no motion.** A plastid that forms a stromule and shows no motion is displayed for a period of 15 minutes (211 frames). Neither the plastid nor the stromule moves.
Movie 14	**Stromule emerges and retracts.** A stromule emerging and retracting from and to the plastid body is shown. Dynamics of branches accompanied by kinking of the stromule are visible. Kinks maintain a 120 ° angle and are easy to distinguish.
Movie 15	**Rubber band effect of stromule losing track.** An elongated stromule is shown, which is losing anchorage. Upon losing halt, the stromule is retracted. The way of retraction reminds of a rubber band that is pulled together in its neutral form.

Movie 16	**The dynamic of stromule branches and kinks 1.** The dynamics of stromule kinks are shown. A stromule kink is transported alongside the stromule. New stromule branches emerge from previously formed kinks. Several kinks with short stromule branches appear throughout the duration of the movie.
Movie 17	**The dynamic of stromule branches and kinks 2.** Stromule branch formation is shown. Some force pulls at the middle of a stromule. A stromule branch seems to be pulled out of an existing stromule. The branch forms very late in the pulling process. Upon branching a stromule kink forming a 120 ° angle is immediately visible. The movie does not show whether a stromule branch or kink is developed in the first place.
Movie 18	**Stromule branching is accompanied by a 120 ° angle of the kink.** A plastid with a stromule is shown. The plastid body shows different dynamics involving stromules throughout the movie. A branch is formed at the stromule at a kinked side already maintaining a 120 ° angle.
Movie 19	**Plastid body pulls and elongates stromule.** A plastid body with an anchored stromule is shown. The plastid body is transported by some force, while the stromule is still anchored. The stromule is elongated and thinned in the process.
Movie 20	**Stromule pulls plastid.** A plastid with a stromule is shown. The plastid moves away from the stromule which pulls it back. The stromule acts as an anchor for the plastid body.
Movie 21	**Plastids move together with another organelle.** Plastids that are assumed to be attached to another organelle are shown. The plastids maintain the grouping around the spherical shape with a diameter of about 10 µm throughout the image series. The object the plastids are attached to moves and the plastids are transported passively. Plastids can also move independently but still seem to be attached to the underlying object.
Movie 22	**The diversity of plastidal movement.** The diversity of plastidal motions involving stromules is shown. Different types of movement are combined by the plastids with stromules giving them enormous dynamic potential. Stromules move independently, plastid bodies move alongside of stromules and are pulled by them. In addition, stromule branches form.
Movie 23	**Plastids use defined routes for directed movement 1.** Several plastids without stromules are shown, which use the same route for directed movement. Plastids undergo directed motions, stop-and-go motions, and wiggling motions. The path of the plastids either leads them in direction of the root hair tip or away from it.
Movie 24	**Plastids use defined routes for directed movement 2.** Several plastids without stromules are shown that use the same route for directed movement. Plastids undergo directed motions, stop-and-go motions, and wiggling motions. As in Movie 23, all plastids are either directed to or from the root hair tip.

Zusammenfassung

Die Funktion einer Zelle ist abhängig von der Zellform. Im Zuge der Evolution haben sich unterschiedliche Zellformen herausgebildet, die in der Regel eine Maximalgröße von 100 µm im Durchmesser nicht überschreiten. Die Größe einer Zelle ist maßgeblich von intrazellulären Transportprozessen abhängig, die unter anderem die sogenannte zytoplasmische Strömung antreiben. Dieses Phänomen ist für eine Vielzahl von Zellen bekannt und wurde sehr genau bei Grünalgen der Familie *Characeae* untersucht, da die zytoplasmische Strömung in dieser Familie sehr ausgeprägt ist. Die zytoplasmische Strömung ist eine prominente Eigenschaft von Pflanzenzellen und ihre Ausprägung und Form ist abhängig von der Pflanzen- und Zellart. Lange Zeit wurde geglaubt, dass neben Nährstoffen auch Zellorganellen passiv im zytoplasmischen Strom treiben. Jedoch wurden des Öfteren Organellen beobachtet, die sich entgegen des zytoplasmischen Stroms bewegten. Des Weiteren konnte gezeigt werden, dass erst durch den aktiven Transport von Organellen die intrazelluläre Zytoplasmaströmung erzeugt wird. Diese Beobachtungen ließen darauf schließen, dass die Positionierung der Organellen in der Zelle sehr definiert ist und einer gewissen Funktion unterliegt. Da im Zuge der Evolution durch Zellorganellen spezielle Reaktionsräume in der Zelle abgegrenzt worden sind, wurde die Grundlage für eine komplexe miteinander verflochtene Zellstruktur geschaffen. Verschiedene metabolische Prozesse finden in separaten Reaktionsräumen statt, die durch Membranen voneinander abgegrenzt sind. Die exakte Funktion der verflochtenen metabolischen Prozesse ist wichtig für den Erhalt der zellulären Homöostase. Dies legt die Schlussfolgerung nahe, dass Organellen für eine einwandfreie Funktion der Zelle Stoffaustausch miteinander betreiben und miteinander kommunizieren müssen. Organelläre Interaktion wurde oft und bei verschiedenen Organellen beschrieben. Für eine optimale Interaktion zwischen den Organellen ist eine variable, aber gezielte Positionierung der Organellen in der Zelle von Nöten. Dies impliziert die Notwendigkeit des gerichteten Transports von Organellen. Gerichteter intrazellulärer Transport wird in der Regel mit Hilfe des Zytoskeletts und Motorproteinen betrieben, die entlang des Zytoskeletts Zellbestandteile durch die Zelle transportieren. In pflanzlichen Zellen findet der meiste aktive intrazelluläre Transport mit Hilfe von Aktin Filamenten und den sich darauf bewegenden Myosin Motorproteinen statt, die Bewegungsgeschwindigkeiten von bis zu 7 µm/sec in der Pflanze *Arabidopsis thaliana* erreichen können. Mikrotubuli und die Motorproteine, die sich auf ihnen bewegen, sogenannte Kinesine, spielen im intrazellulären Transport von Pflanzen eine untergeordnete Rolle. Es konnte gezeigt werden, dass die Bewegung von Peroxisomen, Golgi Stapeln und Mitochondrien mit Hilfe des Aktin-Myosin Gespannes angetrieben wird. Jedoch konnte kein spezifisches Myosinprotein dem Transport einer Zellorganelle zugeordnet werden. Es konnte gezeigt werden, dass die vier am stärksten exprimierten Myosine in der Pflanze *Arabidopsis thaliana* redundante Funktionen in dem Transport der Zellorganellen haben und nur ein multipler Knockout der verschiedenen Gene konnte eine Verlangsamung des Organelltransportes herbeiführen. Obwohl mit den beschriebenen Experimenten eine Beteiligung der Aktin-Myosin Maschine am Transport der drei Organelltypen gezeigt wurde, sind die genauen molekularen Mechanismen, die dem Transport unterliegen bis jetzt nicht genau entschlüsselt. Daher gibt es verschiedene Modelle, mit denen die Organellbewegung beschrieben werden kann. Entweder wird die Organellbewegung durch eine direkte Interaktion von Motorproteinen mit dem Zytoskelett und der entsprechenden Organelle mediiert, durch eine indirekte Interaktion mit dem Motorprotein, indem Organellen miteinander Interagieren, aber

nur eine der Organellen von Motorproteinen transportiert wird, oder durch einen Mixtur, in der Organellen aktiv durch die Zelle transportiert werden, dadurch die zytoplasmische Strömung initiieren mit deren Hilfe andere Organellen durch den Strom in der Zelle verteilt werden. Die Organellbewegung in der Pflanze wurde bisher meistens in grünem Gewebe untersucht. Dazu gehört auch die Bewegung von Chloroplasten, die sehr gut verstanden ist, jedoch einem anderen molekularen Mechanismus folgt, als die klassischen Arbeitsmodelle der Organellbewegung postulieren. Chloroplasten gehören zu der Organellfamilie der Plastiden, die neben den photosynthetischen Chloroplasten im grünen Pflanzengewebe auch diverse bisher meist wenig erforschte Verwandte beherbergt. Da die Bewegung von Chloroplasten durch Blau- und Rotlicht induziert wird, dieses jedoch in der Wurzel normalerweise nicht vorhanden ist, liegt die Vermutung nahe, dass Plastiden in der Wurzel, zumeist Leukoplasten, einen anderen Mechanismus besitzen, der ihre Bewegung antreibt.

Neben der individuellen spezifischen Bewegung können alle Arten von Plastiden tubuläre Ausstülpungen, sogenannte Stromuli bilden. Die Stromuli zeichnen sich dadurch aus, dass sie durch beide Membranen der Plastiden begrenzt sind, sie also mit Plastidenstroma gefüllt sind. Sie können einen Durchmesser von bis zu mehreren hundert Nanometern haben und können sich über eine Strecke von mehreren dutzenden Mikrometern strecken. Als sehr dynamische Strukturen von Plastiden ist ihre Funktion, sowie die molekularen Mechanismen der Stromulientstehung bisher ungeklärt. Man vermutet jedoch, dass sie an dem aktiven Austausch von Stoffwechselprodukten mit anderen Organellen beteiligt sind, da des Öfteren Interaktionen mit anderen Organellen, zum Beispiel dem Zellkern beobachtet worden sind. Neuer Erkenntnisse deuten darauf hin, dass Stromuli durch Komponenten des Zytoplasmas induziert werden können.

Da im Kontrast zu Chloroplasten die Funktion und die Mechanismen der Bewegung von Wurzelleukoplasten bisher weder untersucht, noch verstanden ist, war ein Ziel dieser Arbeit die Plastidenbewegung in der Pflanze *Arabidopsis thaliana* zu untersuchen. Des Weiteren wurde in dieser Arbeit die Dynamik von Stromuli an Wurzelplastiden und deren Beteiligung an der Bewegung und der Positionierung von Plastiden in der Zelle analysiert. In einem dritten Arbeitsabschnitt wurde mit Hilfe von molekularbiologischen Methoden potentielle Interakteure, die an der Bildung von Stromulis beteiligt sind, aufgedeckt.

Für die Untersuchung der Plastidenbewegung in der Wurzel von *Arabidopsis thaliana* wurde die Methodik der Lichtscheibenfluoreszenzmikroskopie verwendet, da diese eine minimalinvasive Methodik für die Pflanze darstellt und in sehr kurzem Zeitraum einen großen Abschnitt der Zelle erfassen kann. Es wurden hierbei 4D Aufnahmen (dreidimensionale Aufnahmen über Zeit) gemacht, welche mit einer automatisierten Pipeline ausgewertet wurden. Im Rahmen der Arbeit wurden die Plastidenbewegungen unter Kontroll-, Salzstress- und Trockenstresskonditionen, sowie unter dem Entzug von supplementierter Saccharose ausgewertet. Zur Auswertung der Bewegung wurde das Programm Arivis Vision 4D genutzt. Die Analysepipeline wurde im Rahmen dieser Arbeit etabliert und war in der Lage einen Großteil der Bewegung der Plastidenkörper zu tracken. Mit Hilfe der automatischen Pipeline konnte eine große Datenmenge in einem übersichtlichen Zeitraum ausgewertet werden. Jedoch waren die automatisch generierten Tracks durch die strukturelle Variabilität der Plastiden, sowie von Stromules, die gebildet worden sind, fehlerbehaftet und mussten manuell korrigiert werden. Die manuelle Korrektur wurde durch

die Visualisierung der getrackten Daten im Programm Arivis Vision 4D mit den darunterliegenden Mikroskopiedaten ermöglicht. Durch die manuelle Korrektur wurde ein Großteil von fehlerbehafteten Tracks aussortiert. Gerade die Tracks, die lange Sprünge mit plötzlichen Richtungsänderungen suggerierten wurden mit Hilfe der manuellen Korrektur aussortiert. Jedoch konnten nicht alle fehlerhaft getrackten Ereignisse ausgesondert werden. Die meisten verbliebenden Ereignisse stellten multiple Segmentierung von Stromuli dar, die wenig Bewegung einschlossen.

Aus den verbliebenden Bewegungsdaten wurden die Geschwindigkeiten aller Bewegungsereignisse der Plastiden mit Hilfe von Vektoranalysen errechnet und in Geschwindigkeitskategorien eingeteilt. Anschließend wurden die Winkel der Plastidenbewegung im Verhältnis zum vorherigen Bewegungsvektor bestimmt. Durch die Winkelbestimmung der einzelnen Bewegung konnte angegeben werden, ob ein Bewegungsereignis eine gerichtete Bewegung mit einer definierten Richtung, oder eine ungerichtete Bewegung, wie eine Vibration an einer Stelle darstellte. Bewegungsereignisse mit einem Winkel von über 90° wurden hierbei als gerichtete Bewegungen behandelt, während Bewegungsereignisse mit Winkel unter 90° mit ungerichteter Bewegung gleichgesetzt wurden. Durch die Bestimmung der relativen Häufigkeiten der gerichteten und ungerichteten Ereignisse innerhalb der einzelnen Geschwindigkeitskategorien konnten Grenzen in der Geschwindigkeit der Plastidenbewegung abgesteckt werden, in welchen vornehmlich gerichtete, oder ungerichtete Bewegung stattfindet. Zeitgleich wurde ermittelt, wie groß die von Arivis Vision 4D errechnete Geschwindigkeit von Plastiden ist, die sich während des beobachteten Zeitraumes nicht bewegten. Der Trackingalgorithmus nutzte für das Erstellen der einzelnen Tracks die geometrische Mitte der segmentierten Plastiden. Da die Segmentierung anhand der Plastidenintensität errechnet wurde, ergaben sich hierbei leichte Unterschiede zwischen den einzelnen Zeitpunkten, welche zu der Generierung von Tracks mit minimaler Bewegung führten. Diese minimale Bewegung wurden als Geschwindigkeiten von bis zu 0.05 µm/Sek errechnet. Dieser Wert wurde als Hintergrundrauschen gewertet und Ereignisse bis zu 0.05 µm/Sek wurden als stationäre Ereignisse eingeordnet. Mit Hilfe der errechneten Bewegungswinkel konnten fünf verschiedene Bewegungsarten innerhalb der gemessenen Geschwindigkeiten definiert werden: 1) keine Bewegung, 2) primär ungerichtete Bewegung, 3) ausgeglichen ungerichtete, sowie gerichtete Bewegung, 4) primär gerichtete Bewegung und 5) gerichtete Bewegung. Mit Hilfe der fünf Gruppen konnten die vorherrschenden Bewegungsarten innerhalb der getesteten Konditionen bestimmt werden. Bewegungen innerhalb von Kontrollkonditionen und Salzstresskonditionen zeigten kaum Unterschiede, während Trockenstress sich negativ auf die Bewegung von Plastiden auswirkte. Die Plastidenbewegung in der saccharosearmen Kondition war drastisch reduziert. Während der Analyse der 4D Daten ist aufgefallen, dass Plastiden mit gerichteter Bewegung innerhalb einer Zelle sich erstaunlich häufig auf ähnlichen Bahnen bewegen. Die Auswertung dieser Plastidentracks ergab, dass es definierte zelluläre Hochgeschwindigkeitsstrecken gibt, auf denen Plastiden gerichtet transportiert werden. Diese Erkenntnisse schließen eine passive Bewegung in einem zytoplasmischen Strom aus, da die von den Plastiden genutzten Routen miteinander verflochten waren und unterschiedliche Richtungen eingeschlagen haben. Aufgrund der gemessenen Geschwindigkeiten und der Richtungsabhängigkeit der Plastidenbewegungen lag die Vermutung nahe, dass es sich dabei um Myosin mediierte Bewegung an Aktinsträngen handelt.

Zusätzlich zur automatisierten 4D Auswertung, wurde die Plastiden und Stromulbewegung innerhalb einer manuellen 3D Analyse ausgewertet. Diese wurde anhand von maximalen Intensitätsprojektionen der

einzelnen Datensets durchgeführt. Die semiautomatisch generierten Ergebnisse zur Plastidenbewegung konnten bestätigt werden. Jedoch wurden auch Schwächen der automatisierten Pipeline aufgezeigt. Zum Beispiel wurden sehr hohe Plastidengeschwidigkeiten nicht zuverlässig vom Algorithmus erkannt. Während die automatisch gemessene Höchstgeschwindigkeit bei 3,21 µm/Sek lag, wurden manuell bis zu 8,5 µm/Sek gemessen. Diese zur vorherigen Untersuchung abweichenden Ereignisse stellten jedoch die Ausnahme dar. Die manuelle Untersuchung zeigte außerdem, dass Wurzelplastiden sich mit anderen Organellen, welche vermutlich den Zellkern darstellten, über den Zeitraum der Aufnahmen synchron bewegten, also höchstwahrscheinlich eine Interaktion mit diesem eingingen und diese trotz zugrundeliegender Bewegung der anderen Organelle aufrecht gehalten haben.

Im Zuge der manuellen 3D Analyse wurde zudem die Dynamik der Stromuli der Wurzelplastiden untersucht. Im Fokus dieser Analyse stand die Frage, inwiefern Stromuli an der Bewegung und der damit verbundenen Positionierung der Plastiden im zellulären Kontext beitragen. In Kontrollkonditionen zeigte ein Großteil der untersuchten Plastiden eine Bildung der tubulären Strukturen. Die Stromulihäufigkeit, sowie deren Dynamik nahm in Salz- und Trockenstresskonditionen ab, und war unter dem Entzug von Saccharose drastisch reduziert. Die Parallelen zur vorherigen ausgewerteten Plastidenbewegung legen nahe, dass die Stromulibildung und Dynamik durch ähnliche Mechanismen, wie die Plastidenbewegung angetrieben wird. Des Weiteren zeigten Stromuli eine Vielzahl an Bewegungsmuster und trugen damit zur Plastidenbewegung und zur Positionierung der Plastiden in der Zelle bei. Auffällig war, dass Plastiden, die eine schnelle, gerichtete Bewegung zeigten, meist keine Stromuli ausbildeten, während Plastiden die stationär in der Zelle lagen oft größer waren und eine Vielzahl an Stromuli bildeten. Die durch die Stromuli vermittelte Dynamik ermöglichte es dem stationären Plastiden Interaktionen mit Zellelementen im Umkreis der Stromulireichweite einzugehen. Die Länge der Stromuli konnte sehr unterschiedlich ausfallen, und zeigte eine Spannweite von einigen µm bis zu 60 µm. Die Stromulspitze konnte sich individuell von der Bewegung des Plastidenkörpers bewegen und Geschwindigkeiten von bis zu 3,2 µm/Sek erreichten. Die von Plastidenkörper unabhängige Bewegung wurde bei fast allen Stromuli gesichtet und stellte eines der Hauptmerkmale ihrer Bewegung dar. Zugleich steht die gemessene Geschwindigkeit der Stromuli der Wurzelplastiden im Kontrast zu bisher gemessenen Geschwindigkeiten von Stromuli an Chloroplasten, welche sich im Bereich von einigen µm/Min bewegen. Die Geschwindigkeit von mehreren µm/Sek konnte bei Verlängerung, sowie der Retraktion der Stromuli beobachtet werden, was die Vermutung nahelegt, dass Stromuliwachstum, sowie Verkürzung durch einen aktiven Prozess angetrieben werden und nicht durch einen passiven zytoplasmischen Strom. Dieser Eindruck wurde dadurch bestätigt, dass die Bewegungsrichtungen von Stromuli variierten. Alle Ergebnisse der Stromulidynamik deuten darauf hin, dass die Dynamik von Stromuli, wie die der Plastidenkörper durch einen aktiven Transport mit Hilfe der Aktin-Myosin Maschinerie angetrieben wird. Abseits der tubulären Struktur konnten Stromuli sich verzweigen und bis zu drei Stromuli konnten an einer Zweigstelle beobachtet werden. Die Winkel an diesen Zweigstellen näherten sich 120° an, was in Einklang mit bisherigen Beobachtungen von Stromuli, sowie mit Modellierungen zur Stromulibildung einhergeht. Die Zweigstellen der Stromuli wiesen hierbei eine erstaunliche Stabilität auf, und konnten mit, sowie ohne ausgebildeten Stromul beobachtet werden, wie sie mit Geschwindigkeiten von bis zu 1 µm/Sek durch die Plastidenmembran transportiert worden sind. Die Stabilität der Zweigstellen lässt darauf schließen, dass sie durch externe Faktoren stabilisiert werden und dadurch die Bildung der Stromuli an definierten Stellen ermöglichen.

Des Weiteren wurde gezeigt, dass Stromuli durch Verankerung in der zellulären Umgebung dazu beitragen können die Bewegung des Plastidenkörpers zu kontrollieren. Stromuli konnten den Bewegungsradius von Plastiden begrenzten, indem sie wie eine Leine fungierten, oder Plastiden amöboide Bewegungen ermöglichten. Diese Vorkommnisse wurden seltener beobachtet als individuelle Stromulibewegung, aber trugen zur allgemeinen Dynamik der Plastiden bei. Die Ergebnisse legen nahe, dass Plastiden die Stromuli bilden von stationärer Natur sind, im Kontrast zu Plastiden, die keine Stromuli ausbilden. Die Stromuli hingegen ermöglichen es den stationären Plastiden dynamisch mit der zellulären Umgebung zu kommunizieren. Eventuelle Membran Kontaktseiten könnten hier auch zu einem Stoffaustausch beitragen.

In einem dritten Abschnitt wurden die molekularen Mechanismen untersucht, die zur Bildung der Stromuli an Plastiden beitragen könnten. Hierzu wurde ein bereits veröffentlichter Assay etabliert, der Stromuli an isolierten Chloroplasten der Pflanze *Nicotiana benthamiana* durch Zugabe von konzentriertem Zellextrakt erzeugen konnte. Der Assay wurde mit Hilfe von isolierten Chloroplasten und Extrakt der Pflanze *Pisum sativum* etabliert. Es konnte gezeigt werden, dass neben Extrakt aus Blattmaterial, Extrakt aus Wurzelmaterial der Pflanzen effektiver darin ist *in vitro* Stromuli an Chloroplasten zu erzeugen. Diese Ergebnisse lassen darauf schließen, dass die Zellbestandteile, die Stromuli induzieren in der Wurzel in höherem Maße vorliegen, aber auch, dass Stromuliinduktion an Chloroplasten und Plastiden vermutlich nach gleichem Prinzip funktioniert. Es konnte eine Abhängigkeit der Menge der induzierten Stromuli von der Proteinkonzentration des Extrakts festgestellt werden. Dass Stromulibildung von den im Extrakt vorhandenen Proteinen mediiert wird konnte mit Hilfe von differentieller Zentrifugation bewiesen werden. Zeitgleich wurde mit Hilfe der differentiellen Zentrifugation gezeigt, dass Stromulibildung nicht abhängig von den im Proteinextrakt verbliebenden Zytoskelettfragmenten ist. Da die im Assay induzierten Stromuli jedoch keinerlei Dynamik aufwiesen, bekräftigten diese Ergebnisse die während der Analyse der Stromulidynamik gemachten Beobachtungen, dass die Stromulidynamik vermutlich Motorprotein mediiert und an die Zytoskelettfragmente gebunden ist. Während eines Thermolysinverdaus der Proteine der äußeren Membran von Chloroplasten konnte keine Reduktion der Häufigkeit induzierter Stromuli festgestellt werden. Damit konnte gezeigt werden, dass die Proteine die zur Stromuliinduktion beitragen höchstwahrscheinlich eine Protein-Lipid Interaktion mit der Membran der Chloroplasten eingehen. Unter Berücksichtigung der Beobachtungen zur Stromuliverzweigung, die während der manuellen 3D Analyse der Mikroskopiedaten gemacht worden sind, wurde geschlussfolgert, dass ein Proteinkomplex entweder eine Interaktion mit der Membran eingeht und eine nadelöhrähnliche Struktur bildet, welche die Ausbildung von Stromuli begünstigt, oder durch Anlagerung an die äußere Membran die Stromulistruktur stabilisiert. Ähnliche Mechanismen sind aus den verschiedenen Vorgängen der Vesikelbildung bekannt.

Unter Berücksichtigung dieser Erkenntnisse wurde eine Pipeline entwickelt, deren Ziel es war, die Faktoren, die zur Stromuliinduktion beitragen zu isolieren und zu bestimmen. Hierzu wurden verschiedenen Methodiken genutzt, um das Zellextrakt zu fraktionieren und die gesuchten Faktoren anzureichern. Es wurde eine Saccharose Dichtegradientenzentrifugation etabliert, die einen Großteil der vorhandenen Proteine ausschloss, während die Proteine, die bei der Stromuliinduktion beteiligt waren, angereichert wurden. Des Weiteren wurde das Extrakt mit Hilfe einer Anionenaustauschchromatographie aufgetrennt. Hierbei konnte gezeigt werden, dass die gesuchten Proteine höchstwahrscheinlich nicht an die genutzte Säule binden konnten, da sie in der Durchflussfraktion zu finden waren, die jedoch einen

großen Anteil der Übrigen im Extrakt befindlichen Proteine ausschloss. Eine Kombination der beiden Fraktionierungsmethoden zeigt eine drastische Reduktion des Proteingehalts des Zellextrakts, während die Faktoren, die zur Stromulibildung beigetragen haben, angereichert worden sind. In einem finalen Schritt wurde die an dem Pflanze *Pisum sativum* etablierte Pipeline auf die Pflanze *Arabidopsis thaliana* übertragen und die so gewonnenen Proben Massenspektroskopisch untersucht. Die Ergebnisse der Massenspektroskopie wurden unter Berücksichtigung einer Protein-Lipid Interaktion ausgewertet und mögliche Proteine, die zur Stromulibildung beitragen könnten, bestimmt. Folgende Arbeiten müssen die hier bestimmten Proteine auf Stromuliinduktion überprüfen.

Abstract

Many metabolic pathways of eukaryotes are carried out in form of interconnected pathways, which take place in organelles. The organelle membrane separates the reaction compartments from each other, making it a key feature of organelle existence in the cell. To maintain cellular homeostasis, organelle positioning in and transport through the cell as well as organelle interaction are important for the organisms. In plants, organellar movement of peroxisomes, Golgi stacks and mitochondria was shown to be mediated by the actin-myosin machinery. The molecular mechanisms are not elucidated, but working models comprise classical movement mechanisms of motor proteins pulling their cargo on cytoskeletal filaments. In contrast, many mechanisms of chloroplasts movement, which are regulated by blue and red light, are deciphered but follow a different molecular mechanism. Plastidal relatives of the chloroplast have long been disregarded by scientific research but carry out important metabolic reactions to maintain cellular homeostasis. The cellular transport and movement mechanisms of root plastids have not been described in detail until now. Additionally, all plastid subspecies can form tubular structures, called stromules. Those are thought to be involved in the organelle communication and metabolite exchange. Since they are very mobile structures, they influence the organellar dynamic of plastids. This work aimed for an in-detail description of the cellular movements of root plastids in the plant *Arabidopsis thaliana* to elucidate underlying mechanisms of their movement. Additionally, the dynamics of root plastid stromules were investigated, led by the questions, if and how stromules are involved in the mediation of plastidal movement and their overall dynamics. Plastidal movement in *Arabidopsis thaliana* was captured using light sheet-based fluorescence microscopy. 4D image data was automatically analyzed using the program Arivis Vision 4D with subsequent manual correction. Additionally to the 4D approach, a manual 3D analysis of plastid and stromule dynamics was performed. The results of the semiautomated analysis displayed heterologous distribution of the plastidal movement. Using a combination of the vector length of each motion event and the angle in relation to previous motion vectors, the proportions of different movement patterns were determined. Main fractions of the data showed undirected motion of plastids, whereas small proportions displayed directed movement with speed up to 8.5 µm/sec. Directed motion was shown to be carried out on defined routes in the cell. Salt stress did not affect plastidal motion, whereas drought stress lead to its reduction. Sucrose depletion led to a drastic decrease of plastidal movement. Additionally, stromule dynamics were investigated using the acquired image data. Stromules were observed in high frequency mainly at stationary plastids giving them the opportunity of dynamic interaction in their cellular surrounding. Stromules reached lengths of up to 60 µm. Additionally, they displayed a variety of movement patterns that contributed greatly to the overall plastid dynamics. Stromule related motion events were captured reaching up to 3.2 µm/sec. Similar to determined plastid dynamics, stromule motions were reduced during drought stress and sucrose depletion, but also were negatively influenced by salt stress. Those results strongly favor an actin-myosin mediated movement machinery mediating the plastidal and stromule movement. This stands in contrast to previous results describing the movement mechanisms of light induced chloroplast movement.

In an additional approach, the molecular mechanisms underlying stromule formation were analyzed. Previous results describe that stromule formation can be induced at isolated chloroplasts of the plant *Nicotiana benthamiana* by mixing it with concentrated cell extract. During this work, a variation of the

described assay was established using the plant *Pisum sativum*. It was shown that an unknown protein factor presumably undergoing protein-lipid interaction is responsible for *in vitro* stromule formation. Using a combination of sucrose gradient centrifugation and anion exchange chromatography, the desired factor could be enriched, while the majority of unwanted proteins could be reduced drastically. A following LC-MS analysis revealed a selection of proteins with membrane interaction- and unknown functions that might be involved in *in vitro* stromule formation.

1 Introduction

1.1 Intracellular movement

1.1.1 Movement in the cell: Why it is needed

Cells can have different shapes and forms that determine their functions. From yeast, as a single-cell organism, to the way bigger plant cells, all cells have in common that they usually do not exceed a specific cell size. In general, cells have a size ranging between 1-100 µm and just in some exceptions, the cell size is drastically increased (Schweiger 1969.; Wallace, Misulovin, and Etkint 1981). The fact that most cells have a defined size range shows that cell growth is limited by specific factors. Besides their availability (Amodeo & Skotheim, 2016), the intracellular distribution of nutrients was found to be a major factor to influence cell growth (Tominaga et al., 2013). On top, the cell is highly compartmentalized. During evolution and endosymbiosis, the complexity of the cell increased with the addition of other organelles like mitochondria and plastids that offered additional compartmentalization. The organelles got tightly integrated into the cell's metabolisms on various levels and are fulfilling crucial functions to maintain the cell's homeostasis. Additionally, during evolution, metabolic pathways have been interconnected between different organelles of the cell creating a further need for nutrient and intermediate exchange. To keep those pathways running, mechanisms needed to be implemented, that distribute metabolites and allow for communication between the different cellular systems, and ways of interaction between the specialized reaction compartments were introduced. For the distribution of cellular components through the cell, and to ensure cellular well-being, different transport and movement mechanisms evolved. A steady flow of the cytoplasm, so-called cytoplasmic streaming, was described in the green algae *Characeae* more than two centuries ago as the first cellular transport mechanism by Bonaventura Corti in 1774 (Corti 1774). Since then, science has come a far way but up to now, the complexity of cellular transport mechanisms is still not well understood, and most mechanisms of intracellular movement are still under debate. Especially the role of organellar movement and how organellar interaction influences cellular homeostasis is still poorly understood. This holds true for the molecular mechanisms that drive organellar movement but also the functions of organellar movement in a broader cellular context. Several mechanisms of movement spanning from passive movement with the cytoplasmic stream up to targeted intracellular transport of organelles via the cytoskeleton were described in the last decades (Vick & Nebenführ, 2012). With the isolation of GFP in 1994 (Chalfie et al., 1994), a new toolset was made available for scientists to investigate intracellular movement. In combination with advanced fluorescence microscopy techniques, new dimensions opened for the investigation and understanding of intracellular movement. In the following chapters, some aspects of intracellular and organellar movement will be discussed. In addition, specifics of plastids and their role in the cellular dynamics are reviewed.

1.1.2 Cytoplasmic streaming: The driving motor of nutrient distribution

Cytoplasmic or protoplasmic streaming refers to a phenomenon of an actively driven intracellular flow of the cytosol. Firstly reported in 1774 (Corti 1774), cytoplasmic streaming has been described in several organisms, reaching from amoeba (R. D. Allen & Allen, 1978) over fungi (Pieuchot et al., 2015) to the oogenesis in the nematode *Caenorhabditis elegans* (Menon et al., 2021) and the fruit fly (Ganguly et al., 2012). Besides this, the most common representatives of cytoplasmic streaming are algae and plants. The algae family *Characeae* is built by cells with a diameter of up to 1 mm and length of up to 10 cm and exhibits a very strong cytoplasmic flow (Shimmen & Yokota, 1994a). Many insights into the functions and the underlying molecular mechanism have been made in *Characeae*. In 1956, the first in-depth characterization of cytoplasmic streaming in the rhizoid cells of *Nitella flexis* described a rotational stream (Kamiya and Kuroda 1956). Since then, a variety of cytoplasmic streaming patterns has been described including diffuse streaming in the oocytes of *drosophila melanogaster*, radial streams that mostly can be found around the vacuoles in plant cells, or fountain-like flows that have been observed in root hairs or pollen tubes (Figure 1) (Goldstein & van de Meent, 2015). Although cytoplasmic streaming has been described in various organisms, it is strongly developed in plants (Goldstein & van de Meent, 2015).

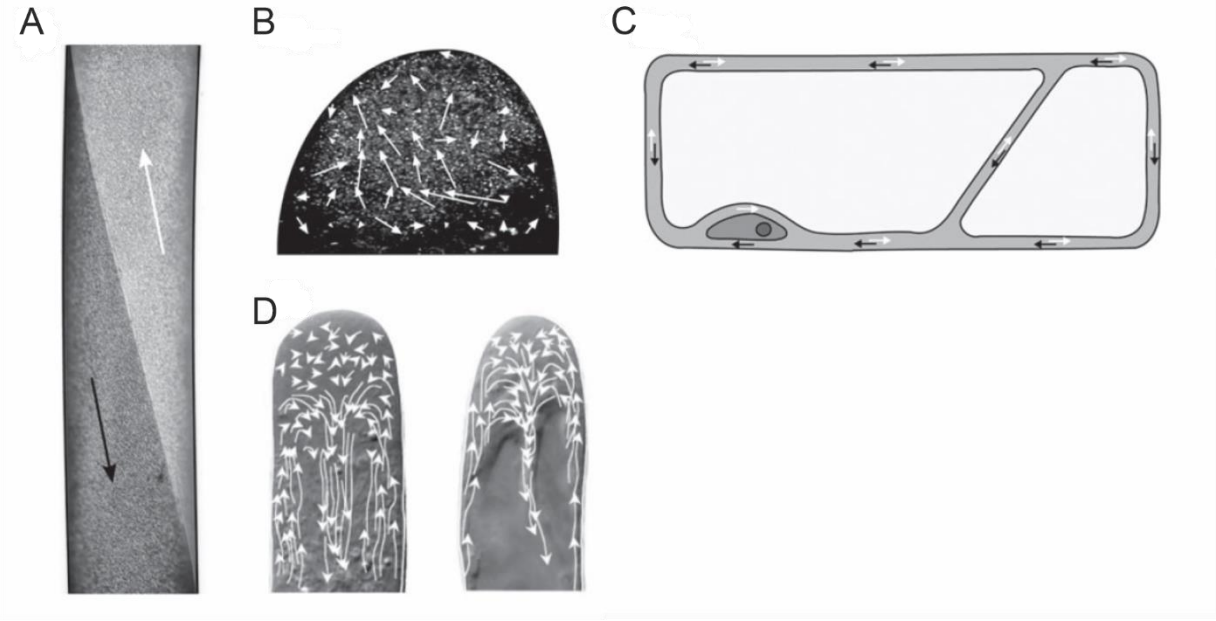

Figure 1: Patterns of cytoplasmic streaming that were observed in different organisms. A) Cytoplasmic streaming in internodal cells of *Chara coralina* displays a rotational stream. B) In developing oocytes of *Drosophila melanogaster* cytoplasmic streaming is organised in a diffuse manner regulated by kinesins. The flow direction and rate can change during development. C) Cytoplasmic streaming in epidermal plant cells is radially organized around big cellular compartments like the vacuole and the nucleus. D) Cytoplasmic streaming in root hairs and pollen tubes is directed in a reverse fountain-like manner. The cytoplasm flows alongside the plasma membrane, changes direction at the tip of the cell and creates a central axial backward flow. (This figure is adapted from (Goldstein & van de Meent, 2015).)

Even though the phenomenon of cytoplasmic streaming is known for over two centuries, the function remains under debate. The most referred to function of cytoplasmic streaming is the nutrient distribution in the cell. Cytoplasmic streaming is believed to act as a driving motor for the transport of nutrients in and

between cells (Bostrom & Walker, 1975; Box et al., 1984; Zawadzki & Fensom, 1986). Specifically for plants, this theory is often proposed since their cells are much bigger than those of other eucaryotes and the cell morphology is more rigid as it is dictated by the cell wall. The flow rate of cytoplasmic streaming differs greatly between cell types and can reach up to 100 µm/sec in *Characeae* (Kamiya & Kuroda, 1956). Given the speed of the cytoplasmic circulation, an actively driven nutrient distribution in the cell was shown to outperform passive diffusion of big molecules (Goldstein & van de Meent, 2015; Pickard, 1974) and aids in preventing local accumulation of macromolecules in the cell by constant mixing of the cytosol. With increasing cell size this effect becomes more interesting, since, depending on the molecule, diffusion mechanisms cannot keep up with the speed of active transport (Goldstein & van de Meent, 2015). However, since cytoplasmic flow rates and directions differ between species and cell types, numbers for the velocity mediated by it are rare. Therefore, specific statements about the functionality of cytoplasmic streaming besides general nutrient distribution are hard to formulate. Further functions of cytoplasmic streaming are still under investigation.

In contrast to the functions of cytoplasmic streaming, the molecular mechanisms are relatively well described. A series of experiments conducted between the 1960s and 1990s showed that cytoplasmic streaming is mediated by the active transport of organelles transported across actin filaments by myosin motor proteins (Shimmen & Yokota, 1994). Further findings demonstrated that the speed of cytoplasmic streaming corresponds to the speed of distinct myosin motors in the respective species (Tominaga, 2003; Yokota et al., 1999). The isolation of myosins from pollen tubes of *Lilium longiflorum* opened doors for further investigations of the motor proteins as the protocol for myosin isolations could be performed on other organisms. Isolated myosins from *Lilium* displayed velocities of 6.0-9.8 µm/sec (Yokota & Shimmen, 1994), whereas myosins from *Chara* displayed movement speed of 40-60 µm/sec (Higashi-Fujime et al., 1995). Those myosin velocities matched the cytoplasmic flow rates of both organisms. Further experiments were executed manipulating the cytoplasmic flow rate by exchanging the myosin motor domains (Tominaga et al., 2013). Different chimeric myosin XI-2 of *Arabidopsis thaliana* were generated, in which the motor domain was exchanged with the one of either *Chara* myosin XI, or *Homo sapiens* myosin Vb. *Arabidopsis* wild-type myosin displayed velocities of 7.2 ± 0.5 µm/sec. The fast-moving chimera reached velocities of 16.0 ± 0.9 µm/sec whereas the slow-moving one displayed a movement speed of 0.19 ± 0.02 µm/sec. Cytoplasmic streaming in epidermal cells of the wild-type plant was measured at 4.3 ± 1 µm/sec, which is in alignment with the streaming rates previously measured for higher plants (Tominaga et al., 2013). Replacement of the wild-type myosin XI-2 resulted in a drastically decreased cytoplasmic streaming velocity of 1.0 ± 0.3 µm/sec for the slow-moving chimera and an enhanced flow rate of 7.5 ± 1.2 µm/sec for the fast-moving one (Tominaga et al., 2013). In addition, plants with lower cytoplasmic streaming velocity showed inhibited growth, which originated not from the reduction of cell number, but reduced cell size, whereas plants with higher flow rates displayed increased growth (Tominaga et al., 2013). Being the first described intracellular movement pattern, this kicked off the debate if and how organelles in the cell move. In plants organelles like chloroplasts were described to move according to the cytoplasmic stream (N. S. Allen & Allen, 1978). However, later findings demonstrated, that organelles can move opposed to the cytoplasmic streaming and fired a completely new debate on organellar transport in the cell (Boevink et al. 1998a; Collings et al. 2002; van Gestel, Köhler, and Verbelen 2002; Jedd and Chua 2002; Mathur, Mathur, and Hülskamp 2002; Nebenführ et al. 1999a).

1.1.3 Cytoskeletal organization in plants

Besides the stabilizing function, that enables the cell to maintain its shape, filaments of the cytoskeleton can be referred to as the "streets" of the cell. In plants, the cytoskeleton consists of actin and microtubule filaments. In contrast to animal cells, in plant cells intermediate filaments are not reported until now. Actin filaments consist of globular-actin (G-actin) monomers, which form two filamentous (F-actin) strands (Pollard, 2016). Two F-actin strands are arranged in form of a helix forming the final actin strand (Pollard, 2016). Since all monomers are oriented in the same direction the actin strand is polar. The ends of the actin filaments are called "pointed" and "barbed" ends (Pollard, 2016). Actin filaments can assemble spontaneously under physiological conditions into small oligomers that can be elongated by the addition of monomers at both ends. In this process, the barbed end of the actin filament grows faster than the pointed one (Pollard, 1986). The stability of the actin filament depends on the nature of the monomers. The G-actin monomer possesses a characteristic ATP/ADP binding domain that can function as an ATPase (Kabsch et al., 1990). Monomers not bound to a nucleotide can associate at the barbed end of the oligomer (de La Cruz et al., 2000), however, the association of nucleotide-carrying monomers is much more likely (Pollard, 2016). During the binding to the polymer, the monomer undergoes conformational changes, favoring the ATPase activity of the protein and the hydrolysis from ATP to ADP (Blanchoin & Pollard, 2002). Both ADP and the resulting γ-phosphate remain bound to the nucleotide-binding domain resulting in ADP-P_i-actin. The γ-phosphate remains bound to the actin monomer, however, due to its repositioning in the protein, the hydrolysis is irreversible (Blanchoin & Pollard, 2002). The hydrolysis of ATP is a spontaneous event (Jégou et al., 2011), but it is discussed, whether those spontaneous events destabilize the neighboring molecules and thereby initiate a zipper-like chain reaction of ATP hydrolysis (Korn et al., 1987). The intermediate ADP-P_i-actin state is relatively stable with a half-life of 102 seconds (Jégou et al., 2011) and its affinity towards the actin oligomer is still comparable to ATP-actin (Fujiwara et al., 2007). With the dissociation of the γ-phosphate, the conformation of the monomer changes, which leads to a destabilization of the filament (Pollard, 2016). Since ATP-actin is more likely to bind at the barbed end, the dissociation of ADP-actin is more likely to happen at the pointed end. Consequently, the shrinking of the filament is more likely to happen at the pointed end (Pollard, 2016). Association, dissociation, and stabilization of the filaments are orchestrated by actin-binding proteins (Pollard, 2016). In short, those proteins are involved in initiation and elongation of new filament strands, capping of barbed or pointed ends to prohibit dissociation and terminate elongation, tearing of filaments, branching, and crosslinking of filaments (Pollard, 2016).

As actin filaments, microtubules are constructed of monomeric proteins, namely α- and β-tubulin. α- and β-tubulin form dimers, called αβ-tubulin which oligomerize to a filamentous structure, the protofilament (Goodson & Jonasson, 2018). Typically, 13 linear protofilaments assemble laterally to a hollow tube in a form that can be described as a spiral staircase, however, the number of associated protofilaments can vary between 12 and 16 (Goodson & Jonasson, 2018). Differences in the number of associated protofilaments result in a seam that is created between the first and the last protofilament. As α- and β-tubulin are attached in the hollow tube laterally, the positioning of the proteins is crucial to give maximal stability to the tube structure (Goodson & Jonasson, 2018). With 13 protofilaments, the proteins are not able to interact laterally thereby creating a seam at one side of the tube. A structure composed of 12, 15 or more filaments can adjust in a way that all neighboring proteins can connect resulting in a stabilized

structure (Goodson & Jonasson, 2018). Varying numbers of protofilaments in microtubule tubes were observed *in vivo* (Sui & Downing, 2010), however, the function of these varying protofilament patterns and the impact on the stability of the microtubule is still not well understood. The number of molecules that are associated with a microtubule, leads to bigger structures compared to actin filaments giving microtubules a higher rigidity. While actin filaments have a diameter of approximately 8 nm and can reach a length of up to approximately 20 µm (Gittes et al., 1993), microtubules have a diameter of approximately 25 nm (Goodson & Jonasson, 2018) and can create structures spanning several thousands of µm (Gittes et al., 1993; Hawkins et al., 2010). As actin filaments, microtubules are polar and assembling of the filament can happen from both sites at varying paces. The fast-growing plus end harbors an exposed β-tubulin, while the slower-growing minus end exposes an α-tubulin (Goodson & Jonasson, 2018). The assembly of new microtubules is initiated by a nucleation process but was shown to be highly unfavorable *in vitro* (Caudron et al., 2002). Therefore, the nucleation process must be regulated tightly by cells to orchestrate difficult processes like the mitotic spindle. Different mechanisms of nucleation exist with the γ-Tubulin ring complex (γ-TuRC), being the best understood complex in promoting nucleation (Kollman et al., 2011). The main function of this nucleation complex is, to provide a template for the attachment of αβ-tubulin and thereby overcoming the unfavorable nucleation energy barrier. After initiation of the nucleation complex, the association of αβ-tubulin is mainly driven by hydrophobic effects (Vulevic & Correia, 1997). The lifespan of a microtubule filament is orchestrated by the hydrolysis of GTP nucleotides. The specifics of the mechanism are still under debate up to date, but the general mechanism is widely accepted (Goodson & Jonasson, 2018). Tubulin can bind to GTP, or GDP, respectively, however, it was shown that only GTP-tubulin will assemble into microtubules (Goodson & Jonasson, 2018). Upon assembly, the hydrolysis of GTP is initiated by the incoming subunit that functions as a GTPase (Nogales et al., 1998). Upon exchange of GTP with the GTP analog guanylyl 5'-a,b-methylenediphosphonate (GMPCPP), which is slower hydrolyzed compared to GTP, it was shown that microtubules formation speed remains the same but the dissociation dynamic of them was drastically slowed down (Hyman et al., 1992). This demonstrated that the disassembly of microtubules is supported by the hydrolysis of GTP. Through GTP hydrolysis the GDP-tubulin undergoes conformational changes and the bonding to the neighboring tubulins gets weaker. The destabilized bonding favors the dissociation of the GDP-tubulin (R. Zhang et al., 2015). The microtubule structure remains stable as long, as a GTP cap is present at the tip, which stabilizes the construct. With no supporting structure, the microtubule structure quickly falls apart in an event called catastrophe (Goodson & Jonasson, 2018). Besides the γ-TuRC nucleation complex, and similar to actin filaments, a variety of other associated proteins is involved in stabilizing, destabilizing, capping, or crosslinking the structure between microtubules or other cellular elements (Goodson & Jonasson, 2018).

Besides providing rigid formations, thereby stabilizing the cell in the form of cytoskeletal elements, the functions of actin and microtubule filaments are much broader. Motor proteins are specialized in "walking" on those filaments and so the cytoskeleton is needed to mediate the intracellular transport processes. In animal cells, most transport is done across microtubules, while in plants the majority of cellular transport is performed across actin filaments, which does not eliminate the transport functions of the other respectively (Geitmann & Nebenführ, 2015). For each filament, specific motor protein classes exist that are solely associated with the filament.

1.1.4 Motor proteins in plants

During the evolution of eukaryotic cells, a variety of motor proteins has evolved, which enables active and directed intracellular transport of cellular components. During evolution, this opened the opportunity for growing much larger cell sizes. All motor proteins display the characteristic feature that they can transform ATP-delivered energy into mechanical force. Generally speaking, three groups of motor proteins exist, which are grouped based on the specific filaments and directions that they can move along said filament. Myosin motor proteins can walk on actin filaments, kinesins walk on microtubules in the minus to plus direction, whereas dyneins walk on microtubules from the plus to the minus end. In the following, a focus is laid on the functional description of myosins and kinesins, since in higher plants besides different dynein light chains, no other components of the dynein complex could be shown (Cao et al., 2017; Nebenführ & Dixit, 2018).
All motor proteins possess a very similar buildup. They all are dimers or oligomers of two or more heavy chains that are involved in the binding of the cytoskeleton, the binding of the cargo and the generation of the mechanical force. Additionally, several light chains help stabilize the heavy chains (Nebenführ & Dixit, 2018; Vale, 2003). The heavy chain itself is divided into a motor domain, which binds the cytoskeleton and converts energy delivered by ATP into a conformational change promoting the movement, a neck domain which functions as a leg-like structure and transits the conformational change of the motor domain into a large step, a dimerization domain, which allows the dimerization (or oligomerization) of three or more heavy chains, and lastly a cargo binding domain that functions as a specific linker between the motor protein and the cargo that needs to be delivered (Nebenführ & Dixit, 2018). The grouping of individual motor protein subfamilies is based on the differences in these four domains (Nebenführ & Dixit, 2018; Vale, 2003). The difference between myosins and kinesins is characterized by the respective motor domain, which is not only specific to the cytoskeletal element, but also differs in chronology of filament binding and ATP hydrolysis (Y. R. J. Lee & Liu, 2004). When bound to ATP myosin motor domains possess a low affinity to actin. Upon hydrolysis of ATP, the conformational change occurs in the molecule. This is accompanied by a rise in affinity to actin and a power stroke is generated (Nebenführ & Dixit, 2018). Kinesin motor domains possess a high affinity to microtubules when ATP is bound, whereas the release from microtubules happens upon ATP hydrolysis. After the release of ADP and the inorganic phosphate, the conformational change is mediated by the binding of a new ATP molecule (Nebenführ & Dixit, 2018).

The number of described myosin and kinesin genes differs drastically in the plant kingdom (Mühlhausen & Kollmar, 2013; Reddy & Day, 2001b; Richardson et al., 2006). In *A. thaliana* the number of identified kinesin genes comprises 61, while the number of identified myosin genes is 17 (Y. R. J. Lee & Liu, 2004; Mühlhausen & Kollmar, 2013; Reddy & Day, 2001a, 2001b). Considering, that plant motor proteins were not extensively studied during the last decades and that the evolutionary divergence between plant motor proteins and other eukaryotic species is very high, relatively little is known about their functions. Nevertheless, kinesins and myosins of all eukaryotes were grouped upon the phylogenetic analysis in different subfamilies. For kinesins family 1-14 (Lawrence et al., 2004), while for myosins family I - XVIII are defined (Berg et al., 2001). The following paragraph will briefly summarize the function of kinesins and myosins in *A. thaliana*.

Since plants do not possess dyneins, kinesin families 7 and 14 compensate for the missing motor protein group. Consequently, those families are widely enlarged in numbers compared to fungi and animal cells (Richardson et al., 2006). Following this, 21 kinesins mainly found in *A. thaliana* kinesin family 14 are minus end directed, while kinesins in fungi and animal cells are plus end directed motor proteins (Reddy & Day, 2001b). The kinesin functions elucidated so far are very broad, family specific and mostly speculative due to the lack of research in this field. Some of the discussed functions of *Arabidopsis* kinesins are the organization of the mitotic and meiotic microtubule spindle apparatuses (Chen et al., 2002; Marcus et al., 2003) or the stabilization of microtubules during different phases of the cell cycle (Mathur & Chua, 2000; Preuss et al., 2003). Furthermore, they are potential dynamic linkers between actin and microtubule filaments during cell growth (Preuss et al., 2004) and can contribute to cellulose microfibril deposition during cell wall synthesis (Zhong et al., 2002). In addition, some kinesins have essential functions in cytokinesis either as activators of a mitogen-activated protein kinase (MAP kinase) cascade (Nishihama et al., 2002; Strompen et al., 2002) or in the organization of the microtubule structure and Golgi derived vesicle transport in the phragmoplast (Y.-R. J. Lee et al., 2001; Pan et al., 2004).

For myosins, only two subfamilies exist in *Arabidopsis.* Phylogenetic analysis revealed that myosin family VIII consists of four members and myosin family XI harbors 13 members in *Arabidopsis thaliana* (Berg et al., 2001; Reddy & Day, 2001a). While both of those myosin families are unique to plants, myosin family XI is closely related to animal and fungal myosin family V (Kinkema & Schiefelbein, 1994; Nebenführ & Dixit, 2018; Reddy & Day, 2001a). In comparison to myosins XI, the efforts in the investigation of myosins VIII have been relatively low and so most of the functions can only be assumed. Localization studies placed one representative of myosin VIII in the cell periphery at newly formed cross-walls giving a basis for speculation about functions during cell plate maturation (Reichelt et al., 1999). Other studies demonstrated that myosin VIII members are involved in endocytosis (Sattarzadeh et al., 2008) and associated with plasmodesmata (Avisar et al., 2008).
The functional roles of myosin XI are under stronger investigation as it has become apparent that members of the myosin XI family are greatly involved in organellar transport and thereby in the mediation of cytoplasmic streaming (Shimmen & Yokota, 1994a). Those findings were manifested in many studies following the early 2000s (Madison et al., 2015; Peremyslov et al., 2008, 2010; Prokhnevsky et al., 2008; Ueda et al., 2010). Furthermore, it was shown that family XI myosins are also involved in the structural organization of actin filaments (Cai et al., 2014; Peremyslov et al., 2010; Ueda et al., 2010). It is noteworthy that neither of those studies could assign specific functions to one member of the myosin XI family. Rather it was shown that members of myosin family XI display redundant functions. With single myosin XI gene-knockouts organellar movement could be slowed down, but not prohibited (Peremyslov et al., 2010). Furthermore, those results demonstrated a rather unspecific assignment of myosin XI to different organelles like Golgi, peroxisomes mitochondria and Endoplasmic Reticulum (ER) (Peremyslov et al., 2010). Besides organellar movement and actin organization, plant growth in total was affected by missing myosin XI (Peremyslov et al., 2010). However, only the loss of function of the four most expressed myosin XI genes led to a total loss of organellar motion and plant growth was affected significantly compared to single myosin XI gene-knockouts (Peremyslov et al., 2010). All those findings hint to non-specific functions of myosin XI motors in the active distribution of organelles and actin organization.

In contrast to the movement speed of kinesins, which reaches up to several nanometers per second, but mostly does not exceed velocities of more than 1 µm/sec (Berg et al 2013), the movement speed of myosin XI-mediated organelle transport is remarkably high, ranging up to 7 µm/sec in flowering plants (Tominaga, 2003). This high motility is facilitated by the long neck region, which is a feature of myosin family XI and allows the motor protein to move with a step length of 35 nm (Tominaga, 2003). This step size is believed to be the reason for the fast movement of the myosin XI family because it enables the protein to walk along the approximately 36 nm helical repeat of actin filaments (Tominaga, 2003). In addition, the fast processing of ATP by myosin XI members is a key element of the movement characteristic. The movement speed is constrained by the release of ADP molecules, which is the limiting step in the reaction cycle and thereby dictates the maximal velocity of the motor protein (Tominaga, 2003). However, the movement speed of organelles transported by myosin XI is not described as a continuous motion. It is proposed that besides the number of attached motor proteins, the actin configuration influences organellar movement (Akkerman et al., 2011). In cell regions where actin accumulated to thick actin bundles a maximal speed of 7 µm/ sec was measured, whereas in regions with thin and unstructured actin filaments, organelles displayed a wiggling effect, indicating no specific transport (Akkerman et al., 2011). The change between undirected wiggling and directed high-speed transport is described at various times for all kinds of organelles (Akkerman et al., 2011; Perico & Sparkes, 2018; Vick & Nebenführ, 2012). The molecular functions of these varying movement patterns are not understood and need to be elucidated.

1.1.5 Organelle movement

During evolution, the eukaryotic cell has developed a high graduate of compartmentalization in form of organelles. Membranes separate the organelles from the rest of the cell creating distinct microenvironments for biochemical reactions. Due to the complexity of the cellular system, the metabolism of the cell is cross-linked but compartmentalized and therefore needs interaction and communication of all involved cellular compartments. A good example of special separation and organellar interaction is lipid synthesis in plants, which is brought out in the cytoplasm, the plastid, and the ER (Chapman & Ohlrogge, 2012). The spatial separation enforces the different compartments to be in a permanent exchange of molecules and information. This arises two questions: I) how is the metabolic transfer between organelles structured and II) how do the organelles communicate with each other to orchestrate the tight regulation of the cellular metabolism. The nutrient turnover cytoplasmic streaming offers is not sufficient to answer those questions. Fluorescence labeling made it possible to show that organelles in plants can move separated from the general direction of cytoplasmic streaming. Independently of each other it was shown that mitochondria (van Gestel et al., 2002), Golgi stacks (Boevink et al., 1998; Nebenfür et al., 1999) and peroxisomes (Collings et al., 2002; Jedd & Chua, 2002; Mathur et al., 2002) undergo stop-and-go motions that cannot be explained with a background of static cytoplasmic streaming. Those results indicate that besides cytoplasmic streaming other mechanisms exist in the cell that mediates the transport of organelles. There is relatively little known about the molecular mechanisms underlying the movement of organelles and even less understood, how organelles communicate with each other. In general, it is accepted that motor proteins bind to the organellar surfaces and pull them through the cell to their target locations (Perico & Sparkes, 2018; Vick & Nebenführ, 2012). Even though molecular mechanisms of most organellar movements are poorly understood, it is dependent on the actin-myosin

machinery. In plants, it has been shown that organellar trafficking is driven by class XI myosin motor proteins (Peremyslov et al., 2008, 2010). Interestingly, although different myosins exist in the plant's genome, their function remains somewhat redundant, and functions of a specific myosin cannot be linked to specific cargo organelles. Singe knockouts of individual plant Myosins XI-K, and XI-2 resulted in three- to four-fold movement reduction of Golgi stacks and peroxisomes, however, no complete stop of motion (Peremyslov et al. 2008). Additionally, for *myosin XI-K* mutant plants it was reported that mitochondria movement speed was reduced four-fold, while in *myosin XI-2* mutants only minor effects on the organellar movement were observed (Peremyslov et al. 2008). Furthermore, while mutation of Myosin XI-K and XI-2 led to a large effect on organellar movement, single mutations of their closest paralogs Myosin XI-1 and XI-B did not cause a great effect on the organellar movement (Peremyslov et al., 2008). Combinations of double mutants of said myosins revealed, a greater impairment on the movement properties of Golgi stacks, peroxisomes and mitochondria, depending on the mutated myosin combination and reflecting an interdependency of myosins regarding their function (Prokhnevsky et al., 2008). During the investigation of triple and quadruple knockouts of the most expressed myosins in *Arabidopsis*, movement of Golgi stacks and peroxisomes was drastically reduced in the triple mutant affecting Myosin XI-K, XI-1 and XI-2 whereas it was completely abolished in the quadruple mutant affecting Myosin XI-K, XI-1, XI-2 and XI-I (Peremyslov et al., 2010). Those results display the importance but also the redundancy and interconnectivity in the functions of class XI myosins during organellar movement.

Besides Golgi stacks, peroxisomes, and mitochondria, the movement of nuclei depends on the actin-myosin machinery, as well. The speed of the light avoidance reaction of nuclei was impaired in mutants of myosin XI-I (Tamura et al., 2013). Additionally, the destruction of the actin cytoskeleton by latrunculin B, a substance that depolymerizes actin filaments, resulted in impaired nuclear movement (Iwabuchi et al., 2010). In contrast, the depolymerization of microtubules did not affect nuclear movement (Iwabuchi et al., 2010), displaying the nuclear movement's dependency on the actin-myosin machinery. Besides their dependency on the actin-myosin machinery, the nuclear movement was also shown to be connected to the light avoidance reaction of chloroplasts. This avoidance reaction is mediated by a different system than the classical organellar transport and does not utilize the filamentous cytoskeleton combined with motor proteins in the classical manner previously described (1.1.3, 1.1.4). The light avoidance reaction of chloroplasts will be described in a later chapter.

Since no exact mechanisms of organellar transport could be elucidated so far, different working models to describe organellar movement in plants were proposed (Figure 2) (Geitmann & Nebenführ, 2015). A first model proposes an active one-to-one association of motor proteins with their cargo (Figure 2 A). This would presume a rather specific association of myosin with particular organelles. A second working model proposes the indirect movement of organelles by attachment to the ER or other organelles, which are actively transported by associated myosins (Figure 2 B). A third model implements cytoplasmic streaming (Figure 2 C). In this model, organelles are transported by myosins, and their movement drives the cytoplasmic streaming. Other organelles that are not attached to cytoskeletal filaments are transported by the passive flow. Since all three working theories are based on results gathered throughout different studies (Cai et al., 2014; Geitmann & Nebenführ, 2015; Madison et al., 2015; Peremyslov et al., 2008; Prokhnevsky et al., 2008; Ueda et al., 2010) organellar movement could be a mixed composition of all three proposed models.

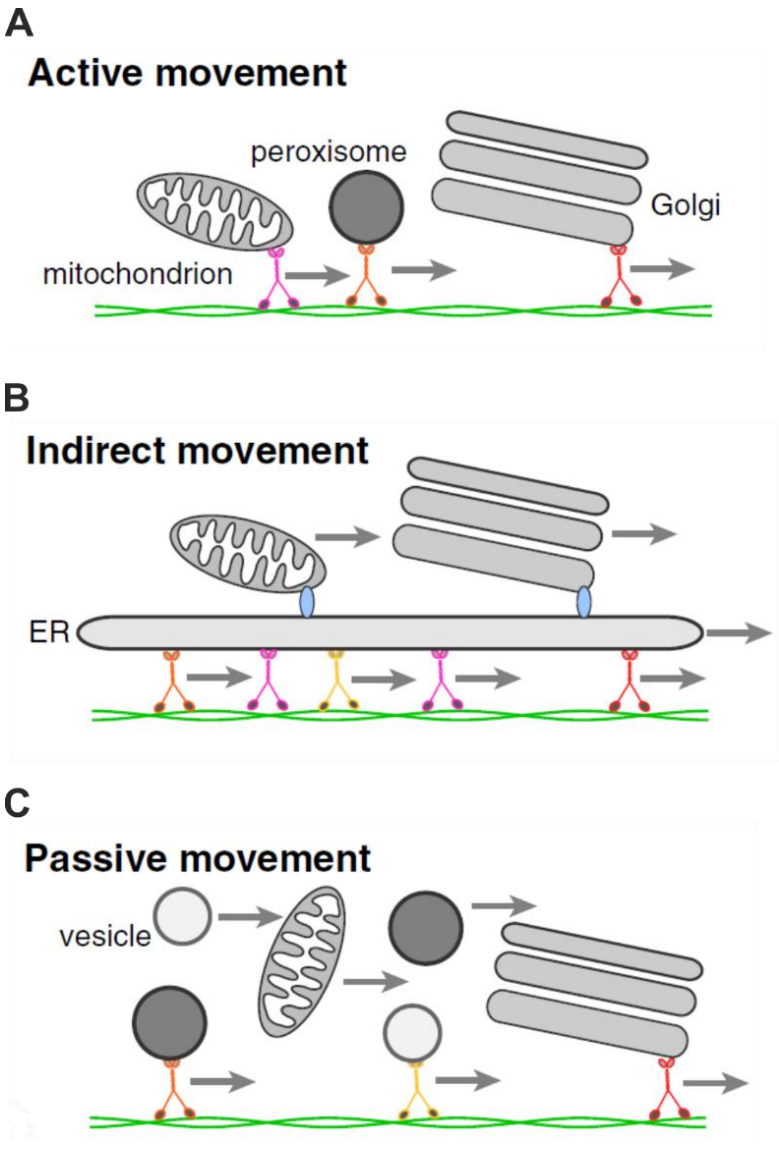

Figure 2 Models of organellar movement. Different models of how organellar movement is mediated. A) Organelles are directly linked to motor proteins that mediate the movement by sliding across cytoskeletal elements. B) Organelles are attached to other organelles like the ER, which are transported actively by motor proteins. The attached organelle moves in a semi-active manner. C) Organelles that are attached to motor proteins and directly transported across cytoskeletal elements mediate cytoplasmic streaming. Movement of other organelles is driven by the cytoplasmic flow (Geitmann & Nebenführ, 2015).

The movement of organelles is crucial for the plant's development. Reduction in organellar movement capacities resulted in a reduction in the plant's growth (Perico & Sparkes, 2018). Functional studies of the organellar movement revealed that organelles do not move continuously, but undergo stop-and-go motions. Individual studies on Golgi stacks (Boevink et al., 1998; Nebenführ et al., 1999), mitochondria (van Gestel et al., 2002) and peroxisomes (Collings et al., 2002; Jedd & Chua, 2002) revealed, that those organelles underwent saltatory, undirected movements, in which phases of the movement were followed by phases of resting. Speculating about the organelle's functions, the resting movements were associated with metabolite delivery or exchange at specific cellular sites or with other organelles, whereas the movement phases were linked to the transport of the organelle to another cellular location (Vick & Nebenführ, 2012). This hypothesis was strengthened by investigations on Golgi stacks delivering cellulose synthase complexes to the plasma membrane. These results displayed that stop motions were directly linked to the delivery of the cellulose synthase complex (Crowell et al., 2009). Additional work revealed

that these stops were mediated by microtubule filaments interacting with the actin filament on which the actual motion was regulated (Wightman & Turner, 2008). Stop motions of other organelles like mitochondria, ER, and peroxisomes could be linked to the presence of microtubules (Hamada et al., 2012). Although a regulatory effect of microtubules could be abstracted from these findings, the stop-and-go patterns of organelles could not be abolished by the disruption of microtubules with oryzalin (Hamada et al., 2012; Wightman & Turner, 2008). This hints to further regulation and functions of the stop-and-go motions of organelles.

1.2 Dynamics of plastids

1.2.1 Plastids and their integration into the plant's metabolism

Plastids are cell organelles specific for plants, which carry out a variety of crucial functions. Originally free-living cyanobacterial ancestors were engulfed during an endosymbiotic event more than 1.6 billion years ago (Yoon et al., 2004). Since then, they evolved to specialized cell organelles that offer compartments for very distinct reactions, like photosynthesis. The term plastid is used to describe a diverse spectrum of organelles all deriving from the proplastid. While all plastid forms share basal metabolic functions that are crucial for the cell, each of them is additionally specialized in specific tasks. From the proplastid, several subspecies of plastids can differentiate (for a detailed evolving pattern see Figure 3) (reviewed by Rolland et al., 2012, 2018). Most plastids are restrained to specific tissues and are characteristic for specific cell types. In general, the discrimination between green and non-green plastids is made. Chloroplasts, and chromoplasts are counted to green plastids (Rolland et al., 2018). Chloroplasts are found in all green tissues carrying out photosynthesis to generate energy for the plant. Chloroplasts, which are not exposed to light, reduce their chlorophyll content and are called etioplasts (Rolland et al., 2018). This state is reversible and upon illumination, the chlorophyll content is reconstituted (Rolland et al., 2018). However, in their bleached form, they cannot carry out photosynthesis. Senescent chloroplasts evolve into gerontoplasts. Their main function is the recycling of their own components (Rolland et al., 2018). Chromoplasts are storage bodies for lipids as well as the source of plant color, through the storage of chromophores (Rolland et al., 2018). They are present in fruits and flowers. All non-green plastids derive from the leucoplast and are present in roots, seeds tuber and fruits (Rolland et al., 2018). Their names are oriented to the function the plastid carries out. Elaioplasts are lipid storage bodies, amyloplasts store starch and reduced carbon, proteinoplasts accumulate proteins (Rolland et al., 2018). Statoliths are special amyloplasts found in the root tip of plants (Morita, 2010). They are involved in gravity sensing. Their sedimentation triggers a signal cascade for the control of root growth (Morita, 2010).

After the endosymbiotic events, the eukaryotic cell compartmentalization was optimized and in result, cellular key reactions of different metabolic pathways were spread around different organelles and the cytoplasm. In consequence, besides the very specific functions, plastids share some cellular key functions for the maintenance of the plant's metabolism with other organelles (Rolland et al., 2018). During evolution, plastids lost most of their genetic material, which was transferred to the plant's nucleus. The plastid genome itself encodes for just a small portion of about 200 proteins (Soll & Schleiff, 2004). This is

not much compared to the proteome of the plastid that harbors approximately 3.500 proteins (Soll & Schleiff, 2004). This raises the need for the import of cytosolic proteins into the chloroplast.

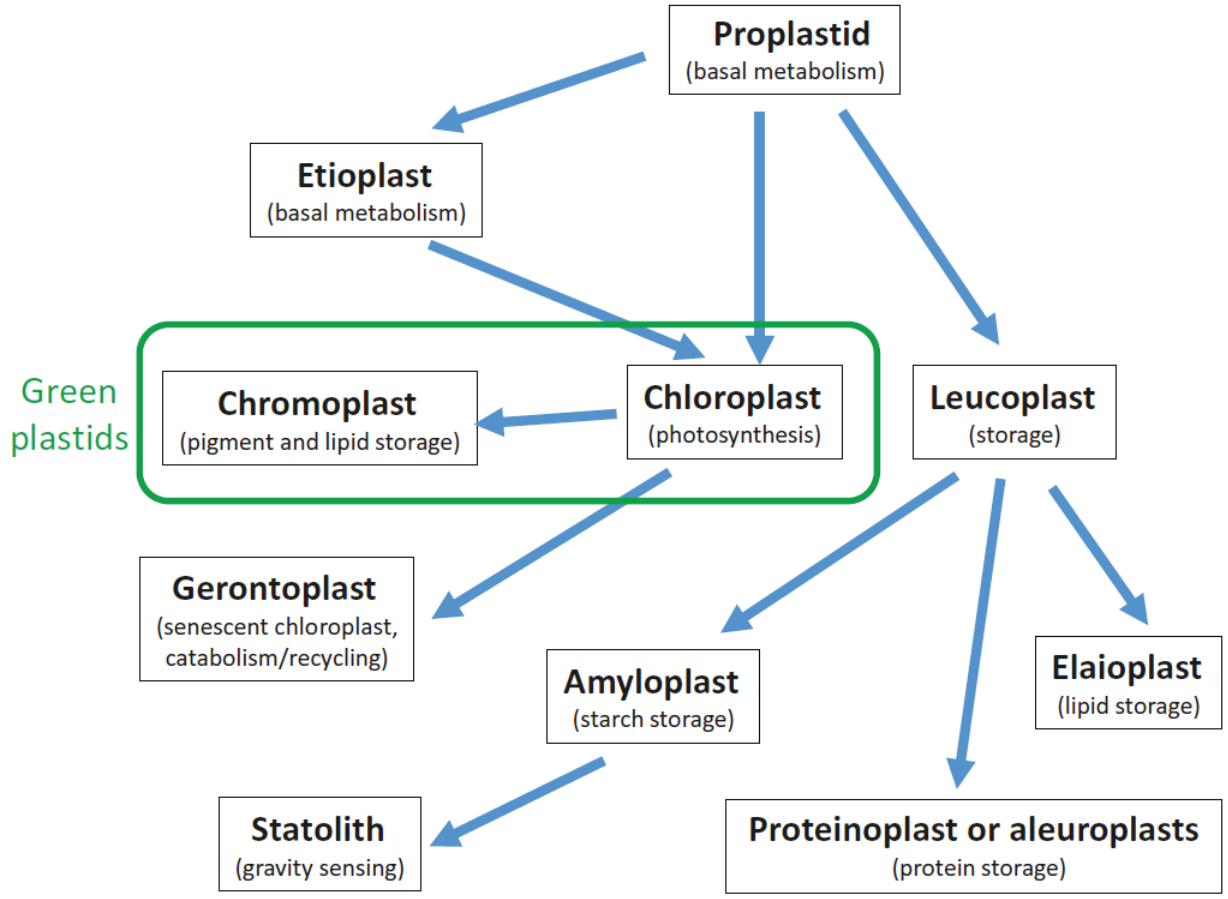

Figure 3 Differentiation pattern of plastids. The diversity of the plastid family is shown. All plastid subtypes originate from the proplastid. Blue arrows indicate the differentiation possibilities of plastid subtypes. Plastid subtypes fulfill specific functions which are indicated in brackets for each type. Chloroplasts and Chromoplasts are classified as green plastids, since they incorporate pigments and thereby are colorful. (Rolland et al., 2018).

By studying the proteins, imported to the plastid, specific functions can be inferred that are carried out by the plastid, although experimental evidence confirming those functions is not always given. Additionally, the functions of the imported proteins are not always well understood but bioinformatic approaches aimed to fill those knowledge gaps by using functional predictions. Several bioinformatical analyses have predicted the plastid proteome based on known genomic sequences and protein sequence predictions (Ferro et al., 2010; Joshi et al., 2011). Besides the bioinformatic approaches that were taken, also proteomic analyses of the plastid proteome were performed (Kleffmann et al., 2004; Zybailov et al., 2008). In consequence, metabolic compartmentalization was inferred even though experimental evidence was not always given.

Besides the well-characterized photosynthesis that is only carried out by chloroplasts, several other metabolic pathways accommodate synthetization steps that are exclusively mediated by the plastid. 10 of

the 20 amino acids have synthetization steps that are exclusively carried out in the plastid. Those amino acids are Arginine, Lysine, Threonine, Leucine, Isoleucine, Valin, Tryptophan, Phenylalanine, Tyrosine, and Histidine (Azevedo et al., 2006; Muralla et al., 2007; Rippert et al., 2009; Rolland et al., 2012; Stepansky & Leustek, 2006). Seven other amino acids, namely Aspartate, Cysteine, Glutamine, Glycine, Serine, and Methionine are partially synthesized in the plastid (Rolland et al., 2012).
The plant's cell membrane is mainly composed of phospholipids. In contrast, the plastid envelope membranes, and the thylakoids in the chloroplast also harbor great amounts of galactolipids. The *de novo* fatty acid synthesis of plants is carried out exclusively in the plastid (Harwood, 1996; Joyard et al., 2010). While glycolipids are further processed at the plastid envelope, the synthesis of phospholipid variants is shared between the plastid and the ER (Harwood, 1996; Joyard et al., 2010). At low phosphate conditions, the glycolipids synthesized in the plastid can also compensate for missing phospholipids at the membranes of other organelles and the plasma membrane and thereby maintain cellular lipid homeostasis (Nakamura, 2013).
Besides amino acid and lipid synthesis, plastids are also involved in the *de novo* synthesis of nucleotides. Disregarding the fact that nucleotide synthesis requires amino acids, which are synthesized by the plastid, also adenosine monophosphate (AMP) is proposed to be exclusively synthesized in the plastid (Zrenner et al., 2006). Proteins that catalyze the synthesis of different vitamins, which are crucial for the plant's life cycle, have been found to localize either in the plastid stroma or at the plastid envelope. They are involved in the biosynthesis of tocopherols and tocotrienols (vitamin E), carotenoids (pro vitamin A), phylloquinone (vitamin K1), riboflavin (vitamin B2), and thiamine diphosphate (vitamin B1) (Frelin et al., 2012; Goyer, 2010; Jordan et al., 1999; Joyard et al., 2009).

Besides taking part in diverse metabolic pathways to maintain the plant's homeostasis, the plastid is furthermore described to be involved in diverse retrograde signaling pathways like ROS-, redox-, and gene expression signaling (Eberhard et al., 2008), as well as in ionic signaling pathways (McAinsh & Pittman, 2009). However, these findings were made in photosynthetic active chloroplasts that take a unique role keeping in mind that they are exposed to destructive effects caused by photodamage. Nevertheless, all plastid types take leading roles in keeping the cellular machinery running. Therefore, strict interaction and communication with other cellular compartments must be assured. So far, it is not well understood how this communication is carried out but the need for direct interaction with other cellular components and organelles is given by those metabolic interrelations. It is believed that tubular extensions, which are a feature of plastids, called stromules, are involved in the cellular communication system.

1.2.2 Stromules

Plastids, like other organelles (Cutler et al., 2000; Logan et al., 2004), can form tubular membrane extrusions. These protuberances were described first more than 100 years ago (Svenn, 1908) but due to methodical limitations restricting light microscopy, their investigation was very difficult for a very long time. The investigation of tubular membrane extrusions came back to the focus of research with the isolation and utilization of the green fluorescent protein (GFP) in the early 90s (Chalfie et al., 1994). With the implementation of GFP into the molecular toolset, targeted labeling of the plastid's stroma made the investigation of the tubular membrane extrusions easy and focused research could be executed. Soon they

were observed in all parts of plants throughout the higher plant kingdom (Köhler et al. 1997; Langeveld et al. 2000; Tirlapur et al. 1999). To differentiate between the different organellar protuberances, the term stromules was given specifically for tubulations of the plastid (Köhler and Hanson 2000). The name is oriented to the fact that both, the inner and outer membranes surround the tubulations and therefore the formed tube is filled with stroma, which allows free flow of macromolecules (Köhler et al. 1997). Besides thylakoids, DNA and ribosomes, all small components of the stroma can pass through stromules making them favorable locations for potential nutrient exchange (Hanson & Hines, 2018). Stromules are very dynamic structures with varying lengths that can reach from several µm (Köhler et al. 1997; Pyke and Howells 2002) up to 200 µm (Waters et al., 2004). In contrast to their length stromules are very thin structures, spanning 0.3-0.85 µm in diameter (Arimura et al., 2001; Natesan et al., 2005). In addition to being long tubular structures, they can take on different shapes by branching and kinking (Gunning, 2005). Their dynamic structure is highlighted by the fact that they were observed to extend and retract with speeds of up to 1.1 µm/sec at chloroplasts (Gunning, 2005). In addition, the tips of stromules can undergo so-called "tip-shedding" (Gunning, 2005), a process, where the tip of the stromule is constricted and vesiculated. The fate of the vesicles is not clear up to now, but they are discussed to be involved in cellular signaling or plastid degradation (Hanson & Hines, 2018).

Stromules have been observed in all kinds of tissues and at all plastid subtypes. Although they have much more often been observed in root tissue, the functions of stromules are not elucidated so far. It was observed that stromules in chloroplasts predominantly formed upon stress treatment of the plant like salt, drought, or oxidative stress (Gray et al., 2012). Also, the addition of external sugars like mannitol or sucrose induced stromule formation (Gray et al. 2012; Schattat and Klösgen 2011). Furthermore, stromule formation was observed during immune reactions of the plant or exogenous application of pro defense signals like H_2O_2 or salicylic acid (Caplan et al., 2015; Gu & Dong, 2015). Interestingly, stromules formed during and apart from immune reactions are described to be associated with the nucleus (Caplan et al. 2015; Erickson, Kantek, and Schattat 2017; Gu and Dong 2015; Kumar et al. 2018). This led to the hypothesis that stromules are involved in retrograde signaling of chloroplasts with the nucleus for transcriptional changes and speculation about pathogen sensing mechanisms of the chloroplast (Caplan et al., 2015; Gu & Dong, 2015). In addition, it was observed that chloroplasts and associated stromules form a physical barrier around the nucleus during triggered immune response (Caplan et al., 2015; Gu & Dong, 2015; Kumar et al., 2018) strengthening assumptions about their functional role in defense mechanisms of the plant. Besides nuclei, stromule localization was often observed with other organelles (Köhler and Hanson 2000; E. Y. Kwok and Hanson 2004) and a functional role of stromules in metabolite transport between the plastid and other organelles was suggested. Specifically, for stromule interaction with the ER, dynamic colocalization and colocalized reorganization were observed (M. Schattat et al., 2011). These findings suggested organellar interaction with the stromules based on colocalization and proximity. Although no membrane fusion was detected so far, membrane contact sites and the exchange of molecules via stromules were observed multiple times (Caplan et al., 2015; Guirimand et al., 2020; Mehrshahi et al., 2013). Additionally, interactions of different plastids are mediated by stromules, although stromules do not form a "plastidal network" in the cell (Köhler & Hanson, 2000). The functional role of stromules was discussed various times, but defined functions that stromules uniquely carry out

could not be proven up to now. However, the fact that stromules physically increase the surface of plastids and thereby allowing for more membrane contact sites for metabolite exchange is generally accepted.

1.2.3 Plastid movement

Although the family of plastids comprises a variety of differentiated organelles with specific functions, all of them carry out basal metabolic functions and thereby maintain the well-being of the plant. As previously depicted, plastids need to undergo interaction and communication with other organelles to properly carry out their tasks. Additionally, since plants are sessile organisms, they need to react to external environmental stimuli. To do so, and to maintain the well-being of the plant, they need to be transported through the cell to either ensure close and proper communication and nutrient exchange with other organelles or to protect themselves against environmental stimuli. Although the plastid family is quite diverse, the focus of research during the last decades was laid on green chloroplasts. This is mainly reasoned by the accessibility of the chloroplasts constituted in times before targeted fluorescence labeling of organelles was possible, but also their ability to carry out photosynthesis, thereby making them one of the driving forces of life. Besides chloroplasts also root amyloplasts have gained some attention of science, since it is believed, that those organelles mediate the gravitropic response of the plant. Unfortunately, other plastid types remain disregarded to a great extent, especially in terms of research on organelle motility and dynamics. However, the movement of plastids has been proven to fulfill specific functions. Especially for chloroplasts, the so-called accumulation and light avoidance reactions were studied intensively, and many essentials of the underlying molecular movement mechanisms are understood now.

Chloroplast movement is a crucial mechanism to ensure efficient photosynthesis under low light conditions, but also to ensure plant survival at high light conditions. During low light conditions, they perform an accumulation response and accumulate at the upper and the lower areas of the cell, where they spread out to gather as much light as possible to ensure efficient photosynthesis (Suetsugu and Wada 2012). Under high light conditions, chloroplast undergo a light avoidance response and gather at the sidewalls of a cell. They stack upon each other in the direction of light to minimize irradiation caused by the strong light and thereby minimizing light stress (Suetsugu & Wada, 2012). These movements were first described in the mid of the 19th century (Böhm 1856), and the first initial experiments on this matter were performed in the early 1900's (Senn 1910). It was also an accomplishment of those studies that displayed the chloroplast's movement dependency on blue light stimuli (Senn 1910). Science has come a long way since then and the molecular mechanisms of the chloroplast photorelocation are much more elucidated today. During the avoidance reaction, which is triggered by blue light, the positioning of the chloroplasts in the cell is regulated by red light (Kong & Wada, 2014; Suetsugu & Wada, 2012). The current model of the chloroplast relocation is described as followed (reviewed by Wada & Kong, 2018): The light accumulation and avoidance reaction is mediated by the signaling of two different blue light receptors phot1 and phot2. Phot 2 is located at the outer envelope of the chloroplast and is mainly involved in the signaling of the avoidance reaction under strong light. Phot1 and phot2 are both also localized at the plasma membrane and mediate the signaling of the accumulation response under low light conditions. The signaling is detected by a so far unknown signal receptor that is probably associated with the protein Chloroplast Unusual Positioning 1 (CHUP1). CHUP1 is anchored at the outer envelope of the chloroplast

and is a key mediator of the chloroplasts' movement. CHUP1 anchors the chloroplast at the plasma membrane by association with a so far unknown protein. Additionally, it mediates the recruitment of profilin-actin and interacts with kinesin-like proteins for actin-based chloroplast movement (KACs). KACs, in an interplay with CHUP1, facilitate the polymerization of the profilin-actin to chloroplast-actin (cp-actin) filaments, which are connected by the protein Thrumin I to the plasma membrane. The filamentous cp-actin is synthesized in a way between the chloroplast and the plasma membrane so that the chloroplast slides in the direction of the newly synthesized actin filaments. The movement that is mediated by this mechanism creates velocity for the avoidance response of 1-2 µm/min (Kimura & Kagawa, 2009), whereas the velocity of the accumulation response is relatively stable localized at 1 µm/min in *Arabidopsis thaliana* (Kong & Wada, 2014).

Aside from the movement of chloroplasts, the only plastid movement that has attracted the attention of research was the amyloplast movement during gravity sensing. Gravity-sensing organs in plants contain starch-filled amyloplasts, which are believed to mediate the gravitropic response by their sedimentation and interaction with the actin cytoskeleton (Morita, 2010). These amyloplasts are not stationary anchored in the cell and thereby can undergo passive sedimentation movements (Morita, 2010). Those sedimentation movements are described to reach velocities up to 2 µm/min in various plant types, but in some cases, movement speeds of several dozen µm/min were observed (Sack et al., 1984; Saito et al., 2005; Yoder et al., 2001). Aside from passive sedimentation, it was also described, that amyloplasts undergo saltatory movements that can be directed against gravity, and which are dependent on F-actin (Saito et al., 2005). Although those saltatory movements have been described in different plant species (Sack et al., 1986; Saito et al., 2005), not much is known about them. However, it is hypothesized that they are mediated by cytoplasmic streaming (Morita, 2010).

Although other plastids play crucial roles in the plant's homeostasis, not much is known about their movement. Especially for other root plastids besides gravity-sensing amyloplasts, information about their dynamics is lacking. Light-induced movement regulation mediating chloroplast movement seems unlikely since no light is present in the roots and one key mediator of the chloroplast movement, CHUP1, is barely expressed in root cells (Oikawa et al., 2003). Since chloroplasts and root amyloplasts exhibit special forms of organellar transport, which are rather exceptional compared to the actin-myosin or cytoplasmic streaming-mediated movement of other organelles described previously (Figure 2), other plastid types could possess other, new mechanisms of organellar movement. The frequent formation of stromules at plastids hints at a dynamic movement and communication system for these organelles.

1.3 Regulation of the plastidal dynamics

1.3.1 Organelle-organelle interaction of plastids

As previously stated, plastids are integrated into a variety of metabolic pathways in the plant cell. These metabolic interdependencies create the need for the exchange of metabolites and reactants with the cellular surrounding, or other organelles. For example, during photorespiration metabolic intermediates are transported in-between chloroplasts, peroxisomes, and mitochondria (Bauwe et al., 2010) while during lipid synthesis, fatty acids and lipids need to be exchanged between the plastid and the ER (Harwood, 1996). Close contact that ensures proper communication and metabolite exchange between the involved organelles can be premised as a key element in these organellar interactions and the metabolic pathways. Those organellar interactions occur normally at so-called membrane contact sites at which the membranes of interacting organelles are within a range of 10-30 nm from each other (Perico & Sparkes, 2018). In mammals and yeast, the tight interaction of organelles at membrane contact sites has been proven to facilitate the exchange of lipids and calcium and thereby displayed a great influence on the positioning of the organelle (Prinz, 2014). Although information about organellar contacts in plants is limited, close contact of plastids with other organelles could be observed by electron and fluorescence microscopy. Microscopic evaluation of membrane contact sites can only be preliminary because those contact sites could also be created by chance, but in terms of plastids, the molecular evidence is expanding that those contact sites fulfill specific functions (Pérez-Sancho et al., 2016). As with most research regarding plastids, most investigations focused on the interactions of chloroplasts with other organelles. For many organellar interactions of chloroplasts, photosynthesis is the causing factor. Since all plastid types perform different tasks that are crucial for plant homeostasis and which are dependent on organellar intermediate exchange, other organellar interactions are possible. The following will discuss described organelle-organelle interactions of plastids disregarding their subtype. A key element in the organelle-organelle interaction of plastids are stromules. As previously stated (1.2.2), those membrane perturbations enlarge the plastid's surface and although their functions are still not elucidated, it is assumed, that they are engaged in a variety of organellar interactions.

Organellar interactions between the ER and plastids have often been described in electron (McLean Whatley, and Juniper 1988; Renaudin and Capdepon 1977; Whatley, McLean, and Juniper 1991) and fluorescence microscopic studies (Hanson and Köhler 2001; Schattat et al. 2011). The fact that during chloroplast purification, fractions of the ER are co-purified also supports a functional interaction of both organelles (Andersson et al., 2007). Additionally, the elongation of stromules has been described to happen alongside ER tubules which led to the hypothesis, that contact sites between stromule and ER guide the stromule dynamic (M.Schattat et al. 2011; M. H. Schattat and Klösgen 2011). A functional basis for the membrane contact sites of plastids and ER could be found in the lipid synthesis of plants. While the *de novo* fatty acid synthesis is carried out exclusively in the plastid envelope, the processing of lipids to phospholipids is shared between the plastid and the ER (Harwood, 1996; Joyard et al., 2010). It is believed that the transfer of lipids occurs via a nonvesicular pathway at membrane contact sites (Block & Jouhet, 2015). However, the proteins involved in lipid transport at membrane contact sites are not elucidated so far. The candidates that are believed to execute the lipid transfer are the Trigalactosyldiacylglycerol (TGD) complex which is located in the outer and inner envelope of the plastid (Hurlock et al., 2014), and the long-

chain acyl-CoA synthetases 4 and 9 (LACS4, LACS9) (Jessen et al., 2015). LACS4 is located at the ER membrane, whereas LACS9 is targeted to the outer envelope of the plastid (Jessen et al., 2015). Additionally, a lipid flippase Ala10, a member of the P4-ATPase family located in the ER could eventually play a role in lipid exchange between plastid and ER (Botella et al., 2016). Evidence exists that all three components could mediate the lipid transfer between plastid and ER at least partially, but until now no direct proof could be found (Mueller-Schuessele & Michaud, 2018).

Interactions between plastids and mitochondria have been described by light (Barton et al., 2018) and by electron microscopy (Jouhet et al., 2004; Lütz & Engel, 2007). The interaction of chloroplasts and mitochondria is not surprising, since both play key roles in the energy metabolism of the plant. Aside, mitochondria are involved in the liquidation of excess reducing equivalents that accumulate at the plastid during photosynthesis at high light conditions that would otherwise lead to photoinhibition and damage of the organelle (Noguchi & Yoshida, 2008). However, it is not clear if the exchange of reducing agents happens through membrane contact sites or via diffusion through the cytosol (Mueller-Schuessele & Michaud, 2018). Besides energy metabolism, also lipid transfer could be provided by organellar interactions between plastids and mitochondria. The envelopes of mitochondria are predominantly composed of phospholipids (Jouhet et al., 2004). Under phosphate starvation, the lipid composition of mitochondria, the tonoplast, and the plasma membrane change drastically, and phospholipids get degraded to use the free phosphate for the maintenance of crucial cellular functions (Jouhet et al., 2003). To maintain membrane integrity of the organelles, the plant incorporates high levels of digalactosyldiacylglycerol (DGDG) (Jouhet et al., 2004). DGDG is synthesized in the plastid envelope (Harwood, 1996) and it was reported that the number of membrane contact sites between plastids and mitochondria increased by the number of three upon phosphate starvation (Jouhet et al., 2004). Successively a mitochondrial transmembrane lipoprotein complex (MTL) was identified, which contains transmembrane proteins localized in the outer and inner membrane of mitochondria, but also comprises other proteins localized in extramitochondrial compartments like plastids (Michaud et al., 2016). A key protein AtMic60 was identified that is proposed to mediate the import of galactoglycerolipids and the export of phospholipids during phosphate starvation (Michaud et al., 2016). Although the plastidal proteins that are involved in the exchange process are not known up to now, the Outer Envelope Proteins 7 and 24 (OEP7, OEP24) are highly abundant in the MTL complex and could mediate the lipid transfer (Michaud et al., 2016).

During photosynthesis the oxygenase activity of Ribulose-1,5-bisphosphate-carboxylase/-oxygenase (RuBisCo) generates phosphoglycerate. Phosphoglycerate is a toxic compound for the plant and needs to be recycled to 3-phophoglycerate, which can be introduced in the Calvin Cycle (Bauwe et al., 2010). This reaction, called photorespiration, is mediated by eight core enzymes that are distributed across the chloroplast, the peroxisome, and the mitochondria (Bauwe et al., 2010). The distribution of those enzymes creates the need for interaction and metabolite exchange between all three organelles. Consequently, proximity between all three organelles was demonstrated by electron microscopy (Frederick et al., 1975) and the *in vivo* interaction between chloroplasts and peroxisomes was shown as well (Gao et al., 2016; Oikawa et al., 2015). Additionally, those interactions were shown to be dependent on light exposure and required photosynthesis, but not photorespiration, photoreceptors, or actin filaments (Oikawa et al., 2015). Similar results were shown for the interaction of mitochondria, chloroplasts, and peroxisomes

(Oikawa et al., 2015). However, experimental evidence of direct organellar contact that enhances the rate of metabolic exchange between those three organelles is still not available. In terms of plastid-peroxisome contact sites a potential interacting protein, Pex10, was identified, which is targeted to the peroxisome membrane and forms a complex with Pex2 and Pex12 (Reumann & Bartel, 2016). *pex10* mutants displayed altered peroxisome morphology and reduced association of peroxisomes and chloroplasts (Prestele et al., 2010; Schumann et al., 2007). However further investigations are needed to understand the complex metabolite exchange between chloroplasts, peroxisomes, and mitochondria during photorespiration.

Plastid-nucleus interaction has often been described under various conditions (Barton et al. 2018; Caplan et al. 2015; Erickson, Kantek, and Schattat 2017). Since the plastid possesses its own genome, which encodes only for a very small portion of proteins needed for a proper organellar function, the protein import of nuclear encoded proteins rises the need for proximity between both organelles (Soll & Schleiff, 2004). Additionally, during stress situations, proper retrograde signaling from the plastid to the nucleus needs to be ensured for a quick translation of stress signals into altered protein expression (Dietz et al., 2016). A key function in the communication between plastids and nuclei is thought to be mediated by stromules. In the upper epidermal cells of *Arabidopsis thaliana* most plastids are localized within 8 µm from the nucleus (Erickson, Kantek, and Schattat 2017). At these plastids, the amount of stromules pointing to the nucleus is increased compared to other plastids in the cell (Erickson, Kantek, and Schattat 2017). Stromules are believed to strengthen the communication between the plastid and the nucleus. The number of stromules interacting with the nucleus can be increased during the plant's immune response (Caplan et al., 2015; Kumar et al., 2018). Those interactions are believed to transport immune signals like the defense protein N receptor interacting protein 1 (NRIP) which is considered a pro-defense signal for plants or the defense transmitter H_2O_2 (Caplan et al., 2008; Higa, Suetsugu, Kong, et al., 2014; Suetsugu et al., 2015). Direct H_2O_2 transfer was measured from chloroplast to nuclei demonstrating the functional interaction between those two organelles in reactive oxygen species (ROS) signaling. Additionally, during high light conditions, nuclei undergo a light avoidance reaction, similar to chloroplasts. (Higa, Suetsugu, Kong, et al., 2014). Mutations in the key protein mediating chloroplast photo relocation, CHUP1, do not only suppress chloroplast photo relocation, but also the relocation of the nucleus (Higa, Suetsugu, Kong, et al., 2014; Suetsugu et al., 2015). Those results hint at a close relationship between plastids and nuclei with a shared basis underlying their transport.

Although direct contact sites between plastids and other organelles have been reported and some functional interactions have been demonstrated, the mechanisms that mediate and regulate those membrane contact sites, and metabolite exchange remain poorly understood. However, direct organellar interaction at membrane contact sites seems to be crucial for the plant. Although they could not be shown explicitly until now, it is believed that stromules play a key role in forming membrane contact sites with other organelles.

1.3.2 Principles of the stromule formation

Even though the dynamics of stromules have been studied extensively, the molecular mechanisms of the stromule formation are not elucidated so far. Two hypotheses of the stromule formation exist. The first proposes a mechanism in which external force from outside the plastid body is delivered punctually to the membrane and pulls out the tubular formation. The second discusses an intrinsic mechanism, in which variations of outward pressure of the chloroplast in combination with internal membrane deformations or a supporting structure at the membrane are responsible for tubulation (Hanson & Hines, 2018). Also, internal variations in lipid composition could lead to membrane deformation and tubulation (Hanson & Hines, 2018). *In vitro* experiments on lipid bilayers showed that tubular structures can be induced by either short peptides (Domanov & Kinnunen, 2006) or protein crowding (Stachowiak et al., 2010). Alterations in the plastidal membrane caused by the overexpression of the outer envelope proteins AtLACS9 (Breuers et al., 2012), OEP7 or the transmembrane domain of CHUP1 (Machettira et al., 2012) were able to introduce tubulation not just from the outer, but also the inner envelope at chloroplasts *in vivo*. These findings led to the new assumption that stromules might serve as a storage site for proteins of the outer envelope (Machettira et al., 2012). It is also discussed if stromules are a relic of defective chloroplast division since stromule appearance is enhanced in *arc3*, *arc5,* and *arc6* mutants (Holzinger et al., 2008), as well as in *atminE1* mutants (M. T. Fujiwara et al., 2015). All proteins are regulators in the chloroplast division. Newer results of *in vitro* stromule formation on isolated chloroplasts highlighted the fact, that stromules could also be induced without the support of cytoskeletal elements (Brunkard et al., 2016; Ho & Theg, 2016). Especially the observation that isolated chloroplasts formed stromules upon the addition of cellular extract drew attention to the topic of stromule formation (Ho & Theg, 2016).

While the mechanisms of stromule formation are still speculative, some physical restrictions underlie the general concept of membrane tubulation and two general requirements must be fulfilled for membrane protuberances to form. Firstly, the plastid needs to have an excess amount of membrane that can be formed into tubular structures. Experiments on *msl2* and *msl3* mutants, both involved in osmoregulation of the plastid, show uncontrolled water influx into the plastid, resulting in an inflated, balloon-like shape of the organelle accompanied by the loss of stromule formation (Haswell & Meyerowitz, 2006; Veley et al., 2012). Additionally, *in vitro* experiments on vesicles have demonstrated, that tubular structures extend to a point at which tension is delivered on the whole membrane and inhibits further tubulation (Kantsler et al., 2008). Theoretical approaches underline those findings. Different modeling approaches resulted in the findings that the ratio of membrane to volume of the organelle is a key element in the formation of tubular structures (Bahrami & Hummer, 2017; Maike Jung, 2021). However, a strict reduction of the volume by keeping the area of the membrane constant resulted in worm-like tubules (Bahrami & Hummer, 2017). The introduction of tubular structures to spheroid organelles needed either a constant core shape or external factors stabilizing the membrane (Bahrami & Hummer, 2017).

This leads to the second requirement for membrane tubulation. Forces, whether intrinsic or extrinsic must work on the membrane for it to bend (Erickson & Schattat, 2018). General concepts have been developed so far to describe how membrane curvature could be introduced to a membrane. To shape the membrane in a tubular form, very specific forces are needed (for additional information see McMahon & Boucrot, 2015). Theoretically, polymerization of the internal cytoskeleton pushing the envelope from the inside can

form tubular structures. Membrane restructuring was observed at vesicles *in vitro* (Cortese et al., 1989; Fygenson et al., 1997), which shows the principal functionality of the idea, but no evidence was found to support this hypothesis *in vivo*. More so, *in vivo* data of the versatile stromule dynamics disprove this theoretical approach since the speed of internal assembly of cytoskeletal structures would not match the speed of reshaping stromules *in vivo* (Gunning, 2005). Membrane curvature mediated by protein insertion was described previously (Machettira et al., 2012), but the dynamics of stromules that can act on the level of seconds dismisses this as the main cause for stromule formation *in vivo*. The accumulation of proteins in the outer envelope takes up hours and days of time which is far too much to explain *in vivo* stromule dynamics.

Polymerization of membrane-associated proteins at the outer envelope has been described various times in the context of membrane curvature. Bar domain proteins possess a crescent shape and are known to be involved in membrane curvature by association and self-polymerization at the membrane (Mim & Unger, 2012; Rao & Haucke, 2011). Also, the self-assembly of spiral-shaped dynamin, a GTPase involved in receptor-mediated endocytosis (Sweitzer & Hinshaw, 1998), was proposed to be involved in plastidal tubulation. However, experimental evidence shows that those proteins are more likely to be involved in vesiculation than in dynamic tubulation (Boucrot et al., 2012; Erickson & Schattat, 2018; McMahon & Boucrot, 2015; Sweitzer & Hinshaw, 1998). Also the reconstruction of membrane internal lipids mediated by cytosolic protein factors could be involved in tubulation (McMahon & Boucrot, 2015). No explicit evidence exists that these mechanisms are involved in stromule formation, but the latest results of *in vitro* stromule induction on isolated chloroplasts are in favor of comparable mechanisms (Ho & Theg, 2016). At least the mechanism of motor proteins associated with the outer envelope pulling the membrane while moving across cytoskeletal filaments would generate enough force for membrane tubulation (Erickson & Schattat, 2018). Experimental evidence strongly supports that these mechanisms are involved in stromule formation (Holzinger et al., 2007; Kwok & Hanson, 2003, 2004a; Natesan et al., 2009). The manner of cytoskeleton involvement in stromule formation and dynamics is discussed intensively. While direct interaction of myosin motor proteins and stromules has been suggested in favor of the pulling theory (Erickson et al., 2018; Hanson & Sattarzadeh, 2011; Natesan et al., 2009) and the stromule extension speed was comparable to those of myosin XI movement speeds *in vitro* with a maximum velocity of 0.5 µm/sec (Erickson et al., 2018), the extension of stromule tips could not be solely associated with the colocalization of actin (Kumar et al., 2018). In addition, microtubules were shown to be associated with stromule extension, kinking, and branching. By depolymerization of microtubules shrinking of chloroplast stromules was observed, while stabilizing of microtubules favored the stromule formation (Erickson et al., 2018; Kumar et al., 2018). The mechanisms of stromule formation seem to be very versatile and are likely to be mediated by more than just one factor. Altogether the findings of stromule formation and dynamics highlight the functional relevance of stromules in the cellular context. However, more research is needed for a complete understanding of stromule formation.

1.3.3 Salt and drought stress in plants

Due to their sessile lifestyle, plants must cope with abiotic stresses like heat, cold, salinity or drought stress. Those stresses often are faced simultaneously and introduce similar damages to the plant. Therefore, the plant's signaling pathways and coping mechanisms can be very alike. Salt and drought stress are both osmotic stresses for the plant, triggering similar responses (Ahluwalia et al., 2021). The exact mechanisms of the signal transductions and stress responses is not deciphered up to date, but the effects of those two stresses on the plant should be very briefly summarized in the following. Both stresses are sensed by the root (Bijalwan et al., 2022; Zhao et al., 2021), and besides that, have much in common.

Salt stress has many effects on the plant. The salt concentration of the soil limits the water uptake of the plant and thereby influences the nutrients absorbed by the plant (Gong, 2021). Lack of nutrients and water results in osmotic and ionic stress, which induces several physiological and molecular changes leading to reduced plant growth, photosynthesis, and cell division (van Zelm et al., 2020; Zhu, 2002). Additionally, the sugar signaling involving sucrose, fructose, and glycolysis is hampered during salt stress (Shumilina et al., 2019). The salt stress response mechanism in plants is carried out at several levels and involves many regulatory elements. Some of them are phytohormones, lipids, the cell wall, or the cytoskeleton (Gong, 2021; van Zelm et al., 2020; Zhu, 2002). The focus of the plant's response is keeping the Na^+ concentration in the cell at a low level. Na^+/H^+ antiporters in the plasma membrane and the vacuolar membrane transport Na^+ into the vacuole or the apoplast (Zhu, 2002). The regulation of those transporters is one key aspect of the cellular response to high salt concentrations (Zhao et al., 2021). Salt stress also induces osmotic stress resulting in turgor pressure leading to damage to the plasma membrane and alterations at the cell wall (Park et al., 2016). To counteract the osmotic pressure, the plant stores osmolytes like proline, polyols, and sugars (Zhao et al., 2021). In response to the variations within the cell during salt stress, the cytoskeletal architecture is reorganized (Lian et al., 2021; Q. Zhang et al., 2012). The cytoskeleton is involved in different aspects of salt stress defense and acts as a mediator for calcium and ROS signaling during salt stress (S. G. Liu et al., 2012; Qian & Xiang, 2019).
Like salt stress, drought stress is accompanied with osmotic pressure for the plant, leading to similar problems the plant must face, resulting in similar solutions. The plant's main aspect during drought stress is to prohibit water loss by closing of the stomata, regulated by abscisic acid (ABA) (Cutler et al., 2010; Nakashima et al., 2014). Besides, maintenance of the osmotic potential of the cytosol is a key regulatory mechanism of the plants in response to drought stress (Ahluwalia et al., 2021). Osmolytes are stored in the cytoplasm to prevent loss of water (Bijalwan et al., 2022). Also, the accumulation of signal molecules as ABA and Ca^{2+} are produced to regulate the stress response (Bijalwan et al., 2022). The outcome of the stress response is a reduced growth and an increased proportion of the root compared to the shoot to minimize water loss, while maximizing water uptake (Ahluwalia et al., 2021).
For both stresses, the main aspect for the plant is the osmotic stress and damage. Those effects are accompanied by usual problems of abiotic stress, like potential protein, lipid and DNA damage that can occur as a consequence of the production of reactive oxygen species (Bijalwan et al., 2022; Gong, 2021; Zhao et al., 2021). Neither effects on the organellar trafficking, nor contributions of organellar trafficking during salt or drought stress are described. Since plastids are involved in a variety of cellular functions (Rolland et al., 2018), those could be affected and the positioning and transport of plastids in the cell could be drastically influenced by both stresses.

1.4 Objectives of the study

Plastids carry out several vital functions in the plant cell (Rolland et al., 2018). Although chloroplasts make up only a fraction of the total pool of plastids in plants, investigations in the last decades focused on their characterization and their role in the context of the plant cell. With increasing amount of information about chloroplast dynamics, which are greatly influenced by photosynthesis, it became obvious that functional mechanisms cannot be transferred to other plastid types. During the last years, research began to focus also on the investigations of other plastid types, however, besides plastids in the root tips mediating the plant's gravitropism, other members of the plastid family were barely touched by those efforts.

The plastid population in the plant's root is versatile and often referred to as leucoplasts. Their specific-, as well as their general functions in the cellular metabolism remain crucial for the cell. The most common population of plastids in the roots are amyloplasts, which act as carbon storage sites. Root plastids are known for the frequent formation of stromules, their proposed function as pure storage bodies seems to be far-fetched (1.2.2, 1.3.2). The molecular mechanisms driving chloroplast movement are broadly deciphered by now. This is not true for the mechanisms driving plastidal motions (1.2.3). Since their dynamics do not seem to be regulated by the key protein that drives chloroplast movement, CHUP1, this study focused on a deep characterization of the movement patterns of root plastids to gather information about potential molecular mechanisms driving their motion including the formation of stromules and their participation in the plastid dynamic.

To generate sufficient data for a deep characterization of the plastidal motion to obtain information about molecular mechanisms driving them, an automated segmentation and tracking approach of fluorescently labeled plastids was established based on 4D light sheet-based fluorescence recordings. The pipeline should be usable in a high throughput approach to process high amounts of image data for the generation of a wide data basis that covers the broad spectrum of potential plastid dynamics. For future studies, this pipeline should be able to process image data containing differently labeled organelles to perform organellar interaction studies in a 4D surrounding to deepen the information about organellar interaction in the cellular context. Since the knowledge about plastidal dynamics is very limited up to now (1.2.3) different abiotic stress conditions were applied during light sheet-based fluorescence microcopy and the influence on the plastidal dynamic was determined. Since the plastidal functions are well interconnected in the cell (1.2.1) these results gave further information about the regulation of the plastidal movement and the underlying molecular mechanisms. In addition, deep characterization of the plastidal movement patterns was executed using the generated image sets. The analysis included the dynamics of stromules, which are preferentially formed by root plastids. Different functions of stromules were proposed in the last decades and most of them target organelle interaction (1.2.2). This study focused on the question of whether stromules are able to mediate plastidal movements and if so, in which manner they contribute to the plastidal dynamics and potential organellar interaction. The characterization of plastids and stromules led to a deeper understanding of the function of the tubular structures in the cellular context and gave insights into general molecular mechanisms underlying the stromule formation.

Additionally to the tracking analysis of plastids and stromules, an *in vitro* approach was followed to get insights into the molecular mechanisms contributing to the formation of stromules. In recent findings, it

was demonstrated that stromules can be introduced *in vitro* by the addition of concentrated cell extract (Ho & Theg, 2016). These findings created new possibilities for scientists investigating the mechanisms of stromule formation, since stromules are formed with the help of external mechanisms. Those results should be used as a basis to find potential interaction partners that contribute to the formation of stromules. Additional experiments were performed to deepen the understanding of the phenomenon of stromule formation and were combined with a fractionation pipeline to limit the number of potential candidates that mediate stromule formation. The fractionation led to an analysis with the aim to find potential factors that contribute to the formation of stromules.

2 Materials and methods

2.1 Plant material

Wilt-type plant lines utilized during this study were *Arabidopsis thaliana* ecotype Columbia 0 (Col-0) and *Pisum sativum.* T-DNA Insertion line of *Arabidopsis thaliana* constitutively expressing GFP fused to the transit peptide of the small subunit of RUBISCO (tpssu-GFP) that was used during light-sheet-based fluorescence microscopy, was generated by Daniela Bublak (Table 1). Pea used for chloroplast isolation and full protein extract of the leaves and roots were grown under greenhouse conditions for seven to eight days at 12 hours light and 22 °C and 12 houes dark and 18 °C. *A. thaliana* used for isolation of protein for mass spectrometric analysis were grown on sterile ½ MS plates at 16 h light (120 µmol/m^2/sec) at 22 °C and 8 hours dark at 18 °C.

Table 1 Mutant plants utilized in the study.

Name	Host line	Mutagenesis	Lab ID	Reference
wt:tpSSU-GFP	Col-0	T-DNA insertion	S01-49	Daniela Bublak, unpublished

2.2 Establishment of a 4D plastid tracking pipeline

2.2.1 Sample preparation for light sheet-based fluorescence microscopy

The automated tracking of organellar movement is a difficult task to perform and needs very specific adjustments. This study aimed for tracking of plastids in the root of *Arabidopsis thaliana*. In specific, a workflow and an analysis pipeline should be established to automatically track the movement of plastid bodies in a 3D environment over time. Given, that plastids in the roots form stromules on a very frequent basis (Natesan et al., 2005), the effect of stromules on the automated analysis should be kept to a minimum.

Since this study aimed for organellar visualization in close to natural conditions light sheet-based microscopy (LSFM) was the microscopic method of choice. Light sheet-based fluorescence microscopy reduces phototoxic effect introduced into the sample to a minimum and therefore is often used during developmental studies (Stelzer, 2014). For light sheet-based fluorescence microscopy only *Arabidopsis thaliana* T-DNA insertion line wt:tpSSU-GFP was used. Before utilization, seeds were surface sterilized for 1 minute with 15 % (v/v) sodium hypochlorite solution, followed by two steps of treatment with 70 % (v/v) ethanol for 1 minute. Sterilized seeds were subsequently washed four times with freshly autoclaved ddH_2O, before the seeds were stored in ddH2O at 4°C in the dark for 48-72 hours to synchronize germination.

To mimic natural conditions, the plants were grown and imaged in a solidified medium filled in glass capillaries (3mm in diameter, 20 mm in height) supported by a carbon rod (0.28 mm in diameter, 30 mm in height) (both kindly provided by the Stelzer lab) (Figure 4). Prior to application, both materials were cleaned in an ultrasound unit with water and then autoclaved, following a minimum of 72 hours at 37 °C for evaporation to remove any excess water that was collected in the glass capillaries during autoclaving. As a sample holder, the cut top parts of 15 ml falcon tubes were used. Tubes were cut 4 cm above the lid and a cut top part of a 10 µl pipet with an approximate diameter of 3 mm was glued into the lid as the holder for the glass cuvette. The assembled sample holder was sterilized before use for 5 minutes with 15 % (v/v) sodium hypochlorite following 30 minutes of treatment with 70 % (v/v) ethanol and 4 wash steps with freshly autoclaved ddH_2O. Medium used for the LSFM sample preparation was ½ strength Murashige and Skoog Medium (MS-Medium) (Murashige and Skoog. 1962) containing 2.3 % (w/v) MS salts (Duchefa Biochemie) and 0.97 % (w/v) 2-(*N*-morpholino)ethanesulfonic acid (MES) solidified with 0.5 % (w/v) Phytagel (Sigma-Aldrich), and supplemented with either 1 % (w/v) sucrose (control condition), 1 % (w/v) sucrose and 0. 1 M NaCl (0.1 M NaCl condition), 1 % Sucrose and 5 % PEG 4000 (5 % PEG condition) or was used without further supplements (½ MS-Sucrose condition). Following medium preparation, the medium was autoclaved and stored at room temperature until usage. Prior to usage, media were liquefied by microwaving for several minutes at 700 W.

The use of solidified medium was accompanied by the disadvantage that the excitation and emission light had to pass through the medium. The optical density of the medium as well as the root led to light scattering. The deeper the root was embedded into the medium, the more light scattering was observed. As a result, the level of detail in the recorded images decreased. For the analysis of the organellar movement and more so for the investigation of the stromule dynamics, a very high picture quality was premised. Therefore, the samples needed to be generated in a very specific manner:

Sample preparation for light sheet-based fluorescence microscopy imaging was performed following a sample holder technique proposed by Daniel von Wangenheim (von Wangenheim, 2014). In this procedure, the root was forced to grow at the inner wall of the capillaries by tilting the sample holder at 45 ° thereby minimizing light scattering during image acquisition (Figure 4). In short: Glass cuvettes were placed in a 96-well plate which was tilted at 45 °. A carbon rod was placed for support of the medium in the cuvettes and liquefied medium was pipetted into each cuvette. After hardening of the medium, cuvettes were transferred into the falcon tube sample holder. One seed was placed on the medium of each cuvette. The sample holder was filled with sterile liquid medium matching the solidified medium minus the supplementation of Phytagel. The sample holders were sealed with fresh Parafilm (noeLab) and were placed onto a 12-well plate. The plate was tilted at a 45 ° angle to promote root growth against the inner wall of the glass cuvette. Plants were grown under long-day conditions (14 hours light with 120 µmol/m^2/s at 22 °C, 10 hours dark at 18 °C) for 10 days until imaging.

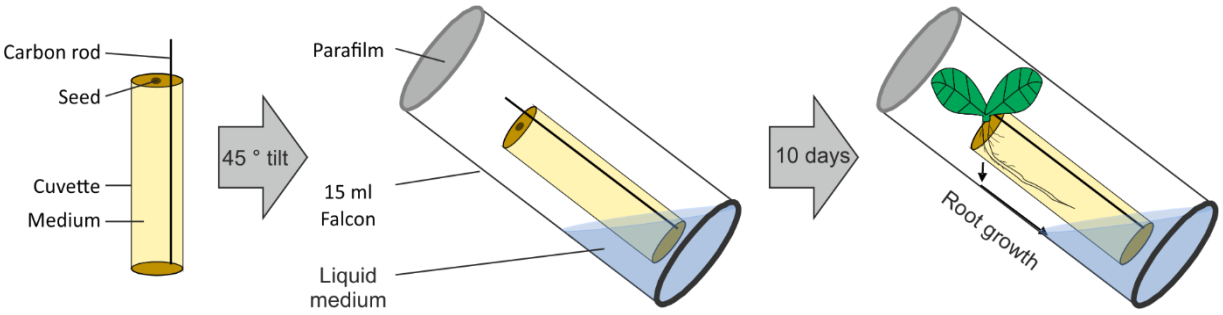

Figure 4 Schematic display of plant sample preparations for light sheet-based microscopy. To reduce the light scattering effects of the medium during image acquisition, the root of the plant was forced to grow at the inner wall of a sample holder glass cuvette. The glass cuvette was filled with solidified medium, which was supported by a carbon rod. The seed was placed on top of the cuvette. The cuvette was placed in a cut 15 ml falcon that was partially filled with liquid medium, sealed with Parafilm, and tilted at a 45 ° angle. The tilt forced the root to grow at the inner wall of the cuvette instead of its center.

2.2.2 Light sheet-based fluorescence microscopy

Light sheet-based microscopy is a technological term, which is used to describe the fact, that the sample is illuminated by a thin sheet of light. In this study, a monolithic digital scanning light sheet microscope (mDSLM) was utilized which forms the light sheet by scanning a focused laser beam up and down. The aperture is an improved version of the DSLM described by Keller et al. (2010). This version differs from the described one in having all optical parts built in a single block of aluminum. For the illumination, an EC Plan Neofluar 5x/0.16 air (Zeiss) was used and combined with a WN Achroplan 40x/0.75 W (Zeiss) as a detecting objective. GFP was excited by a laser diode at 488 nm and detected between 500 and 550 nm utilizing a bandpass filter 525/47. The data was acquired by an EMCCD Andor Clara Camera. Plants were illuminated by a minimal laser power between 5-10 mW, depending on the signal intensity of the sample, and an exposure time of 20 ms to keep the light-induced damage to a minimum (for a detailed setup of the mDLSM that was utilized during this work see Keller et al., 2010; von Wangenheim, 2014). The combination of the detection objective and EMCCD camera gave a display window of 224.46 µm x 168.7 µm that is composed of 1392 x 1040 pixels. This setup resulted in one pixel covering a length of 0.16125 nm in each direction.

For illumination, the chamber was filled with a liquid medium matching the solidified medium that was used to culture the plants in the sample holder (2.2.1). The 10 days old *Arabidopsis* plants were pushed out of the capillaries by about 0.2 cm by pressing the capillary onto a MS-Plate containing ½ strength MS media, which was solidified, with 2 % Phytagel, to create a strong bottom for the capillaries. The plants were successively mounted on the sample holder with the roots being exposed to the detecting objective. Successful imaging relied on the stability of the root in the sample holder and the medium. The root was pushed as far out of the capillary that the leaves did not drown in the liquid medium, but no glass remained in the optical path between the detection objective and the root.

The recordings were taken in the differentiation zone of the root (Figure 5 A). They were started at the first signals detectable of the root epidermis. Root hairs were not considered as a starting point for the recordings. The level of detail was considered sufficient if the stromule structure was identifiable.

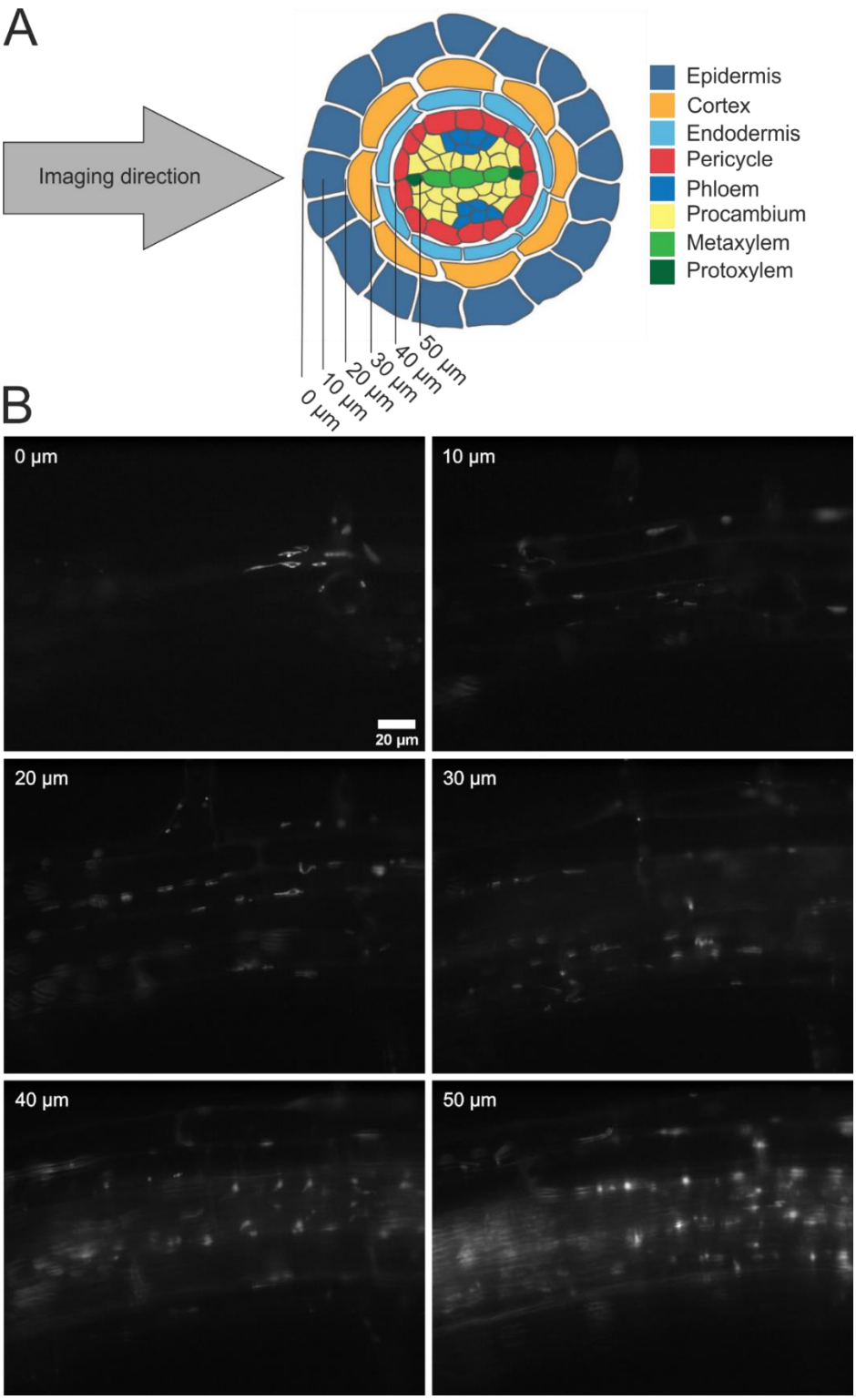

Figure 5 Cross-sectioning of the *Arabidopsis thaliana* root by light sheet microscopy. Using light sheet-based microscopy the *Arabidopsis* root was scanned. A) Schematic cross-sectioning of the differentiation zone in *Arabidopsis thaliana* with the indicated direction of imaging which can be referred to as the Z-axis of the image data. Root hairs are omitted for clarification reasons. Different tissues are colored and named in the legend aside. Schematic sectioning in 10 µm steps is marked. (Adapted from Petricka et al, 2012) B) 50 µm deep imaging scan alongside the Z-axis into the root of *Arabidopsis thaliana* starting with the first visible plastids in the root epidermis. Sectioning that is indicated in A) is applied. The level of detail determined at the plastid structure is decreasing with increasing depth of the root tissue.

To determine the image quality during processing through the root, recordings were taken reaching up to 50 µm in depth along the Z-axis into the root (Figure 5 B). In general, the stromule structure was distinguishable from the background up to a depth of around 30 µm. This strongly depended on the

structure of the root and the amount of media for the emitted light to cross. Different recordings did not comprise similar resolutions but could have many or few levels of detail in different sections of the pictured root (Movie 1-8). Considering this, 31 planes with a 1 µm distance between each layer were chosen as the depth of the detection regime. Generally speaking, this depth covers the first two cell layers of the root in the differentiation zone of *Arabidopsis thaliana* (Figure 5 A). The minimum amount of time needed for the aperture to finish a full detection cycle and start another stack with an exposure time of 20 milliseconds per frame was ≈ 4.3 seconds resulting in 211 frames over 15 minutes. Considering that the maximal velocity for organelles so far detected in *Arabidopsis* is driven by myosin motor proteins and is settled around 7 µm/sec (Tominaga, 2003; Tominaga et al., 2013), the time frame of 4.3 seconds is sufficient to capture such events of the plastidal motion in cells covering ca. 100 µm in length. During image acquisition different numbers of replicates were generated for control conditions, 0.1 M NaCl, 5 % PEG 4000 and ½ MS-Sucrose. These replicates are referred to as image datasets or simply datasets in the following.

The detection regime was chosen to give a good resolution and visualization for the plastids. While the previous section discussed the level of detail gained in the X- and Y-axis of the recordings, the spatial resolution in the Z-axis is crucial for 4D organelle tracking. The Z-resolution in light sheet-based microscopy hardly depends on the adjustments of the sample illumination. In the best case, only the detected plane is illuminated. Here, enhanced by light scattering of the sample, the narrowest point of the illumination still covered a region of a few µm. Therefore, some structures layered on each side of the focal plane were also illuminated and could irradiate into the visualized plane. The Z-resolution showed that single plastids were distinguishable but those possessed an elongation along the Z-axis that was not expected (Figure 6). This prohibited any inference that could be drawn from a correlation between plastid movement and plastid size.

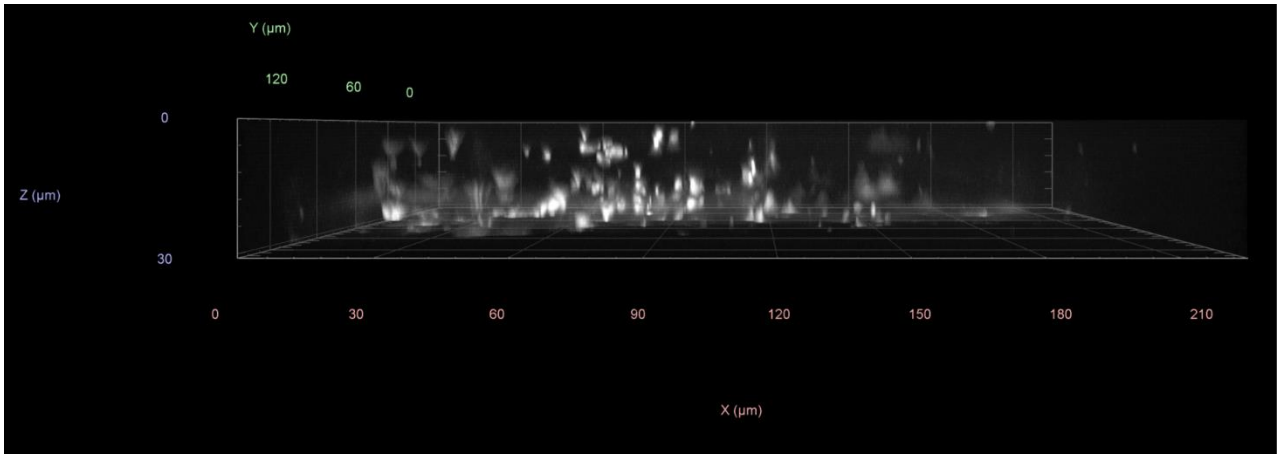

Figure 6 Spatial resolution of the Z-dimension. A 3D visualization of a Z-stack is shown from a side view (for directionality see Figure 5). The dimensions and the orientation of the stack are indicated in µm. The Z-resolution of the plastids is decreased due to the microscopic setup and the light scattering induced by the medium of the sample. Spherical plastid structures are still visible and automated tracking could be performed using the data.

2.2.3 Automated analysis of the plastidal movement

For the automated analysis of the plastidal movement, the program “Arivis Vision 4D” (Version 3.5.0) (Arivis a Zeiss company) was used. Since the software makes use of a very specific .sis data format, the acquired datasets were converted with the help of the software “Arivis Sis Converter” (Version 3.3.0) (Arivis a Zeiss company). The scales for the pixel size of the X- and Y-axes were set to 0.16125 nm, 1 µm was set as a value for Z-sectioning. Arivis Vision 4D is capable of automatic segmentation and tracking. These automated features were necessary to analyze a large number of datasets. To treat every dataset equally, the same analysis conditions were used for each replicate. To achieve this, a pipeline was set up, with the aim of enhancing the picture quality and tracking the movement of the plastid bodies (Figure 7-Figure 11).

Following the loading of a dataset into the program, the selection of the region of interest (ROI) was set. At this option, the whole dataset was selected without exceptions. An initial threshold filter was chosen to enhance the signal-to-noise ratio. The filter aimed to preserve the bright pixels of the dataset and to zero the intensity of all pixels below an intensity value of 50 (Figure 7).

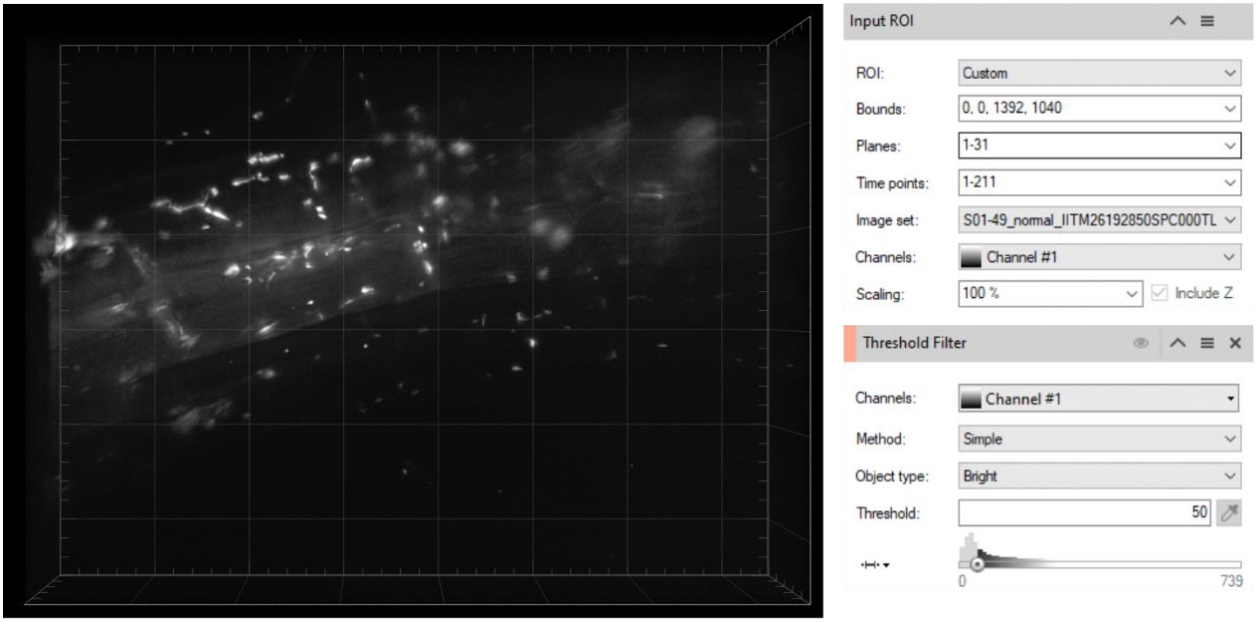

Figure 7 Arivis Vision 4D automated tracking pipeline step 1. The example dataset is loaded into the program, and the resulting visualization is shown from a top view. The initial steps, namely input of the region of interest (ROI) and a threshold filter for reduction of the background were performed. As ROI the whole dataset was considered, the threshold filter was chosen to zero every intensity below a value of 50 and to preserve everything above that threshold. Selected options of each menu are shown.

The resulting image showed a drastic reduction of background and preservation of the bright pixels in the dataset (Figure 8). Most of the plastid structures of bright plastids were preserved, including stromules, which could not be excluded, since they were very bright structures. Very small plastids showing low levels of fluorescence (ca. 1-2 µm in diameter) were also excluded from further analysis by this operation. The

resulting image set was saved internally for further processing. For the segmentation of the plastids, different mechanisms were tested, but the best results were achieved by using the “Blob Finder” option of Arvis Vision 4D. This segmentation method is preferred to find spherical 2D or 3D shapes in a noisy image by its diameter. For this reason, the diameter of the plastids was measured and set generally to 5 µm. The probability threshold which defines how likely a structure is considered a wanted segment was set to 20 %, the split sensitivity, which defined the sensitivity with which nearby structures are split was set to 80 %.

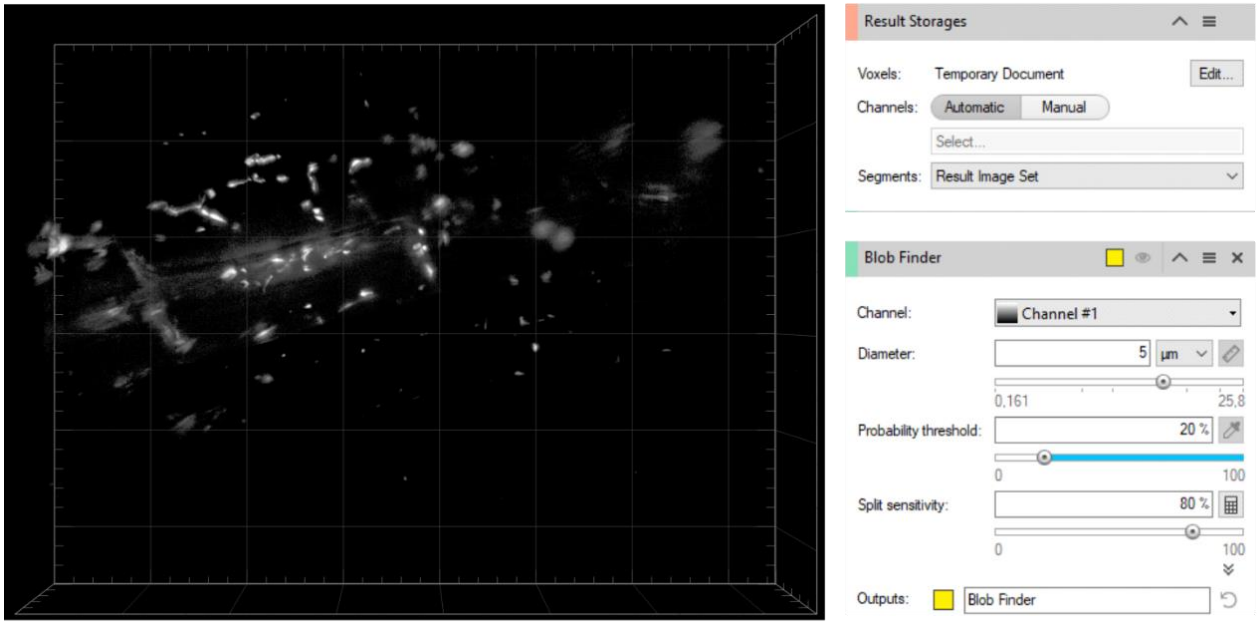

Figure 8 Arivis Vision 4D automated tracking pipeline step 2. The resulting image after running of the threshold filter is shown. The image set was stored internally for further processing and preserved bright parts of the image were segmented using the blob finder option. Selected options of each menu are shown.

The resulting segments (Figure 9) were predominantly plastid bodies but also very bright stromules besides very small objects like the remaining background. Those small objects interfered greatly with the tracking analysis, which considered every available segment. Since background intensities usually changed slightly during the imaging, the appearance of those very small segments was randomized and therefore created false tracks in the tracking analysis. To get rid of those small interfering segments, a segment filter was used to eliminate all objects with a voxel size below 50. A voxel is the equivalent of a pixel in 3D space.

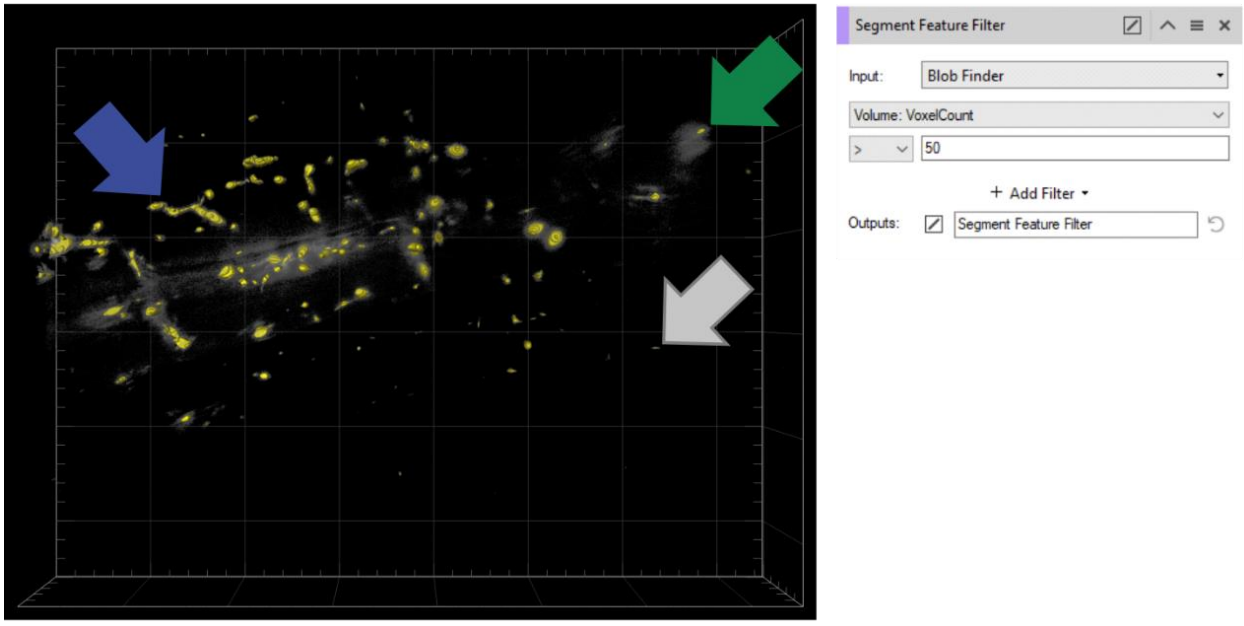

Figure 9 Arivis Vision 4D automated tracking pipeline step 3. A segmented image set resulting from the blob finder option is shown. Computed segments are visualized in a spheric approximation and shown in yellow. Mainly plastid bodies are segmented, but also stromules (blue arrow), background that was not deleted by the threshold filter (green arrow) and small segments, being either very small plastids, or very small remains of background noise (grey arrow). For the deletion of the randomly apparent small segments, a segment feature filter was chosen deleting every segment with a voxel size below 50. Selected options of each menu are shown.

The resulting image (Figure 10) was used as input for the automated tracking algorithm. The parameters for this option were set as followed: Since different motion types from straight movement to wobble motions needed to be investigated, the option “Brownian Motion” was chosen as a parameter for the motion type, which focusses on segments that move predominantly random. As the centroid, the geometric center of the segments was set, no divisions or fusions between tracks were allowed and the maximal time gap in which a segment of a track would not be computed by the algorithm was set to 1 frame.

The tracks computed by the algorithm (Figure 11) were underlaid in different colors for better visualization and traceability. Segments and tracks assigned during the process were saved for further editing.

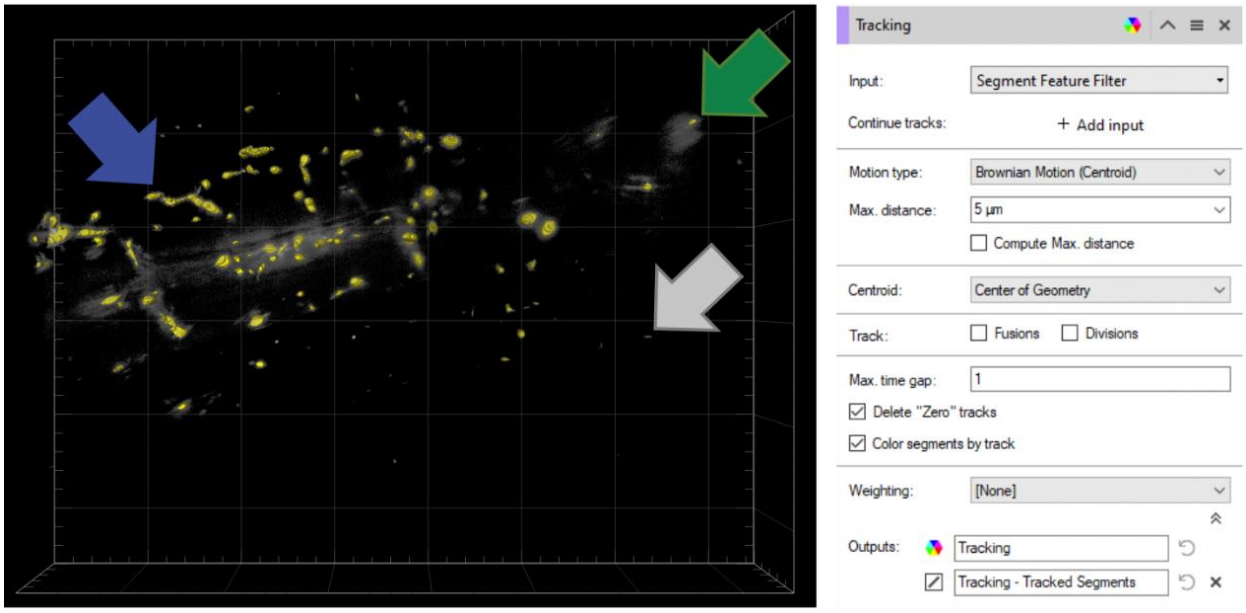

Figure 10 Arivis Vision 4D automated tracking pipeline step 4. The resulting image set after the segment filter was applied. Small segments, like indicated by the grey arrow are deleted, marked by the absence of yellow color displaying a segmentation. Bigger segments were preserved, independently of wrong segmentation displayed by blue and green arrows. The remaining segments were used as input data for the final tracking algorithm. Selected options of each menu are shown.

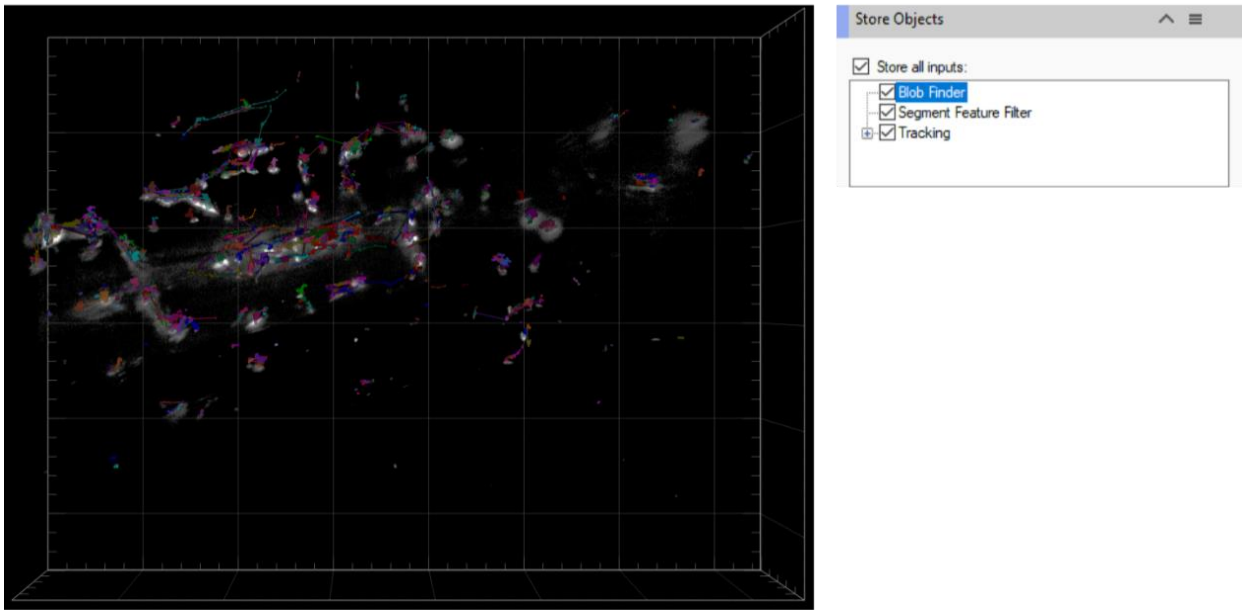

Figure 11 Arivis Vision 4D automated tracking pipeline step 5. Resulting visualization of the tracked segments generated by the automated tracking algorithm. Track lines are drawn between Segments that are attributed to a track. Segments and track lines are colored in the same color. The color set is chosen randomly. All segments and tracks generated during the pipeline were saved for later processing and editing. Selected options of each menu are shown.

2.2.4 From coordinates to movement data

The previously generated data (2.2.3) comprised the X-, Y- and Z-coordinates of the center of geometry calculated from the individual segments and each timepoint in µm. Each segment that was attributed to a track was addressed with a timepoint (which equals the frame in which the segment was identified) and a dedicated track number. Tracks and attributed segments were ordered chronologically. The length of the connecting vectors between two consecutive points were calculated by the formula:

$$\vec{v} = \sqrt{(x_2 - x_1)^2 + (y_2 - y_1)^2 + (z_2 - z_1)^2}$$

The result was divided by 4.3 sec since this was the time between the start of each image stack. The resulting values were displayed in µm/sec. Each movement of a segment between two timepoints was classified as one event. For an overview about the general velocity distribution, all events were classified in groups with increasing velocity ranges. The relative number of events was depicted for each group in relation to the total number of events (Figure 12). The distribution of the movement patterns showed a variety of different velocity events during the image recording. The greatest section of movement events (ca. 80 %) was distributed within movement speed up to 0.1 µm/sec. Another great portion of about 16 % of the classified events showed increased movement events between 0.1 and 0.3 µm/sec. The remaining 4 % of movement events displayed movements greater than 0.3 µm/sec. Generally, most events were classified within 0.02 and 0.03 µm/sec followed by a negatively exponential trend. 0.5 % of all events classified showed the movement of more than 1 µm/sec.

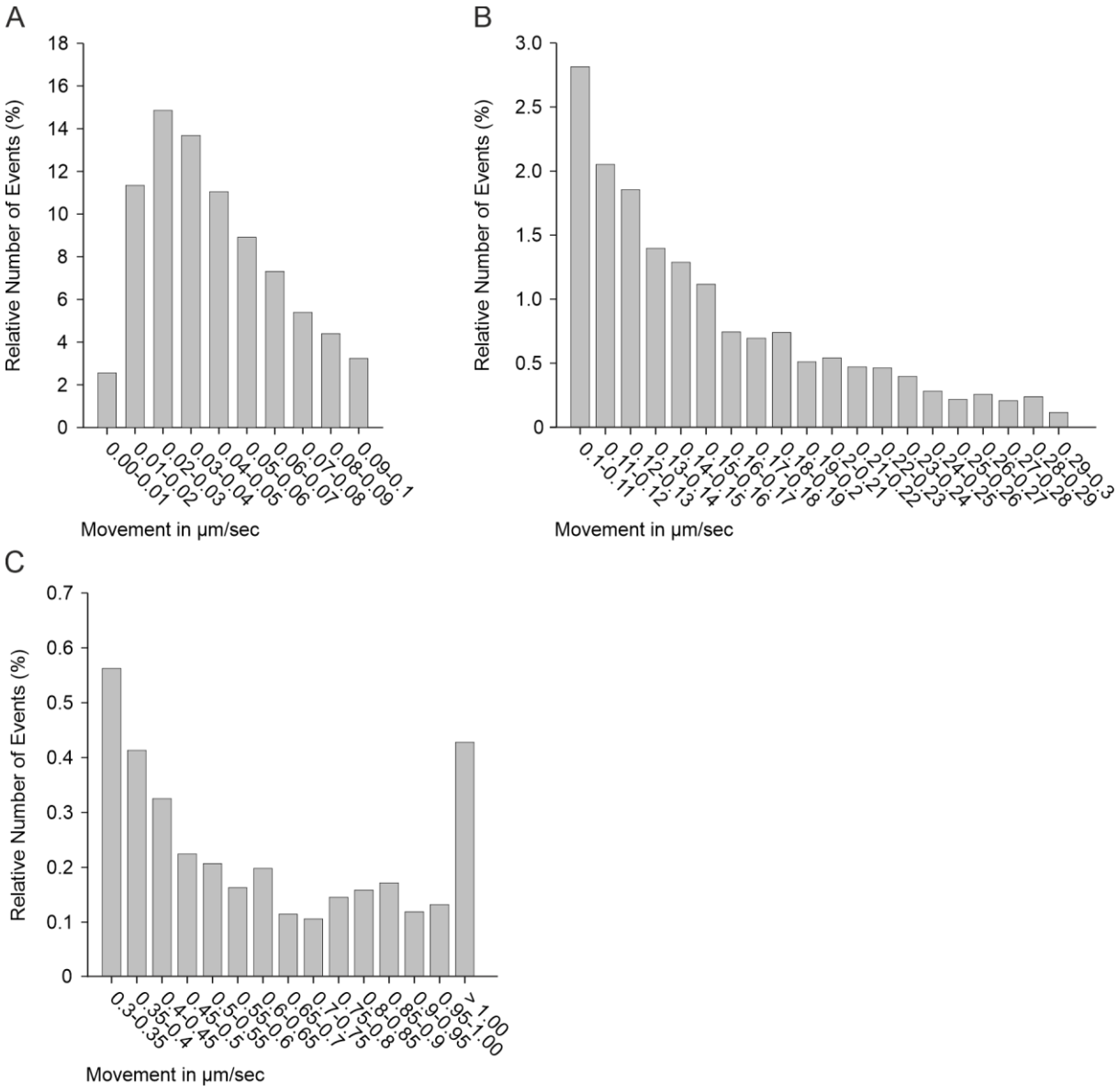

Figure 12 Classification of events of an exemplary dataset. Movement events of segments were classified in different velocity ranges and are shown in in relation to the total amount of events in the image set. The graph is split into three sections for the proper scaling of the Y-axis. Velocity events are shown in A) between 0 and 0.1 µm/sec, B) between 0.1 and 0.3 µm/sec in 0.01 µm/sec steps respectively C) between 0.3 and 1 µm/sec in 0.05 µm/sec steps and all events exceeding 1 µm/sec as a cluster.

2.2.5 Manual data correction

To process a big amount of data and create a comprehensive picture, an automated approach for organelle tracking was needed and established. Besides the upside that much data could be processed in a relatively short amount of time, the automated approach came with some drawbacks. Generally, an automated approach works best within a uniform dataset, in which the tracked segments show low variety in their morphology and motion patterns. The results generated by the automated tracking algorithm of Arivis Vision 4D (Figure 12) showed a comprehensive distribution of movement events.

Nevertheless, taking the visualization of the tracking results into account (Figure 13 A), it displayed a variety of movement events that differed from the underlying image data. These differences greatly became noticeable through large jumps of tracks spanning several micrometers. Those jumps indicated that the automated tracking algorithm was error-prone, and that the data needed to be corrected. Since the original image data was visible under the segmented visualization of Arvisi Vision 4D, the correction of the tracks was performed manually. This action aimed to delete the most abundant wrongly assigned tracks and to rearrange wrongly assigned segments to get a convincing result. For this reason, every track that consisted of only two tracked timepoints was deleted, since these tracks showed to be error-prone and mostly responsible for wrongly assigned large track jumps. Additionally, wrongly assigned segments were reassigned by hand until not comprehensible data points were eliminated (Figure 13 B). It needs to be mentioned that the procedure did not result in error-free track sets, but the proportion of errors was lowered, and the overall data was much more comprehensible.

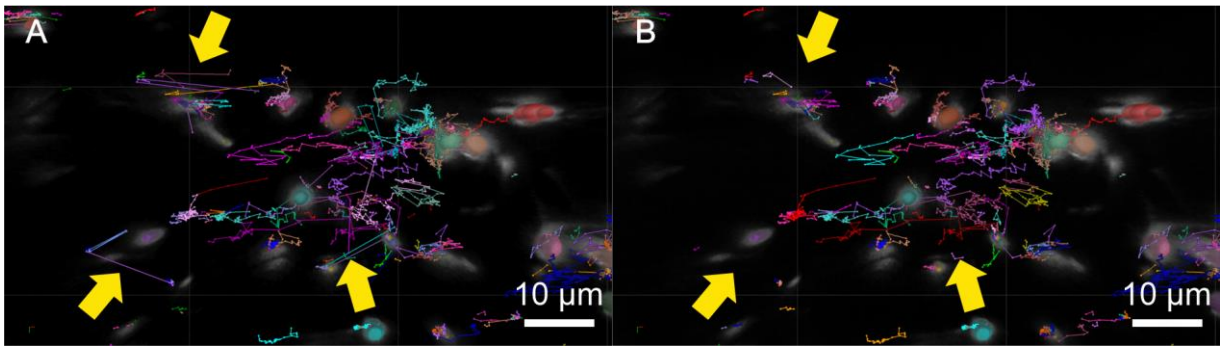

Figure 13 Visual presentation of uncorrected and corrected tracks. The visual 3D presentation of Arivis Vision 4D of tracks in an exemplary image dataset. The scene is shown from a top view. Colored lines are drawn between segments that are assigned to the same track. The same color was attributed to the corresponding segments. The coloring of lines and segments is random and can vary between A and B. The visualization based on image intensity is still seen in white under the visualized segmentation and was used for the correction of the tracking data. A) Presentation after the automated tracking was performed. Yellow arrows indicate areas with a high quantity of unspecific long track jumps of several µm. B) Manual corrected version of A. Yellow arrows indicate the same areas as in A, but the manual correction deleted unspecific tracks. Tracks are much more comprehensible after manual correction.

For a comparison of changes introduced by the correction, the corrected data were categorized the same way as previously described (2.2.4) and compared to the automated, uncorrected results (Figure 14). The general appearance of the graph did not change drastically, but in distinguished areas, the data points showed drastic changes. Movement events between 0.01 and 0.06 µm/ sec, as well as events around 0.3 µm/sec the corrected data gained in relative strength compared to the fully automated approach. In large movement events greater than 0.35 µm/sec the corrected data showed decreased amount of data points, most likely pushed by the deletion of wrongly assigned long unspecific track jumps. The resulting data points were much less defective and therefore were considered as the basis for the actual data analysis and comparison.

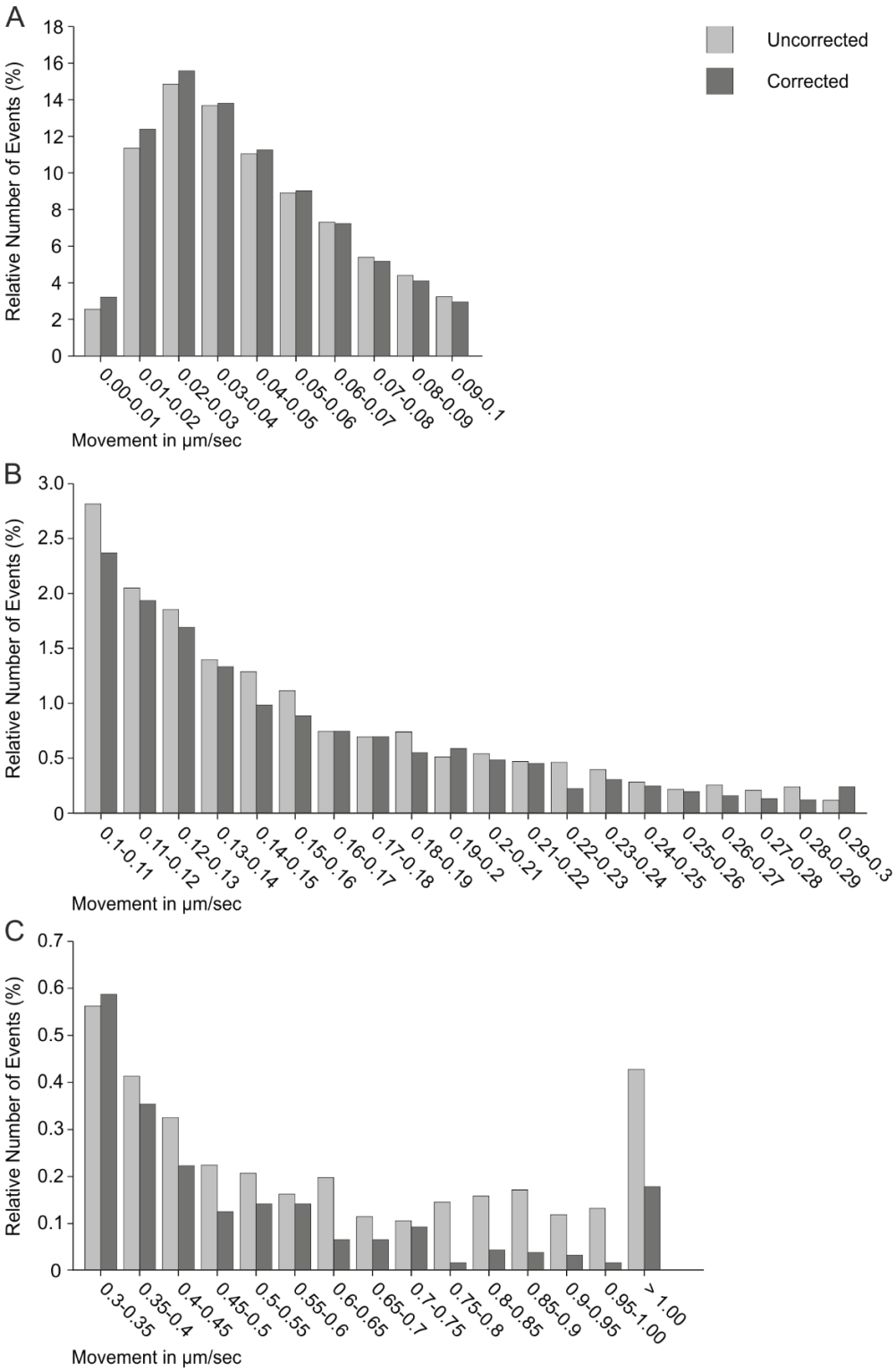

Figure 14 Comparison of the relative number of events in velocity categories between uncorrected and corrected data. The presentation of Figure 12 is extended by the numbers of the corrected dataset. Movement events of segments were classified in different velocity ranges and shown in relative amount in relation to the total amount of events in the image set. The relative number of events is shown in % against the velocity categorization in µm/sec described in 2.2.4. The graph is split into three sections for the proper scaling of the Y-axis. Velocity events are shown in A) between 0 and 0.1 µm/sec, B) between 0.1 and 0.3 µm/sec in 0.01 µm/sec steps respectively, C) between 0.3 and 1 µm/sec in 0.05 µm/sec steps and all events exceeding 1 µm/sec as a cluster.

2.2.6 Corrected vs uncorrected data

Besides the tracking algorithm, which was error-prone in a dataset showing a variety of different object structures and intensities, the segmentation of the image data was another crucial step in the automated tracking pipeline. As the automated approach worked best within a uniform dataset, it was extremely challenged by the plastid shape, which can create unique structures of variable size, not only because of the broad size spectrum of plastids but also by the existence of stromules that dictate the plastid appearance in great measure (Figure 15 A top panel). The blob finder segmentation algorithm of Arivis Vision 4D was shown to perform very well in the broad spectrum of shapes throughout the image sets, however, it struggled with the segmentation of plastids that possessed stromules. For plastids with stromules often many segments were computed reflecting different structures throughout the stromules. This was not intended but also not preventable keeping in mind that the automated approach was needed for the number of datasets analyzed, which displayed heterogeneous plastid morphology. Besides the plastid body, a variable number of additional segments was calculated for stromule-rich regions (Figure 15 A middle panel). The stromule-rich regions could show drastic changes in intensity and movement that led to the swapping and merging of segments in consecutive frames. The swapped and merged segments led to additional tracks in the final tracking that interfered with the consecutive tacking analysis (Figure 15 A bottom panel). Therefore, the number of stromules had a great influence on the number of segments and tracks in each dataset. To determine the amount of false positive movement events generated by the false segmentation of stromules, tracks of five random image datasets from plants cultivated under control conditions were scanned for faulty assignments of tracks caused by false segmentation of stromules (Figure 15 B). For the analysis, all events of the categories 0.1-03 µm/sec and greater than 0.3 µm/sec of corrected tracking data were checked in the datasets for correct or false assignment of segments to the corresponding tracks. Category spanning 0-0.1 µm/sec was not incorporated into the analysis because of the high amount of data. If a track was not traceable with the help of the underlying intensity data, the event was classified as false, if the tracking was comprehensible, it was classified as correct. In both categories, the analyzed data showed a correct assignment of about 70 %. That leaves about 30 % of the data, that is not assigned correctly and that was not found during the manual correction. The amount of false data was very reliant on the equality of the underlying image data. Datasets showing a good level of detail were less error-prone than bad-quality image data with a low level of detail. Most of the false assignments were made because of multiple segmentation of plastid stromules. Therefore, datasets with a huge amount of stromule movement showed a very high error in this analysis. Spherical plastids without stromules and steady movement up to 0.5 µm/sec showed to produce the most error-free data caused by automated segmentation.

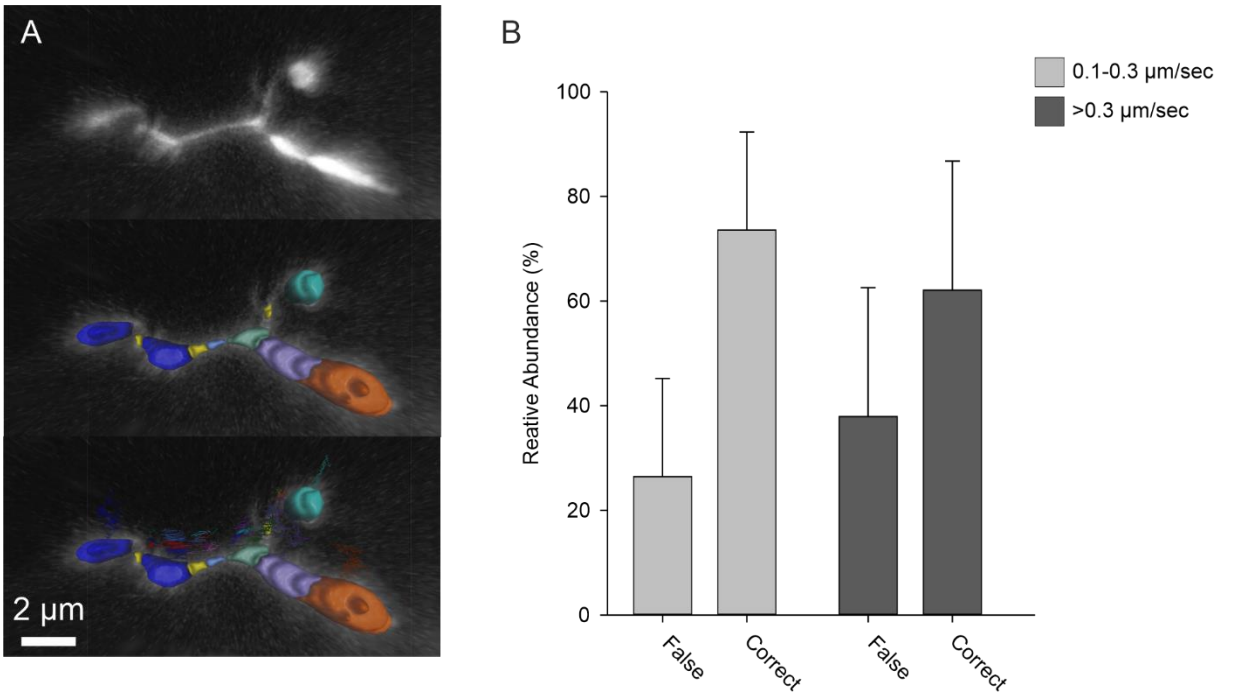

Figure 15 Multiple segmentation of stromules leads to false tracking data. A) Presentation of a stromule with plastids from a top view. The top panel shows the intensity data, the middle panel displays the automated segmentation of the structure, bottom panel the segmentation with assigned tracks. Tracks of all segments were computed separately and led to a surplus of tracking data. B) The comprehensibility of tracks was reviewed. The relative amount of false and correct tracks in the categories 0.1-0.3 µm/sec (light gray) and >0.3 µm/sec (dark grey) of five randomly chosen image sets are shown. Error bars indicate standard deviation.

2.2.7 Determination of noise in the movement data

The segmentation of the plastids is a crucial step during the automated tracking pipeline and is highly dependent on the intensity of the investigated objects. During imaging, the intensity of a fluorescently labeled organelle like the plastid varies not only because of photobleaching, which leads to a successive lowering of the object's intensity but also because of natural variation of the fluorescence intensity. Those are caused by minimal variations in either excitation or emission caused by changes in the cellular environment blocking or disturbing the light path leading to slightly different segmentation outlines in each frame for every object. In addition, slight variations in the plastid shape led to small differences in the segmentation. For tracking the segments, the geometric center of each segment was used. The slight variations in the object segmentation between each frame led to differences in the geometric center between frames of non-moving plastids, which generated movement data for stationary segments. To determine the velocity of movement events caused by non-moving objects, 45 different plastids of control conditions were chosen randomly that did not show a delocalization of more than 2 µm in relation to their first appearance throughout the imaging process (Figure 16 A). Those plastids were classified as stationary. The movement speed of each movement event and the mean movement speed of all resulting events (n=3686) were calculated in µm/sec (Figure 16 B). The average movement speed of those variations in the segmentation was about 0.05 µm/sec. Therefore, all movement events up to 0.05 µm/sec were considered as noise caused by slight variations in the object intensity. It needs to be mentioned that the velocity of

the noise events was strongly dependent on the size of the segment. Bigger segments had the capacity for more change caused by fluorescence fluctuation, leading to bigger movement events.

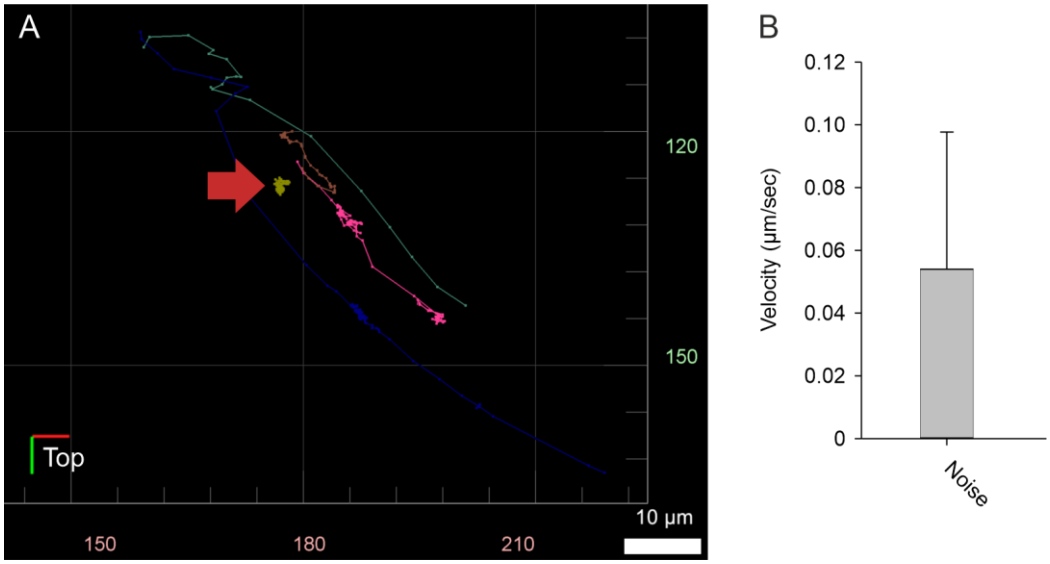

Figure 16 Determination of background noise in the tracking data. A) Top view of a 3D representation of different tracks. 3D orientation is indicated by the directionality marker in the bottom left. The X-dimension is shown in red, Y-dimension in green and Z-dimension in blue. The yellow track, which is marked by a red arrow, displays an exemplary stationary track, in which all segments did not exceed a distance of 2 µm from the initial segment. B) The graph displays the mean of all velocity events (n=3686) in µm/sec of 45 different stationary tracks of control condition. Error bars indicate standard deviation.

2.2.8 Assignment of plastid speed to movement patterns using angles between connecting vectors

For an initial overview of the distribution of the plastidal movement speed, the movement events have been divided into several groups (2.2.4). The classification was used to determine movement events that were mostly affected by the manual correction. However, the distribution of the movement speed did not allow conclusions about the underlying movement patterns of the plastids. A variation of movement patterns has been described for other organelles, including directed movement, where the organelle moves in a directed manner from one location to another and undirected “wiggling” motions, in which the organelle maintains the location and moves around one spot. Both are described to happen at various speeds and can be mixed. Motions that change between directed and undirected patterns are called stop-and-go motions and happen commonly in the cell. For a detailed analysis of the movement patterns underlying a particular track, this track needs to be analyzed. This work aimed for a broad automated analysis, capable of processing multiple datasets, not an individual track analysis. However, for a description of the categorized movements, a classification of movement events in directed and undirected motion patterns was desired. For the analysis of the movement patterns, the angle of the movement vector in relation to the prior movement vector can give information about the direction of the movement

event in relation to the previous one. The movement of a segment between two frames can be described as a connecting vector by the formula:

$$\overrightarrow{\mathrm{AB}} = \begin{pmatrix} \mathrm{b}_1 \\ \mathrm{b}_2 \\ \mathrm{b}_3 \end{pmatrix} - \begin{pmatrix} \mathrm{a}_1 \\ \mathrm{a}_2 \\ \mathrm{a}_3 \end{pmatrix} = \begin{pmatrix} \mathrm{b}_1 - a_1 \\ \mathrm{b}_2 - \mathrm{a}_2 \\ \mathrm{b}_3 - \mathrm{a}_3 \end{pmatrix}$$

The angle between two consecutive vectors $\overrightarrow{AB}$ and $\overrightarrow{BC}$ was calculated by the formula:

$$\alpha = 180 - \left(\arccos \left(\frac{\overrightarrow{AB} \circ \overrightarrow{BC}}{\left|\overrightarrow{AB}\right| \cdot \left|\overrightarrow{BC}\right|} \right) \cdot \frac{180}{\pi} \right)$$

Since the angle is located between two individual movement events, it can be assigned to either of the two movement vectors. For the following work, the angle was assigned for the motion of the second vector giving each vector a direction of the motion it described.

In an exemplary track, directed and undirected motions were identified (Figure 17 A) and angles were calculated for each motion vector. Directed movement events were predominantly characterized by angles between two vectors that were greater than 90 ° (Figure 17 B), whereas undirected wiggling motions around one spot or area were most often accompanied by an angle of less than 90 ° between two vectors (Figure 17 B). In a follow-up step, the corresponding angle for each movement event (described in 2.2.6) of the control condition replicates was calculated with the aim to classify the movement events in clusters that describe the majority of included movement patterns. All movement events were separated into two groups. The first group displayed an angle of less than 90 ° the second one displayed an angle of more than 90 °. All movement events with an angle of less than 90 ° were classified as undirected movements, whereas all movement events with an angle of more than 90 ° were classified as directed movements. All movement events were successively assigned to the velocity groups (defined in 2.2.4) and the relative amount of undirected and directed movement for each velocity group was calculated (Figure 18). Most movement events between 0 and 0.05 µm/sec displayed undirected motion (Figure 18 A). Since these motions were previously classified as noise (2.2.7), this result was expected. Consequently, movement events between 0 and 0.05 µm/sec were classified as no motion. Movement events between 0.05 and 0.14 µm/sec displayed mostly undirected movement (Figure 18 A) therefore these movement events were classified as predominantly wiggling motions. Movement events between 0.14 and 0.3 µm/sec displayed the same amount of undirected and directed movement patterns (Figure 18 B). Since the number of directed and undirected movement events was comparable, movement events in this velocity range were classified as a mixture of directed and undirected motion. Movement events greater than 0.3 µm/sec displayed mostly directed motion (Figure 18 C). This effect was more drastic in movement events greater than 1 µm/sec. Therefore, movement events in the velocity range of 0.3-1 µm per second were classified as predominantly targeted motions, whereas the motion events with velocities of more than 1 µm/sec were classified as targeted motions. For each of the five categories (no motion, predominantly undirected, mixture of directed and undirected, predominantly directed, and directed) the relative number of events in relation to the overall number of events for each replicate was determined and compared with each other.

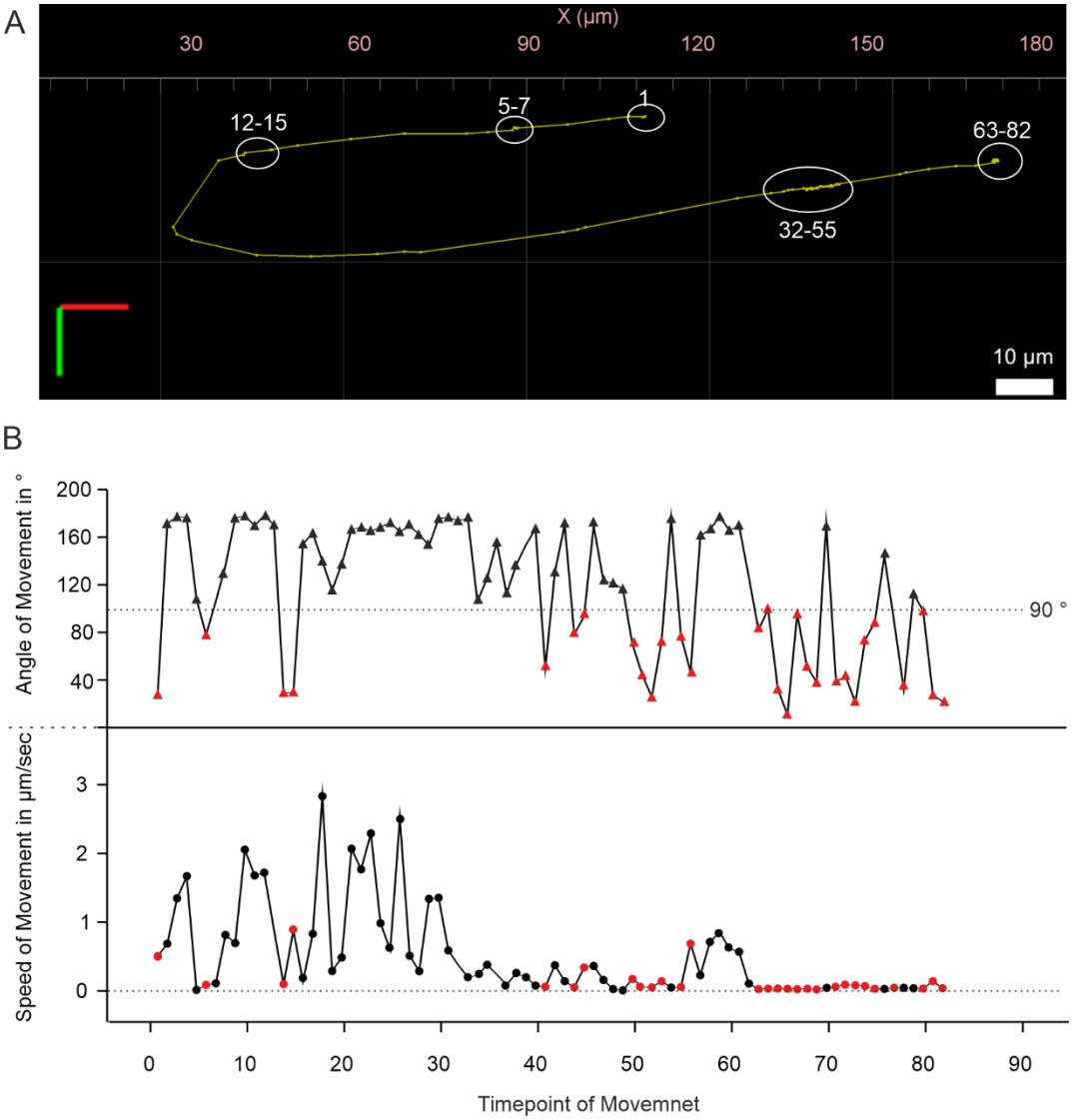

Figure 17 Exemplary visualization of the dependency of plastid speed and angle of the movement event. A) A top view of an exemplary track that shows directed and undirected movement patterns. 3D orientation is indicated by the directionality marker in the bottom left. X-dimension is shown in red, Y-dimension in green and Z-dimension in blue. Each movement event is indicated by a small square starting at timepoint 1. Zones of undirected movement patterns of the track are indicated by white circles and the corresponding timepoints. B) The angle in degree and the movement speed in µm/sec for each event are displayed for each timepoint. Angles of the movement events are divided in more and less than 90 °. Each movement event with an angle of less than 90 ° is marked in red; each movement event with an angle of more than 90 ° is marked in black. Movement events that display an angle of less than 90 ° are more likely to be in the zones of undirected movement with a low velocity, whereas movement events displaying an angle of more than 90 ° are more likely to possess higher movement speed of up to several µm/sec and show directed movement.

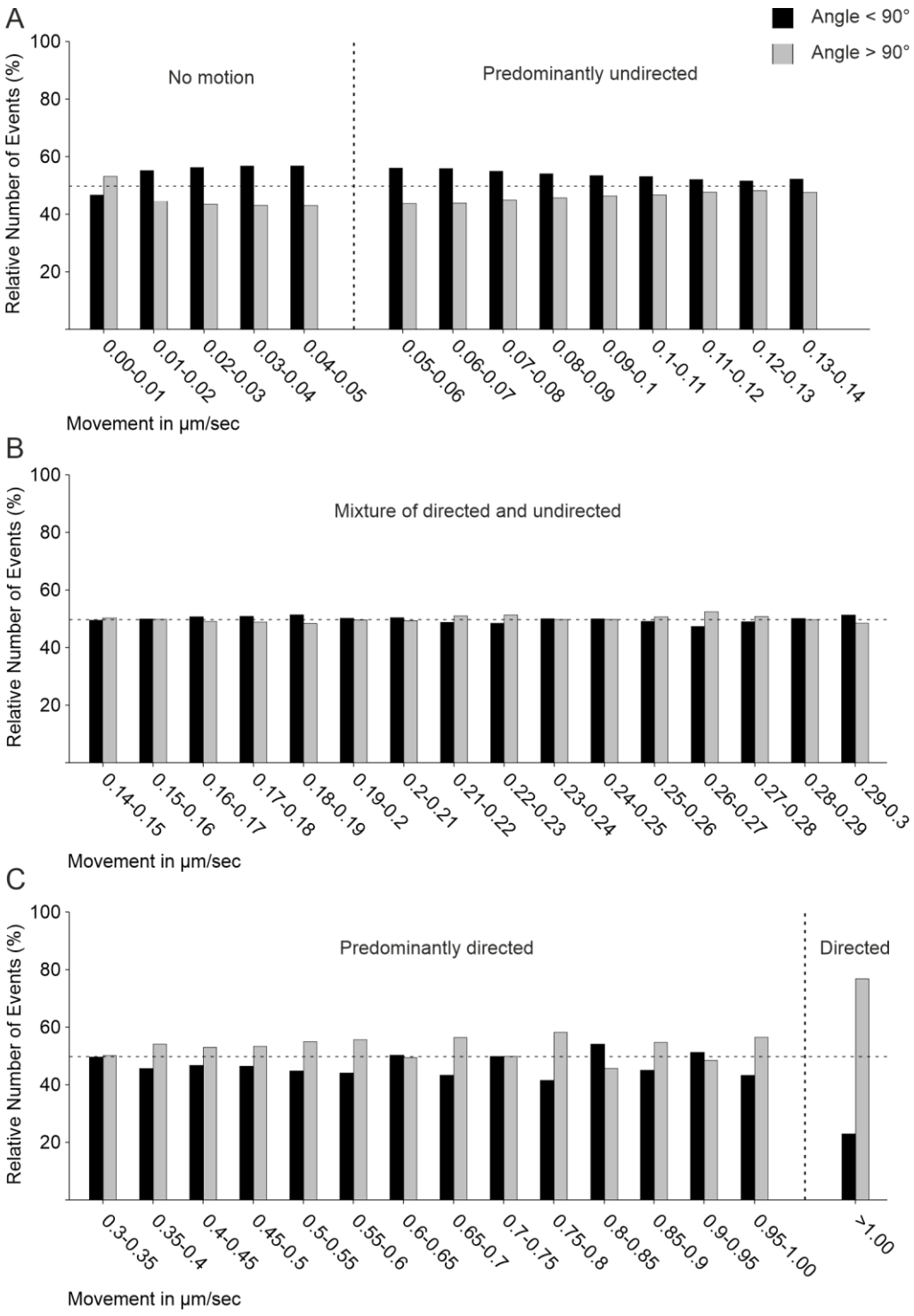

Figure 18 Classification of movement events using angles. Angles are assigned to each movement event of control conditions and all events were separated into movement events with angles greater or smaller than 90 °. The relative amount for each velocity category (defined in 2.2.4) for movement with more and less than 90 ° angles was calculated and is displayed in A, B and C. Based on the majority of movement events, different velocity categories were assigned to movement patterns that are dominantly performed in the velocity range A) Movement events with a velocity of 0-0.05 µm were classified as no motion. Movement events with 0.05-0.14 µm/sec were classified as predominantly undirected motions. B) Movement events between 0.14 and 0.3 µm/sec were classified as a mixture of directed and undirected motions. C) Movement events with 0.3-1 µm/sec are classified as predominantly directed, whereas movement events with more than 1 µm/sec are classified as directed.

2.3 Additional measurements done for the 4D tracking

2.3.1 Cell size

The determination of the cell size was performed to illustrate potential differences in growth for different conditions and to determine the number of plastids per cell. Stacks of the image data were loaded in ImageJ (Fiji) ver. 1.53c (Schindelin et al., 2012) for differentiation of the cell size. By enhancing the gamma values of the image data, the autofluorescence of components of the cell wall or the cell membrane got visible. This allowed a measurement of X- and Y dimensions of each cell (Figure 19). The Z-resolution however was not sufficient (Figure 6) to illustrate the cell border. Therefore, cell depth was approximated by the number of planes, the X- and Y-borders were visible. Since generally only a few whole cells were visualized in the image sets, up to two individual cells were measured per dataset and the cell size was averaged.

2.3.2 Number of cells

The average volume of all measured cells was determined for each condition representing the average cell size. Stacks of the image data were loaded in ImageJ (Fiji) ver. 1.53c (Schindelin et al., 2012) for the determination of the number of cells per dataset. Since most cells in the image frames were cut by the image borders and Z-borders for the cells could not be determined, the number of cells for each image set was approximated. To do so, the length and width of each root were measured (Figure 19). The root was considered as a cubic object since in general, the first few planes covered the whole width of the roots. The length and width of each root were multiplied by 30 µm of depth, for this reason, resulting in the approximated volume of each root. The volumes of the roots of each replicate were divided by the average cell size of each corresponding condition, resulting in the approximated number of cells.

2.3.3 Number of plastids

The number of plastids was counted using maximum intensity projections of each replicate. The resulting number was divided by the approximated number of cells to gather the number of plastids per cell. The total number of plastids was divided by the total volume covered in each image set to determine the number of plastids per μm^3 cell volume.

2.4 2D analysis of light sheet data

The automated 4D analysis of the data generated a reasonable overview of the general movement of plastids. Unfortunately, stromule formation did greatly interfere with the automatic analysis of plastidal motions. To gather additional information on the plastidal motion and for the investigation of the involvement of stromules in the plastidal motion, a detailed analysis of the plastidal movement patterns including stromules was performed in 3D (2D over time) eliminating the Z-plane. Previous results on those image data showed, that up to 90 % of the observed plastidal movement can be described by only considering the X- and Y-axes (Plomer, unpublished). Maximum intensity projections of all Z-stacks were prepared, and all frames were arranged to a 3D projection. For a detailed analysis of the different plastidal motions the software ImageJ (Fiji) ver. 1.53c (Schindelin et al., 2012) was used. The pixel size of each dataset was set to 0.16125 µm. The detailed procedures for the individual analysis are listed below.

2.4.1 Relative number of plastids with/without stromules and stromule branches

To calculate the relative number of plastids with stromules of each dataset, the amount of all visible plastids was counted in the first frame of every dataset. For this calculation, only areas of the recordings were used, which showed a proper resolution for distinguishing if a plastid possessed a stromule. Subsequently those plastids were categorized in two groups: A) plastids with stromules b) plastids without stromules. A stromule was defined as a tubular structure that visibly emerges from the plastid body for more than 1 µm (Figure 28). The relative amount of each group was calculated for every replicate and condition. From the plastids that showed stromules the number of stromule branches was counted. The number of branches in every dataset was set in relation to the number of plastids with stromules.

2.4.2 Stromule length

The stromule length of all visible stromules was measured in frame 1 of all datasets in all conditions. Stromule length was measured using the freehand tool of ImageJ (Fiji) ver. 1.53c (Schindelin et al., 2012).

2.4.3 Relative number of movement event classifications

For a detailed reflection of the plastidal motion patterns, different movement events were classified. In each dataset, 10-20 randomly chosen plastids were analyzed over the full period of 211 frames and movement patterns were analyzed in terms of the classified movement patterns. The classifications were: plastids without stromule shows movement, plastid without stromule shows no movement, plastid with stromule shows no movement, plastid with stromule shows stromule movement, plastid body of plastid with stromule is pulled by the stromule, plastid body moves and thereby pulls out a stromule. The relative number of observed events was calculated in relation to the total number of plastids in each dataset and each condition.

2.4.4 Measurement of maximal speed of plastids without stromules

Since the total amount of plastids without stromules that showed movement was too much to analyze by hand, the maximal speed of plastids in each dataset was determined. Therefore, coordinates of plastids with high mobility were recorded over the full period of 211 frames, or in the sections in which they were

present in the observed frame. Connecting vector length between consecutive frames was calculated with the formula $\sqrt{(x2-x1)^2+(y2-y1)^2}$ and divided by 4.3 sec. The maximal velocity was chosen for each dataset.

2.4.5 Measurement of stromule elongation and retraction speed

For the measurement of stromule elongation and retraction speed, the freehand tool of ImageJ (Fiji) ver. 1.53c (Schindelin et al., 2012) was used. In every dataset, three to five plastids with stromules were chosen displaying the highest stromule mobility. The distance between the stromule origin and the stromule tip was measured and differences between the frames were calculated and divided by 4.3 sec. Negative values were considered as retraction speed, and positive values were considered as elongation speed.

2.4.6 Speed of plastid bodies that pulled or moved alongside stromules

For the measurement of the speed of plastid bodies that pulled out stromules, which were anchored in the cellular context as well as the speed of the plastid bodies that move alongside stromules, the pointing tool of ImageJ (Fiji) ver. 1.53c (Schindelin et al., 2012) was used. Since those two events were rarely seen over a great period, all visible events have been considered in the measurements. Measurements were taken out over the full period of 211 frames, or until plastids were not identifiable anymore. The coordinates of the stromule origin and the stromule tip were recorded and vector length between these two points was calculated using the formula: $\sqrt{(x2-x1)^2+(y2-y1)^2}$. For the calculation of the velocity of each event the changes in the vector length between frames were calculated and divided by 4.3 sec.

2.4.7 Stromule branch movement speed

Stromule branch movement speed was measured using the point tool of ImageJ (Fiji) ver. 1.53c (Schindelin et al., 2012). For the measurement, all visible stromule branches that showed movement were considered. The coordinates of all branches were determined over the full period of 211 frames, or until branches were not identifiable anymore. The vector length between two consecutive points was calculated and differences between two frames were determined and divided by 4.3 sec.

2.4.8 Measurement of angles between stromules

The angle enclosed by two stromules was measured using the angle tool of ImageJ (Fiji) ver. 1.53c (Schindelin et al., 2012). Stromules that displayed a stable angle for a minimum of two frames were considered in this analysis.

2.5 Analysis of *in vitro* stromule formation

2.5.1 Chloroplast isolation

Chloroplasts were isolated from seven to eight days old *Pisum sativum* leaves. Plants were grown under greenhouse conditions on vermiculite at 12 hours light and 22 °C and 12 hours dark and 18 °C. Chloroplast isolation was performed as described by Bionda and Schleiff (Bionda & Schleiff, 2010). In summary: All working steps were performed either at 4 °C or on ice, precooled equipment was used. The afternoon before isolation, pea trays were put at 4 °C in the dark. On the isolation day, pea leaves were harvested and briefly cut with a kitchen blender and a scissor in an isolation medium (330 mM Sorbit; 20 mM Mops; 13 mM Tris; 0.1 % bovine serum albumin (BSA) Fraction V). The suspension was filtered through four layers of cheesecloth and one layer of gaze. The suspension was centrifuged for 2 min at 1,460xg in 50 ml polypropylene tubes. The supernatant was discarded, and the pellet was resuspended in 1 ml wash buffer (330 mM Sorbit; 50 mM Hepes / KOH pH 7.6). The suspension was layered on top of a Percoll gradient (40 % Percoll was underlaid with 80 % Percoll (Sigma-Aldrich) (both 330 mM Sorbit; 50 mM Hepes / KOH pH 7.6)) and centrifuged in a swing bucket rotor at 8,000xg for 10 minutes with a low deceleration. The fraction that got caught on top of the 80 % Percoll layer contained the intact chloroplasts and was collected in a fresh 50 ml polypropylene tube and filled up with wash buffer to remove the remaining Percoll. Tubes were centrifuged at 1,460xg for 2 minutes, the supernatant was removed, and the procedure was repeated a second time. The remaining pellet was collected in 1 ml of wash buffer and the chlorophyll content was determined according to Arnon (Arnon, 1949). Samples were successively adjusted to a concentration of 1 µg/µl chlorophyll and kept on ice for a maximum amount of two hours before further usage.

2.5.2 Calcein AM staining of chloroplasts

Isolated chloroplasts were stained with Calcein AM (Thermo Fisher). Calcein AM was solubilized in freshly opened Dimethyl sulfoxide (DMSO) to a concentration of 1 µg/µl. To determine a concentration of Calcein AM sufficient for confocal microscopic visualization of plastidal extrusions, different concentrations were tested on chloroplast samples with a total chlorophyll concentration of 50 µg. The determined concentration, which gave the best signal while keeping the amount of used Calcein AM to a minimum, was 0.04 µg per µg chlorophyll. Upon mixing Calcein AM with the chloroplasts, samples were incubated on ice for 90-120 minutes in the dark and were mixed every 20 minutes. Before microscopic imaging, the concentration of chloroplasts was reduced to 0.1 µg/µl by adding chloroplast wash buffer.

2.5.3 Isolation and concentration of total root and leaf protein extract from *P. sativum*

According to Ho and Theg (Ho & Theg, 2016), stromules can be induced at isolated chloroplasts by concentrated leaf extract, collected after the first centrifugation step during the chloroplast isolation procedure (2.5.1). In pursuance of those findings, full protein content of *P. sativum* leaves and roots was extracted. All steps of the procedure were performed either at 4 °C or on ice. For the protein extraction, 8-9 days old peas, grown under greenhouse conditions on vermiculite at 12 hours light and 22 °C and 12 hours dark and 18 °C respectively were used. For leave extract, top leaves were harvested, for root extract, roots were washed to free them from vermiculite and successively cut. Roots or leaves were blended with

a kitchen blender in chloroplast wash buffer (330 mM Sorbit; 50 mM HEPES / KOH pH 7.6) and the suspension was filtered through two layers of gaze. Protein extract was gathered in 50 ml polypropylene tubes and sonicated (2x 20 pulses at 30 % amplitude, Bandelin Sonoplus HD70, Bandelin electronic GmbH & Co. KG) before centrifugation for 45 minutes at 50,000xg to clear the extracts of leftover cell debris and big cytoskeletal elements (centrifugation step was introduced after 3.3.5). Following centrifugation, the extract was either concentrated for stromule induction assay, or ready to use for other downstream applications. Concentration was performed using Amicon Ultra-0.5 ml centrifugal filters (Merck) with a cutoff of 10 kDa. Those filter units were utilized at several points throughout this work. In the following, they will be referred to as Amicon filter units. The concentration of the extract is dependent on the extraction volume and material quantity used in the extraction process. For reaching high concentrations of the extract several rounds of concentration were performed keeping the concentrate in the filter unit while discarding the flowthrough until the intended concentration was reached. Protein concentration was either determined using the amido black method (Popov et al., 1975) or using the Bradford reagent (BioRoad) following manufacturer's instructions. Protein concentration was adjusted by adding a wash buffer if needed.

2.5.4 *In vitro* stromule induction assay using confocal microscopy

For confocal visualization of chloroplasts and stromules, a Zeiss LSM 780 confocal laser scanning microscopic system was utilized, using a Plan-Apochromat 63x/1.40 Oil DiC M27 (Zeiss) objective. Calcein was excited with an argon laser at 488 nm and emission wavelength was detected at 493-616 nm. Chlorophyll B was excited at 633 nm by a diode and emission signals were detected at 638-721 nm. Right before imaging, a sample of Calcein AM stained chloroplasts containing 3 µg chlorophyll in total was centrifuged to settle the chloroplasts with a desk centrifuge for 1 min. The supernatant was discarded, and the pellet containing the chloroplasts was mixed with the respective concentrated protein extract. The samples were examined using a 96-well glass bottom plate (Corning, Thermo Fisher). After 3 minutes of incubation and time for the chloroplasts to settle down, samples were imaged. The stromule number was determined using ImageJ (Fiji) ver. 1.53c (Schindelin et al., 2012). All images were visualized in z-stack format because the samples showed too much movement for maximum intensity projection. The number of chloroplasts showing Calcein AM fluorescence was determined. Of those chloroplasts, the number of chloroplasts that formed stromules was determined. Chloroplasts with no visible Calcein AM fluorescence were considered broken and were not included in the analysis.

2.5.5 SDS-PAGE

For the separation of proteins in dependence on their molecular weight the Tris glycine-based sodium dodecyl sulfate polyacrylamide gel electrophoresis (SDS-PAGE) was used, described by Laemmli (Laemmli, 1970). For the separation, either a 10 %, or a 12 % concentration of polyacrylamide was used in dependence on the molecular weight of the proteins that were separated. Proteins samples were mixed with 4x SDS Loading Dye (0.2 M Tris/HCL pH 6.8; 8 % SDS; 40 % (w/v) glycerol; bromophenol blue arbitrary, the stock was stored at 4 °C in portions of 800 µl, directly before use 200 µl 2 M dithiothreitol (DTT) were added), cooked at 95 °C for 5 minutes and successively loaded onto the gel. Samples were run with 1 X SDS running buffer (50 mM Tris; 200 mM glycine; 0.1 % SDS) for 75 min at 0.4 mA/cm^2. As a marker Unstained Protein Molecular Weight Marker (Thermo Fisher) was used. Following the run, gels were either

stained with Coomassie brilliant blue (Green & Sambrook, 2012), silver stain (Nesterenko et al., 1994), or conducted to western blotting.

2.5.6 Coomassie brilliant blue staining of protein gels

Gels were stained with Coomassie brilliant blue for the visualization of protein amounts at several steps in various protein purification processes following protocols from Green and Sambrook (Green & Sambrook, 2012). Gels were stained with Coomassie Brilliant blue (0.125 % (w/v) Coomassie brilliant blue R250; 0.125 % (w/v) Coomassie brilliant blue G250 in wash buffer (50 % (v/v) methanol; 10 % (v/v) acetic acid; 40 % ddH_2O)) for up to seven days, but at least for two hours. Gels were successively de-stained by several washes with wash buffer until protein bands were visible. Gels were scanned for documentation but beforehand, gels were washed two times with ddH_2O for 3-5 minutes for better band visualization.

2.5.7 Silver staining of protein gels

Silver staining of protein gels was performed according to Nesterenko (Nesterenko et al., 1994). In short: For every step 60 ml solution per gel was used. All actions besides rinsing were performed under constant shaking. All solutions were prepared freshly from stock solutions. Stock solutions were 50% acetone in ddH_2O; 50 % trichloroacetic acid (TCA) in ddH_2O; 20 % $AgNO_3$ (w/v) in ddH_2O; 10 % $Na_2S_2O_3 \cdot 5H_2O$(w/v) in ddH_2O. Starting the procedure, gels were incubated for 5 min in a fixing solution (60 ml acetone stock; 1.5 ml TCA stock; 25 µl 37 % formaldehyde), rinsed with water three times, washed extensively with ddH_2O for 5 min, rinsed again with ddH_2O for three times and treated with 50 % acetone for 5 min. Successively gels were incubated for 1 min in a pretreat solution (100 µl $Na_2S_2O_3 \cdot 5H_2O$ stock; 60 ml ddH_2O), rinsed three times with ddH_2O and incubated with an impregnating solution (0.8 ml $AgNO_3$ stock 0.6 ml 37 % formaldehyde; 60 ml ddH_2O). Gels were rinsed three times with ddH_2O and incubated in a development solution (1.2 g Na_2CO_3; 25 µl 37 % formaldehyde; 25 µl $Na_2S_2O_3 \cdot 5H_2O$ stock; 60 ml ddH_2O) until protein bands were visible. Reaction was stopped with stopping solution (1 % (v/v) glacial acid and 50 mM ethylenediaminetetraacetic acid (EDTA)) for 1 minute. Gels were rinsed a final time with ddH_2O and successively scanned for documentation.

2.5.8 Differential centrifugation of protein extract

To determine the components of the total protein extract that are responsible for stromule formation, differential centrifugation for the separation of different cellular components was performed on the isolated cell extract (Campbell & Reece, 2009). The following regimes were performed: 10 min 2,000xg for sedimentation of whole cells, cell debris, nuclei, and big cytoskeletal elements; 20 min 20,000xg for sedimentation of mitochondria, lysosomes, and peroxisomes; 1h 80,000xg for sedimentation of microsomes and small vesicles; 3h 300,000xg for sedimentation of large macromolecules and ribosomes. The remaining pellets were resolved in 1 ml chloroplast wash buffer which resulted in 50 fold concentration of the respective pellets. The remaining supernatant was concentrated using Amicon centrifugal units (0) also tested for stromule induction.

2.5.9 Nucleus isolation

For the determination of a potential association of stromules and nuclei during *in vitro* stromule formation, nuclei were isolated from *Pisum sativum* following the protocol for nucleolus isolation from Palm et al. (Palm et al., 2016). Peas were cultured as previously described (2.1). Nuclei were isolated from freshly cut pea leaves. 10 g of pea leaves were ground in liquid nitrogen and taken in HNB buffer (5 % sucrose; 5 % glycerol; 25 mM Hepes pH 7.5; 25 mM NaCl; 5 mM $MgCl_2$; 1 mM EDTA pH 8.0; 2 mM $CaCl_2$; protease inhibitor cocktail (PIC, Sigma)). The suspension was incubated on ice for 15 minutes and Nonidet-P40 was added to the samples to a final concentration of 1 %. The samples were vortexed vigorously before they were underlaid with a cushion of 10 % sucrose in HNB buffer. Samples were centrifuged at 2,150xg at 4 °C for 10 minutes in a swing bucket rotor with low deceleration. The supernatant, which contained the cytoplasmic fraction was discarded, and the pellet, which contained the nuclei was resuspended in chloroplast wash buffer. Nuclei were further stained with 4',6-Diamidino-2-phenylindol (DAPI) (Thermo Fisher) following the manufacturer's instructions and were further analyzed in the *in vitro* stromule induction assay.

2.5.10 Thermolysin treatment

To determine, if proteins interact with lipids or proteins of the outer chloroplast membrane to induce stromule formation, a Thermolysin treatment was performed, to reduce the number of accessible proteins in the outer envelope (Bionda & Schleiff, 2010). Following the isolation procedure, a fraction of the chloroplasts containing 20 µg chlorophyll was used for each reaction individually. All procedures were performed at 4 °C or on ice. Chloroplasts were centrifuged at 1,300xg for 1 min, the supernatant was removed, and the pellet was resuspended in 500 µl wash buffer 2 (330 mM Sorbit; 50 mM HEPES/KOH pH 7.6; 0.5 mM $CaCl_2$). The samples were centrifuged at 1,300xg for 1 min, the supernatant was discarded, and the pellet was resuspended in 200 µl wash buffer 2. The samples were mixed with 5 µg Thermolysin (Calbiochem) and incubated for 20 min on ice in the dark. The reaction was stopped with 2 µl 0.5 M EDTA, to reach a final concentration of 5 mM. The samples were centrifuged for 1 min at 1,300xg and the pellet was collected in 200 µl wash buffer 3 (330 mM Sorbit; 50 mM HEPES/KOH pH 7.6; 5 mM EDTA). The digested samples were either used for microscopic imaging, or SDS-PAGE following western blotting.

2.5.11 Western blot

For immunoblot analysis of proteins separated via SDS-PAGE, semidry western blotting was performed (Ausubel et al., 1987). Proteins were transferred to a nitrocellulose membrane (Amersham Protran 0.45 µm, Merck) in a blotting buffer (40 mM Tris; 39 mM Glycine; 0.039 % (w/v) SDS; 20 % (v/v) methanol. Blotting was performed at 1 mA cm^{-1} gel size for 75 min. Following the blotting procedure, nitrocellulose membranes were stained with direct blue 71 (DB 71) (0.008 % (W/v) DB71; 10 % (v/v) acetic acid; 40 % ethanol) until protein bands were visible for the validation of correct transfer of the proteins and the detection of the transferred marker. DB71 stained blots were de-stained with de-stain solution (1 M Sodium bicarbonate; 50 % (v/v) ethanol) and washed extensively 4-5 times with ddH_2O for 1 minute. Subsequently, free binding sites of the membrane were blocked with blocking solution (5 % (w/v) non-fat dry milk powder in phosphate buffered saline (PBS) (140 mM NaCl; 2.6 mM KCl; 10 mM NaH_2PO_4; 1.8 mM KH_2PO_4)) for 1 hour at room temperature or up to 72 hours at 4 °C

under constant shaking following the incubation with the primary antibody for 1 hour at room temperature or up to 72 hours at 4 °C under constant shaking. Primary antibodies were diluted (for concentration see Table 2) in 5 % milk in PBS. The blots were washed three times for 10 min with PBS at room temperature under constant shaking. For detection of the primary antibody, the blots were incubated with a secondary antibody conjugated to horseradish peroxidase (HRP) (Sigma Aldrich). Secondary antibodies were diluted 1:10,000 in 5 % milk in PBS and the blots were incubated in the solution for 1 hour at room temperature under constant shaking. Antibody signals were detected using the Enhanced Chemiluminescence Kit (ECL kit, Perkin-Elmer Life Science) and a ChemoStar PC ECL & Fluorescence Imager (Intas Science Imaging).

2.5.12 Antibodies used for western blotting

Table 2: Antibodies utilized in this study.

Name	Variety	Antigen Source	Secondary Antibody	Dilution	Conjugate	Reference
Tic 110	Polyclonal	*P. sativum*	Rabbit	1:2,000	-	(Schleiff et al., 2003)
Toc 159G P.s.	Polyclonal	*P. sativum*	Rabbit	1:5,000	-	(Sommer et al., 2011)
Toc 34G P.s.	Polyclonal	*P. sativum*	rabbit	1:5,000	-	(Sommer et al., 2011)
Anti-Rabbit-HRP	Polyclonal	Rabbit	-	1:10,000	HRP	Sigma Aldric (Cat # A9169)

2.5.13 Sucrose gradient centrifugation

For separation of the total protein extract (0) sucrose density ultracentrifugation was performed (Berg et al. 2013). Linear sucrose gradients were prepared following (Luthe, 1983). Gradients were prepared in 10 ml polypropylene tubes (Beckmann Coutler) in a range between 10 % and 60 % sucrose in chloroplast wash buffer. Sucrose concentrations of 10, 20, 30, 40, 50, and 60 % were prepared, 1.33 ml of each sucrose concentration was used. Starting with 60 % sucrose the solution was filled in the tubes, which were successively frozen in liquid nitrogen, before overlaid with the next concentration. The sucrose concentration of each layer decreased by 10 %. The procedure was repeated for each concentration. Gradients were stored at -80 °C. On the day before use, gradients were transferred to 4 °C at a vibration-free space. Before separation, pea protein extract was concentrated to reduce loading volume using Amicon Filter units. The required amount of protein was loaded onto the gradient and was centrifuged at 4 °C over night at 250,000xg with low deceleration. The next day, fractions were taken from the top in 1 ml steps and either directly conducted to SDS-PAGE, anion exchange chromatography or concentrated completely and washed four times with chloroplast wash buffer in Amicon filter units before the stromule induction capacity of each fraction was determined in the stromule induction assay.

2.5.14 Anion exchange chromatography

To fractionate the crude cell lysate (0) and to maintain a protein factor that is responsible for *in vitro* stromule induction, anion exchange chromatography was performed with the protein lysate, or with fractions of the protein lysate, which was separated via sucrose density centrifugation. For the separation of the total protein extract and accumulation of wanted protein, the protein extract was separated with an anion exchanger. Diethylaminoethylcellulose (DEAE) Sephadex A-50 (Pharmacie) was used following the manufacturer's protocol. In short: Column material was swollen in freshly autoclaved 0.1 M NaCl at 95 °C for 2 hours, following an incubation at 4 °C over night. The next day, the column material was washed with 10 volumes equal to the column material of 20 % (v/v) ethanol. Column material was stored in 20 % (v/v) ethanol at 4 °C until further use. Protein lysate was separated using a maximum of 3 mg total protein per ml swollen column material to avoid saturation of the column material. Separation was performed at 4 °C. The column material was equilibrated with 10x column volume chloroplast wash buffer. The protein lysate was run three times over the column material to ensure maximal binding of proteins before the column was washed two times with double the amount of column volume with chloroplast wash buffer. Proteins were eluted with increasing concentrations of NaCl in chloroplast wash buffer and the eluates were ready to use for downstream applications. For microscopic analysis in the stromule induction assay, complete fractions were concentrated to ensure equal distribution of the proteins using Amicon filter units. Following concentration, the concentrated protein lysates were maintained in the filter units and washed four times with 500 µl chloroplast wash buffer to reduce the salt concentration in the samples to a minimum. Protein lysates were subsequently used in the chloroplast induction assay, or for SDS-PAGE.

2.5.15 Sucrose cushion centrifugation

To reduce the amount of loaded protein and thereby avoid overloading of the sucrose gradients, a sucrose cushion centrifugation was performed for samples with quantities of protein greater than 50 µg total protein extract. Sucrose cushion centrifugation was performed in the morning of the same day, on which the linear sucrose gradient was performed, to reduce the overall time needed for protein separation to a maximum of 36 hours to prohibit degradation of the wanted protein factor. The wanted protein factor remained in fraction 1 of the sucrose density gradient, reaching approximately from 0-15 % sucrose. Therefore, chloroplast wash buffer was supplemented with 15 % sucrose during protein extraction (0). 4 ml of the protein extract were underlaid with 40 % sucrose in chloroplast wash buffer in 7 ml ultracentrifugation columns and samples were centrifuged for 4 hours at 400,000xg in a fixed angle rotor. The top 3.5 ml fraction of the columns was taken for further processing. The amount of overall protein was reduced in the samples as shown by Coomassie staining (Figure 45) and Bradford protein concentration determination. Samples were further prepared for sucrose density centrifugation. For this, protein extract was concentrated with Amicon filter units, to reduce loading volume for the sucrose gradient and washed four times with chloroplast wash buffer to remove the sucrose and ensure proper loading on the linear sucrose gradient. Samples were afterward loaded onto the linear sucrose gradient.

2.5.16 Preparation of samples for mass spectrometry

For the preparation of mass spectrometry samples, sucrose cushion centrifugation (0), sucrose gradient centrifugation (2.5.13) and ion exchange chromatography (2.5.14) were coupled in this order. Samples prepared from *A. thaliana* were cultured on 12 cm squared petri dishes (as described in 2.1). For all steps of the anion exchange chromatography MS-grade water and low protein retention tips were used. Flowthrough, 0.1 M NaCl, 0.2 M NaCl, 0.35 M NaCl fractions were captured as stromule induction capacity of those fractions showed significant differences. Samples were concentrated using fresh Amicon centrifugal units and precipitated with acetone (Rehm & Letzel, 2016). To do so, 6-9 volumes of -20 °C cold 100 % acetone was added to the sample. The sample was vortexed and incubated at -20 °C for 16 hours. Successively, the sample was centrifuged for 15 minutes at a minimum of 13,000xg and washed with 90 % acetone two times. Samples were dries at room temperature for up to 30 minutes. Proteins were dissolved in 25 µl SDC-buffer (2 % Deoxycholate (DOC); 1 mM Tris(2-carboxyethyl)phosphine (TCEP) 4 mM chloroacetamide (CAA); 50 mM Tris pH 8.5) and heated for 10 minutes at 60 °C. Samples were cooled down to room temperature and condensates gathered at the lid were collected with short centrifugation with a table top centrifuge. 25 µl Trypsin stock (50 mM Tris pH 8.5; 20 ng/µl Trypsin) was added to the samples and samples were digested for 14 hours at 37 °C. Digestion was stopped with 150 µl 1 % Trifluoroacetic acid (TFA) in isopropanol. Samples were centrifuged for 5 minutes at 14,000xg and the supernatant was transferred into a fresh tube. For a solid phase extraction, the samples were given onto 10 µg of Styrenedivinylbenzene – Reverse Phase Sulfonate (SDB-RPS, Empore) columns and centrifuged for five minutes. During this process, all centrifugation steps were performed at 3,500xg. 200 µl 1 % TFA in isopropanol was added and the samples were centrifuged for 5 minutes. This step was repeated one time. 200 µl 0.2 % TFA in water was added and centrifugation for 5 minutes was carried out. This procedure was repeated one time. The samples were eluted into a 1.5 ml LoBind tube using 60 µl of 80 % Acetonitrile (ACN) and 1.25 % ammoniac by centrifugation for 5 minutes. The elution solution was evaporated using a Speed Vac and stored at -20 °C until analysis by liquid chromatography coupled to mass spectrometry (LC-MS)

2.5.17 LC-MS of protein samples

Before LC-MS analysis, the samples were resuspended in 10 µl 2 % ACN and 0.1 % TFA. The MS analysis was performed by Georg Tascher of the quantitative Proteomics Unit at the Institute of Biochemestry 2 (Goethe University in Frankfurt a. M.). The samples were analyzed on a Q Exative HF coupled to an easy nLC 1,200 (Thermo Fisher) using a 35 cm ling, 75 µm ID fused silica column packed in house with 1.9 µm C18 particles and kept at 50 °C using an integrated column oven (Sonation). For controlling the instrument, the software Tune version 2.9 (Thermo Fisher) was used. For the control and processing of the data, the software Xcalibur version 4.0.27.10 (Thermo Fisher) was utilized. The peptides were eluted by a non-linear gradient (4-32 % acetonitrile) over a timeframe of 90 min. The eluted peptides were directly sprayed into the mass spectrometer equipped with a nanoFlex ion source (Thermo Fisher). Full scan MS spectra (350-1,650 m/z) were acquired in Profile mode at a resolution of 60,000 at m/z 200, a maximum injection time of 20 ms, and an AGC target value of 3×10^6 charges. Up to 15 of the most intense peptides per full scan were isolated using a 1.4 Th window and fragmented using higher energy collisional dissociation (normalized collision energy of 27). MS/MS spectra were acquired in centroid mode with a resolution of

15,000, a maximum injection time of 25 ms and an AGC target value of 1 x 10^5. Single-charged ions, ions with a charge state above 5, and ions with unassigned charge states were not considered for fragmentation and dynamic exclusion was set to 25s to minimize repeated fragmentation of already selected precursors.

2.5.18 LC-MS data analysis

For the analysis of LS-MS raw data, the software MaxQuant (Ver. 1.5.5) (Cox & Mann, 2008) was utilized. For "Group specific parameters", default options were chosen. Options "Modifications" were set as followed: "Oxidation (M)", "Acetyl (Protein N-tem)", and "Deamidation (NQ)". At "fixed modification" option, "Carbamino methyl (C)" was set. For "Digestion" option "Trypsin/P" was selected, "Maximal Missed Cleavages" were set to 2. At "Label-free Quantification" settings, "LFQ" was set with maintaining the default settings. As reference for the identification of proteins the Uniprot *Arabidopsis* proteome database UP000006548 in FASTA format was loaded at "Global Parameters" option. For "protein Quantification" option, the previously chosen modifications were added again and "iBAQ" option was chosen at "Label-free Quantification slider". After MaxQuant processing of the data, it was analyzed using the software Perseus (Ver. 2.0.3.1) (Tyanova et al., 2016).

2.6 Statistics

All statistics were performed using SigmaPlot 13.0.0.83. A student's t-test was performed to compare normally distributed populations, whereas for not gaussian distributions a Mann-Whitney rank sum test was used for comparison. Statistical difference was asserted by $p < 0.05$.

3 Results

3.1 4D tracking of plastids

3.1.1 Description of control conditions

In plants, organelle movement is believed to be mainly mediated by motor proteins transporting organelles across cytoskeletal elements (Geitmann & Nebenführ, 2015; Nebenführ & Dixit, 2018; Vick & Nebenführ, 2012). However, the machinery comprised of cytoskeletal elements and motor proteins is variable and the exact molecular mechanisms are not understood by now. Central questions of organellar transport are, whether it is mediated actively through active attachment and transport of the organelle by motor proteins, or passively by cytoplasmic streaming or other factors. To get insight into the movement dynamics and the transport of root plastids, an automated 4D tracking analysis of image stacks, acquired via light sheet-based fluorescence microscopy, was piloted. The recorded tissue was the mature zone of the root, also known as differentiation zone (Figure 5 A). The area of recording was limited due to the experimental setup (Figure 5 B). Different replicates of control conditions were taken out, in the latter referred to as image datasets. To establish a detailed description of the cellular context of the recordings, the cell size and plastid number of each control condition replicate was examined.

Since the cell wall and the plasma membrane were not fluorescently labeled in the plants used for this study, the borders of the cell could only be observed using its' autofluorescence. The investigation under increased gamma values made it possible to distinguish the cell walls of the cell in X- and Y-dimensions but it was not applicable to visualize the Z-borders of the cell (2.3.1). Therefore, cell depth was assumed by the presence of the borders in X- and Y-dimensions (Figure 19 A). By this method, the average cell size under control conditions was settled at 125 x 20 x 19 µm = 47,500 µm³. Being dependent on the microscopic frame, most of the visualized cells were cut by the image border (Figure 19 A) making it difficult to determine the exact cell number in each replicate. However, total cells were measured, and the general cell size was determined for each replicate, respectively (Figure 19 B). The average visible cell measured about 50,000 µm³ with a minimum of 20,000 µm³ and a maximum of 80,000 µm³. Taking the average cell size, an estimation of the visualized number of cells was done, even though most of them were not fully pictured. For the approximation, the framed image of the root was treated as a cuboid, disregarding the spherical structure of the root, which was not visible in a great portion of the acquired image data. The root volume for each image dataset was determined using the diameter and the length of the root (Figure 19 A) as well as the 30 µm of depth that was used as a standard during image acquisition. For an estimation of the average cell number that was comprised in the image sets in control conditions, the root volume of each replicate was divided by the average cell size. One frame depicted about 16 cells with only slight variations throughout the control sets.

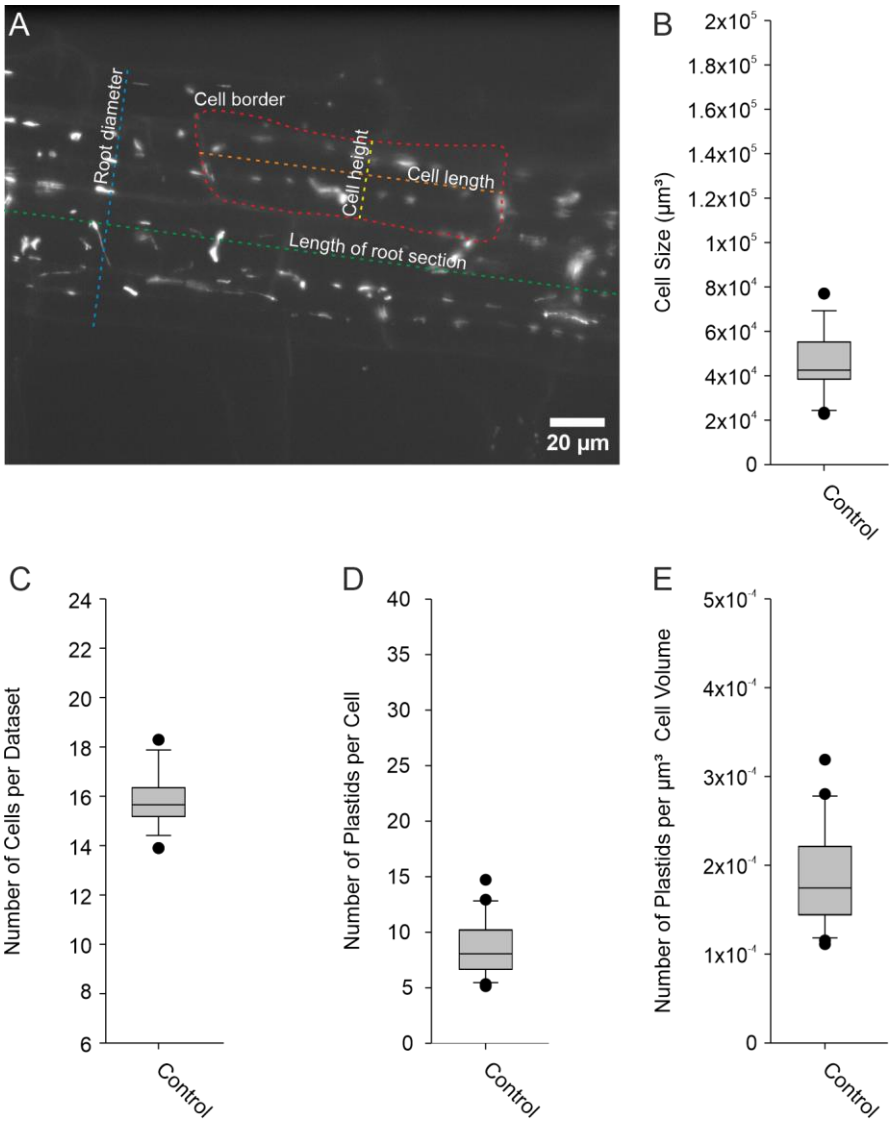

Figure 19 Description of the cell size and plastid number. . Image Data were acquired from n=25 control image datasets. A) Maximum intensity projection of an exemplary image frame of control conditions. Cell size could be measured using the cell walls' autofluorescence indicated in red, the root diameter and the length of the root in the display window shown in green. Cell size was approximated using the length (orange) and the height (yellow) of the cell. Cell depth was determined by the number of frames that showed cell wall autofluorescence. B) Number of cells represented in control condition image datasets was estimated by the average cell diameter and the size of the root respectively. C) Cell size was estimated in µm³ for each control image dataset and shown as a boxplot. D) Plastids were counted in each image dataset and divided by the estimated number of cells for each image dataset respectively. E) Number of plastids per µm³ of each image dataset is shown. B)-E) Values are shown as a boxplot. Boxplots display the distribution of determined values. Boxplots show the 10 %, 25 %, 50 %, 75 %, and 90 % quartiles. Outliers are indicated as points outside of the boxplots.

In contrast to the cell number, which needed to be approximated, the number of plastids was counted. For the procedure all plastids in the first frame of every image dataset were counted, using maximum intensity projections of the acquired data. The total number of plastids was divided by the average approximated cell size and was settled at maximal 15 plastids per cell. The median value across all replicates was 8 plastids (Figure 19 C). Using the average cell size, the number of plastids was also

calculated in relation to the displayed cell volume and was settled at 0.0002 ± 0.0001 plastids per µm³. Besides the number of plastids, the plastid size was not determined, because the structural variety that was shown by the plastids was too high. Furthermore, the Z-resolution was too weak (Figure 6) to display stromules and therefore a general approximation of the plastid volume was not performed. However, plastid size showed variations (Movie 1,2). The overall number of plastids in the root epidermis appeared to be smaller compared to plastids in the root cortex but no general rule was formed due to lack of robust data and difficulties in the discrimination of the two cell layers.

3.1.2 Plastid velocity distribution in control conditions

So far, a variety of organellar motions have been described (Geitmann and Nebenführ 2015; Nebenführ et al. 1999a; Vick and Nebenführ 2012). The most extreme movement patterns are directed movements, displaying a distinct directionality in their movement, with varying velocities up to 7 µm/sec (Tominaga et al. 2013; Tominaga et al 2003). The movement is believed to be actively mediated by motor proteins but could also be driven by cytoplasmic streaming (Tominaga et al. 2013). Other movement patterns like wiggling motions which describe undirected movements around a location and no movement at all were described (Vick & Nebenführ, 2012). Wiggling motions can be compared to Brownian motion patterns (Vick & Nebenführ, 2012). Both extremes can be performed on one organelle within minutes and with varying velocities (Perico & Sparkes, 2018; Vick & Nebenführ, 2012). The mechanisms and functionality of most organellar movement is not well understood so far. Although it is suggested that wiggling motions are stop points at specific sites of the cell for metabolite exchange with other organelles (Perico & Sparkes, 2018; Vick & Nebenführ, 2012). Plastidal movement in the root has not extensively been studied to date, disregarding the statolith movement in the root columella cells. To capture and describe the variety of plastidal movement in *Arabidopsis thaliana* roots, it was necessary to process a great amount of image data not just in control conditions, but also in different stress situations. To allow for the analysis of the data in a reasonable amount of time, an automated tracking pipeline was established (2.2) which followed the aim to track the movement of the plastid bodies (Figure 7-Figure 11). The problems faced during the automated approach and how they were tackled have previously been described (2.2.5, 2.2.6). For a general description of the plastidal motion patterns and to set a baseline for following stress treatments, control conditions were examined. The data were analyzed using the 4D visualization and the tracking output tables of the analyzed image sets.

The visualization of the tracking data was a crucial step for the verification and manual correction (2.2.5) of tracks (Figure 13). Following correction, a variety of motion patterns was observed (Figure 20). The directed movements of some plastids across defined routes were striking. Plastids that showed directed movement eventually stopped at one location for a certain amount of time, displaying undirected wiggling motion, before moving further in a directed manner (Movie 23, 24). Most directed tracks captured were of a limited length and did not span the whole timeframe of 15 minutes. During the imaging process, they moved outside of the imaged area, thereby limiting the recorded tracks. Many times directed movement of plastids was observed, these plastids were transported either from or into a root hair tip (Movie 24). Besides striking directed movement, many plastids displayed no real change in place. Tracks generated from these plastids mostly wiggled around a defined area generating movement data that was summed

up as background noise (2.2.7). In some cases, they covered bigger volumes with the wiggle motion. Those movements seemed to be a directed repetitive movement between two or more locations. Some tracks displayed a wiggling motion in combination with a direction. They slowly changed place in a zigzag track, mimicking a directed motion. In general, many tracks were not computed for the total duration of 211 timepoints. Difficulties in segmentation mostly caused by stromules led to wrongly assigned segments and early breakup of tracks.

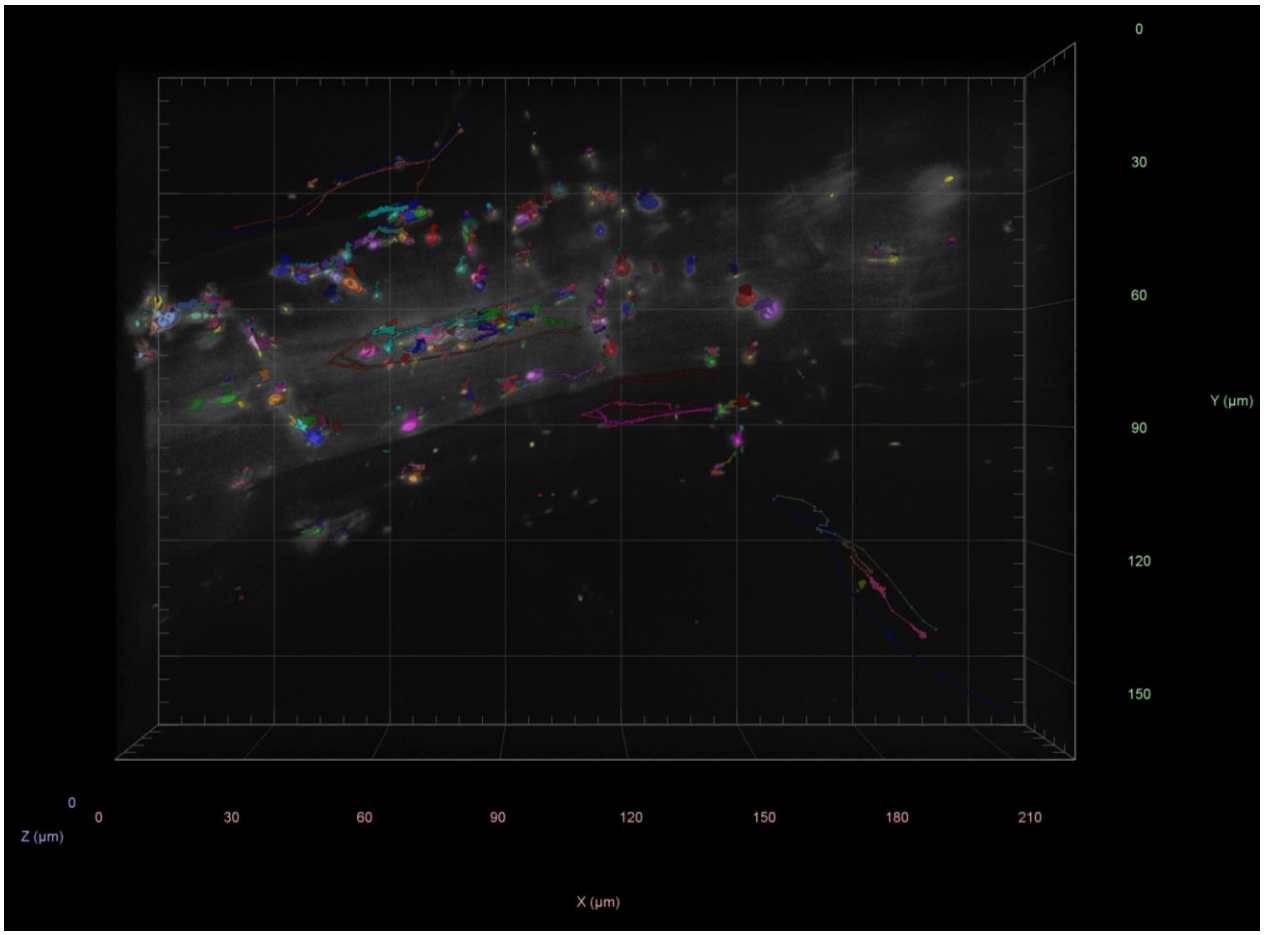

Figure 20 Representative display of corrected tracks in a control image dataset. 3D top-view of manually corrected tracks of an image dataset taken from control conditions is shown. Segmented plastids are marked as colored spheroids, tracks computed for the segments are shown in colored lines. Various tracks are displayed including tracks with no motion and long-distance transport of plastids. Distance is given in µm and indicated by the coordinate system.

Besides visual data, the automated tracking generated a bulk of X-, Y-, and Z-coordinates for each computed segment. To contextualize the generated movement data into potential movement patterns, a classification based on movement speed in relation to the angle of the movement was performed (2.2.8). This classification yielded five different classes of movement. Movement events between 0 and 0.05 µm/sec were classified as no motion since the generated movement data was categorized as noise (2.2.7). Movement events between 0.05 and 0.14 µm/sec were classified as predominantly undirected

motions, which can also be referred as small-step wiggling motions. Movement events between 0.14 and 0.3 µm/sec were classified as a mixture of undirected and directed movements. In this category, directed movements got more prominent with increasing plastid velocities, but undirected wiggling motions still were present in an evenly large amount. Movement events between 0.3 and 1 µm/sec were classified as predominantly directed motions. Most motions were performed in a directed manner, but wiggling motions of larger plastids were still present to some extent. With increasing velocities, the number of directed movements also got bigger and motions with velocities of more than 1 µm/sec were classified as directed motions (Figure 18). The classification of the movement data in five groups of motion patterns allowed for a summary of all movement events in a replicate. The relative amounts of movement events per category could be displayed for control conditions (Figure 21). Between 30 % and 70 % of the data generated were movement events that did not display motion (Figure 21 A). The amount of noise was high in all replicates and was highly influenced by the number of segments generated. Due to additional segments generated by stromules of plastids that did not move (2.2.6) image sets with generally more stromules resulted in a higher amount of segments that did not move and increased the relative number of events that were categorized as noise. 20-25 % of the movement data were classified as predominantly undirected movements (Figure 21 B). Between 5 and 15 % of the movement data in control conditions was categorized as a mixture of undirected and directed motions (Figure 21 C), while between 0.2 and 5% of the movement data of the replicates were classified as predominantly directed (Figure 21 D). In all three categories, the number of events was also influenced by falsely assigned tracks that were missed by the manual correction of the data (2.2.6). A very small number of movement events per replicate reached velocities of more than 1 µm/sec and was classified as directed movement and up to 0.3 % of the control condition movement data were sorted into this group (Figure 21 E). The general movement in the different replicates of control conditions was very versatile. Some replicates showed very low overall movement resulting in a higher amount of undirected movement, whereas some replicates displayed a very high overall movement, leading to higher numbers of directed movement. Also, the maximum speed that was measured in each replicate was highly influenced by this phenomenon. Plastids that displayed directed movement were present in the imaged frame for a limited amount of time and therefore the number of directed movement events is lower than the number of undirected motions. But in contrast to first impressions generated by the segmented image data (Figure 20), directed trafficking of plastids seemed to be exceptional cases of the plastidal motion. The little amount of fast-directed movement nevertheless allowed for speculation about potential transport mechanisms. The maximal velocities of myosins and kinesins moving across cellular filaments are well described in *Arabidopsis* (Nebenführ & Dixit, 2018) and therefore conclusions can be drawn about potential molecular mechanisms that drive the plastidal motion. To do so, the maximum velocity was recorded for each image dataset (Figure 21 E). Maximal recorded velocities ranged between 0.71 to 3.21 µm/sec with a median maximal velocity of 1.5 µm/sec. The variance of the data displayed drastic differences across the replicates in the plastid velocity. Although the movement speed of the plastids varied significantly, the maximal plastidal movement speed measured hinted at a myosin-mediated transport, since all known kinesins are shown to move much slower (Yamada et al., 2017a).

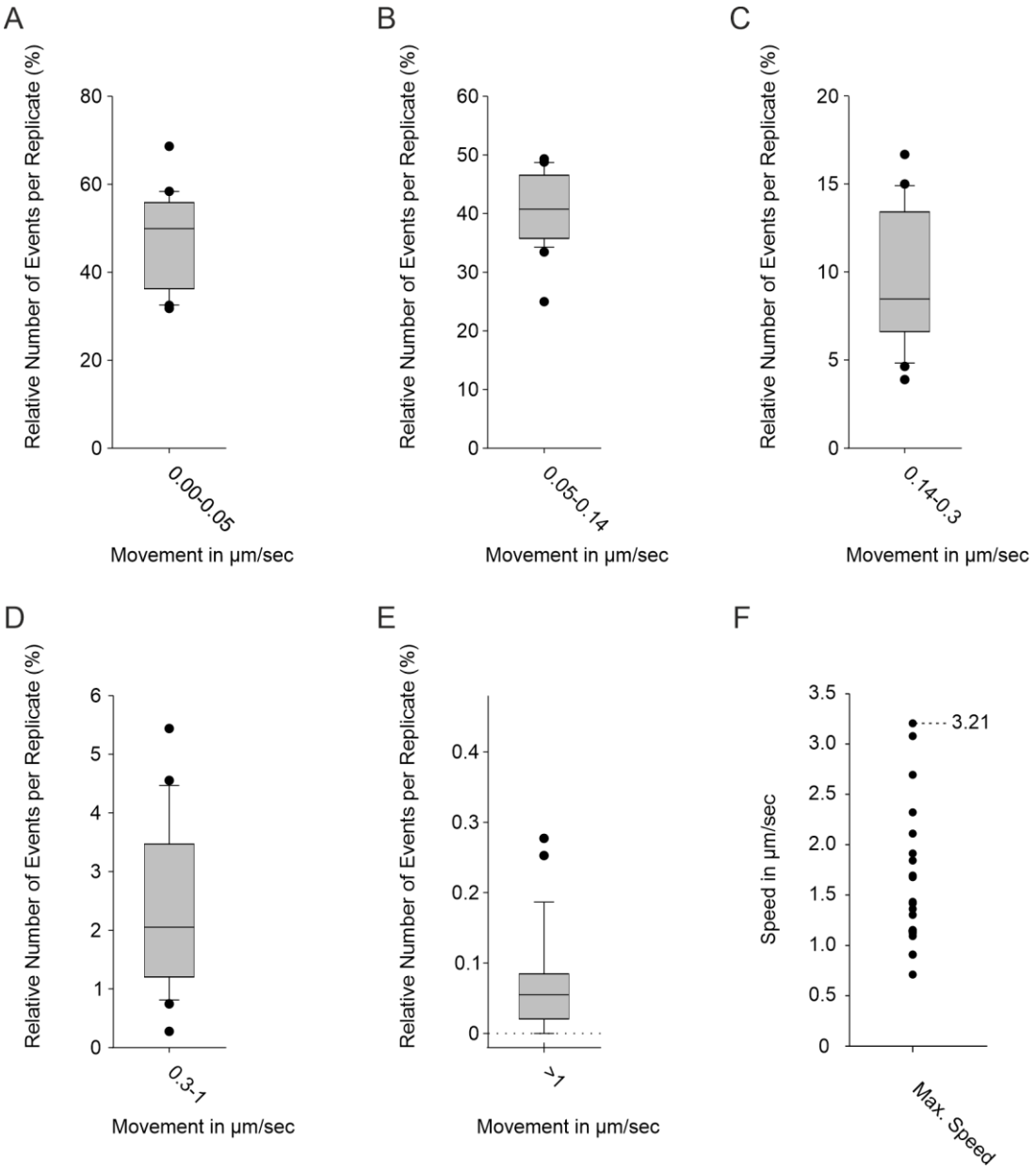

Figure 21 Plastidal movement in control conditions. A)-E) Categorization of movement events into movement patterns is defined in 2.2.8. Relative number of movement events in each category in relation to all movement events of the replicate of all replicates of control conditions (n=25) is summarized in boxplots. Boxplots show the 10 %, 25 %, 50 %, 75 %, and 90 % quartiles. Outliers are indicated as points outside of displayed quartiles. A) Movement events with no motion (0-0.05 µm/sec). B) Movement events with predominantly undirected motions (0.05-0.14 µm/sec). C) Movement events with a mixture of undirected and directed motions (0.14-0.1 µm/sec). D) Movement events with predominantly directed movement (0.3-1 µm/sec). E) Movement events with directed motion (>1 µm/sec). F) Maximal velocity of each control condition replicate is displayed. The maximal velocity measured for control conditions is marked.

3.1.3 Fast plastidal movement is directed and is mediated on distinct cellular highways

The visual analysis of the automated tracking data revealed that the fast movement of plastids was often mediated in a directed manner with a distinct course (Movie 23, 24). 3D analysis of various tracks comprising fast and directed motions with a speed of more than 0.3 µm/sec revealed that directed movement was linked to very distinct tracks in the cell (Figure 22 A, B). Different plastids displaying directed movement eventually would take the same route at different timepoints of an image set, demonstrating that those routes are stable structures. Besides this, those findings showed that fast and directed movement was somehow linked to those specific areas that reminded of cellular "highways". All plastids that moved across those cellular highways displayed the same directionality in the movement that did not reverse itself spontaneously. Exemplary for those kinds of events, three tracks that shared movement across the same cellular highway were picked and analyzed (Figure 22 C). The movement area that was shared by all three plastids was called the area of interest. The three tracks passed the area of interest between different timepoints. Track 1 passed the area between frames 11 and 28, Track 2 passed it between frames 59 and 145, while Track 3 displayed the shortest amount of time on the highway, passing it between frames 86 and 94. The fact that all three tracks passed the area of interest at different timepoints throughout the image set, showed that the cellular highways are somewhat stable structures, keeping their function for at least several minutes. All three tracks shared the same direction while passing the area of interest. However, the tracks differed in their directions prior to entering and after leaving it. While Track 2 and 3 shared a similar route before entering the area of interest, this was not the case for Track 1. Additionally, Tracks 1 and 2 shared a similar route after leaving the area of interest, while Track 3 took a different direction (Figure 22 A, B). This hints to a system in the cell, in which different routes exist that plastids can take for their movement. Those tracks seemed to be interconnected and linked together like a net. Plastids are transported across this cellular street system. With the leaving of the area of interest, Track 3 displayed a drastic loss in movement speed before the plastid changed directions hinting at a potential reorientation of the plastid before the directional change was introduced.

These findings support the assumption that those plastids were directly transported rather than only by passive cytoplasmic streaming. Cytoplasmic streaming would have led all plastids on the same tracks. The patterns reminded of either a splitting and merging highway or an entry and exit system of highways that was dynamically used by the plastids. For such motion to appear, highways needed to exist at least partially in parallel to each other or they needed to connect. The direct transport of all three plastids was performed at velocities of more than 0.3 µm/sec. The track profile revealed (Figure 22 C) that the movements of those plastids were not consistent but underwent stop-and-go patterns with changing velocities. Additionally, while Track 1 and 3 showed a very short duration in the area of interest, Track 2 had a very long dwell time with a phase of nearly no motion ((Figure 22 C) Timepoints 70-130). The same held true for Track 1 after leaving the area of interest (Figure 22 C) after Timepoint 28).

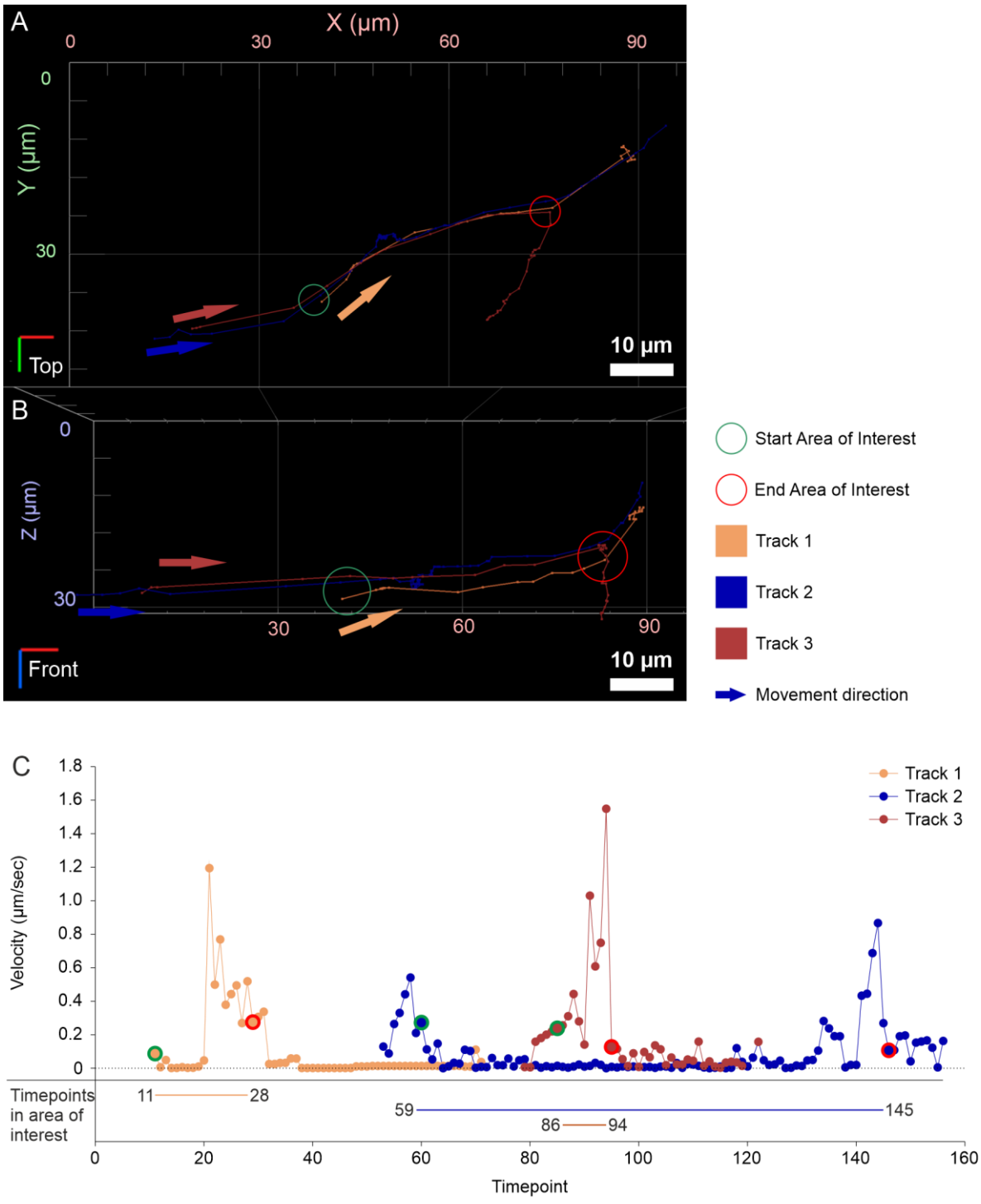

Figure 22 Plastids use distinct tracks for fast, directed movement. 3D Visualization of three plastid tracks showing directed motion through the cell. For simplicity reasons the background is zeroed and just three tracks as results of the automated tracking routine are shown. Tracks are shown from A) top and B) front. 3D directionality is given by the coordinate system and the directionality marker in the lower left. The X-dimension is shown in red, Y-dimension in green, and Z-dimension in blue. Plastids' movement direction is indicated by arrows in the respective color. C) Velocity plot of the full track of each plastid in respective colors. Velocity is given in µm/sec and is shown for each tracked timepoint. Track 1 was tracked from timepoints 10-72, Track 2 from timepoints 52-156, Track 3 from timepoints 78-119. All three tracks move across the area of interest. The start of the area of interest is indicated by a green circle, the end is indicated by a red one in A and B. In C the entering and leaving of the area of interest is marked with corresponding colors in each track. Corresponding timepoints are shown at the bottom. All tracks show

directed fast movement in the area of interest with velocities exceeding 0.3 m/sec. Two tracks also show timepoints with less to no velocity in the area of interest.

Those stop motions displayed that on the cellular highways, plastids are not transported with a uniform velocity and that although those routes seemed to be preferred for fast and directed movement of plastids, the movement could also be stopped while remaining on the cellular highway. Similar patterns have been observed in different datasets (Movie 23, 24). The appearance of such stop motion and the change in directions also hinted at a directed movement across cytoskeletal elements mediated by motor proteins rather than a movement in a passive flow.

3.1.4 Changes in environmental conditions influence the cell size but no the overall plastid number

Naturally, plants are exposed to a variety of stresses. Abiotic stresses, like water, heat, drought, or salinity stress are faced either singularly or in combination by the plants challenging their resistance and defense responses (He et al., 2018a). Since mechanisms and functionality of plastidal movement in the roots have not been investigated so far, the influence of varying conditions has not been tested. Abiotic stresses come with systemic responses by the plant in stress situations that are far from fully understood (Gong, 2021; He et al., 2018b; Nakashima et al., 2014). Salt and drought stresses are both very common, but also severe stresses for the plant, which are accompanied by many changes in the cellular regulations of the plant (Farooq et al., 2009; Zhao et al., 2021). Due to climate change, understanding plant's stress responses is more relevant than ever. Due to the stress response management of the plant, the capacity for organellar transport could be lowered or increased. Since plastids are involved in a variety of cellular functions (Rolland et al., 2018), their reaction to different stresses should be investigated. Besides salt and drought stress, the effect of other abiotic stresses like cold and heat stress on the plastidal movement was attempted to be implemented in this study. All showed low applicability within the used microscopic setup and were terminated in the early steps of the workflow.

In addition, the influence of sucrose on the plastidal movement was investigated. Sucrose is an often-used supplement for plants grown in laboratories (Murashige & Skoog, 1962). It supports the plants' growth in MS medium and is thereby used in diverse studies investigating plants' behaviors. Sucrose can directly be transformed into ATP via glycolysis and the respiratory chain, providing the plant easily accessible energy. Since myosin-related movement is ATP dependent (Nebenführ & Dixit, 2018) the question was asked if variation in the plant's energy levels influences the organellar movement of plants.

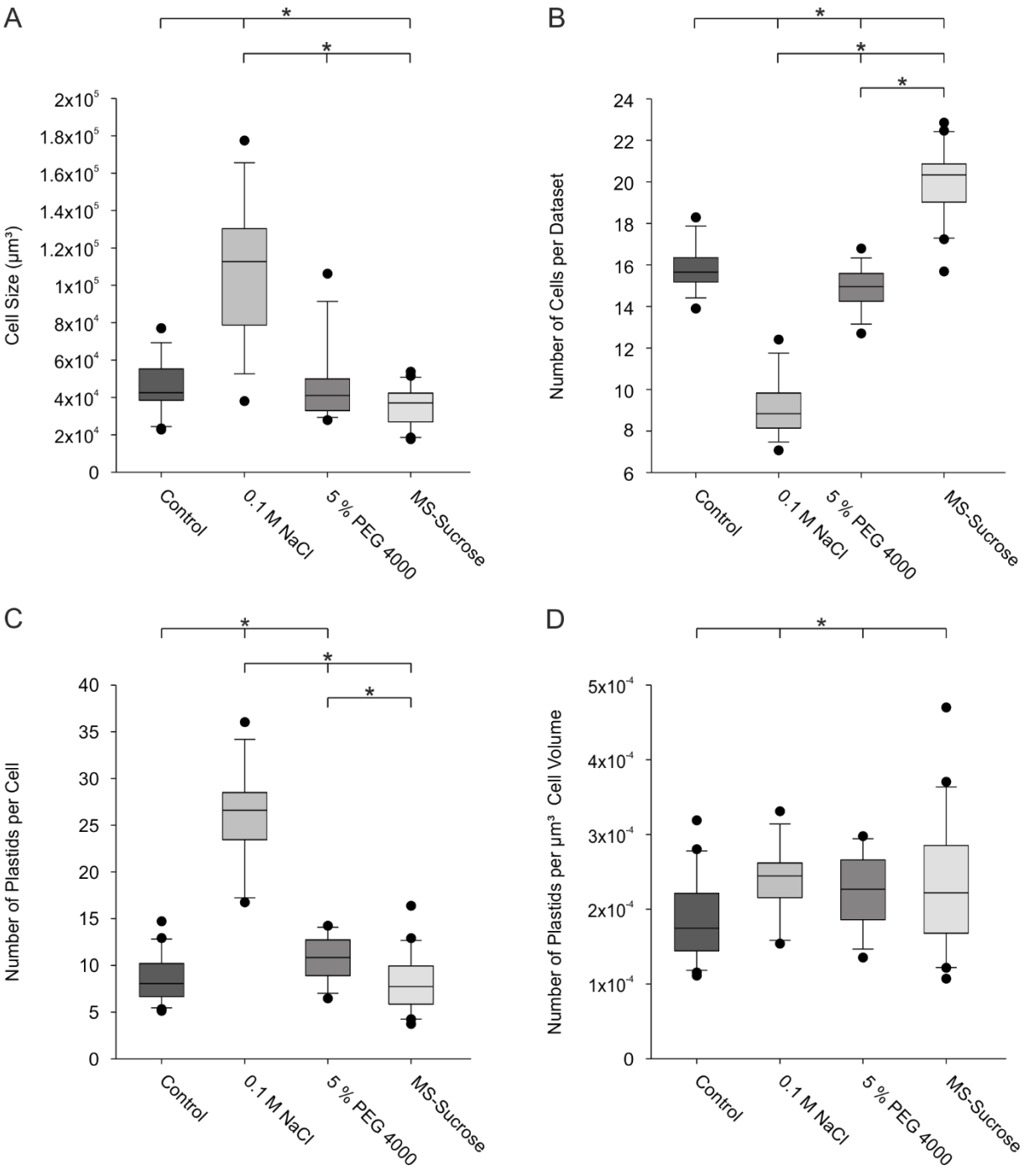

Figure 23 Descriptive analysis of cell size and plastid number in LSFM image datasets in different conditions. The graphs display: A) The distribution of the number of cells, B) the distribution of cell size in µm³, C) the distribution of the number of plastids per cell, D) the distribution of the numbers of plastids per µm³ of cell volume in each examined image dataset of all conditions. Results of control conditions (n=25), 0.1 M NaCl (n=13), 5 % PEG 4000 (n=14), ½ MS-sucrose (n=19) are shown. Boxplots display the distribution of determined values. Boxplots show the 10 %, 25 %, 50 %, 75 %, and 90 % quartiles. Outliers are indicated as points outside of shown quartiles. Statistical analysis was performed using either a student´s t-test or a Mann-Whitney rank sum test. Asterisks indicate statistical differences ($p<0.05$).

To implement salt and drought stress respectively, 0.1 M NaCl as salt stress condition and 5 % PEG 4000 as drought stress condition were chosen as the two previously defined abiotic stress conditions. Both have been applied in previous studies and were demonstrated to mimic the respective stress (Gray et al. 2012). To induce alteration in the cellular energy budget, the supplementation of sucrose to the medium was suspended.

To analyze whether applied conditions influenced the plastids of the plants, the cell size and cell number, as well as the number of plastids in relation to the cell number and the cellular volume was monitored (Figure 23). Salt stress was accompanied by a drastic increase in cell size in relation to all other conditions (Movie 3 and 4 compared with Movie 1, 2, 5-8), while the cell number was drastically decreased. Drought stress induced no significant changes in cell size, but the cell number displayed in the datasets was slightly reduced compared to control conditions, respectively. Sucrose depletion led to a significant increase in cell number compared to all other conditions while cell size was comparable to control conditions (Figure 23 A+B). The enlarged cells in salt stress conditions were accompanied by increased numbers of plastids per cell while the plastid number per cell in other conditions remained comparable to control conditions (Figure 23 C).

The enormous increase in cell size in salt stress conditions came along with an increase in plastid number per cell. To verify, if the increased number of plastids were a compensational mechanism in response to enlarged cells to keep the cellular homeostasis by maintaining the plastid ratio, the number of plastids per µm³ cell volume was calculated (Figure 23 D). All stress conditions showed comparable numbers of plastids per µm³ cell volume with a significant difference compared to control conditions. This showed that the cells in salt stress conditions compensated the enlarged cells with increasing amounts of plastids.

3.1.5 Distribution of movement speed displays hampered movement under drought stress and sucrose depletion

Following the analysis of basic appearances, the plastidal motions in salt and drought stress as well, as sucrose depletion conditions were analyzed using the automated tracking pipeline (2.2.3). The resulting movement events were categorized as previously described (2.2.8) and the relative numbers of events for each replicate were compared with each other (Figure 24). As a standard, the previously analyzed data of control conditions (3.1.2) were utilized. No statistical difference throughout all motion categories was detected between control conditions and salt stress conditions (Figure 24 A-E), showing no effect of salt stress on the plastidal motion. Drought stress conditions displayed a comparable amount of undirected movement to control conditions and salt stress conditions (Figure 24 B, C), but generally displayed a much lower amount of directed motions (Figure 24 D, E). Furthermore, the number of plastids showing no movement was higher than in salt stress and control conditions and was settled between 50 and 70 % of the overall data (Figure 24 A). Drought stress influenced the plastidal motion to some degree but did not abolish it. The highest contrast to the other three conditions was observed in sucrose depletion conditions. Between 60 and 90 % of the movement data was summed up in the no-motion category (Figure 24 A).

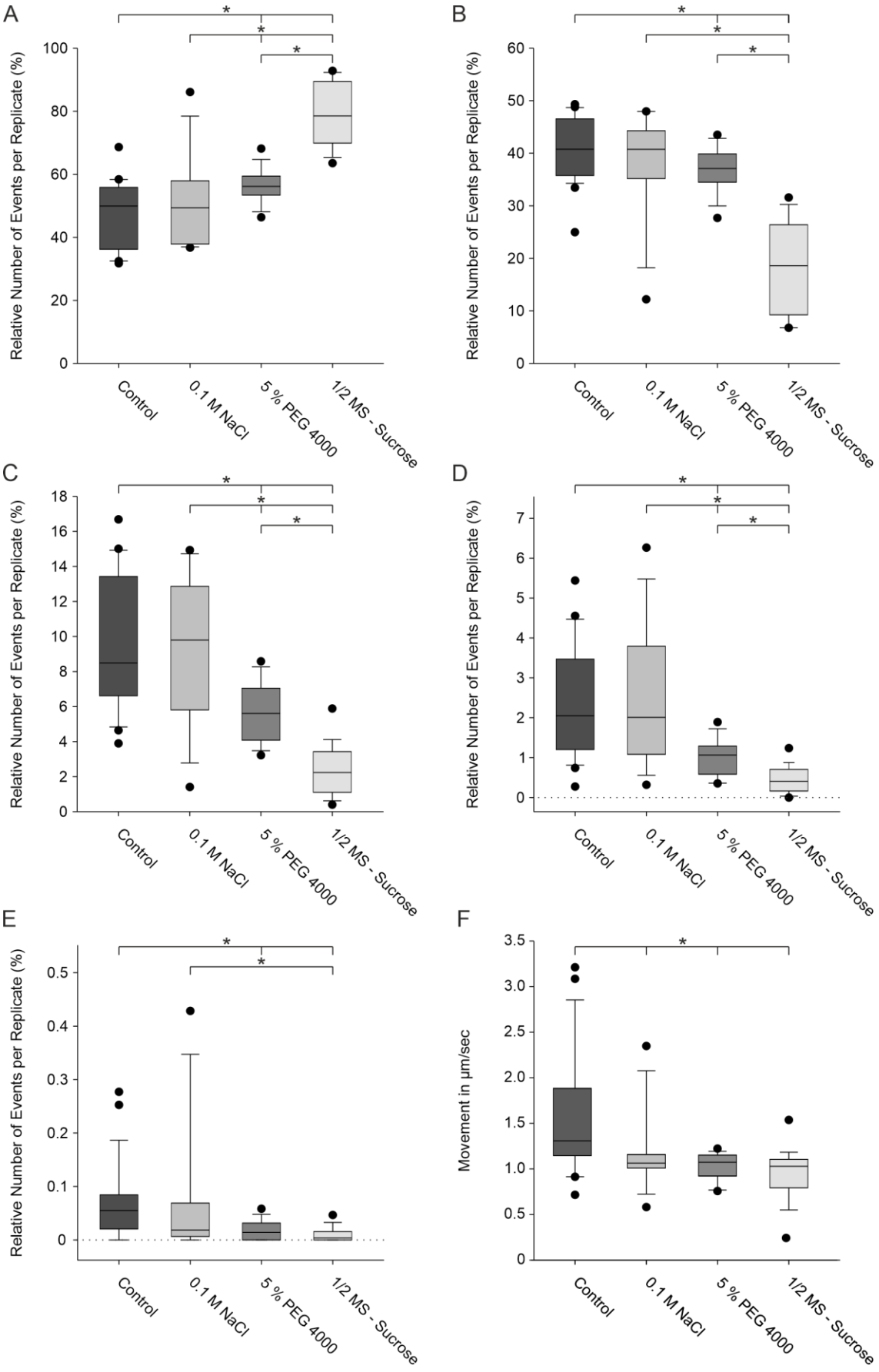
A
Relative Number of Events per Replicate (%)
Control
0.1 M NaCl
5 % PEG 4000
1/2 MS - Sucrose
B
Relative Number of Events per Replicate (%)
C
Relative Number of Events per Replicate (%)
D
Relative Number of Events per Replicate (%)
E
Relative Number of Events per Replicate (%)
F
Movement in µm/sec

Figure 24 Movement event distribution of different conditions. A)-E) Categorization of movement events into movement patterns defined in 2.2.8. Relative number of movement events in each category in relation to all movement events of the replicates of control conditions (n=25) 0.1 M NaCl (n=13), 5 % PEG 4000 (n=14), ½ MS-sucrose (n=20) is summarized in boxplots. A) Movement events with no motion (0-0.05 µm/sec). B) Movement events with predominantly undirected motions (0.05-0.14 µm/sec). C) Movement events with a mixture of undirected and directed motions (0.14-0.3 µm/sec). D) Movement events with predominantly directed movement (0.3-1 µm/sec). E) Movement events with directed motion (>1 µm/sec). F) Maximal velocity of each control condition replicate is displayed. Boxplots show the 10 %, 25 %, 50 %, 75 %, and 90 % quartiles. Outliers are indicated as points outside of displayed quartiles. Statistical analysis was performed using a student's t-test or a Mann-Whitney rank sum test. Asterisks indicate statistical differences ($p<0.05$).

Undirected motions were present in sucrose depletion but to a much lower extent, than in the other three conditions (Figure 24 B, C), while the directed movement was nearly abolished (Figure 24 D, E). Taken together, sucrose depletion influenced the plastidal motion to a very high degree.

Similar to control conditions, the maximal velocity for each replicate was determined to conclude the potential underlying molecular mechanisms (Figure 24 E). While the maximal velocity of control conditions reached more than 3 µm/sec, the maximal velocities of all other conditions were much lower. Salt stress conditions, like control conditions, displayed a big variance in the maximal velocity of the replicates, but still showed a significant difference, with a median maximal velocity of 1.1 µm/sec. In contrast, the median maximal velocity of drought stress and sucrose depletion was settled around 1 µm/sec, but the samples displayed less variance. Although the maximal movement speeds measured in salt stress, drought stress, and sucrose depletion differed significantly from the measured values of control conditions, all velocities hinted at an actin-myosin-mediated transport mechanism for plastids.

3.1.6 Motion of plastids lacking stromules

The automated 4D analysis of the plastidal movement resulted in a broad overview of the general plastidal motion distribution under different conditions. In addition, specific tracks were tracked in detail throughout the 3D environment of the cell. Nevertheless, the automated approach was extremely hampered by the dynamic nature of the root plastids. To gather further information about the plastid motility and to contextualize the automatically generated results, the diversity of the plastidal movement was analyzed manually. Therefore, the 4D image data (3D over time) that was used during the automated tracking analysis was converted into 3D datasets (2D over time) using maximum intensity projections. In addition, to draw a detailed comparison to the tracking data that was acquired automatically, all datasets that were used during automatic 4D tracking were subjected to a detailed analysis of the plastidal motion using ImageJ (Fiji) ver. 1.53c (Schindelin et al., 2012). The image data was examined manually, and different motion patterns were described (2.4). By the deletion of the Z-axis, different results were expected compared to the automated analysis. However, variations were expected to stay minimal, since recent findings on image sets produced during this work showed that up to 90 % of the plastidal movement can be described by the X- and Y-dimensions (Plomer, unpublished).

For a detailed description of the plastidal movement patterns using 3D datasets, the movement patterns of plastids were divided, guided by the morphology of the plastids. Movement patterns of plastids without stromules and movement patterns of plastids displaying stromules were differentiated. As a great

proportion of the examined plastids, the movement patterns of plastids without stromules were analyzed. The lack of stromules limited the opportunities for movement options to either a motion or no motion of the plastid. Plastids that showed a maximal motion of 4 µm throughout the duration of the imaging without forming stromules, were classified as plastids without stromules that showed no motion (Figure 25 A, Movie 10). The geometrical centers of the plastids were used as relation to follow the movements.

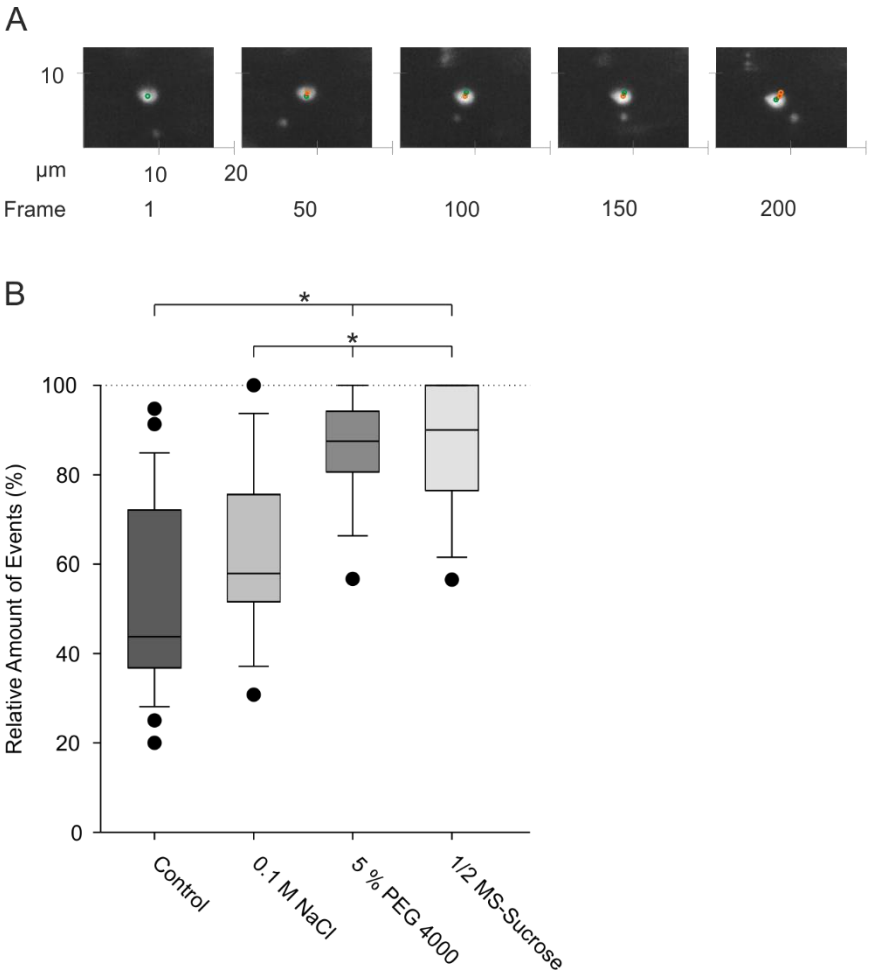

Figure 25 Plastid body shows no motion. Plastids without stromules, that showed no motion throughout the time of the image acquisition were analyzed. A) Schematic display of plastids without stromules and motion. Plastid was followed over a time span of 200 frames representing 852 seconds of image material. The motion of the plastid is indicated with green points marking the plastid location in each respective picture and orange points marking the plastid location in the previous pictures. A red line indicates the path taken by the plastid. Distances are shown in µm and displayed in coordinate systems at each frame. B) Relative number of plastids without stromules and motion of each analyzed dataset (Control condition: n=26, 0.1 M NaCl: n=13, 5 % PEG 4000: n=17, ½ MS-Sucrose: n=19) is displayed in relation to all plastids without stromules observed, respectively. Numbers of all analyzed replicates are displayed as boxplots displaying the 10 %, 25 %, 50 %, 75 %, and 90 % quartiles. Outliers are indicated as points outside of boxplots. Statistical analysis was performed using a student's t-test or a Mann-Whitney rank sum test. Asterisks indicate statistical differences ($p<0.05$).

Successively, the relative number of plastids without stromules and motion was determined. Therefore, all image sets were conducted to a manual analysis, and plastids matching the criteria were picked out and set in relation to the total amount of plastids without stromules for each image dataset, respectively. The median value (Figure 25 B) of the number of plastids without stromules and motion was settled at about 40 % in control conditions, while reaching 60 % for salt stress conditions and about 90 % for drought stress. The second motion option for plastids lacking stromules was to show motion. Again, the geometrical center of the plastids was used to follow the movement. A plastid was classified as moving if its center moved more than 4 µm throughout one image set (Figure 26 A, Movie 11, 23, 24).

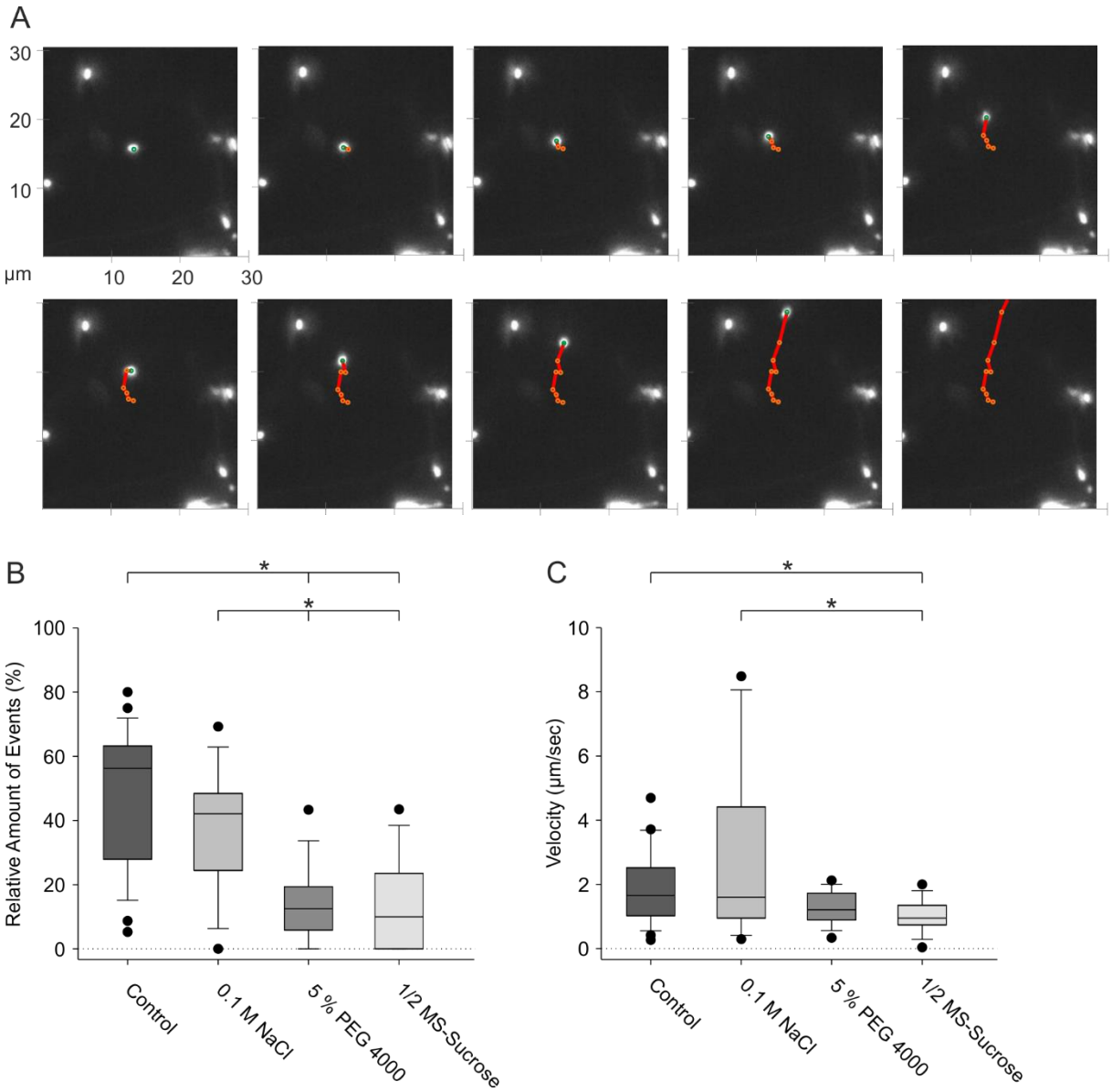

Figure 26 Plastids without stromules show motion. Plastids without stromules that showed motion were analyzed. A) Schematic display of movement events that were classified as plastids without stromules displaying movement. Plastid was followed over a time span of 10 consecutive frames, representing 43 seconds of the image material. Plastid delocalization was followed over time, represented by the red line. Green dots display plastid localization in the respective frame, orange dots represent plastidal localization in the previous frames. Scale is introduced in form of a coordinate system and displays distance in µm. Distances are indicated in the first frame. B) Relative number of plastids without stromules which displayed motion of each analyzed dataset (Control condition: n=26, 0.1 M NaCl: n=13, 5 % PEG 4000: n=17, ½ MS-Sucrose: n=19) is displayed in relation to all plastids without stromules observed, respectively. C) Maximal motion measured in between two frames for each replicate was summarized in form of boxplots. Replicates showing plastids without stromules that displayed motion were integrated (Control condition: n=26, 0.1 M NaCl: n=13, 5 % PEG 4000: n=15, ½ MS-Sucrose: n=14). Velocity is displayed in µm/sec. B+C) Numbers of all analyzed replicates are summarized in form of boxplots displaying the 10 %, 25 %, 50 %, 75 %, and 90 % quartiles. Outliers are indicated as points outside of boxplots. Statistical analysis was performed using the Mann-Whitney rank sum test. Asterisks indicate statistical differences ($p<0.05$).

The number of plastids that showed those defined motions was determined manually for each dataset and set into relation to the total number of plastids without stromules for each replicate respectively (Figure 26 B). Naturally, the relative amounts of plastids without motion matched the numbers presented for the non-moving plastids (Figure 25 B) in a reverse manner. According to the previous results, the majority about 60 % of the plastids lacking stromules displayed movement in control conditions. All stress conditions showed less movement with 40 % in salt stress conditions and 10 % in drought stress and sucrose depletion, respectively. Most of the plastids without stromules were linked to very distinct tracks, which matched the previously discussed track "highways" (Figure 22, Movie 23, 24). As previously mentioned, those tracks showed a diversity of plastid velocities reaching from very low to very high movement speeds. These diversities of motions were also observed during the manual investigation. Generally, motion patterns like stop-and-go motions, wiggling motions and a directed motion were observed for those plastids. To get insights into the underlying movement mechanism that drives plastidal motion, the velocities of the fastest tracks in each dataset were measured and the fastest motion captured for each dataset, was depicted for comparison between the conditions (Figure 26 C). The fastest events were specifically chosen for comparison because the maximal motion allows for conclusions about potential motor proteins that might be associated with the movement. The measured plastids were all transported on seemingly directed paths through the cell. In contrast to the automated analysis, the results taken from the manual analysis were lacking the Z-axis and therefore less motion was expected. Interestingly the maximal motions measured in the manual analysis were higher throughout every condition, pointing out the lacks in the automated analysis. The maximal speed of control conditions was measured at 4.6 µm/sec. In contrast, the maximal velocity measured in salt stress conditions was much higher at 8.5 µm/sec (Movie 12). This was the fastest motion measured throughout all image data. The maximum velocities for drought stress and sucrose depletion are very similar, settled around 2.1 and 2.0 µm/sec, respectively. As with the amount of moving plastids, the overall maximal velocities of all datasets were reduced in drought and sucrose depletion conditions, pointing to a general mechanism that is linked between overall and maximum velocity for plastids without stromules.

3.1.7 Plastidal movement can be associated with other organelles

The function of plastids in the cellular context is widespread (Rolland et al., 2018). They are involved in several crucial cellular pathways, of which most rely on nutrient and molecule exchange with other organelles such as the ER. In addition, retrograde signaling with the nucleus is a crucial mechanism for maintaining plastid and cellular function under normal conditions and more so at pathogen defense (Kumar et al., 2018; Rolland et al., 2018), since most of the plastidal genome was transferred to the nucleus during evolution. One working theory of organellar movement is that organelles can be attached to each other and are transported together through the cell (Vick & Nebenführ, 2012). Even though the image data acquired in this study did just rely on one fluorescent label that was targeted to the stroma of the plastids, such clustering around a cellular component was detected (Figure 27 A, Movie 21). Due to the lack of additional labeling, conclusions were difficult to draw from those findings. However, several times throughout the image datasets various number of plastids were detected, building a sphere like shape, creating the image of surrounding a cellular component.

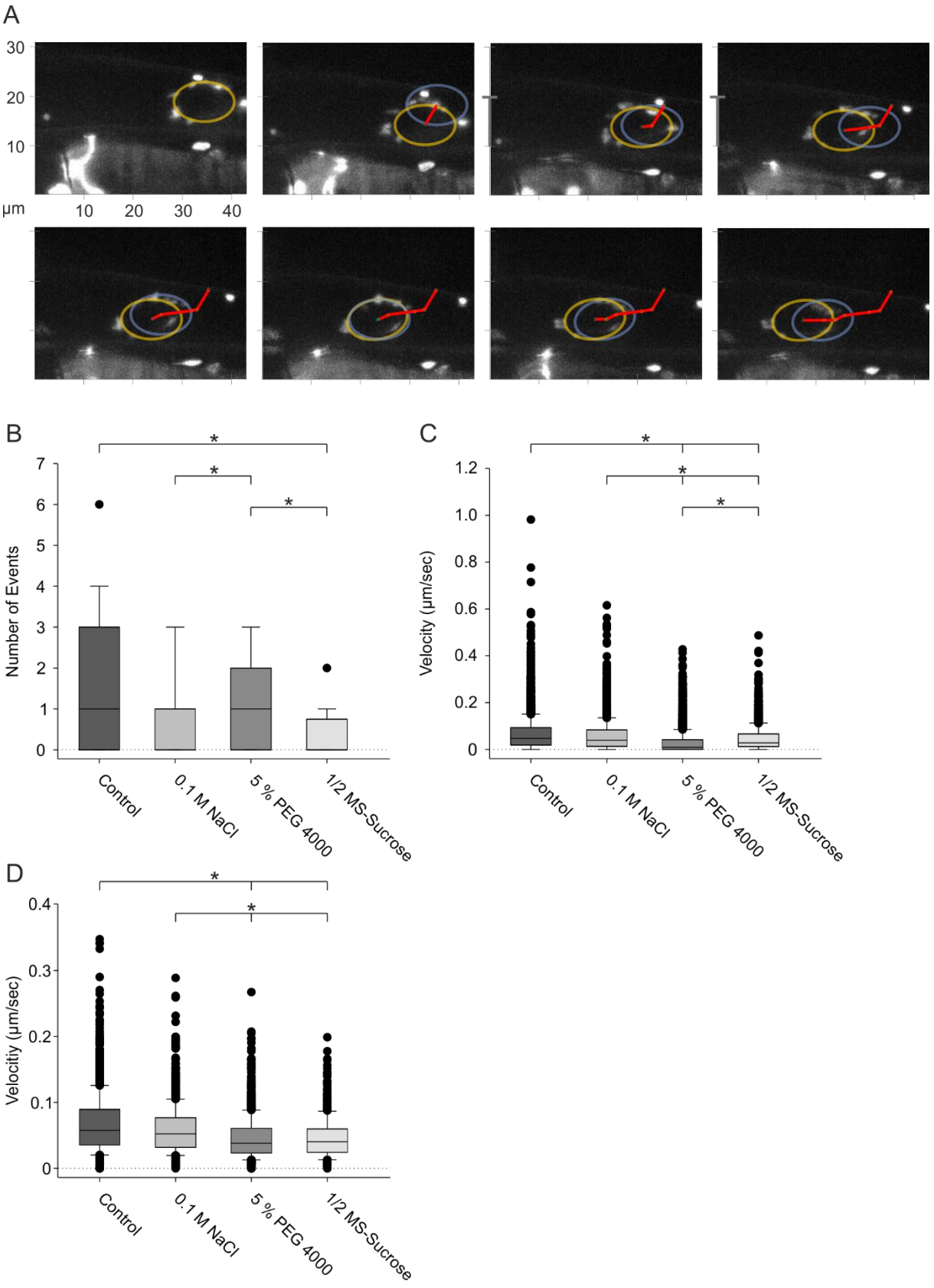

Figure 27 Plastids are attached to another organelle and are transported with it. The movement of plastids that are assumed to be associated to other organelles was followed. A) Schematic display of plastids that are associated with another organelle.

Associated plastids were identified by characteristic clustering. Plastids surrounded a potentially oval or circular shape of up to 10 µm and moved alongside of it in the clustered formation. A described event is displayed in a timeframe of eight consecutive frames. The organelle to which plastids were attached is indicated by circles. Plastids attached to the organelle are visible in all frames maintaining the circular shape. The movement of the organelle was followed indicated by the red line. Green dots represent the center of the organelle. Yellow circles indicate the position of the organelle in the respective frame, blue circles indicate the position of the organelle in the previous frame. Distance is given in µm and indicated in each frame by the coordinate system. B) Number of described events identified in replicates throughout the different conditions (Control condition: n=27, 0.1 M NaCl: n=15, 5 % PEG 4000: n=17, ½ MS-Sucrose: n=20). The number of events of each dataset is summarized in form of boxplots. C) Movement speed of three randomly chosen individual plastids associated with the organelle for one event per replicate was measured. The total number of movement events is displayed in µm/sec in form of boxplots. D) Movement speed of all three plastids measured in C) was averaged for each replicate. The average movement speed of the plastids displays the movement speed of the organelle that moves through the cell. All average velocities are displayed in µm/sec in form of boxplots. Boxplots display the 10 %, 25 %, 50 %, 75 %, and 90 % quartiles. Outliers are indicated as points outside of boxplots. Statistical analysis was performed using either a student´s t-test or a Mann-Whitney rank sum test. Asterisks indicate statistical differences ($p<0.05$).

The size of those events comprised usually between 5 and 10 µm in diameter, leading to the speculation that those plastids were associated with nuclei. This impression was manifested since those were very rare events and did not occur more than one time per cell. Besides being attached to a structure that was most probably the nucleus, the plastids moved together in the clustered formation indicating that not the plastids themselves moved, but the object the plastids were attached to (Figure 27 A, Movie 21). The number of those events detected in each dataset was determined (Figure 27 B). A maximum of six accumulations of plastids moving with a surrounded object was found in all replicates throughout all conditions. Salt stress and sucrose depletion displayed fewer events than control and drought stress conditions. To categorize movement patterns of plastids found in the image data, the movement of those plastids was followed. Besides a steady moving direction of the underlying object, the plastids themselves showed motion. The motions of three randomly chosen plastids were followed over time for at least one clustering event per dataset (Figure 27 C). Many of the analyzed plastids showed individual motion, shifting the organelle across the borders of the spheric shape, on top of the collective motion that transported all associated plastids through the cell. Nevertheless, the movement speed of the analyzed plastids showed that the general velocity of the clustered plastids was very low, normally not reaching 0.05 µm/sec for each condition. The maximal speed measured for the individual plastid motion was 1 µm/sec in control conditions. Other conditions did not pass 0.6 µm/sec in maximal velocity. The shape of plastids was not analyzed in detail, but the clusters harbored plastids that formed stromules, as well as such without membrane extrusions. Since the positioning of those plastids in the cell relied on the movement speed of the underlying object, the movement speed of this object was approximated. Since no labeling was apparent to visualize the nucleus or other cellular compartments than the plastid, the direct measurement of the underlying movement speed was not possible. Nevertheless, to get an impression, the velocity of all plastids measured for each clustering event (Figure 27 C) was averaged for each frame, representing an approximation to the relocation speed of the underlying movement. The median movement speed of the clusters was very slow, not passing 0.1 µm/sec. Peak velocities were measured at 0.3 µm/sec for nearly all conditions. All stress conditions displayed less movement than the control conditions, pointing out deficits in those movement actions. The collective motion of plastids showed that besides moving individually, plastids are also able to associate with other cellular organelles and components and thereby be transported through the cell.

3.2 The dynamics of root plastid stromules

3.2.1 Large fractions of root plastids form stromules

Stromules in roots have been described as a common feature of plastids (Köhler & Hanson, 2000) and besides changing the plastid's appearance from a spherical into a diversity of shapes they have the ability of independent, dynamic movement isolated from the plastid body (Movie 1). Both properties interfered greatly with the automated tracking algorithm and raised questions about the general mechanism underlying the plastidal movement. The only form of motion extensively described in a plastid family is the light avoidance movement of chloroplasts (Higa, Suetsugu, & Wada, 2014; Suetsugu et al., 2016). The driving force of plastidal movement in roots cannot be the same for several reasons. Firstly, the light avoidance movement is triggered by blue light receptors (Jarillo & Cashmore, 2001; Kagawa et al., 2001), which need light that normally does not reach the roots. Secondly, the light avoidance movement of chloroplasts is mediated by the protein CHUP1 (Schmidt Von Braun & Schleiff, 2008). However, this factor is barely transcribed in roots (Oikawa et al., 2008) and as such is very unlikely to mediate the plastidal movement. Thirdly, the movement speed of chloroplasts while performing the light avoidance movement is reaching up to 1 µm/min (Wada & Kong, 2018). Plastids were shown to move at higher velocity levels reaching several µm/sec (Figure 14). All findings indicate that plastidal motion is driven by a different mechanism. Several questions emerged from this assumption: I) What is the movement mechanism that drives plastidal motion? II) Considering that stromules seem to have defined movement and anchor mechanics (Erickson et al., 2018; Kumar et al., 2018): What are the molecular mechanisms driving stromule motion? III) Since stromules are crucial components of root plastids and can show individual motion (Erickson et al., 2018): Are stromules involved in the movement of root plastids and part of the machinery that drives the plastidal motion? IV) Since the visual analysis of the 4D image data revealed a variety of different movement events: Do different forms of motions exist in plastids and if so, what do they look like and how are they affected by stromule formation? In alignment with previous procedures (3.1.6), 3D maximum intensity projections were obtained from all automatically analyzed image datasets and the analysis of the stromule dynamic was performed in a 3D environment. This decision was mainly affected by the fact, that stromules were not resolved in the 4D environment due to a low resolution along the Z-axis (Figure 6).

To tackle the above formulated questions, the number of plastids possessing stromules was determined (Figure 28). The relative number of plastids forming stromules in relation to all plastids was calculated for each replicate. For this determination, only image sets providing a sufficient resolution to distinguish stromules were considered. A stromule was defined as a tubular structure that was distinguishable and expanding from a plastid (Figure 28 A). The number of stromules per plastid was not considered during the analysis. The number of stromules that were formed was highly dependent on the examined condition and showed great variance in the replicates (Figure 28 B, compare Movie 1-8). In control conditions, approximately 70 % of plastids possessed stromules. In comparison, the number of stromules in the other three conditions was significantly reduced. While no difference was observed between salt and drought stress conditions, showing both around 50 % of plastids forming stromules, the number of plastids that formed stromules in sucrose-depleted samples was drastically reduced and was settled around 25 % through the replicates. Generally, plastids of all sizes formed stromules (Movie 1). The stromule length

differed greatly across the plastids but a correlation between plastid size and stromule length was not performed, due to a lack of data regarding plastid size (3.1.1).

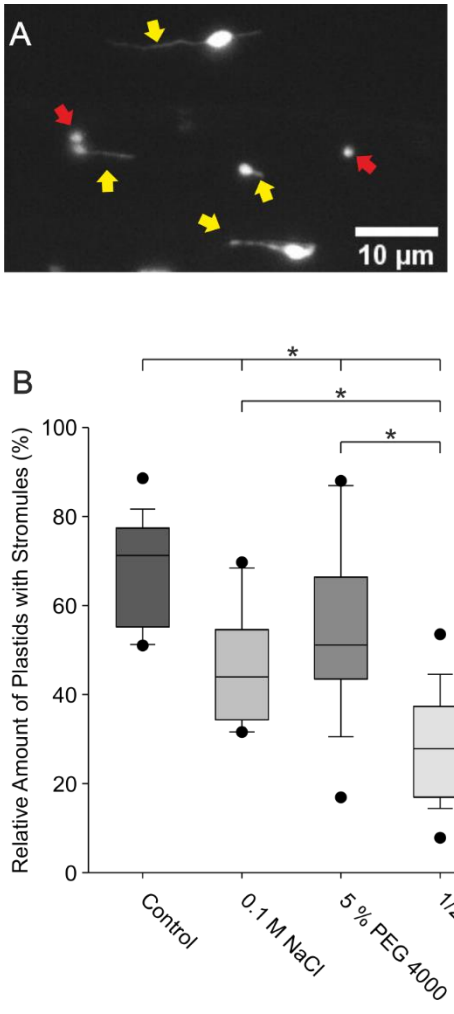

Figure 28 The abundance of stromules in the image data. The number of plastids forming stromules was determined in each image dataset. A) Presentation of plastids that were considered for the evaluation. A stromule was defined as a visible tubular structure that emerged from the plastid body. Yellow arrows indicate plastids that form varying structures, which were considered as stromules, red arrows point to plastids without stromules. B) Relative number of plastids that form stromules was calculated from all plastids in each dataset, respectively. Graphic includes all datasets that showed adequate level of detail to distinguish a stromules from the background (Control condition: n=16, 0.1 M NaCl: n=10, 5 % PEG 4000: n=16, ½ MS-Sucrose: n=20). Relative number of plastids possessing stromules of all included datasets are visualized as boxplots showing the 10 %, 25 %, 50 %, 75 %, and 90 % quartiles. Outliers are indicated as points outside of shown quartiles. Statistical analysis was performed using a Mann-Whitney rank sum test. Asterisks indicate statistical difference ($p<0.05$).

3.2.2 Stromules with varying lengths are often observed in root plastids

All subtypes of plastids can form stromules, but they are preferably formed at root plastids (Köhler & Hanson, 2000). The functionality of those membrane extrusions is under investigation and discussion up to date. Experimental evidence has shown that stromal molecules can flow freely through the stroma filling the protrusions (Kwok & Hanson, 2004b) and thereby supporting the working theory that stromules facilitate the exchange of molecules between organelles (Natesan et al., 2005). It was shown that stromules use different parts of the cytoskeleton for anchoring, whereas the movement and extension of stromules are not clarified by now (Erickson et al., 2018; Kumar et al., 2018). This study aimed for a detailed description of the stromule dynamics and to describe potential connections between stromule and plastidal movement. To do so, the movement of stromules was analyzed individually but also dependence on the plastid body and vice versa. A focus was laid on the appearance of specific motion patterns involving stromules, the overall occurrence of those events and the speed in which different

motion patterns were carried out. Superordinated were the main questions defined in 3.2.1 led by the question, if stromules are involved in the plastidal motion.

Stromules were shown to be very dynamic features, with a great potential for independent velocities merging from the plastid body (Kwok & Hanson, 2004b). By their motion, stromules could facilitate the movement of the plastid body in different forms, for example in an amoeboid manner. Stromules have been found to elongate for up to several hundreds of µm (Waters et al., 2004), offering great potential for mediating the movement of the plastid body. Stromule length was determined by measurement of visible stromules throughout the first frame of each image set (Figure 29). Stromules were defined in between the visible tubulation of the plastid membrane and the end of the stromule (Figure 29 A). Besides linear stromules, also branching stromules were observed (Movie 16). The length was taken only from the longest arm of the branch. The general stromule length differed greatly covering lengths between 1 µm up to several dozen throughout all conditions (Figure 29 B). Control conditions displayed the longest stromules of all tested conditions and harbored the longest stromules with 40 µm in length. Since the stromules measured for this analysis only comprised stromules in the first frame of each replicate, the stromule length could be much higher, than displayed by the analysis. The longest stromule throughout all image data was detected in control conditions reaching out to 60 µm in length (Movie 9).

Salt stress conditions displayed slightly shorter stromules with approximately. 30 µm in maximum length (Figure 29 B), but also the overall length of stromules was higher compared to drought stress and sucrose depletion. The last two conditions displayed very similar stromule lengths, with about 20 and 25 µm at maximum, respectively. The median stromule length of all conditions remained between 4 and 8 µm, showing that long stromules up to several dozen of µm were rather the exception than the rule. Stromule length in general seemed to correlate with the size of the plastid. Small plastids were found to form small stromules and vice versa (Movie 1), demonstrating the necessity of excess membrane for stromule formation.

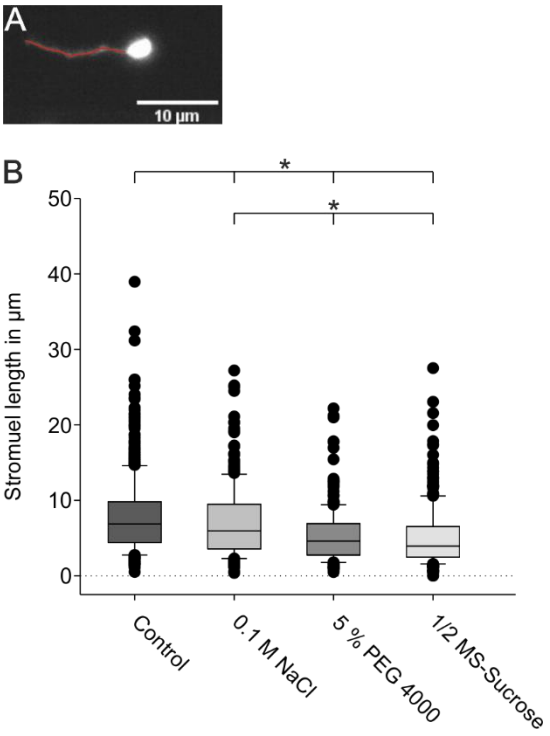

Figure 29 Stromule length distribution of plastids. The Stromule length of plastids forming stromules was determined. A) Stromules were measured from the stromule origin of the plastid body to the stromule tip. The stromule origin was characterized by a visible tubulation of the plastidal surface. Length measurement is indicated exemplarily by the red line. Only the longest stromule of each plastid was considered, although plastids could form more than one stromule. Also, the longest branch was considered if a stromule showed branching. B) Stromule length of all plastids forming stromules visible in frame 1 of each replicate was analyzed (Control condition: n=576, 0.1 M NaCl: n=277, 5 % PEG 4000: n=265, ½ MS-Sucrose: n=310). Stromule length is shown in µm. Lengths of all analyzed stromules are summarized in form of boxplots displaying the 10 %, 25 %, 50 %, 75 %, and 90 % quartiles. Outliers are indicated as points outside of box plots. Statistical analysis was performed using the Mann-Whitney rank sum test. Asterisks indicate statistical differences ($p<0.05$).

3.2.3 Plastids with stromules can show no movement

As demonstrated by the automated tracking analysis, plastids have very different movement patterns. Besides very quick motions, a great proportion of plastids showed little to no motion (Figure 24 A, Movie 13). To describe the movement patterns that were observed by either plastids or stromules and to draw possible conclusions in the leading questions of the stromule dynamic (3.2.1), different movement patterns of plastids with stromules were characterized. As plastids without stromules (Figure 25), plastids that formed stromules could display no movement throughout the image set (Figure 30 A). No movement was characterized as no displacement of either the plastid body or parts of the stromule of more than 4 µm throughout one image set. The relative number of plastids with stromules that displayed no motion was determined throughout all conditions in relation to all plastids that formed stromules (Figure 30 B). In control conditions, the relative number of events of non-moving plastids with stromules was lowest. Nevertheless, the maximal number of non-moving plastids measured for control conditions was higher compared to salt and drought conditions, indicating that the most stromule movement takes place in these conditions. Events of non-moving plastids with stromules under sucrose depletion showed high variability. However, a significantly higher number of events of non-moving plastids with stromules was detected compared to all other conditions.

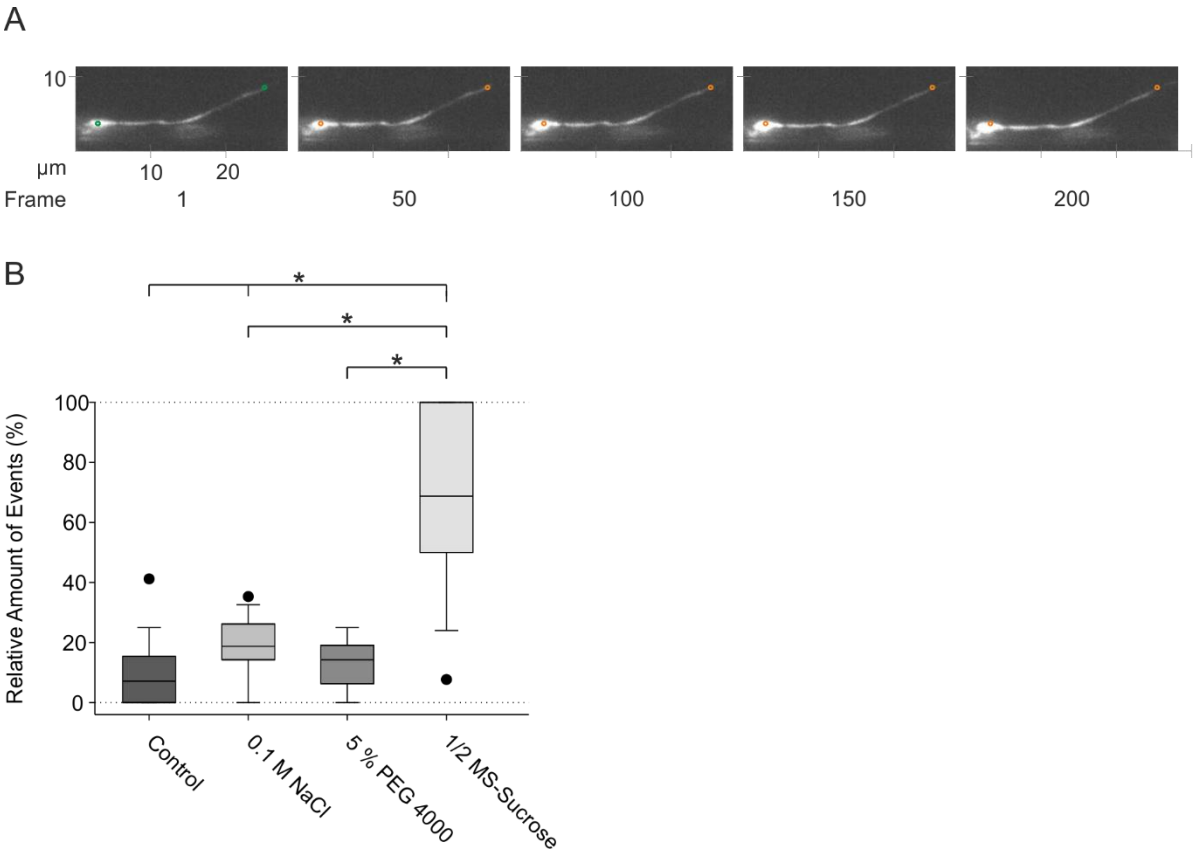

Figure 30 Plastids with stromules show no motion. Plastids with stromules and no visible motion were analyzed. A) Schematic display of a plastid with a stromule that showed no motion throughout an image series. Plastid is shown in frames 1, 50, 100, 150, and 200. Locations of the plastid body and the stromule tip in the first frame are marked in green for frame 1 and orange for consecutive frames. Distance is given in µm and indicated by the coordinate system in each frame. B) Relative amount of plastids with stromules that displayed no movement is shown in relation to all plastids forming stromules that were registered in the respective replicate. Relative number of events of each analyzed replicate (Control condition: n=27, 0.1 M NaCl: n=13, 5 % PEG 4000: n=17, ½ MS-Sucrose: n=19) was summarized in form of boxplots. Boxplots display the 10 %, 25 %, 50 %, 75 %, and 90 % quartiles. Outliers are indicated as points outside of boxplots. Statistical analysis was performed using either a student´s t-test or a Mann-Whitney rank sum test. Asterisks indicate statistical differences ($p<0.05$).

3.2.4 Stromules can move independently with varying velocities

As very dynamic structures, stromules have been shown to associate with the cytoskeleton and other organelles (Erickson et al., 2018; Köhler & Hanson, 2000; Kumar et al., 2018; M. H. Schattat & Klösgen, 2011). The exact mechanisms of stromule dynamics are still not elucidated and are under investigation. It was shown that stromules use actin filaments as anchor points (Kumar et al., 2018), and that the movement relies on the presence of myosin family XI motor proteins (Natesan et al., 2009), suggesting an underlying interaction with the actin-myosin machinery or cytoplasmic streaming to be the motor behind the movement. Besides, stromule branches have been shown to co-locate with microtubules and movement has been associated with microtubules (Erickson et al., 2018; Kumar et al., 2018), which challenges the myosin-dependent movements that were described. The dynamic of stromule formation is still under investigation and different assumptions of stromule dynamics are discussed up to now. The debates about the mediation of the stromule movement cover various options, associations with the

cytoskeletal movement machineries or cytoplasmic steaming are in favor of the discussions and generally accepted (Erickson & Schattat, 2018). However, most of the data generated on stromule dynamics were gathered from chloroplasts, not root plastids (Jessica L. Erickson et al. 2018). Following the results of this work, root plastid movement differs greatly from chloroplast movement in the green tissue.

Here, the stromule dynamics were analyzed with the ambition to characterize how stromule dynamics contribute to the plastidal motion individually and in relation to the movement of the plastid body. To tackle those questions, the stromule growth and retraction velocities were measured (Figure 31 A). Stromules were observed to individually prolong and retract from plastid bodies (Movie 14). Most of the time, the plastid bodies stayed in place during stromule elongation/retraction, therefore excluding the possibility that stromules are singularly formed by attachment of the stromule tip to cytoskeletal elements and sole movement of the plastid body. Furthermore, no distinct directionality of stromule extension and retraction was found reducing the chance of possible cytoplasmic streaming effects involved in stromule formation. Stromule tips were found to co-locate with other plastids in the observed 2D perspective hinting at plastidal interaction (Movie 1, 6). The stromule movement with a fixed plastid body was a very common feature of plastids throughout the observed image material (Movie 1-8). To quantify these findings, the relative number of anchored plastids with moving stromules was calculated in relation to the overall number of plastids forming stromules (Figure 31 B). Observation of the frequency of the movement events displayed that the majority of about 90 % of plastids forming stromules in control conditions possessed stromules that showed movement independent from the plastid body. The frequency of those events was reduced in several datasets of salt stress conditions and more so in the entirety of the sucrose depletion datasets. In drought stress conditions, the overall frequency of events was slightly reduced compared to control conditions. Data throughout all conditions displayed that independent stromule movement is a very common feature of root plastids but can be hampered by cutting off external sucrose supply.

Stromules are very mobile features of plastids that can be extended to several µm in length (Figure 29, Figure 31, Movie 9). The question of the force-generating mechanisms has been discussed over the last decades. To provide possible explanations to those questions and to subsequently characterize the stromule behavior, the variations in length were followed for three randomly chosen stromules in each dataset for the entirety of the stromule appearance. Length changes were separated into positive and negative values, displaying either stromule elongation (Figure 31 C), or retraction speed (Figure 31 D, Movie 14). Maximal stromule elongation and retraction speed in control conditions ranged between 0 µm/sec and 3.2 µm/sec. All stress conditions showed decreased stromule movement in general but also lacked maximal speed compared to control conditions. The maximal velocity measured for salt stress condition was settled at 1.5 µm/sec, whereas for drought stress and sucrose depletion maximal stromule elongation and retraction speed was measured between 0.8 and 1 µm/sec. The velocity distribution of elongation and retraction for each condition matched perfectly, and no statistical difference was observed upon the change of algebraic sign (not shown). This hinted at a uniform mechanism that drives both, the elongation and retraction of stromules. The varying directionality of the stromule movement also allowed for the exclusion of the potential involvement of cytoplasmic streaming in the stromule formation.

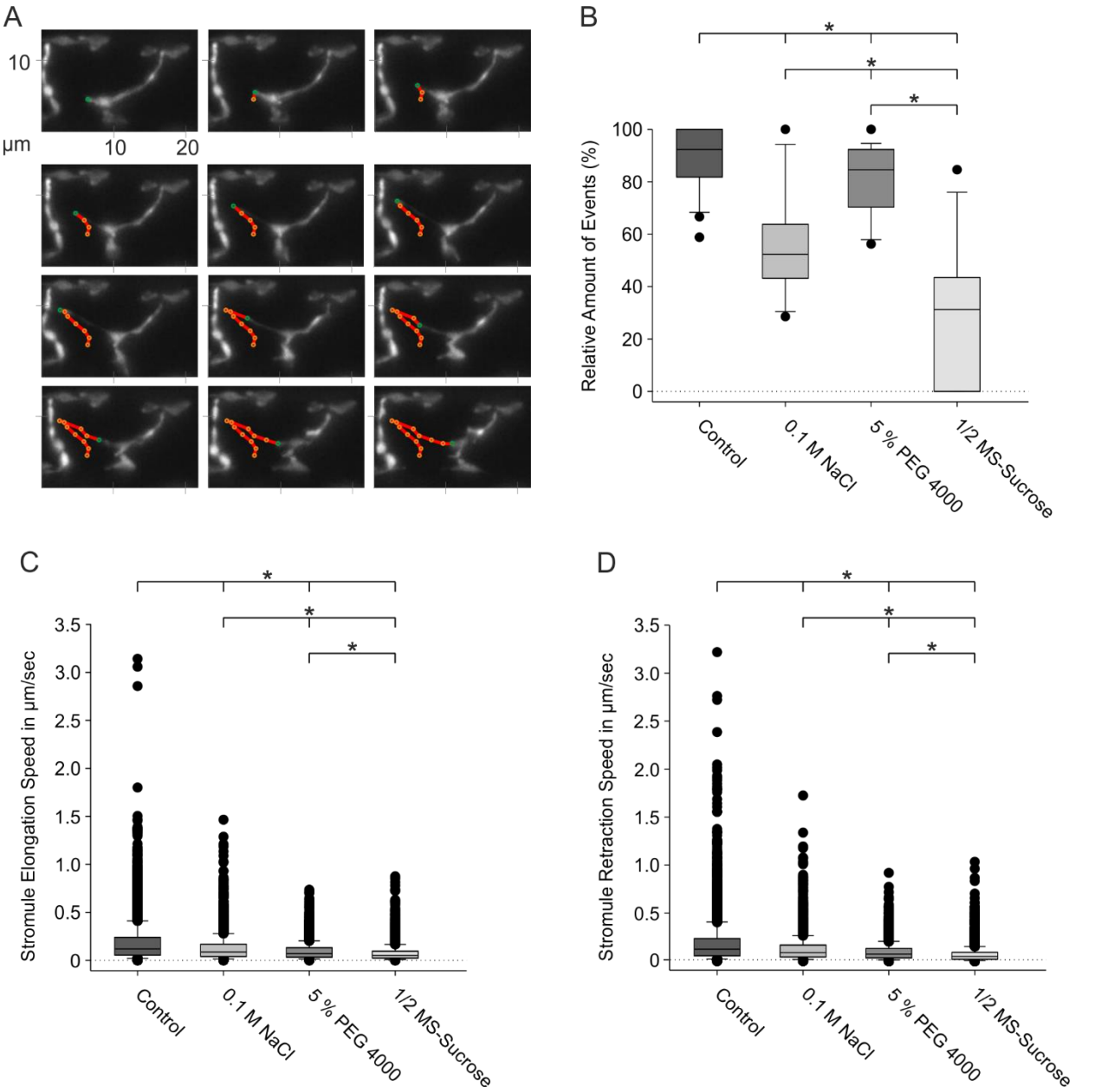

Figure 31 Stromule moves independently from the plastid body. Stromule movement observed independently from the plastid body was analyzed. A) Schematic display of motion pattern that was shown by moving stromules. The Stromule tip elongated from the plastid body (Frames 1-7) or was retracted (Frames 8-12). The Stromule tip was followed for 12 consecutive frames, representing 51 seconds of the total image series. The Red line indicates the movement of stromule tip throughout the displayed image series. Green dot represents the localization of the stromule tip in the respective picture, and orange points reflect the motion of the stromule tip throughout previous frames. Scale is shown in µm and indicated by the coordinate system in each frame. B) Relative number of plastids with stromules that displayed independent stromule movement is shown in relation to all plastids forming stromules that were registered in the respective replicate. Relative number of events of each analyzed replicate (Control condition: n=27, 0.1 M NaCl: n=13, 5 % PEG 4000: n=17, ½ MS-Sucrose: n=19) was summarized in form of boxplots. C) Stromule elongation and D) Stromule retraction speed was measured for a maximum of three randomly chosen stromules in each analyzed dataset as indicated previously (Figure 29 A) throughout the whole image series or stromule visibility. All documented movement events that displayed elongation of the stromule (Control condition: n=5196, 0.1 M NaCl: n=2778, 5 % PEG 4000: n=4702, ½ MS-Sucrose: n=3598) are displayed in C), all events that displayed shortening of the stromule (Control condition: n=5352, 0.1 M NaCl: n=2778, 5 % PEG 4000: n=4771, ½ MS-Sucrose: n=3698) are displayed in D) in form of boxplots. Movement speed is shown in µm/sec. Boxplots display the 10 %, 25 %, 50 %, 75 %, and 90 % quartiles. Outliers are indicated as points outside

of boxplots. Statistical analysis was performed using either a student´s t-test or a Mann-Whitney rank sum test. Asterisks indicate statistical differences ($p<0.05$).

The data led to the speculation that stromules are formed and retracted actively in both directions. Contrary to these findings were the observations that retracting stromules often performed motions that could be compared to a rubber band that is snapping back in place after stretching (Movie 15). Retracting stromules showed bending and diffuse movement of the stromule tip for at least some frames, before the stromule tip seemed to be stabilized in place again and the diffuse rubber band-like motion stopped. Those diffuse movements could be explained by the force of the membrane pulling back stromules that lost anchorage from a cytoskeletal element. The difference in the stromule movement speed (Figure 31 C, Figure 31 D) and the movement speed of plastids without stromules displaying directed motion (Figure 26 C) is significant and therefore different mechanisms seem to drive the plastid body motion and the stromule motion. Even though stromule movement data gathered here is represented by a random selection of stromules and thereby does not reflect the potential maximum speed of stromule elongation and retraction, those findings reinforce the functionality questions of stromules in the cellular context.

3.2.5 Stromule branches are stable structures and able to relocate throughout the plastidal membrane

Stromules can branch and split the stromule into several tips (Kumar et al., 2018; Kwok & Hanson, 2004b). The branches between two stromule tips normally constitute a very characteristic angle of 120° in each direction (Maike Jung, 2021; M. Schattat et al., 2011). Additionally, in contrast to stromule tips, stromule branches have been shown to associate with microtubules (Erickson et al., 2018; M. Schattat et al., 2011). The functionality of stromule branches is up to date very speculative.

By visual examination of the image data, stromule branches have often been observed. Those stromule branches are characterized by a prominent angle enclosed by one or two stromules (Figure 32 A). The shape of stromules varied in timescales of several seconds (Movie 1, 9, 14, 16) thereby not only influencing the shape of the stromule but also of the stromule branch. Although the dynamics of stromules happened on a timescale of seconds, the stromule branches and the enclosed angle remained somewhat stable. For an analysis of the angle between stromules at the branches, various angles at stromule branches were measured in all four conditions (Figure 32 B). For this analysis, angles of stromules that maintained their position for more than two frames were included to ensure a stable position of the stromule. The angles were measured at a 2D level, excluding the Z-dimension. This introduced the possibility of disturbances of the analysis caused by the angle of visualization. However, the average of all measured angles resulted in 120° ± 1° reflecting the previous studies about angles between stromules.

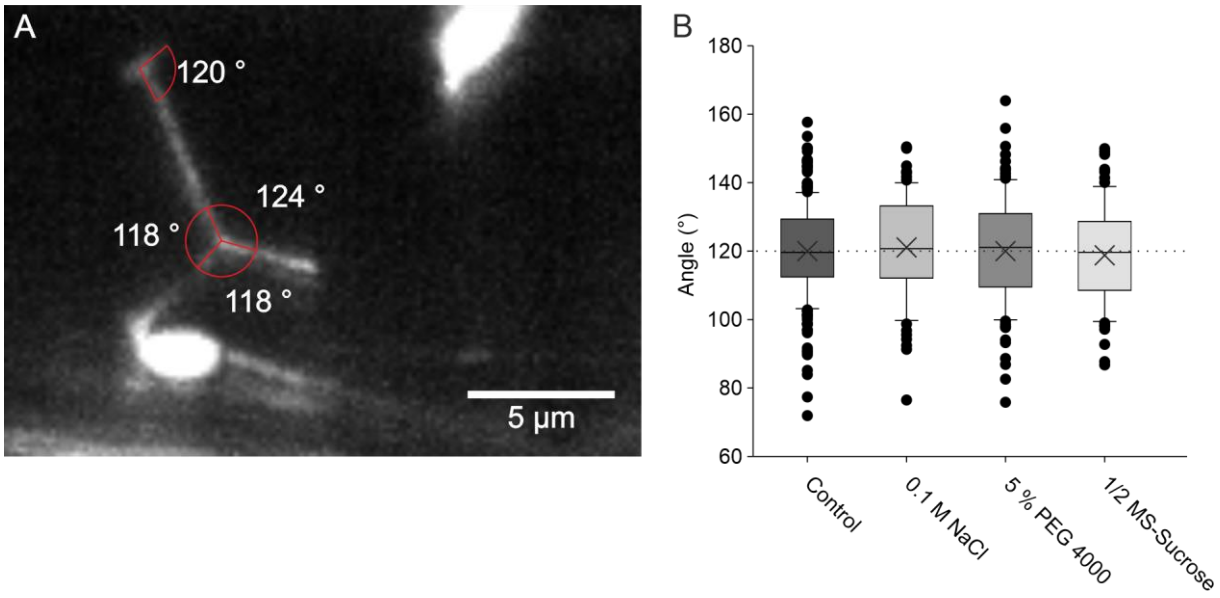

Figure 32 Stromules maintain an angle of 120°. A) Exemplary and characteristic visualization of angles formed by stromules. Angles enclosed by stromules formed by a branch maintain angles close to 120 °. B) Angles formed by stromules of different plastids were measured in control condition (n=226), 0.1 M NaCl (n=79), 5 % PEG 4000 (n=114), and ½ MS-sucrose (n=78). All measured angles are displayed as boxplots for each condition. Boxplots display the 10 %, 25 %, 50 %, 75 %, and 90 % quartiles. Outliers are indicated as points outside of boxplots. The average of each condition is marked with a cross.

Even though most branches displayed an angle of 120 °, most of the time a third stromule tip emerging from the branch was missing (Movie 17, 18). Only one kink of the branch keeping the angle stayed visible. In addition, kinks are very stable structures (Movie 16). Stromule tips could eventually grow from those kink positions, but not from different positions of the stromule (Movie 16-18). The fact that in most cases the kink was visible before the stromule tip emerged could hint at the possibility that stromule kinks could offer origin points from stromule tips to emerge from. For further characterization of the stromule dynamics, the relative number of stromules that showed branching and kinking was calculated (Figure 33 C). The number of stromules that formed branches varied greatly between 5 and 30 % throughout the control, salt, and drought stress conditions, with a slight increase displayed in control conditions (Movie 1-8). Sucrose depletion showed significantly fewer stromule branches. This effect was expected since many datasets in this condition did not display stromules at all. Visual examination of the image data showed that stromules of all lengths were able to create those branches, but longer stromules often possessed multiple branches (Movie 16-18). Besides always maintaining 120° in angle, visual examination of the image data revealed that stromule branches and kinks were very mobile structures and able to move through the stromule (Movie 16). Those structures could be easily tracked over time by following the maintained 120° angle through the stromule (Figure 33 A). Kinking and branching are discussed to be mediated by anchoring at microtubules (Erickson et al., 2018; M. Schattat et al., 2011).

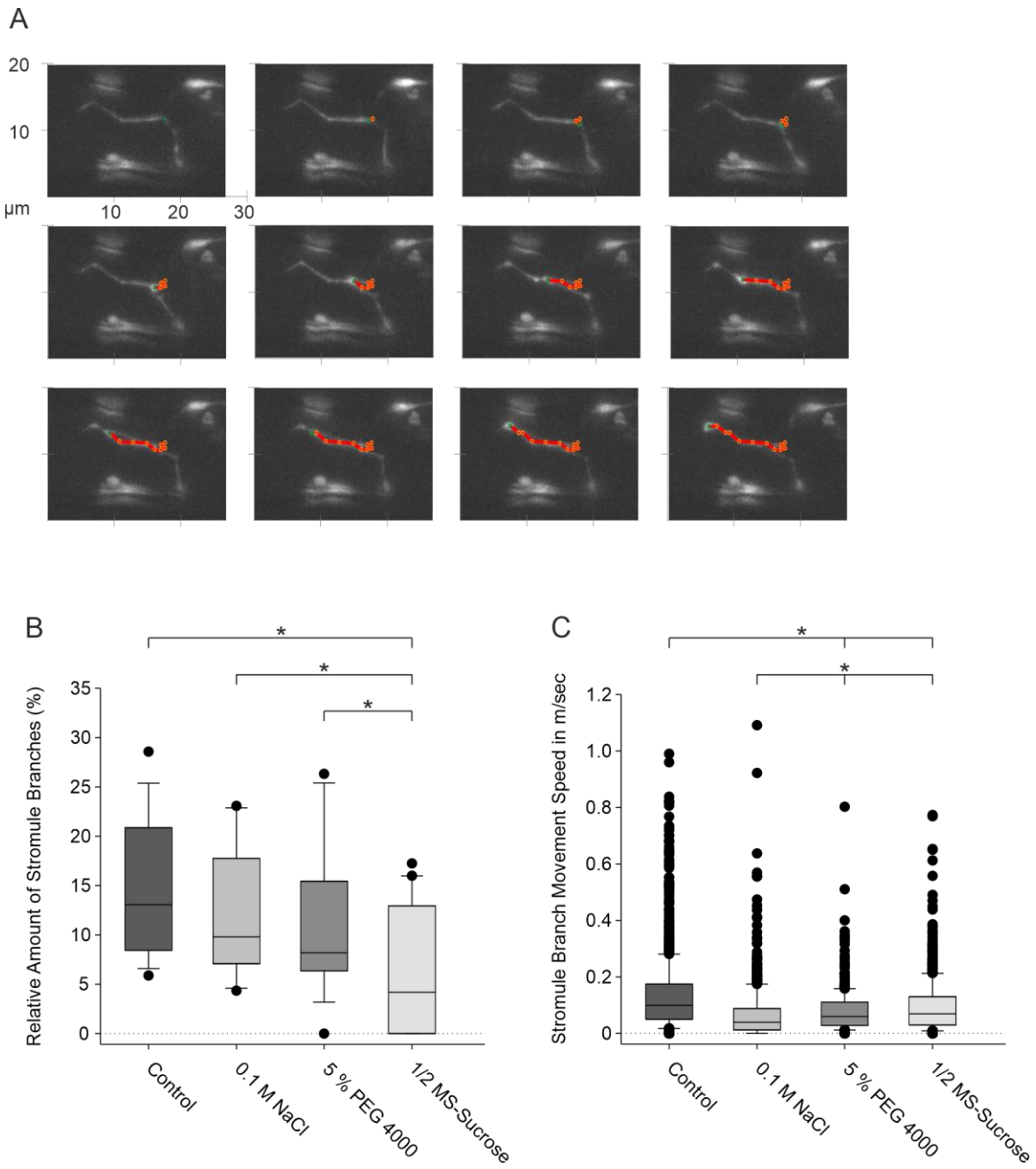

Figure 33 Stromule origin and branch movement. The movement and the behavior of stromule origins and stromule branches were analyzed. A) Schematic display of motion pattern that was integrated in this analysis. The Stromule branch that moved alongside of the stromule it emerged from was followed over a time of 12 consecutive frames representing 51 seconds of the total image series. The path taken by the branch during this image series is indicated by a red line. Green dots mark the position of the branch in the respective frames, orange dots mark the positions in the previous frames. Independently of stromules that emerged from branches, branches could be observed by the 120° angle they formed and maintained. Angles are quite prominent and are seen in all frames. Distance is shown in µm and indicated by a coordinate system across all frames. B) Relative amount of stromule branches were identified in the first frame of all analyzed replicates (Control condition: n=16, 0.1 M NaCl: n=10, 5 % PEG 4000: n=12, ½ MS-Sucrose: n=20) in relation to all plastids that formed stromules. Values of each replicate are summarized in form of boxplots. C) Stromule branch speed was analyzed by following a maximum of three randomly chosen stromule branches throughout the time of movement or visibility. The resulting movement events (Control condition: n=1359, 0.1 M NaCl: n=551, 5 % PEG 4000: n=362, ½ MS-Sucrose: n=657) are displayed in form of boxplots. Movement speed is shown in µm/sec. Boxplots display the 10 %, 25 %, 50 %, 75 %, and 90 % quartiles. Outliers are indicated as points outside of boxplots. Statistical analysis was performed using either a student´s t-test or a Mann-Whitney rank sum test. Asterisks indicate statistical differences ($p<0.05$).

To get insights, if the process of kink movement is actively mediated from an external motor protein, or intrinsically by passing of the kink through the plastidal membrane, the movement speed of various kinks and branches was followed. A maximum of three kinks per dataset were followed throughout their motion processes, depending on the number of appearances (Figure 33 C). Comparison of velocities between conditions showed that control conditions possessed a higher median speed compared to all other conditions, with salt stress conditions being hampered the most. However, the maximal velocity of kinks throughout all conditions remained between 0.8 and 1.2 µm/sec, displaying only slight effects between the conditions. A comparison to the velocities of the stromule tip's elongation and retraction (Figure 31 D) showed clear differences in the maximal speed capacities, especially in control conditions. These results indicated that different mechanisms are responsible for pulling out a stromule tip and moving the stromule kink. With the repositioning, stromule kinks seem not only to provide origin points for stromules but also can reposition for optimal localization of potential stromules. In addition, the stableness of kinks and branches suggests that stromule kinking is provided by the restructuring of the plastidal membrane comparable to lipid rafts.

3.2.6 Stromules can be pulled out by the movement of the plastid body

The mechanism that underlies stromule development and extension is still under investigation and being discussed intensively. One assumption proposes that stromules are actively pulled out from the plastid body by attachment of a motor protein to the membrane (Erickson & Schattat, 2018). The motor protein pulls the membrane, thereby creating the stromule. However, this mechanism is not proven yet. Data provided in this study support a potential role of motor proteins (Figure 31, Movie 16-18) by either direct interaction with the organellar membrane or by providing the driving force in cytoplasmic streaming. Besides that, stromules seem to need an origin point that is provided by kinking (Figure 33). As another mechanism for stromule elongation, the anchoring of stromules to the cytoskeleton with a simultaneous cellular force pulling the plastid body elongating the stromule, is proposed (Erickson & Schattat, 2018).

Visual analysis of the image datasets also supports that this kind of stromule elongation exists *in vivo* (Figure 34 A, Movie 19). To draw conclusions, in what proportion this mechanism is responsible for stromule development, the relative number of events of the plastid body actively pulling out stromules in relation to all plastids possessing stromules was determined (Figure 34 B). In contrast to stromules that elongate while the plastid body remains in position (Figure 31), plastid bodies that pulled out stromules were seen less often. In control conditions, a maximum of 40 % of plastids showed this behavior, while it was nearly abolished in drought stress and sucrose depletion conditions.

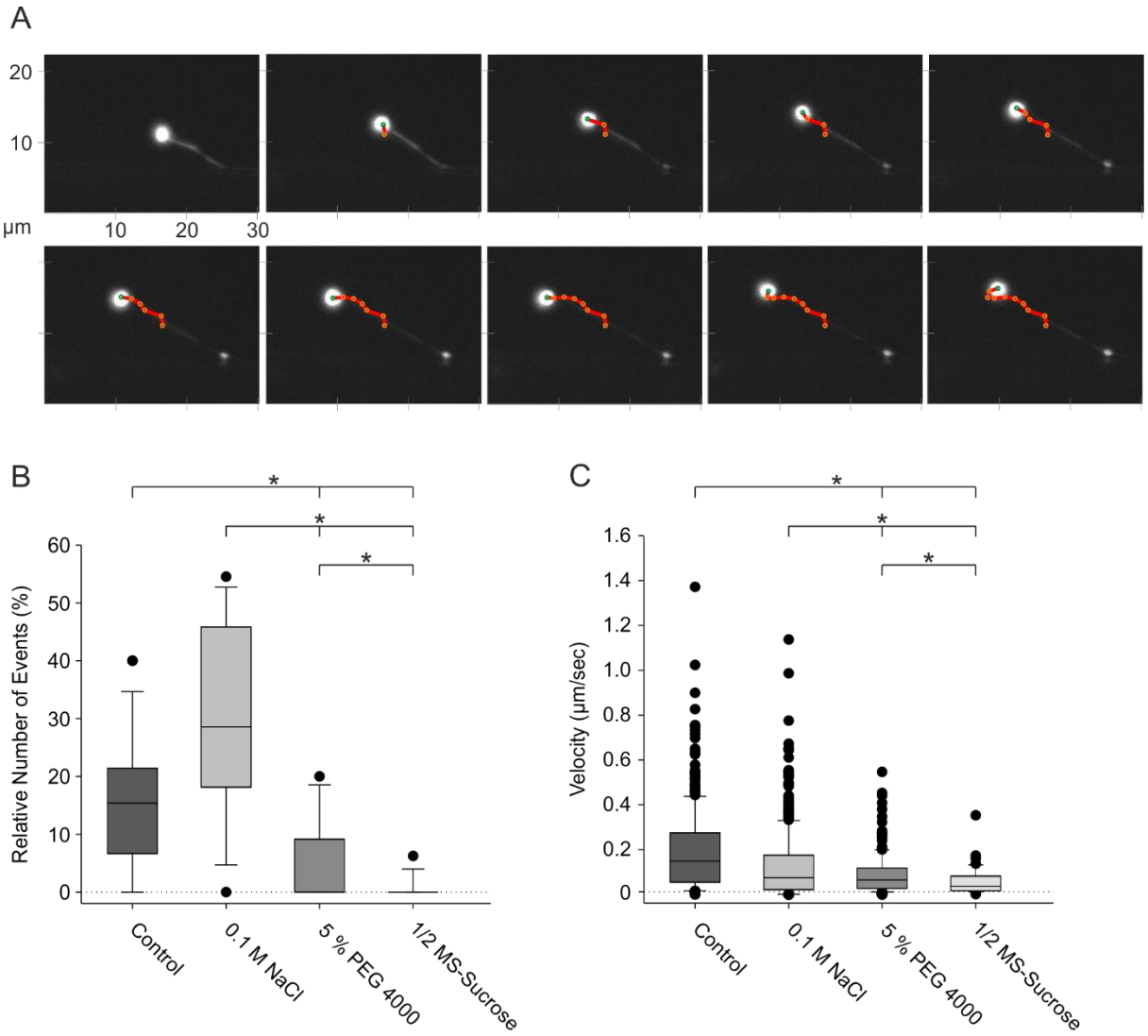

Figure 34 Plastid body moves while the stromule is anchored and elongates. The movement of plastid bodies possessing stromules that were anchored was analyzed. A) Schematic display of motion pattern that was analyzed. The shown plastid possesses a stromule that is anchored in the cellular context. The plastid body moves away from the stromule anchor point, elongating the stromule. The movement of the plastid body was followed for 10 consecutive frames, representing 43 seconds of the total image timeframe. The movement of the plastid body was followed throughout the image series, indicated by the red line. The position of the plastid body in the respective frame is indicated by a green dot, orange dots indicate the positions of the plastid body in the previous frames. Distance is given in µm and indicated by the coordinate system at each frame. B) Number of plastids that showed described behavior in relation to all plastids with stromules for the respective image dataset. Relative number of events of all analyzed replicates (Control condition: n=27, 0.1 M NaCl: n=13, 5 % PEG 4000: n=17, ½ MS-Sucrose: n=19) was summarized in form of boxplots. C) The movement speed of plastid bodies that displayed described behavior was analyzed. Up to three independent movement events were analyzed throughout the time of the movement in each replicate and the total number of movement events (Control condition: n=392, 0.1 M NaCl: n=406, 5 % PEG 4000: n=183, ½ MS-Sucrose: n=43) is displayed in form of boxplots. Velocity is given in µm/sec. Boxplots display the 10 %, 25 %, 50 %, 75 %, and 90 % quartiles. Outliers are indicated as points outside of boxplots. Statistical analysis was performed using either a student´s t-test or a Mann-Whitney rank sum test. Asterisks indicate statistical differences ($p<0.05$).

Surprisingly, salt stress conditions displayed the most events throughout the replicates with a maximum of 60 % of plastids displaying this behavior. To contextualize the molecular mechanism that underlies those motions, a maximum of three events per dataset was followed and velocities of plastids being transported while their stromules were anchored were determined (Figure 34 C). Since those motions were best compared to motions of plastids, which displayed no stromules (Figure 26) a relatively high movement speed was expected. Surprisingly, the velocities measured did not catch up to those expectations (Figure 34 C). The median velocity of the motion was very low reaching from 0.05 µm/sec in sucrose depletion to a maximum of 0.15 µm/sec in control conditions. Maximum velocities measured for each condition were largely behind velocities measured for plastids without stromules, reaching a maximum of 1.4 µm/sec in control conditions. All other conditions displayed drastically decreased maximum velocities with 1.2 µm/sec for salt stress, 0.6 µm/sec for drought stress, and 0.4 µm/sec for sucrose depletion. Those results indicate that either the track, on which the plastid is transported, influenced the velocity of the organelle, or that the movement mechanism of those plastids was different compared to movement of plastids without stromules (Figure 26). In addition, the stromule could influence the plastid speed by generating force on the membrane that stretched thereby pulling the plastid backwards, slowing it down. Most events that were seen, did not span distances of more than a few µm. Considering the number of events, this form of motion does exist, but does not seem to be the preferred motion pattern of plastids. In addition, this movement could be a byproduct of organellar interaction or general cytoplasmic streaming.

3.2.7 The plastid body can be pulled by the stromule or move alongside a stromule

The functions of stromules in the cellular context are not elucidated so far. It is discussed if stromules increase the organellar surface and interact with other organelles for nutrient and molecule exchange (Caplan et al., 2015; Gu & Dong, 2015; Hanson & Hines, 2018; Natesan et al., 2005). One main aspect of this study was to shed light on the question whether stromules are involved in the movement of plastids. So far, different stromule movement patterns were presented here, showing, that stromules are very dynamic and mobile structures (Figure 31-Figure 34, Movie 9-19). These dynamics can contribute to the organellar function in different ways. Besides being able to move independently, or to anchor the plastid in some form to a cellular component, visual analysis of the image datasets revealed, that stromules can also be used by the plastid for movement in an amoeboid manner (Figure 35 A, Movie 20). Different types of such movements were registered. Firstly, the plastid body was seen to be “pulled” by a stromule that is anchored at a cellular component (Movie 20). Secondly, the plastid body was shifted like a marble on a chain between several stromules that emerge from the plastid and were anchored in the cell (Movie 18, 22). Both mechanisms were categorized in the same movement patterns since the plastid body moved alongside the stromule. The number of such events was determined in relation to all plastids forming stromules (Figure 35 B). In control condition replicates, the number of such motions was widely spread across the replicates, spanning 20 % to over 80 % of stromules that showed this behavior.

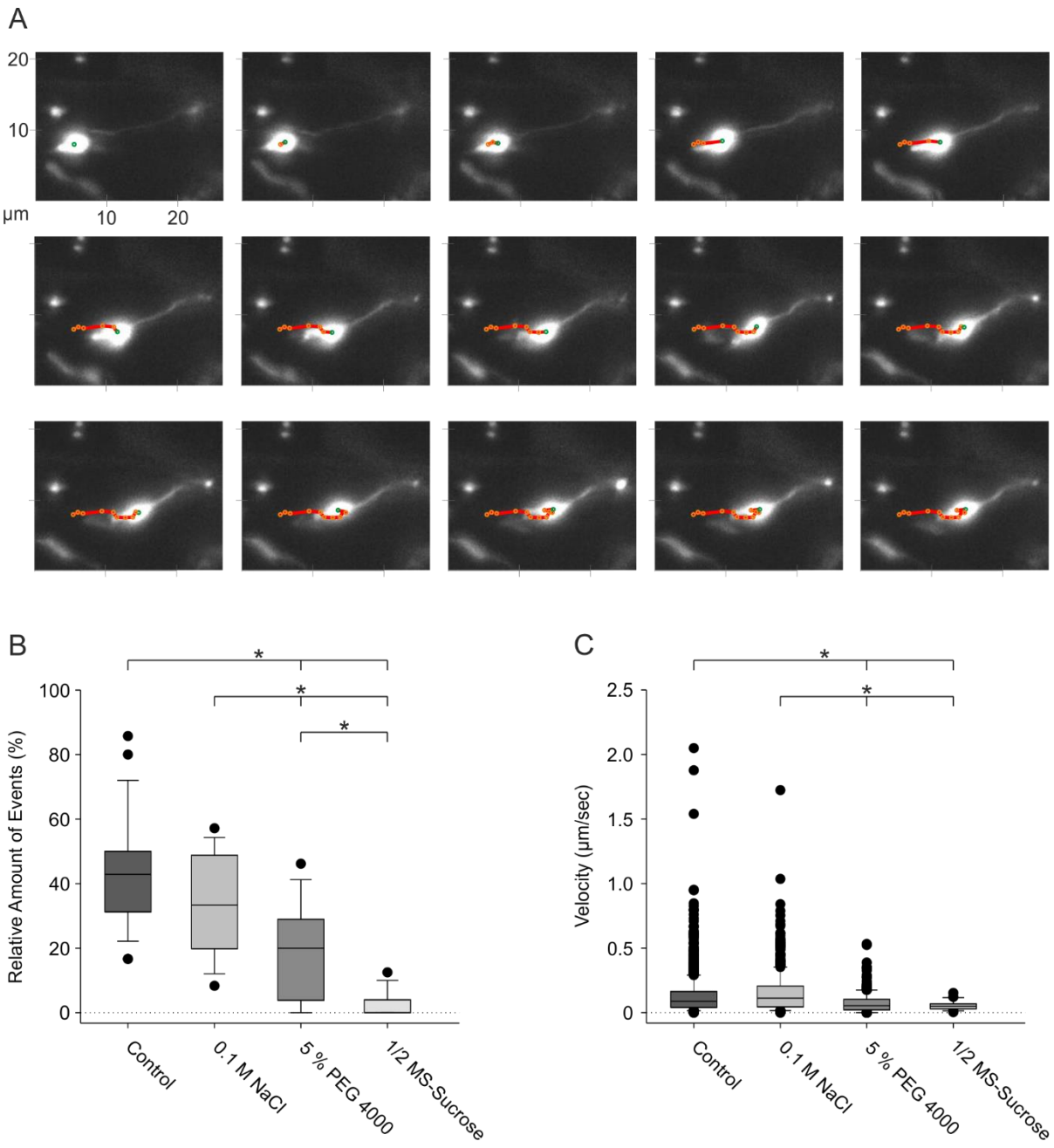

Figure 35 Plastid body is pulled by it's stromule. The movement of plastid bodies that were pulled by their own stromule was analyzed. A) Schematic display of the motion pattern. A plastid with a stromule that is anchored at a cellular component is shown for 15 consecutive frames representing 64 seconds of the image series. The plastid body is pulled by the anchored stromule. Movement of the plastid body was followed and is indicated by the red line. Green dots represent the plastid body location in the respective image, orange spots represent the positions of the plastid body in the previous frames. Distance is given in µm and indicated in each frame as a coordinate system. B) Relative amount of described events was determined in each replicate (Control condition: n=27, 0.1 M NaCl: n=13, 5 % PEG 4000: n=17, ½ MS-Sucrose: n=19) in relation to the total amount of plastids with stromules in the respective replicate. The individual numbers of the replicates are summarized in form of boxplots. C) Movement speed of plastid bodies that displayed described movement behavior was analyzed. A maximum of three randomly chosen motion events were followed in each replicate. Total number of registered movement speeds between the frames (Control condition: n=1141, 0.1 M NaCl: n=451, 5 % PEG 4000: n=333, ½ MS-Sucrose: n=22) are displayed in form of boxplots and shown in µm/sec. Boxplots display the 10 %, 25 %, 50 %, 75 %, and 90 % quartiles. Outliers are indicated as points outside of box plots. Statistical analysis was performed using either a student´s t-test or a Mann-Whitney rank sum test. Asterisks indicate statistical differences ($p<0.05$).

The relative number of events was drastically reduced in all stress conditions, while the number of events determined throughout the replicates was widely spread. In salt and drought stress conditions this form of movement was less common compared to control conditions. In salt stress, a maximum of 55 % and in drought stress a maximum of 40 % of plastids with stromules showed this behavior. In sucrose depletion, this movement action was nearly abolished, again influenced by the overall absence of stromules. To compare the speed of motion with other plastidal movement actions, the speed in which the plastid body was transported alongside the stromule was determined. A maximum of three randomly chosen movement events per dataset dependent on availability was analyzed by following the stromule origin point at the plastid body. The velocities in control and salt stress conditions were comparable (Figure 35 C), with salt stress displaying a slightly higher median movement speed and control conditions showing the highest maximal movement speed of all conditions reaching 2 µm/sec. Drought stress and sucrose depletion both displayed drastically reduced velocities of the plastid body. Drought stress showed a maximal velocity of 0.5 µm/sec and sucrose depletion displayed close to no movement speed. This demonstrates that the function of stromules could be broader than just providing interaction sites to other organelles. Here it is shown that stromules can also contribute to the plastidal motion to some degree. The movement speed of those motions is also quite high and comparable to the active transport of plastids that has been discussed previously. These findings make the stromule-mediated movement a valid option for plastids in terms of relocation.

3.3 *In vitro* analysis of stromule induction and identification of factors potentially involved in stromule formation

3.3.1 Stromules can be introduced *in vitro*

Stromules as a characteristic feature of plastids were first described more than 100 years ago (Svenn, 1908). Since then, numerous experiments were made, that all led to a descriptive characterization of the plastidal tubulations (Hanson & Hines, 2018; Kwok & Hanson, 2004b; Natesan et al., 2005). Most studies introduced stromules *in vivo* by introducing stress conditions (Gray et al., 2012; M. H. Schattat & Klösgen, 2011) or stimulating immune reactions of the plant (Caplan et al., 2015; Gu & Dong, 2015; Kumar et al., 2018). On the molecular level, many studies proposed the cytoskeletal and motor protein-driven transport system to be involved in the stromule dynamics (Erickson et al., 2018; Kumar et al., 2018; Kwok & Hanson, 2004a; Natesan et al., 2009). However, the molecular mechanisms that drive the stromule dynamics are not known until now and many questions remain unanswered. Most urgent questions are, what molecular mechanisms directly form the tubular structures, move them, and keep them in shape (Erickson & Schattat, 2018). This work showed that stromules could form in several ways, independently and in dependence of the plastid body (Figure 31-Figure 35). In summary, the phenomenon of stromule formation could not be fully explained by descriptive analysis so far. In 2016, an *in vitro* approach was published, stating that stromules can be induced at isolated chloroplasts from *Nicotiana benthamiana* by adding concentrated cell extract to the chloroplasts (Ho & Theg, 2016). This molecular approach demonstrated that stromules can be introduced lacking the cellular environment. Most importantly, stromules were often shown to be dependent on the cytoskeleton and the molecular motor proteins

(Erickson et al., 2018; Kumar et al., 2018; Kwok & Hanson, 2004a; Natesan et al., 2009). If cytoskeletal elements are present during the *in vitro* assay, they are fragmented and not a great support for the tubular structures. Therefore, it was assumed that stromules can be induced at chloroplasts by an external factor that is available in the cell and either binds to a membrane element or gets incorporated into the chloroplast, mediating the stromule formation. The publication from Ho and Theg (Ho & Theg, 2016) was taken as a basis for this study to answer the leading question, what cellular factors mediate the stromule formation.

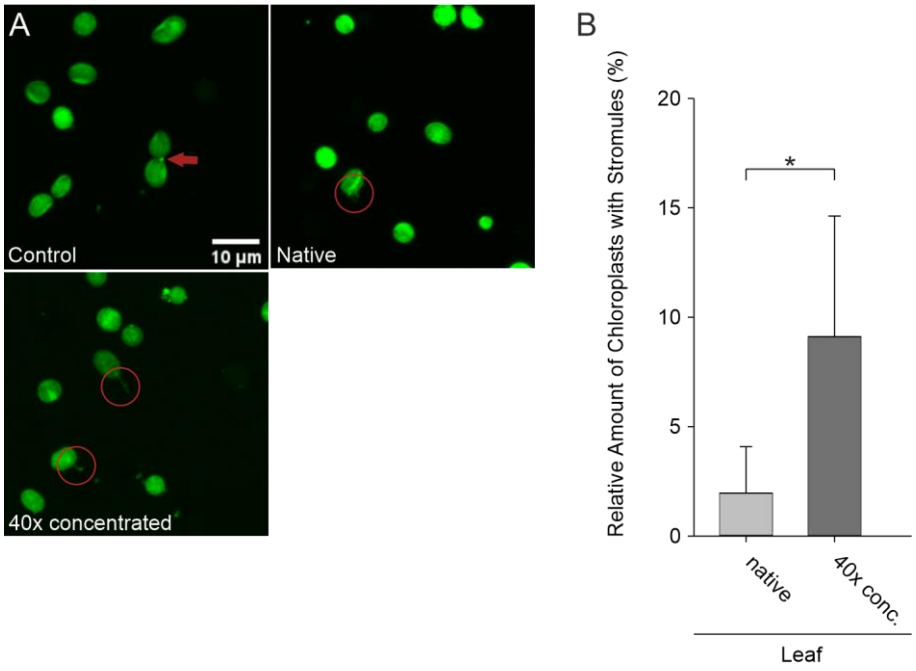

Figure 36 Stromule induction *in vitro* by the addition of concentrated cell extract. Following previous publications (Ho & Theg, 2016) an assay for in vitro stromule formation was established. Stromules were induced at isolated chloroplasts by the addition of concentrated cell extract. A) Isolated chloroplasts stained with Calcein AM at control conditions, with the addition of native cell extract and with the addition of 40x concentrated cell extract. The red arrow in the control frame indicates structures that could be mistaken as a stromule. Red circles indicate stromules that formed upon addition of either native or concentrated extract. B) Relative amount of chloroplasts that formed stromules was analyzed throughout five technical replicates. Average values are shown for native and concentrated leaf extract. Results of control conditions were substracted prior to visualization. Error bars represent standard deviation of five technical replicates. Statistical analysis was performed using a student´s t-test. Asterisks indicate statistical difference ($p<0.05$).

To establish this *in vitro* assay, the experimental procedures described in the publication (Ho & Theg, 2016) were followed (Figure 36 A). Instead of tobacco, pea plants were used. Pea leaves were carefully shred into pieces, the extract was filtered, and chloroplasts were spun down. The remaining cellular extract was preserved and concentrated approximately 40x using Amicon filter units. Chloroplasts were stained using Calcein AM and successively spun down and mixed before imaging with the concentrated extract. As controls, the native extract as well as the chloroplast isolation buffer was tested. The stromule induction was determined using confocal fluorescence microscopy and manual counting of the stromule-forming chloroplasts (Figure 36). Despite lacking explicit tubular structures, chloroplasts in control conditions

formed structures that could be compared to buddying yeast (Figure 36 A control). Those structures were not considered stromules. However, since those structures were seen in each condition tested and could be mistaken for stromules, they were counted. The number of buds that were detected in the control condition of each experiment was subtracted from all conditions. Defined tubular structures emerging from the chloroplasts were visible in the native as well as the concentrated extract (Figure 36 A). The number of stromules was determined in each replicate and set in relation to the total number of vital chloroplasts marked by the Calcein AM fluorescence (Figure 36 B). The analysis revealed that even though the native extract induced stromules, the number of stromules drastically increased with the adding of the concentrated extract. With this observation, the stromule induction assay was established and was further used for the investigation of cellular factors that contribute to the formation of stromules.

3.3.2 Root extract forms more stromules *in vitro* than leaf extract

Stromules were often described to be primarily present in root plastids, whereas chloroplasts in the leaf and hypocotyl can form stromules, but on a far smaller basis (Köhler & Hanson, 2000). So far, no data are available, whether stromule formation in chloroplasts and root plastids is induced by similar molecular mechanisms. Since chloroplast movement and root plastid movement differ greatly from each other (Wada and Kong 2018, Figure 18, Figure 22), different mechanisms could be responsible for stromule formation in green tissue and roots. If the stromule-forming mechanisms follow the same molecular mechanisms, root extract should be able to introduce stromules at chloroplasts. Following this idea, root and leaf extracts were generated from the same pea batch by harvesting the leaves and roots, respectively. Roots were washed extensively before crushing. Concentrated extracts were adjusted to 25 µg/µl protein concentration, which represented 40x concentration of at least one of the two generated extracts. The adjusted protein extract was tested for stromule induction capacity (Figure 37). Confocal images showed that leaf extract as well as root extract induced stromule formation *in vitro* (Figure 37 A). Visual examination of the stromules did not reveal any differences between leaf and root extract. To contextualize the findings, the number of chloroplasts with stromules was set in relation to the total number of vital chloroplasts (Figure 37 B). The result depicted that root extract had a higher stromule induction capacity compared to leaf extract and also led to the suggestion, that the molecular mechanism of stromule formation in leaves and roots at plastids are the same.

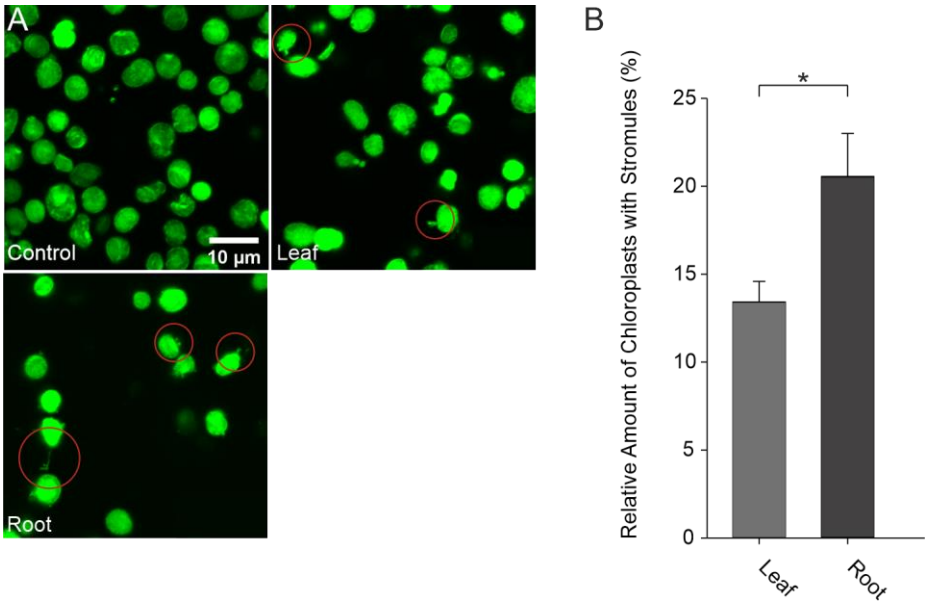

Figure 37 Concentrated root extract is more potent in forming stromules than leaf extract. A comparison between concentrated leaf and concentrated root extract was made. Each extract was gathered and adjusted to 25 µg/µl. A) The stromule induction capacity of both extracts was analyzed at isolated chloroplasts stained with Calcein AM. Control conditions represent chloroplast isolation buffer. Red circles indicate stromules in concentrated leaf and root extract conditions. B) Image data from A) was evaluated and the relative amount of chloroplasts that formed stromules was analyzed. Average values are shown for concentrated cell extract of leaves and roots. Results of control conditions were substracted before visualization. Error bars represent standard deviation of five technical replicates. Statistical analysis was performed using a student´s t-test. Asterisks indicate statistical difference ($p<0.05$).

3.3.3 Stromule induction *in vitro* is dependent on the concentration of protein extract

The publication used as a template for this method (Ho & Theg, 2016) stated that a 40x concentrated extract, gathered from leaves during chloroplast extraction, was used for stromule induction. The concentration of the extract is highly dependent on the amount of plant material and buffer used during the isolation process. Therefore, the concentration factor does not state how much protein is introduced onto the chloroplasts and how much protein is needed to induce stromule formation. A dilution curve reaching from 0 to 32 µm/µl protein concentration of leaf and root extract was prepared and tested for stromule induction capacity (Figure 38). Leaf extract (Figure 38 A) and root extract (Figure 38 B) showed a linear relation between protein concentration and stromule-forming chloroplasts between 0 and 8 µg/µl. As expected, root extract was more potent than leaf extract in terms of stromule formation capacity. Chloroplasts mixed with root extract showed double the number of stromules formed at each concentration compared to leaves. At 32 µg/µl for leaves and 16 µm/µl for roots, the curve flattens and seems to reach a plateau giving the curve a sigmoidal appearance. The maximal number of chloroplasts with stromules was in both cases 25 % of the chloroplasts, indicating that the stromule-forming capacities of the extracts were limited to a maximal value. It is necessary to state that the counting of stromules was interfered with by the viscosity of high protein concentrations prompting the chloroplasts not to properly sediment during the assay, which interfered with the data analysis.

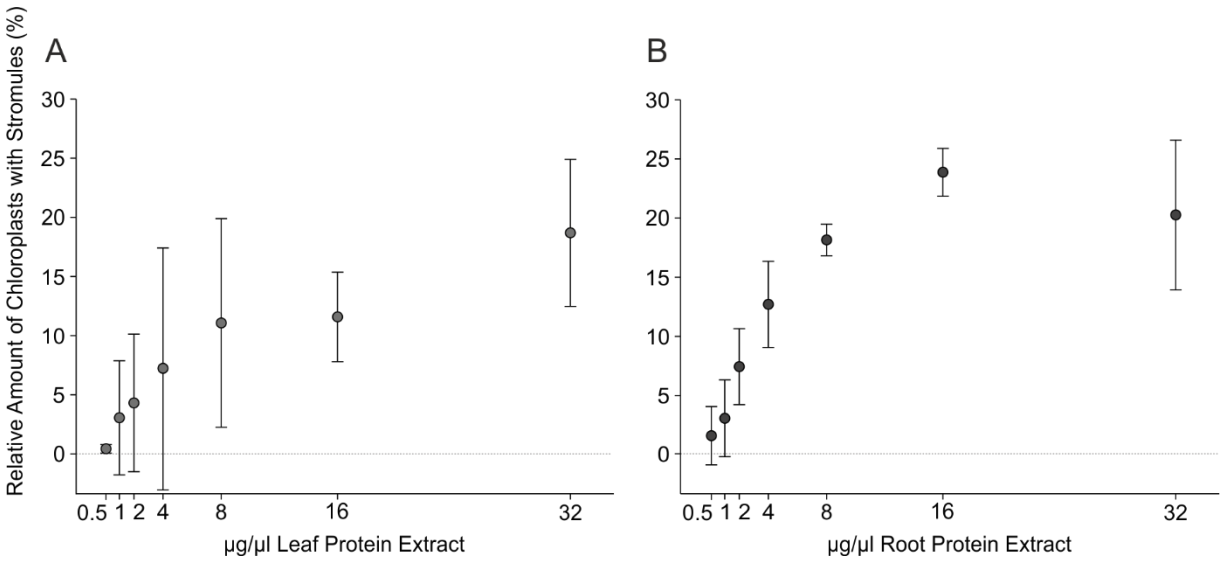

Figure 38 Stromule induction depends on the protein concentration. Different concentrations of A) leaf and B) root extract were prepared and tested for *in vitro* stromule induction capacity on isolated chloroplasts. Concentrations are indicated by the X-axis in µg/µl. The relative amount of chloroplasts forming stromules was determined throughout five technical replicates. Error bars represent standard deviation of n=3 biological replicates.

Therefore, the maximal number of stromules may vary drastically in higher protein concentrations. These findings indicated that root extract is two times more effective in stromule formation than leaf extract, hinting at a greater abundance of the involved factors. In addition, these results displayed that the number of stromules is dependent on the protein concentration of the extract. In following experiments using this method, these findings were incorporated, and the protein concentration of the extract was not determined anymore. Concentration adjustments were just applied for experiments needing exact biological replicates (Figure 41).

3.3.4 Stromules cannot be induced by external factors without cell extract

Even though the *in vitro* assay was established, and root extract was shown to be more potent in stromule induction, the main question of the crucial cellular factor that induces stromule formation remains unanswered. A cellular extract harbors a variety of substances that could contribute to the formation of stromules. Even though most evidence supports the theory that an external factor is needed that interacts with the membrane, it is not excluded that an external factor could cross the chloroplast membrane to induce an intrinsic pathway, leading to stromule formation (Erickson & Schattat, 2018). *In vivo* stromule formation was often observed in association with the nucleus (Caplan et al., 2015; Erickson et al., 2017; Gu & Dong, 2015). Stromule-nucleus contact was not only observed under stress conditions but also at normal conditions, leading to the assumption that plastids form stromules for retrograde signaling with the nucleus. These findings lead to the hypothesis that the outer membrane of nuclei could harbor factors, which facilitate stromule induction. In previous findings, plastid-nuclear complexes were proposed to be involved in stromule formation (Mullineaux et al., 2020). Factors associated with the nuclei could also be

present in the cell extract even though intact nuclei are excluded in the extract. To analyze whether nuclei harbor stromule inducing factors, the *in vitro* stromule induction assay was used in combination with isolated nuclei (Figure 39).

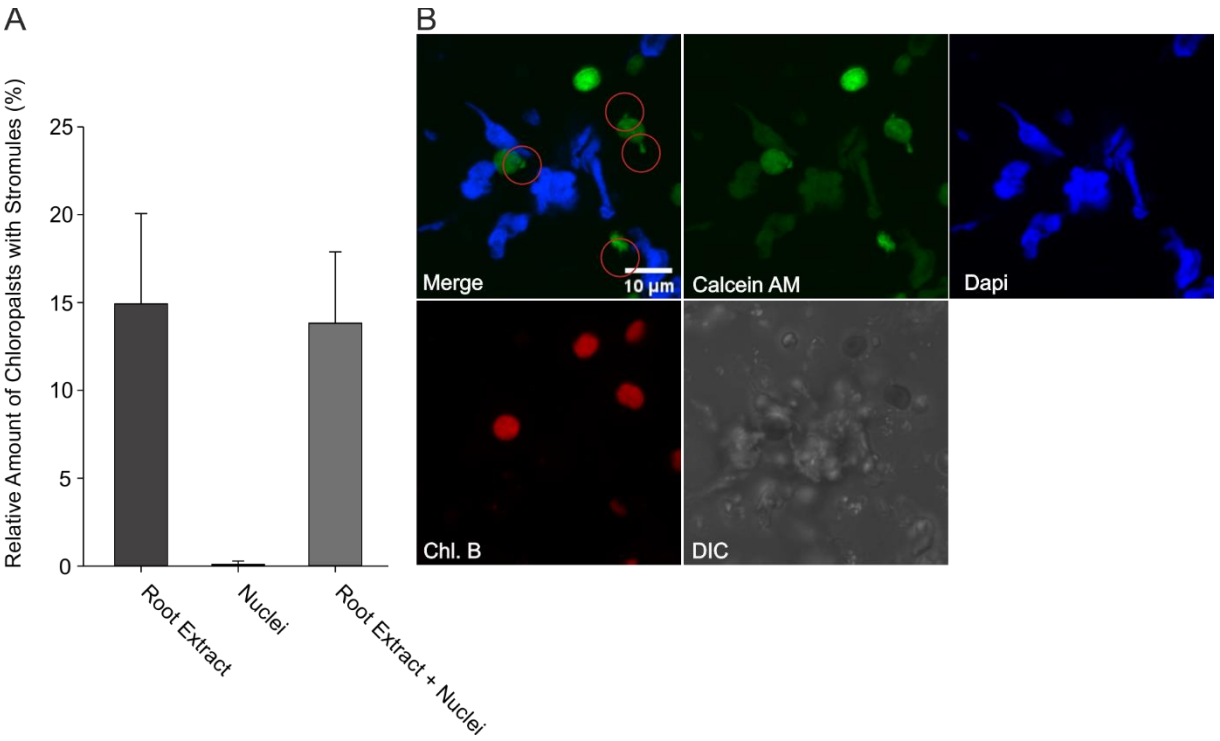

Figure 39 Stromule induction capacity of isolated nuclei. Representative assay on the stromule-inducing capacities of isolated nuclei. A) Nuclei were isolated from pea leaves and tested for stromule induction capacity *in vitro*. Stromule induction capacity is shown either alone or in combination with concentrated root extract on isolated chloroplasts. As positive control concentrated root extract is shown. Results from control conditions were substracted before visualization. Error bars represent the standard deviation of five technical replicates. B) Confocal images displaying either Calcein AM stained chloroplasts (green), Dapi stained nuclei (blue), the chlorophyll b fluorescence of chloroplasts (red), differential interference contrast and merge of all channels. Pictures were taken from conditions containing root extract and nuclei, to determine if formed stromules interact with nuclei. Stromules of chloroplasts are highlighted with red circles. Stromules show no interaction with nuclei.

Nuclei were isolated either from leaves or from roots. Due to too much cell debris in isolated root nuclei that interfered with the microscopic analysis, only leaf nuclei were analyzed. Relative numbers of chloroplasts with stromules were determined either by the addition of root extract, and nuclei, or in combination with root extract and nuclei (Figure 39 A). Images were taken especially of positions, where plastids and nuclei had close contact with each other. Stromule induction is facilitated in all conditions, in which the root extract is present. Nuclei were not able to facilitate stromule induction. In combination, the number of stromules induced by the cellular extract did not rise, showing that nuclei do not harbor any factors that facilitate stromule induction *in vitro*. In addition to a determination of stromule formation capacities, a visual analysis of the stromules induced during this assay was performed to determine if any connection between stromules and nuclei is facilitated (Figure 39 B). During this assay, no direct connection between nuclei and stromules was observed. This gives more evidence that stromule

formation is not facilitated by nuclei *in vitro* and that additional external factors are needed to mediate not only stromule induction but also the contact with the nucleus.

3.3.5 Stromule induction is facilitated by protein factors *in vitro*

Taking the previous findings into consideration (Figure 36, Figure 39), stromule formation is most likely to be mediated by a cellular factor that is present in the cell extract. Since it has been shown to be dependent on the protein concentration of the extract (Figure 38), proteins are highly in favor of mediating the stromule formation. However, during the generation of the extract, some centrifugation steps at low speeds up to 2,000xg were applied to clear the cell extract from tissue debris and nuclei. All other cellular components were present in the extract.

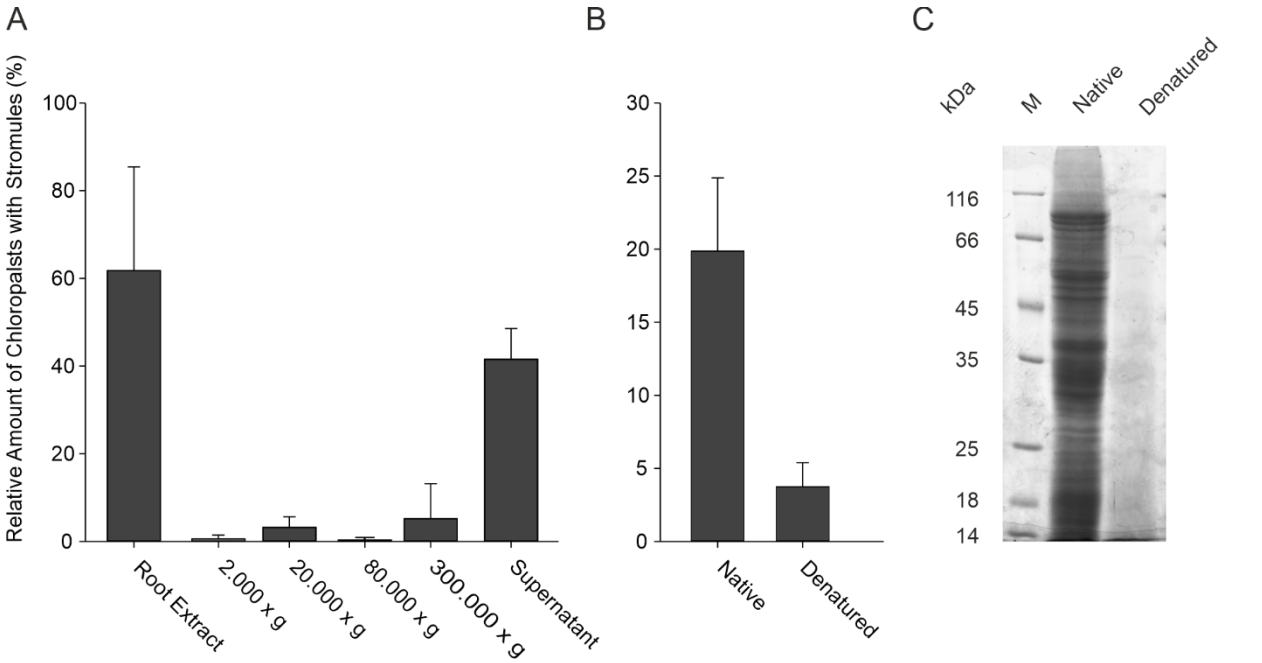

Figure 40 Cytosolic proteins induce stromule formation *in vitro*. Within a process of elimination, it was shown that presumably cytosolic proteins are responsible for *in vitro* chloroplast formation. A) A differential centrifugation was performed using root cell extract. The pellets in each centrifugation step were resolved in 1 ml chloroplast isolation buffer resulting in 50x concentration. The supernatant was concentrated. All samples were analyzed for *in vitro* stromule induction capacity on isolated chloroplasts. The relative amount of chloroplasts forming stromules for each fraction is shown. Error bars represent standard deviation of five technical replicates. Results of control conditions were subtracted from all conditions before visualization. B) Supernatant fraction from A) was subjected to a denaturation process at 95 °C. Native and denatured extract were concentrated and analyzed for *in vitro* stromule induction capacity on isolated chloroplasts. The relative amount of chloroplasts with stromules is shown. Error bars represent the standard deviation of five technical replicates. Results of control conditions were subtracted from all conditions prior to visualization. C) Native and denatured samples from B) were subjected to SDS-Page followed by Coomassie staining. Results are shown. Protein content after the denaturation process is drastically reduced. Molecular weights of marker bands (M) are indicated in kDa.

This included remaining cell debris, membrane debris, small organelles, small cytoskeletal elements, Ribosomes, RNAs, and all kinds of cellular proteins. For the concentration process of the cellular extract, Amicon filter units with a 10 kDa cutoff were used. Therefore, all cellular components bigger than the cutoff were present in the concentrated extract. To clarify what cellular component present in the cell extract is mediating stromule formation, differential centrifugation was performed with the extract (2.5.8, Figure 40 A).

The stromule induction capacity of each sedimented fraction and the concentrated supernatant was compared with concentrated root extract (Figure 40 A). Again, problems with extract viscosity were faced as previously indicated (3.3.3). Nevertheless, the number of chloroplasts with stromules determined in this assay was very high, reaching 60 % of chloroplasts. This shows again that the number of stromules that could be formed is highly dependent on the cellular extract. In comparison, the stromule induction capacity of cellular fractions except the supernatant was quite low. Investigation of stromule abundance was also interfered with the cellular components in lower centrifugation steps, and thereby hard to determine. However, only the supernatant showed well-defined tubular structures of the chloroplast membrane, indicating that the factors responsible for stromule formation were only present in this fraction. The supernatant as the cytosolic fraction of the cell included soluble proteins and RNAs. The question raised was, which of those cell components mediated stromule formation? To answer this, the supernatant was further processed and treated at 95 °C for 20 minutes to denature available proteins. Samples were centrifuged for 10 minutes at 20,000xg to sediment aggregated proteins and the supernatant was analyzed for stromule induction capacity (Figure 40 B+C). As revealed by Coomassie staining, the denaturation process eliminated a big portion of the soluble proteins (Figure 40 C). In comparison to the native concentrated extract, the denatured concentrated extract showed less stromule induction, showing that an interaction of the chloroplast with protein factors is necessary for stromule formation *in vitro*. Although fractions that underwent higher centrifugation steps than 20,000xg were much easier to examine in the microscopic analysis, because of the lack of cellular debris. In the following analyses of the cell extract an additional 50,000xg centrifugation step for 45 minutes after sonication was introduced to clear the crude cell extract.

3.3.6 Thermolysin treatment of the outer envelope protein does not reduce stromule formation

The mechanism of membrane tubulation is a form of membrane curvature (Stachowiak et al., 2010). The membrane of the outer envelope, as any other cellular membrane, is a very complex and highly dynamic component of the cell. The understanding of membrane behavior is still limited in animal and yeast cells and more so in plant cells (Erickson & Schattat, 2018; Stachowiak et al., 2010). Nevertheless, mechanisms of membrane curvature are assumed to work similarly. Although membrane tubulation could theoretically be an internal mechanism of the plastid, it is highly unlikely that stromule formation is solely mediated from the stromal site of the plastid. This puts external interactions with the outer envelope of the plastid in the foreground of investigations. (Erickson & Schattat, 2018; Stachowiak et al., 2010). Membrane curvature can be introduced membrane-intrinsically by differently shaped lipids or integrated proteins which can be orchestrated by the attachment of proteins on the outer envelope (Erickson & Schattat,

2018; Stachowiak et al., 2010). It can also be introduced by external proteins that directly interact either with the lipid bilayer, or with integrated proteins providing a structure for the membrane bend (Erickson & Schattat, 2018; Stachowiak et al., 2010). Since an external protein factor from the cell extract is needed for stromule induction *in vitro*, the conclusion was drawn that a protein abundant in the cytosol, undergoes either protein-lipid or protein-protein interaction and thereby facilitates membrane tubulation. Thermolysin is a protease that was shown to effectively cleave proteins in the outer envelope, but not proteins of the inner envelope (Cline et al., 1984). If stromules are introduced *in vitro* by protein-protein interaction, the number of stromules formed on Thermolysin treated chloroplasts should be reduced by the lack of interaction domains of integrated membrane proteins. To determine, if a protein-protein or a protein-lipid interaction is responsible for mediating membrane tubulation, isolated chloroplasts were treated with Thermolysin prior to testing for stromule induction *in vitro* (Figure 41 A).

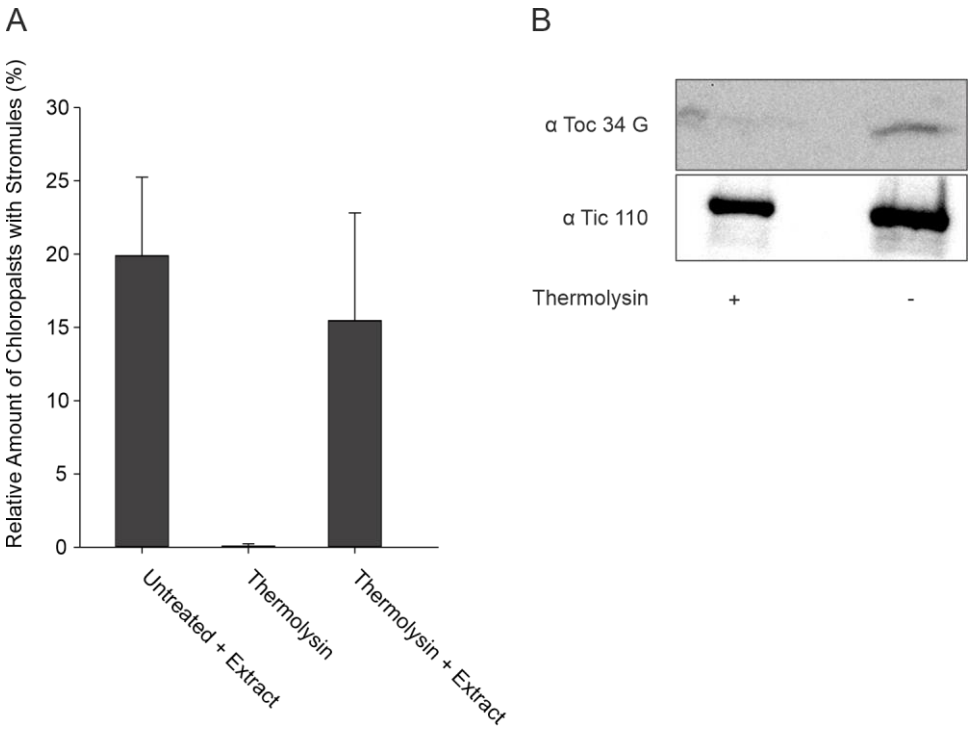

Figure 41 Thermolysin treatment of chloroplasts does not inhibit stromule formation. To analyze whether proteins of the outer envelope are associated with *in vitro* stromule formation, isolated chloroplasts were treated with Thermolysin. A) Untreated and treated chloroplasts were analyzed for *in vitro* stromule induction with concentrated root extract. Results display a relative amount of chloroplasts forming stromules. Error bars indicate the standard deviation of n=3 biological replicates. B) Representative immunoblot analysis of untreated and Thermolysin treated chloroplasts used for the *in vitro* assay displayed in A) is shown. To prove the functionality of the Thermolysin treatment, an antibody specific to the cytosolic G-domain of Toc 34 was used. As a control that proteins of the inner envelope were not affected by the thermolysin treatment, an α Tic 110 antibody was used.

Thermolysin treatment was controlled by western blot with treated and untreated chloroplasts (Figure 41 B). The abundance of the cytosolic-oriented G-domain of the outer envelope protein Toc 34 and the inner envelope protein Tic 110 was tested with antibodies. Successful Thermolysin treatment was characterized by a signal loss of Toc 34 indicating that cytosolic domains of outer envelope proteins are successfully digested. Retention of the Tic 110 signal demonstrated that proteins of the inner envelope were not affected by the treatment. Successful Thermolysin treatment was detected (Figure 41 B) and treated chloroplasts were analyzed for stromule formation (Figure 41 A). Interestingly, the stromule induction capacity of Thermolysin-treated chloroplasts did not decrease drastically compared to the control with untreated chloroplasts. These findings lead to the assumption that the factor available in the cellular extract undergoes a protein-lipid interaction, thereby mediating the tubulation of the membrane even though an internal regulation of the plastid stromule formation could not be excluded.

3.3.7 Fractionation of the crude cell extract using a linear sucrose gradient

Only limited molecular approaches are available to study the formation of stromules. The main question of this section of the work was, what factor available in the crude cell extract taken from pea roots is responsible for the induction of stromule formation. As previously stated, the factor is most likely a protein that interacts with the lipids of the outer envelope of the chloroplasts. For the identification of the unknown protein factor, a mass spectrometric analysis was intended. The crude cell extract of any plant contains several thousands of proteins. To limit the number of proteins that are possibly involved in stromule formation, the cell extract was fractionated using different methods. The superordinated aim was that all fractions needed to be analyzed for the stromule induction capacity using the *in vitro* stromule induction assay to ensure the factor that mediates stromule induction was still present. However, the factor needed to be maintained in a native condition, giving a time restriction for the experimental procedures. Experiments on an extract that was not freshly produced on the day used, hinting at protein degradation. Both factors constricted the methods usable for the approach.

Linear sucrose gradients separate cellular proteins according to their sedimentation coefficient (Berg et al. 2013). As a first approach, a linear sucrose gradient ranging from 10-60 % sucrose was applied to separate the protein lysate. The protein extract was generated as usual and successively concentrated using 10 kDa Amicon filter units to reduce the volume of extract layered on top of the gradient. Continuous sucrose gradients were prepared (Luthe, 1983) and concentrated crude cell extract was loaded on top of the gradient. The gradient was centrifuged for 16 hours at 250,000xg. After centrifugation, the gradient was split into eight fractions starting from the top. Each fraction was concentrated to a full extent to the same volume ensuring the same proportion of proteins present in each sample. Samples were successively tested for stromule induction capacity (Figure 42 A). Fraction 1 showed a strong induction of stromules. The number of induced stromules decreased over samples 2 and 3, showing that the factors responsible for stromule induction did not run a long distance in the gradient. The fractions were also loaded onto an SDS-gel to analyze the distribution of the proteins gathered from the gradient by Coomassie staining (Figure 42 B).

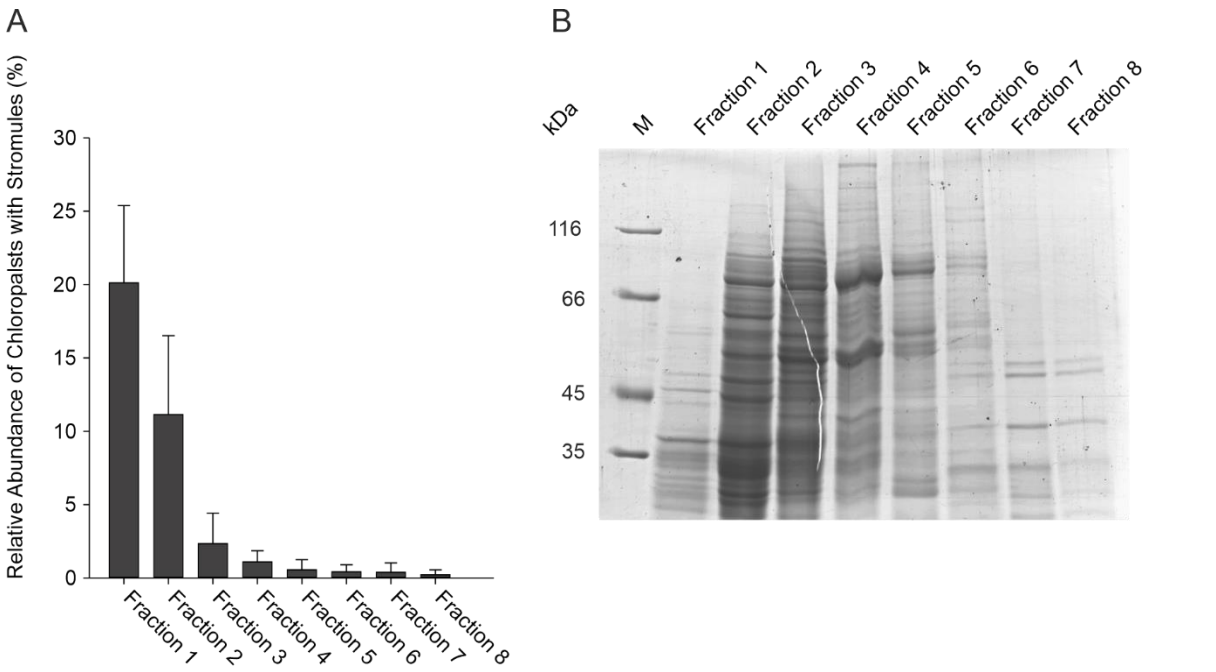

Figure 42 Protein extract fractionation using a linear sucrose gradient. For the separation of the crude root cell extract, a linear sucrose gradient was used. Eight fractions were taken from the top of the gradient. The results displayed in this graphic are representative. A) All fractions from the linear sucrose gradient were analyzed for *in vitro* stromule induction on isolated chloroplasts. The relative abundance of chloroplasts forming stromules is shown. Error bars represent standard deviation of five technical replicates. B) Fractions from the sucrose gradient tested in A) were subsequently subjected to SDS-Page followed by Coomassie staining. The resulting gel is shown. Molecular weights of the marker bands (M) is given in kDa.

Most proteins were observed in fractions 2, 3, 4 and 5. Only a very small subfraction of proteins was observed in fraction 1, 6, 7 and 8. Even though Coomassie is not a very sensitive detection method, the number of proteins in fraction 1 was drastically reduced compared to fraction 2. Since the first fraction was the one with the highest stromule induction capacity, the number of protein candidates responsible for stromule induction could be decreased drastically using the continuous sucrose gradient.

3.3.8 Fractionation of the crude cell extract using anion exchange chromatography

Besides a linear sucrose gradient, ion exchange chromatography was performed to separate proteins according to their molecular net charge. Like the sucrose gradient, this method aimed for fractionation of the crude cell extract and limiting the pool of potential candidates that needed to be examined in a mass spectrometric approach. As column material, the anion exchanger DEAE Sephadex A-50 was used. The crude cell extract was generated as described previously and was directly used for ion exchange chromatography. Different protein fractions were obtained by eluting with increasing amounts of NaCl. The fractions were concentrated and tested for their stromule induction capacity (Figure 43 A). Interestingly, all fractions tested were able to induce stromules. Of all fractions, the flowthrough fraction was the most potent in terms of stromule induction. Comparing the number of stromules obtained in each fraction with previous experiments, the number of proteins used in this experiment was quite high, leading

to overall high stromule induction. The results of the stromule induction assay led to the assumption that the wanted factor did not bind to the column and was retained not just in the flowthrough fraction, but also was washed from the column successively. Since the wash fraction possessed double the volume in contrast to all other elution fractions, it was not fully concentrated because of time reasons. The lower amount of stromules in the wash fraction could be influenced by this treatment in comparison with the other fractions. All fractions were also conducted to SDS-Page, followed by Coomassie staining (Figure 43 B).

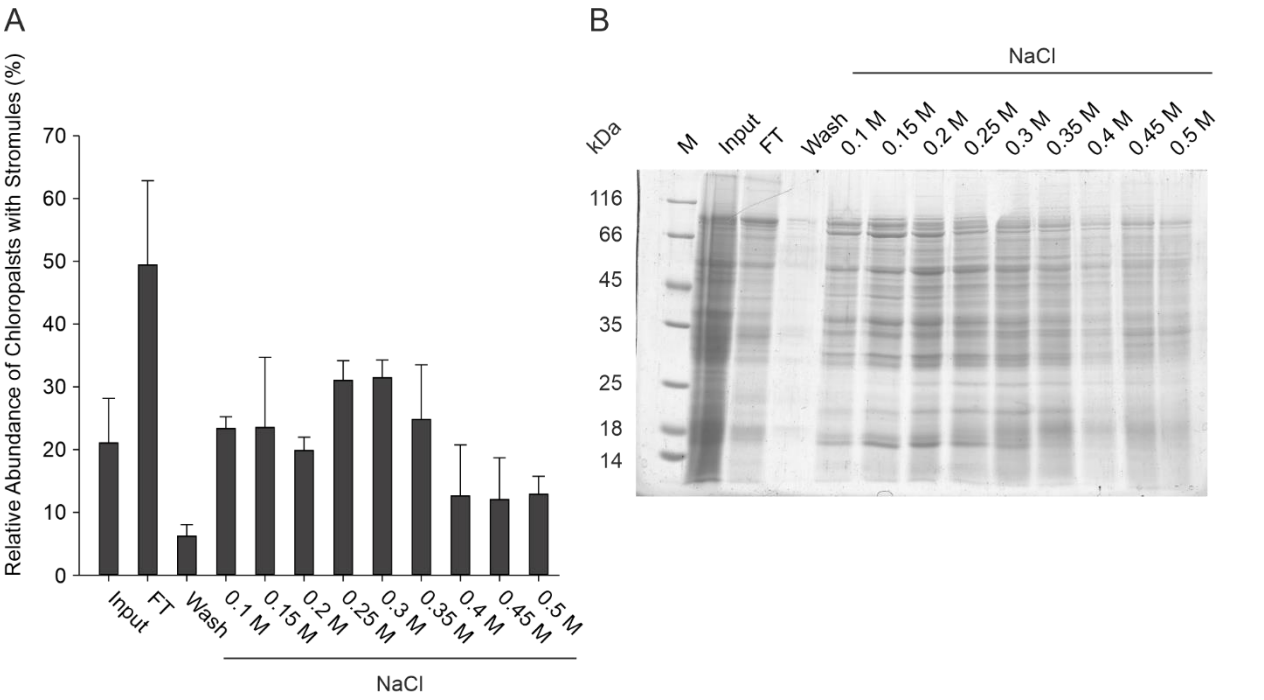

Figure 43 Protein extract fractionation via anion exchange chromatography. For the separation of the crude root cell extract, an anion exchange chromatography was performed. Input, flowthrough, wash, and nine elution fractions eluted with increasing concentrations of NaCl were taken. The results displayed in this graphic are representative. A) All fractions taken from the anion exchange chromatography were analyzed for *in vitro* stromule induction on isolated chloroplasts. The relative abundance of chloroplasts forming stromules is shown. Error bars represent the standard deviation of five technical replicates. B) Fractions taken from the anion exchange chromatography tested in A) were subsequently subjected to SDS-Page followed by Coomassie staining. The resulting gel is shown. Molecular weights of the marker bands (M) is given in kDa.

The input fraction displayed that the amount of overall protein used in this assay was quite high. This was expected and probably the reason for the high stromule induction capacities of all fractions. The wash fraction showed that the column was not overloaded, which led to the question of why all fractions were able to induce stromules in the *in vitro* assay. Although elution fractions were very similar in terms of protein composition, a different protein composition was present in the flowthrough. Taken together, the results showed that the wanted factor could be obtained in the flowthrough of the anion exchanger. About half of the cytosolic proteins in *A. thaliana* are negatively charged (D. Requião et al., 2017), reducing the number of potential proteins in the flowthrough section drastically with this approach.

3.3.9 The combination of linear sucrose gradient and ion exchange chromatography drastically reduces the number of potential protein candidates

Having two methods established that each effectively reduces the number of potential proteins responsible for stromule formation, the two methods were combined. Fraction one of the linear sucrose gradients harbored very few proteins and showed great potential in stromule induction (Figure 42). Therefore, it was decided to obtain fraction one from the sucrose gradient and subsequently conduct the fraction to anion exchange chromatography.

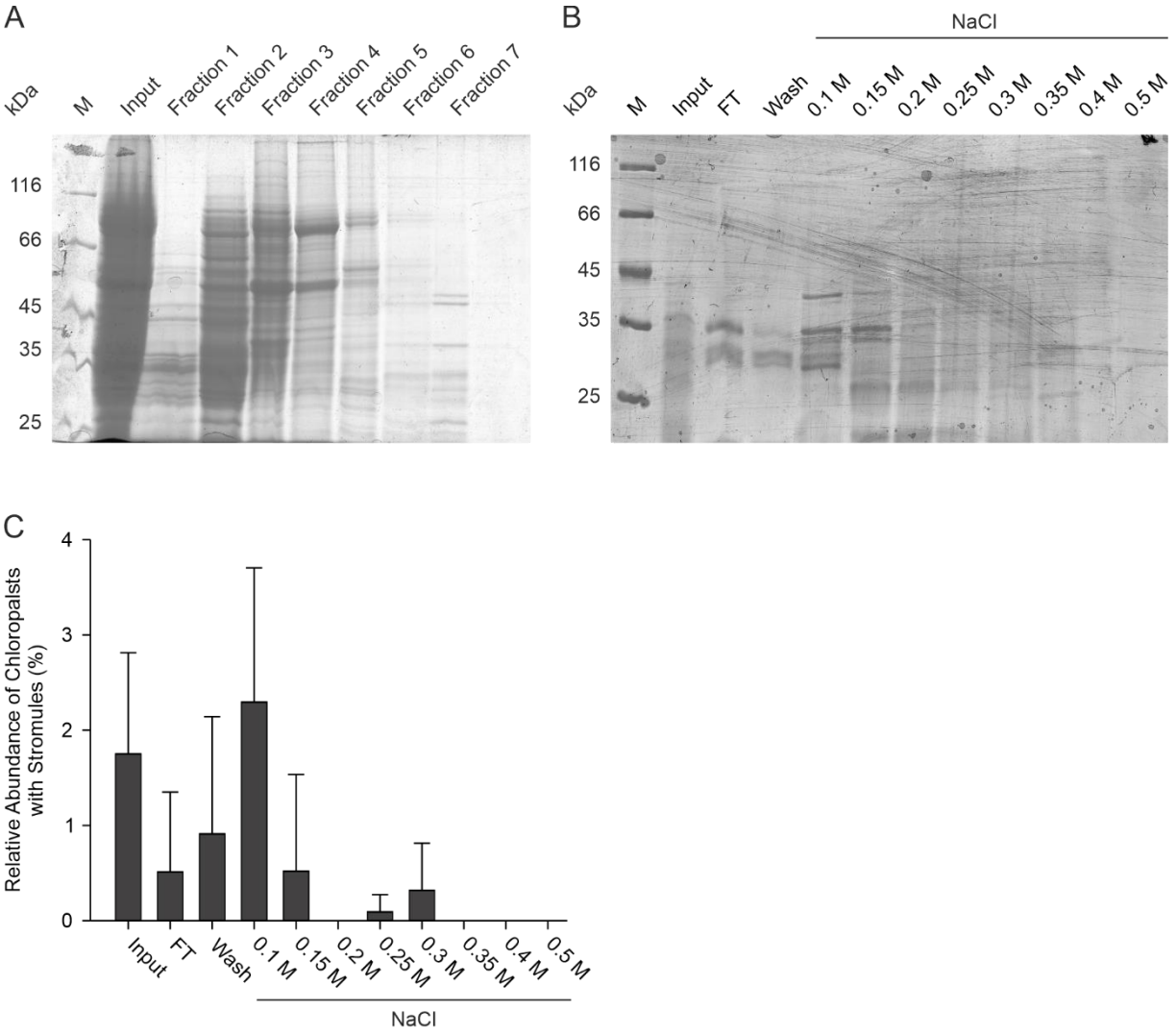

Figure 44 The combination of sucrose gradient and anion exchange chromatography results in a drastic reduction of proteins. For reducing the overall protein content, while maintaining the factors that induce stromule formation, fractionation of the crude cell extract by the sucrose gradient (Figure 42) and the anion exchange chromatography (Figure 43) were combined. A) Before anion exchange chromatography, the linear sucrose gradient fractionation was performed. To maintain protein levels in the final *in vitro* analysis, the protein amount was scaled up. Coomassie-stained gel including input fraction and fractions 1-8 from the sucrose gradient is shown. Molecular weights of the marker bands (M) are given in kDa. B) Fraction 1 obtained in A) was successively used in anion exchange chromatography. Coomassie-stained gel of input, flowthrough, wash and elution fractions is shown. Molecular weights of the marker bands (M) are given in kDa. C) Fractions obtained in B) were analyzed for *in vitro* stromule induction capacity on isolated chloroplasts. The relative abundance of chloroplasts forming stromules is shown. Error bars represent the standard deviation of five technical replicates.

As previously, the subordinated aim was to retain enough protein material to analyze each fraction in a final *in vitro* stromule induction assay. Each of the applied steps came with a great reduction of overall protein. This led to the problem that the initial amount of protein needed to be very high to maintain the wanted factors in sufficient amounts for microscopic analysis (Figure 44 A). Fraction 1 of the gradient was successively concentrated, washed, and further fractionated using anion exchange chromatography. Coomassie staining of the different fractions showed a drastic reduction of overall proteins and a clear difference between flowthrough and elution fractions (Figure 44 C). Although the initial protein content used for the sucrose gradient was very high, the amount of protein obtained after the anion exchange chromatography was very low. Fractions were subsequently analyzed for stromule induction capacity (Figure 44 D). The overall stromule induction capacity of the retained lysate was very weak. A maximum of 2 % of chloroplasts formed stromules during this analysis, showing that the amount of protein remaining after the procedure was very low. The increasing amount of stromule induction capacity in the consecutive fractions: flowthrough, wash, and 0.1 M NaCl strengthened the assumption that the wanted factor did not bind to the ion exchange column and was retained in the column throughout the wash fraction. Wash fractions were not fully concentrated during the workflow, because they possessed two times the volume of the other fractions. The concentration of the full volume would have taken too much time. The factor could have remained in the column and successively been washed away by the elution fractions. The procedure was applied with some changes for further experiments.

To enrich the protein factor in relation to the overall protein content of the lysate, a sucrose cushion centrifugation was applied (Figure 45 A) prior to the sucrose gradient. In contrast to the linear gradient centrifugation, the procedure was conducted at 400,000xg, which allowed for a very quick centrifugation procedure of 4 hours lowering the concentration of high molecular weight proteins.

Since the wanted factor was retained in the upper fractions of the linear sucrose gradient containing sucrose up to approximately 15 %, the cell lysate was collected in 15 % sucrose ensuring that the wanted factor would not pass the density of the sucrose during centrifugation. Cell extract gathered in isolation buffer supplemented with 15 % sucrose was underlaid with 40 % sucrose solution and centrifuged at 400,000xg for 4 hours to reduce the overall protein content and enrich the proportion of the wanted factor. The two phases of different sucrose contents were separated into three fractions (Figure 45 A). A top fraction contained the wanted factors and a bottom fraction contained undesired proteins. The intermediate fraction at the separation border of the two phases contained the wanted factor plus proteins that could not pass into the 40 % sucrose phase. Proteins from the intermediate fraction and the bottom fraction were excluded from the following analysis. All fractions were conducted to SDS-Page followed by Coomassie staining (Figure 45 B). The amount of protein in the intermediate and bottom fraction showed that the overall amount of protein was reduced by using the cushion centrifugation. The top fraction was concentrated, and the sucrose was washed out using Amicon filter units. Afterward, the concentrate was placed on the linear sucrose gradient. Coomassie staining of the fractions obtained from the gradient displayed proteins in between fraction one and four, showing that the initial cushion centrifugation eliminated all proteins that were not able to sediment through 40 % sucrose (Figure 45 C).

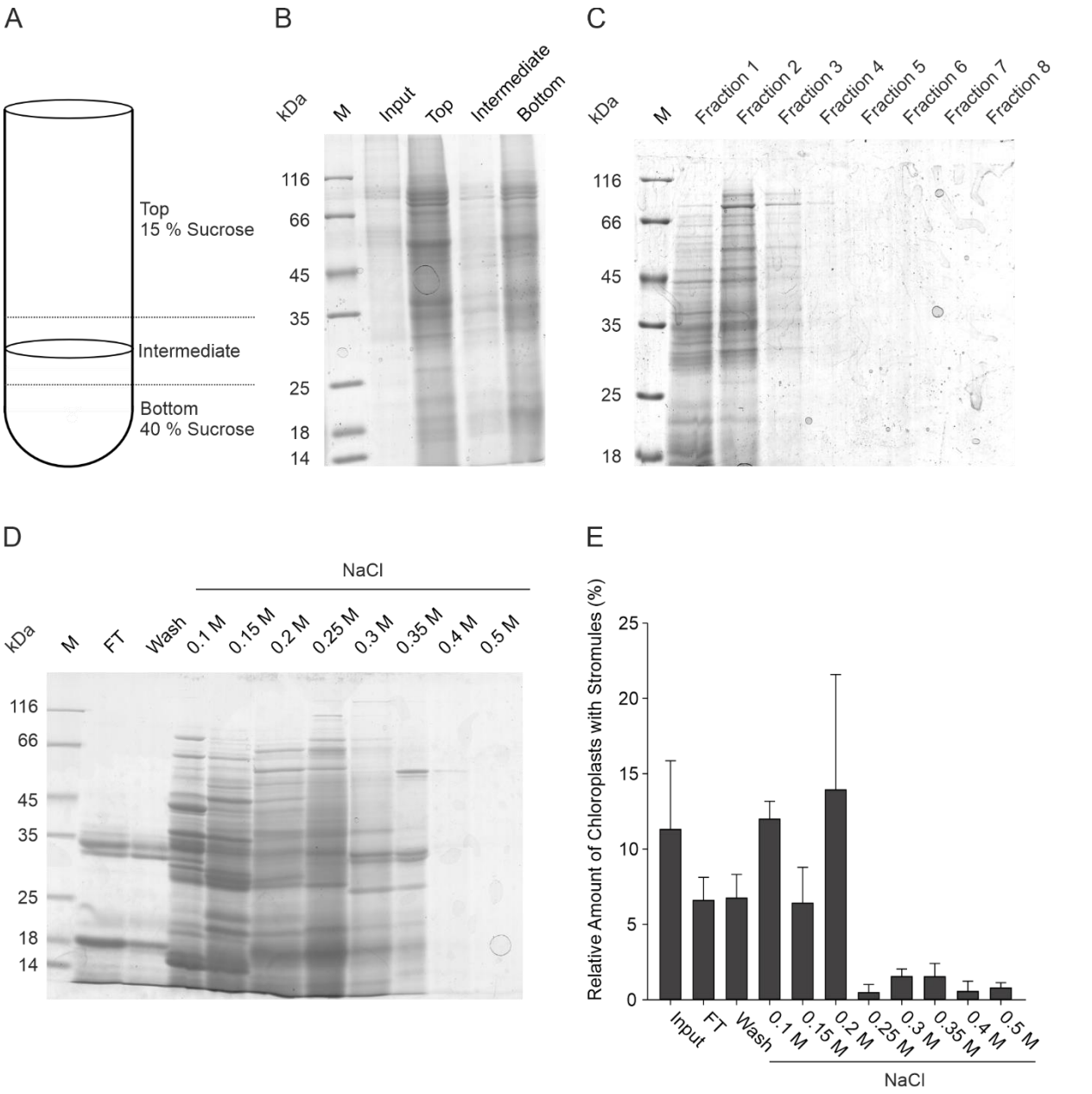

Figure 45 Sucrose cushion centrifugation before coupled fractionation procedure increases protein concentration. Due to low protein concentration in previous fractionation attempts (Figure 45), a sucrose cushion centrifugation was included before the pipeline to enrich the wanted factor in proportion to the overall protein content. A) Schematic visualization of the sucrose cushion centrifugation. Cell extract was collected in isolation buffer with 15 % sucrose and the solution was underlaid with 40 % sucrose solution. For further processing and analysis, of whether large molecular weight proteins are separated by this procedure, three fractions were assigned indicated by dotted lines. B) The three fractions obtained from the sucrose cushion centrifugation were conducted to SDS-Page, followed by Coomassie staining. Input, top, intermediate and bottom fraction are displayed. The top fraction was concentrated before gel analysis, therefore protein content is not comparable to other fractions. Molecular weights of the marker bands (M) are given in kDa. C) The top fraction of the sucrose cushion was layered on top af a linear sucrose gradient. Fractions obtained from the gradient were conducted to SDS-Page, followed by Coomassie staining. The resulting gel showing fractions taken from the gradient is shown. Molecular weights of the marker bands (M) are given in kDa. D) Fraction 1 obtained in C) was successively conducted to an anion exchange chromatography. Coomassie-stained gel of flowthrough, wash and elution fractions are shown. Molecular weights of the marker bands (M) are given in kDa. E) Fractions obtained in D) were analyzed for *in vitro* stromule induction capacity on isolated chloroplasts. The relative abundance of chloroplasts forming stromules is shown. Error bars represent the standard deviation of five technical replicates.

The amount of protein in fraction 1 was higher compared to previous experiments (Figure 44), indicating a higher concentration of protein, for what was aimed with this approach. Fraction 1 was gathered and subsequently used for ion exchange chromatography. SDS-Page followed by Coomassie staining revealed a significant reduction of proteins in the flowthrough fraction, while the protein content in the elution fractions was very high (Figure 45 D). Fractions were concentrated and conducted to the *in vitro* stromule induction assay (Figure 45 E). The overall stromule abundance was much higher than in the previous approach. In addition, the flowthrough fraction showed stromule induction, demonstrating that the wanted factor was present in this fraction. Again, the stromule induction capacity of the subsequent following fractions indicates that the factor did not bind to the column and was retained in fractions up to 0.2 M NaCl. As flowthrough was the fraction containing the least amount of protein but showed remaining stromule-inducing capacities, it was depicted as one of the final fractions that should be analyzed by mass spectrometry. As a second fraction 0.1 M NaCl was chosen. This fraction included the wanted factor each time the experiment was executed and the amount of protein in this fraction was quite high (Figure 45 D), making it possible to compare the fraction to other obtained elution fractions. As a third fraction 0.2 M NaCl was chosen to be analyzed via mass spectrometry. Most of the time the factor was also present in 0.2 M NaCl, while the elution pattern looked very different compared to 0.1 M NaCl (Figure 45 D) giving the potential to further reduce the amounts of proteins involved in stromule formation. As a last fraction 0.35 M NaCl was chosen, most of the time not containing much of the wanted protein factor, but still containing Coomassie visible amounts of proteins (Figure 45 D). The abundant proteins in this fraction were most likely not involved in stromule formation. Therefore, abundant proteins gathered in this elution fraction could be excluded as potential factors responsible for stromule induction.

To sum up the findings of the fractionation process: The number of abundant proteins in the final fractions was drastically reduced compared to the crude cell extract and four fractions were appointed which should be conducted to LC-MS analysis.

3.3.10 LC-MS analysis of the fractionated protein extract

The pipeline for the generation of fractions that could be conducted to mass spectrometry was established using root extract from *Pisum sativum* (Figure 42-Figure 45). Peas were used, because the amount of plant material, which could be gathered in a relatively short amount of time, was very high. Proteomic databases of *Pisum sativum* are still lacking information compared to databases of *Arabidopsis thaliana*. Because of this, *Arabidopsis thaliana* was used for the sample preparation process for the LC-MS analysis. Attempts to gather enough plant and protein material from *Arabidopsis* to show stromule induction using the *in vitro* assay were not successful. However, data generated during light sheet-based fluorescence microscopy of root plastids (Figure 31-Figure 35) showed the abundance of stromules at root plastids of *Arabidopsis* grown at normal conditions. Therefore, it was assumed that the factor of interest was also present in the roots of *Arabidopsis*. *Arabidopsis* plants were grown upright on ½-strength MS medium with 1% sucrose supplementation to mediate root growth for 4 weeks. Roots were harvested and the established fractionation procedure (Figure 45) was performed. The resulting fractions were conducted to SDS-PAGE. The gel was subsequently silver stained for visual analysis of the very low concentrated fractions (Figure 46). The resulting fractions were comparable to the ones obtained from *Pisum sativum*

(Figure 45 D). Both fractions were very similar which indicated that the pipeline led to the same protein output in *Arabidopsis thaliana* and *Pisum sativum*. Triplicates of the fractions were obtained and conducted to LC-MS analysis.

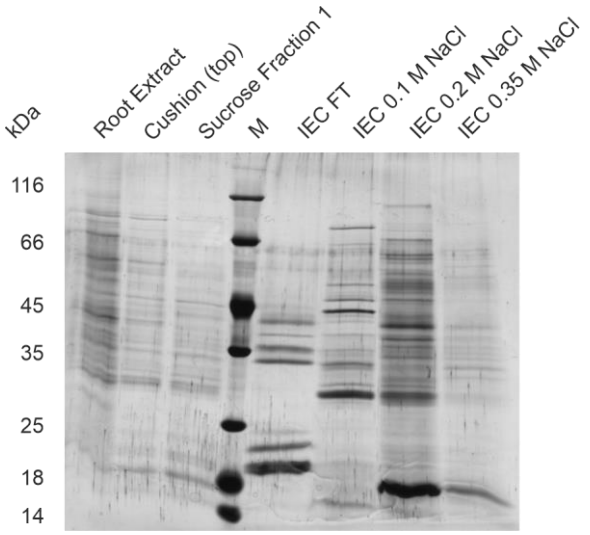

Figure 46 Representative gel picture of *Arabidopsis thaliana* samples that were fractionated for mass spectrometric analysis. The fractionation pipeline established previously (Figure 45) was used to fractionate the root extract of *Arabidopsis thaliana*. Fractions of intermediate steps and final elution fractions that were used for mass spectrometric analysis were conducted to SDS-Page followed by silver staining of the gel. The gel shows proteins of the unfractionated root extract, the top fraction of the cushion centrifugation (cushion (top)), fraction 1 of the linear sucrose gradient (sucrose fraction 1), and four fractions of the final anion exchange chromatography (IEC) namely flowthrough (FT) and the elution fractions 0.1 M, 0.2 M, and 0.35 M NaCl. Molecular weights of the marker bands (M) are given in kDa

After the deletion of potential contaminants, the LC-MS analysis revealed 3,214 hits that were found throughout all replicates of all four samples. To limit the number of contaminants in the triplicates of the fractions, each hit that was found less than two times throughout the replicates were excluded. This left 1925 hits that were present in two of the three replicates for at least one fraction. Those hits were utilized for the generation of a Venn diagram (Figure 47). 358 hits were identified in the flowthrough section, 1,024 in 0.1 M NaCl, 1,269 in 0.2 M NaCl and 845 in 0.35 M NaCl. The distribution of the identified proteins was expected when compared to the protein abundance displayed in the gel picture (Figure 46). Considering that the protein factors responsible for *in vitro* stromule formation were found in the flowthrough section, only hits that were present in the flowthrough section were included for the following analysis. This reduced the amount of potential proteins to 358. Of those 358 protein candidates, 104 were solely found in the flowthrough section, 104 in flowthrough and 0.1 M NaCl, 43 in flowthrough, 0.1 M NaCl and 0.2 M NaCl, and 103 in all four fractions. Following the previous analysis (3.3.9), all hits that were present in all four fractions were excluded from the analysis, since the 0.35 M NaCl fraction did not induce stromule formation during the *in vitro* assay. Additionally, since the 0.1 M NaCl fraction displayed a stromule induction during the *in vitro* assay, all proteins that were found in the 0.2 M NaCl fraction, but not in the 0.1 M NaCl fraction were excluded from the analysis. This left a maximum of 251 potential protein candidates (Supplemental Table 1) distributed in the three remaining combinations of fractions: Flowthrough, flowthrough, and 0.1 M NaCl, flowthrough and 0.1 M NaCl and 0.2 M NaCl. The wanted protein factor was present in all three fractions during the *in vitro* stromule formation assay. Therefore, 43 hits found in all three fractions were conducted for a bioinformatical analysis of potential protein functions. Since previous results also displayed variations in the stromule-inducing capacities of the elution fractions (Figure 44, Figure 45), also proteins that were found solely in the wash fraction and proteins that

were present in the wash fraction combined with the 0.1 M NaCl elution fraction were considered in the bioinformatical analysis.

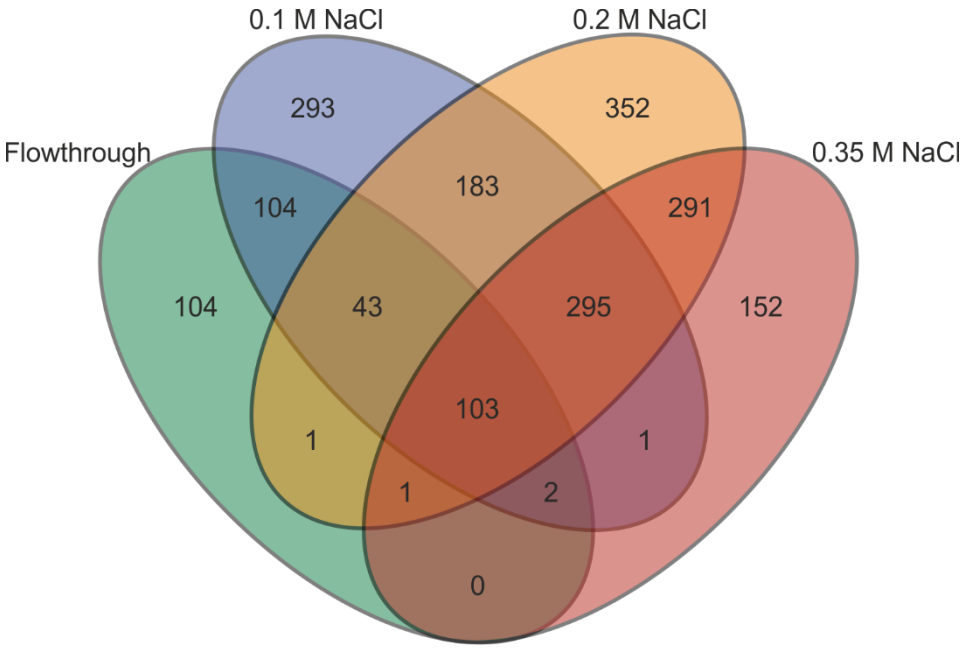

Figure 47 Venn-diagram of the LC-MS analysis. The results obtained by mass spectrometry were analyzed and a Venn diagram was generated displaying the distribution of proteins identified in at least two of the three replicates in each sample.

The size of proteins found was predominantly very small showing the effect of the sucrose gradient centrifugation. The functions of the identified proteins were very broad and scattered around all kinds of cellular functions. In addition, a variety of proteins with unknown functions was present. Earlier experiments suggested that protein factors with lipid binding functions could be involved in stromule formation (Figure 41). For this reason, a focus was laid on proteins with potential or proven functions in membrane or lipid interaction. All proteins that fitted the regime or that were of unknown function were carried to a final collection of potential candidates responsible for *in vitro* stromule formation. Throughout the analysis, no protein candidate was found that had a known function in membrane tubulation. The combination of hits found in all three fractions revealed 11 potential candidates (Table 3), of which two were predicted to be involved in membrane organization, five candidates had potential functions in vesiculation while nothing was known about the function of the remaining four. Hits that were found solely in the flowthrough section revealed 22 potential candidates (Table 4). Of those protein candidates, one was assigned to be involved in lipid interaction, one had a potential sterol binding function, four were involved in the organization of vesicle formation at various cell sides, and 16 candidates were of unknown function. The combination of the flowthrough with the 0.1 M NaCl fraction revealed 21 potential candidates (Table 5), of which one was potentially involved in sterol binding, three were potentially involved in vesicle formation at various cellular sides, and the remaining 16 candidates were not associated with specific functions. Even though no candidate was found that directly fitted the regime, this list

harbored some proteins that were involved in protein-lipid or protein-membrane interaction. Those proteins could potentially be involved in stromule formation. In addition, all proteins with unknown functions could potentially be involved in stromule formation. Further studies of those protein candidates could give a deeper understanding of the molecular mechanisms underlying stromule dynamics.

Table 3: Potential protein candidates involved in stromule formation identified in LC-MS analysis. Candidates were found with a minimum of two hits in flowthrough, 0.1 M NaCl, and 0.2 M NaCl fractions. Protein candidates with two hits in 0.35 M NaCl were excluded. Shown candidates are potentially involved in membrane organization, vesicle formation or no function could be assigned up to date.

Gene Number	Name	Function
At4g15410	Plant UBX domain-containing protein 5	Membrane organization
At4g22150	Plant UBX domain-containing protein 3	Membrane organization
At5g22770	AP-2 complex subunit alpha-1;AP-2 complex subunit alpha-2	Vesicle organization
At3g62560	GTP-binding protein SAR1A	Vesicle organization
At1g04750	Vesicle-associated membrane protein 721	Vesicle organization
At3g46060	Ras-related protein RABE1c	Vesicle organization
At3g09900	Ras-related protein RABE1a	Vesicle organization
At2g04690	---	Unknown function
At3g07460	---	Unknown function
At5g20060	Abhydrolase_2 domain-containing protein	Unknown function
At1g23130	---	Unknown function

Table 4: Potential protein candidates involved in stromule formation identified in LC-MS analysis. Candidates were found with a minimum of two hits in flowthrough fraction. Protein candidates with two hits in 0.35 M NaCl were excluded. Shown candidates are potentially involved in lipid interaction, sterol binding, vesicle organization or no function could be assigned up to date.

Gene Number	Name	Function
At2g33470	Glycolipid transfer protein 1	Lipid Interaction
At2g16005	MD-2-related lipid-recognition protein ROSY1	Sterol binding
At1g23900	AP-1 complex subunit gamma-1	Vesicle organization
At5g22360	Vesicle-associated membrane protein 714	Vesicle organization
At3g08530	Clathrin heavy chain 1	Vesicle organization
At1g60070	AP-1 complex subunit gamma-2	Vesicle organization
At1g76020	---	Unknown function
At2g04170	TRAF-like family protein	Unknown function
At4g17480	Alpha/beta-Hydrolases superfamily protein	Unknown function
At4g00752	Plant UBX domain-containing protein 9	Unknown function
At5g04750	MUK11.3	Unknown function
At4g27520	Early nodulin-like protein 3	Unknown function
At4g08280	Glutaredoxin-like protein	Unknown function

At4g34150	---	Unknown function
At1g14930	Major latex homologue type2	Unknown function
At1g35260	MLP-like protein 165	Unknown function
At1g07040	---	Unknown function
At3g58550	Non-specific lipid transfer protein GPI-anchored 22	Unknown function
At3g08030	---	Unknown function
At1g76160	---	Unknown function
At4g07820	---	Unknown function
At2g38870	Putative protease inhibitor	Unknown function

Table 5: Potential protein candidates involved in stromule formation identified in LC-MS analysis. Candidates were found with a minimum of two hits in flowthrough and 0.1 M NaCl fractions. Protein candidates with two hits in 0.35 M NaCl were excluded. Shown candidates are potentially involved in sterol binding, vesicle formation or no function could be assigned up to date.

Gene Number	Name	Function
At1g45015	---	Sterol binding
At4g26750	Protein HOMOLOG OF MAMMALIAN LYST-INTERACTING PROTEIN 5	Vesicle organization
At5g58060	VAMP-like protein YKT61	Vesicle organization
At4g32150	Vesicle-associated membrane protein 711	Vesicle organization
At1g72230	---	Unknown function
At5g26280	---	Unknown function
At1g51850	Leucine-rich repeat protein kinase family protein	Unknown function
At5g44130	Fasciclin-like arabinogalactan protein 13	Unknown function
At2g25980	Jacalin-related lectin 20	Unknown function
At2g26210	Ankyrin repeat family protein	Unknown function
At4g10300	---	Unknown function
At1g58270	---	Unknown function
At3g20370	---	Unknown function
At1g56580	SMALLER WITH VARIABLE BRANCHES	Unknown function
At1g27030	DUF1338 domain-containing protein	Unknown function
At1g51840	Malectin_like domain-containing protein	Unknown function
At1g21090	---	Unknown function
At5g26330	---	Unknown function
At3g17840	Probable inactive receptor kinase RLK902	Unknown function
At2g27060	Leucine-rich repeat receptor-like protein kinase	Unknown function
At5g46230	CRAL-TRIO domain-containing protein	Unknown function

4 Discussion

4.1 The spatial and temporal resolution must fit the needs of the study

Plastids are a diverse group of organelles each specialized in distinct functions. Mostly because of accessibility and the fact that they carry out photosynthesis, most research targeted chloroplasts while their relatives got somehow disregarded. The insights gathered about the light avoidance reaction of chloroplasts are a fine example of the difference in attention that has come to the subspecies of the plastid family (Oikawa et al., 2003; Schmidt Von Braun & Schleiff, 2008; Suetsugu et al., 2016; Wada & Kong, 2018). While all plastids differ in their specific function for the plant, all types contribute to basic metabolic pathways (Rolland et al., 2018). This creates a need for organellar transport for site-specific nutrient distribution and exchange of metabolites with other organelles. The transport mechanisms of chloroplasts are still under investigation, but the main aspects of the molecular mechanisms have been discovered (Schmidt Von Braun & Schleiff, 2008; Suetsugu et al., 2016; Wada & Kong, 2018). However, the transport mechanisms of chloroplasts and plastids in the roots differ greatly since the chloroplast's movement is induced by light (Wada, 2018). This work strived for an investigation of the plastidal movement in *Arabidopsis thaliana* using light sheet-based fluorescence microscopy. Light sheet-based fluorescence microscopy has been shown to reduce phototoxic effects during imaging of the samples while drastically enhancing the record time compared to confocal laser scanning or bright field microscopy (Stelzer, 2014). Earlier work demonstrated that plants can successfully be implemented into a light sheet-based microscopic setup (von Wangenheim, 2014) and the utilized mechanisms were applied in this work. Even though light sheet-based fluorescence microscopy was advantageous for the needs of the study, the experimental setup restricted the imaging to very specific parts of the root. Even though different structural parts of the roots were accessible, the differentiation zone of the root was chosen to be analyzed to generate comparable data between replicates and conditions (Figure 5 A). The differentiation zone as a mature part of the root is heavily engaged in nutrient uptake and is characterized by the presence of root hairs. For this reason, the differentiation zone is easy to distinguish in the 3D environment. Initial experiments on the plants (Figure 5 B) showed that the microscopic setup limited the image acquisition to the two outer layers of the *Arabidopsis* root, namely the epidermal and the cortex cell layer. The acquisition of deeper layered tissue resulted in a dramatic decrease in resolution and was therefore not suitable for the combination of light sheet microscopic setup and sample preparation that was used. For a wholesome analysis of root plastid movements, coverage of a cross-section of the root would be desirable. The information gathered in an analysis of a more wholesome approach would deepen the understanding of the plastid's functions in the cell, because the root is composed of different tissues that could affect the plastid's function in the cell. Such analysis however would create a drastic need for additional marking of the cell wall or membrane components to differentiate between tissues. However, the increase of spatial coverage is inevitably linked to a decrease in temporal resolution. The temporal resolution defines the number of data points that are gathered from moving objects and by increasing the spatial coverage, the possibility of missing out on very fast-moving objects increases as well. The time consumed by the acquisition of 31 frames in this study was 4.3 seconds (2.2.2). The analysis of directed plastidal movement (Figure 26 C, Movie 9, 12) and stromule dynamics (Figure 31 C, Movie 9) showed that

a decrease in temporal resolution would result in a drastic loss of information regarding fast-moving plastids and stromules analyzed here. The temporal resolution of 4.3 seconds per frame was guided by the maximal transport speed of 7 µm/sec measured for *Arabidopsis* myosin XI-2 so far (Tominaga et al., 2013) and the average size of an *Arabidopsis* root cell (Figure 23). Even in case of additional movement speed, a plastid covering the length of the root would be captured every 30-40 µm and be visible in multiple frames. Even though higher motions than 7-8 µm/sec were not expected, the adapted temporal resolution would exclude such motion patterns. However, the manual analysis of all image data acquired during this study (Figure 27, Figure 28) gave no need for the assumption that a higher speed of plastidal transport exists in *Arabidopsis*. Therefore, the spatial and temporal coverage chosen for this study seemed to be sufficient for a description of the plastidal motions in a cellular context and more so for the description of all existing plastidal motion patterns. However, one frame each 4.3 seconds still has the capacity for information loss. A lower spatial resolution spanning not two, but just one cell layer could be taken out to increase the temporal resolution. A lower temporal resolution for further studies is not recommended for the imaged frame size.

4.2 The automated tracking analysis needs to be refined for tracking of root plastids

One of the key aspects of this study was the establishment of an automated high throughput analysis approach for the tracking of root organelles. Besides this study, such a tracking pipeline was created to utilize it in future co-analyzes of differently labeled organelles and thereby generating information about cellular communication and transport systems. Since the manual tracking and colocalization analysis is very time-consuming and prone to human errors, an automated tracking pipeline for high throughput analysis is recommended to process data from high replicate numbers. The variety of different movement characteristics observed in replicates of the same conditions during this study (Movie 1 and 8) is proof of concept that a thorough picture of the organellar movement needs a high number of replicates to be analyzed. This is the only way to generate a sufficient database to abstract cellular functions.

The automated 4D tracking approach itself depends on several variables that greatly influence the outcome of the tracking. Mostly, the automated approach relies on the intensity values of the image set. For the performance of an automated approach on different replicates, the image quality needs to be very consistent. Especially inconsistency in the background and differences in the focus (compare Movie 1 to Movie 3 or 6) challenges the automated approach. Therefore, the setup of the automated tracking pipeline, which uses the same conditions for each dataset (Figure 7, Figure 11), needed to make compromises between the stringency and general applicableness of varying image qualities. As a result, the performance of the automated tracking approach varied greatly between the analyzed image sets and the need for manual correction (Figure 13, Figure 14).

The segmentation of objects can be appointed as the most critical step during the tracking routine. Since the segmentation of objects is purely intensity based, tradeoffs needed to be made for the algorithm to work on noisy as well as crowded image sets. In addition, great variation in shapes needed to be detected. Due to the many shapes, sizes, and intensities that were displayed by the plastids (Movie 1- 8) a tradeoff

needed to be made between too much and too little segmentation of the dataset. On one hand, smaller plastids with very little intensity needed to be included in the analysis and created the need for low stringency in the segmentation. On the other hand, the non-consistent shape of stromules created the need for a very high stringency in segmentation (Figure 9 and Figure 10). On top, the Z-resolution (Figure 6) greatly influenced the segmentation in the 3D environment and favored large and more intense structures upon the smaller and darker plastids. A compromise was established, with a regime that mostly segmented plastidal bodies and that was set to disregard stromules. However, due to some stromules displaying very high intensity values, those were also segmented by the algorithm. In summary, the segmentation of the image data delivered good results in the segmentation of plastid bodies and excluded only very small plastids with low intensity (Figure 9, Figure 10). However, it was also very error-prone in the segmentation of plastids with stromules (Figure 15 A).

The automated tracking was the second vulnerable step during the tracking pipeline. To perform well, the tracking algorithm required a very clear segmentation and, in the best case, steady movement of the segmented objects in-between frames. Since the different shapes of plastids greatly interfered with the segmentation, the requirements for proper tracking were hardly fulfilled. Nevertheless, a great portion of the data generated during the automated tracking (Figure 12-Figure 14) was assigned correctly and gave a good basis for the following analysis. Even though wrongly assigned tracks made up a small portion of the overall tracking data, it interfered especially in segments of very high and very low velocity of plastids, leading to great jumps in movement tracks (Figure 13 - Figure 14 A, C) The correction of the wrongly assigned tracks was necessary for the overall data to generate a comprehensible picture of the cellular activities. Keeping in mind that later studies should make use of this automated approach to analyze organellar interaction, the wrongly assigned track could greatly interfere with such analysis. Even though the manual correction missed out a lot of wrongly assigned tracks, especially for segments created by the segmentation of stromules (Figure 15), it generated acceptable data for the plastidal motions, especially for very bright and segmented objects. Very small objects that were either not properly segmented or that moved very fast were not captured well in this analysis (compare Figure 21 D+C with Figure 26 C or Movie 12). For the tracking of more uniform cell organelles, the automated approach established during this work is sufficient. For follow-up studies, the analysis of organellar interaction is necessary to gather information about the function of organellar movement. However, for adequate tracking of differently shaped structures, either a more specific approach or an adaption of the post-processing of the generated data would be advised.

The automated analysis was greatly disturbed by structural variation (Figure 15) and limited by the Z-resolution (Figure 6) obtained during image acquisition. In another study of the plastidal movement patterns, based on the acquired image sets, it was shown that about 90 % of information that was found by the 4D analysis was covered by a 3D analysis, condensing the images to a maximum intensity projection leaving a 2D environment over time (Plomer, unpublished). This effect was probably introduced due to the elongated shape of the cell and the space, taken by the vacuole. By subtracting the Z-dimension, the manual analysis in a 3D environment could be carried out with only minor information loss. Due to the structural variety of plastids, the specifics of the plastidal motion were of great interest to this study. The automated analysis generated an overview of plastidal motion patterns based on the angle between movement vectors and the vector length in-between two frames (Figure 18). However, it did not deliver

specifics of the plastidal movement. To analyze the variety of plastidal motions and analyze the possible role of stromules in the plastidal movement, a manual analysis of the data was inevitable. The information gathered in the manual analysis (Figure 25-Figure 35) provided a detailed analysis of the plastidal motion patterns. The manual analysis needed a significantly higher amount of time compared to the automated analysis, but the level of detail in the description was much higher. Although the results differed in some terms from the automatically generated ones, especially in terms of maximal velocities covered (Figure 21, Figure 26), the trends of the general motion distribution and the changes in motion throughout different conditions matched the automated approach (Figure 24-Figure 27). As long as automated approaches are hindered by structural variabilities, like those in root plastids, such a semi-automated analysis of movement patterns combining the throughput capacities of the automated approach with the level of detail provided by a manual inspection, could be suitable for further studies.

4.3 The variety of plastidal motions is not driven by cytoplasmic streaming

The plastidal motion between two consecutive frames defined the velocity of each plastidal movement event. These movement events were the basis for the analysis of the plastidal motion (Figure 24, Figure 26, Figure 24-Figure 27). Even though the automated analysis of the plastidal movement was error-prone, especially in terms of higher velocities, it rendered the different motion types displayed by root plastids. The velocity of plastids is either driven in a directed manner by the direct attachment of motor proteins, in a semi-directed manner by the transport of other attached organelles, or in an undirected manner by cytoplasmic streaming (Vick & Nebenführ, 2012). Due to the lack of differently labeled organelles besides plastids, no interaction or colocalization analysis could be performed in this study. This limits the conclusions about the function of the plastidal motions that can be drawn from the findings. However, the data allowed for statements and speculations about the directed or undirected movement mechanisms of plastids and the underlying driving forces.

The outcome of the automated 4D analysis displayed the distribution of different plastidal movement patterns in the root (Figure 21, Figure 24). Motions up to 0.05 µm/sec were associated with background noise signal induced by intensity changes of the plastids between frames (Figure 16). The determination of noise for this study is based on the average movement displayed by plastids that did not show a delocalization of more than 2 µm throughout the time of imaging. This very practical approach disregarded the different sizes and shapes of plastids. Since the tracking algorithm calculated the tracks from the geometrical center of each segment, bigger plastids with higher capacity for fluctuation could lead to bigger steps in between two frames. For a detailed analysis of the noise generated during this study, the plastids should be clustered by size and individual noise for each size category should be subtracted from each movement event. However, due to a low Z-resolution (Figure 6), the measurement of the plastid size was falsified and a correlation between plastid size and the noise was not generated. However, taking the averaged value of 0.05 µm/sec as a hallmark for noise, 4D data showed that about half of the recognized events in each dataset were classified as no motion (Figure 21 A, Figure 24 A). The number of stationary plastids determined in the 3D analysis (Figure 25, Figure 26, Figure 30) supported those findings. The cytoplasmic streaming in *Arabidopsis* was shown to be driven by a member of the myosin XI family (Tominaga et al., 2013). A general cytoplasmic flow should affect all organelles in similar ways and should

contribute to a monotone flow that can be observed at different organelles. The fact that plastids lacking motion as well as the high-speed movement of plastids were observed in the same cell (Figure 20, Figure 22, Movie 1, 2, 24) hints at very specific regulation of the plastidal transport rather than a general transport in a cytoplasmic stream. In addition, the high amount of stop-and-go motions recognized in the automated analysis (Figure 21 B, C, D, Figure 24 B, C, D) points to very specific mechanisms underlying the plastidal transportation in the cell, mediating either the transport or the stop. Due to the broad range of functions plastids can carry out, no further speculation should be made about the cellular functions of the stop-and-go motions. However, the absence of intense wiggling motions in stationary plastids (Movie 10, 13) and stop motions (Movie 24) contradicts the theory that the plastidal motion is mediated solely by cytoplasmic streaming. The maximal motions captured during this analysis (Figure 26 C) hint at a myosin XI family-mediated transport either by direct or indirect attachment to the organelles. However, the plastidal motion palette is very versatile (Figure 24-Figure 35), and the data gathered in this study allow assumptions about different movement mechanisms that drive the plastidal movement. Since the data cannot show direct myosin XI regulation of these movement patterns, some of them might be driven by cytoplasmic streaming.

4.4 Directed transport of plastids is mediated by the actin-myosin machinery

Partially directed and directed transport of plastids made up the smallest proportions of the classified plastidal movements in the automated analysis (Figure 21 D, E, Figure 24 D, E). Mechanisms of the molecular machinery mediating plastid transport in the cell were derived. The term directed stands for plastids that show a directionality in their movement rather than unspecific motion with many turns. Directed transport of plastids could occur in any velocity (Figure 18, Figure 20, Figure 22, Figure 26, Movie 1, 3, 11, 12, 23, 24) and was observed in many cases with very high velocities over 1 µm/sec (Figure 21 E, Figure 24 E, Figure 26 C, Movie 12). The highest velocity observed for directed tracking was traced manually at 8 µm/sec in salt stress conditions (Figure 26 C, Movie 12). Movements of more than 7 µm/sec were observed in two different replicates of salt stress conditions (Figure 26 C). Notably, those movement speeds were traced in a 2D environment and therefore could well be faster by the addition of the Z-layer. The fastest movement of a motor protein in *Arabidopsis* described so far was mediated by a member of the myosin XI family, namely myosin XI-2 with 7.2 ± 0.5 µm/sec (Tominaga, 2003; Tominaga et al., 2013). The observed movements could therefore be mediated by this member of the myosin XI family, although it has been shown that organellar transport, in general, is broadly distributed in the myosin XI family (Peremyslov, Prokhnevsky, and Dolja 2010). Most directed movements that were observed displayed velocities between 0.5 and 4 µm/sec (Figure 26). Even though no final proof can be given by the findings of those studies, the fact that directed movement was significantly reduced in sucrose-depleted plants (Figure 24 E, Figure 26 B) leads to the assumption that movement speed is dependent on the energy that is available for the motor proteins and assembley of cytoskeletal structures. The function and velocity of myosins is dependent on the availability of ATP (Tominaga, 2003). However, besides the energy delivered by sucrose, other factors need to be involved in the speed of directed movement, since the maximal velocities observed in different conditions differed greatly.

The directed movement was observed in all cells, but an assignment of the cell layer was not always possible, because the Z-resolution did not allow for a distinct analysis of the cell borders (Figure 6). Conspicuously, the most directed movement was found in the epidermal cell layer in cells that possessed root hairs (Figure 20, Movie 24). The final destination or turning point of the plastids could not be determined, but much-directed transport was performed on tracks from and to the root hairs. Root hairs are a very rapidly growing structure. With a growing speed of up to 1 µm/min (Grierson & Schiefelbein, 2002) they need to be constantly provided with metabolites to mediate the growth of the cell, which is executed at the tip of the cell (Mendrinna & Persson, 2015). Those tip-growing events are commonly found in root hairs and pollen tubers (Mendrinna and Persson 2015) and need to be highly regulated. Upon the broad functions plastids can carry out, the storage of starch and lipids, as well as the synthesis of lipids, could play key roles in the fast growth of root hairs by providing the material and energy that is necessary for the expansion of the cell. The directed movement of plastids from and to the root tip could therefore be linked to tight regulation of the cellular transport mechanisms to provide a constant pool of material and resources for the growth process.

Many plastids displaying directed motion, especially plastids that were transported from and to the root tip, seemed to use the same routes for their movement (Figure 22, Movie 23, 24). The 4D analysis allowed for specific descriptions of the cellular routes and displayed high similarity of various tracks (Figure 22). The directed movements on those tracks were tightly bound to one movement direction that was not spontaneously reversed. The observation of stop-and-go motions, as well as the finding that plastids can enter and leave these tracks at different locations (Figure 22), led to the assumption that the directed movements of plastids are mediated by cytoskeletal filaments of the cell and not by static cytoplasmic streaming. The stop-and-go patterns can be explained by the occasional anchorage of the plastids at cellular components while floating in a stream. Meanwhile, the distinct overlapping usage of some routes that can be entered or left at different locations is difficult to explain by a constant cytoplasmic flow. This strengthens the assumption that the directed motion of plastids is specifically mediated by attached motor proteins. Since in plants mostly members of the myosin XI family are known to reach velocities of more than 1 µm/sec (Jonsson et al., 2015; Prokhnevsky et al., 2008; Tominaga et al., 2013), the directed transport is likely to be mediated via actin filaments. Furthermore, the disruption of actin filaments was shown to eliminate fast organellar movement (Nebenführ & Dixit, 2018). Even though this was not shown for plastids, this strengthens the theory that the directed movement observed in this study is actin-myosin-dependent. Actin filaments are short structures that can reach up to several dozen µm (Gittes et al. 1993) and the plant cell was shown to be veined with several actin cables that are interconnected in between each other (Durand-Smet et al. 2020). The stop-and-go motion of directed plastids observed in this study (Figure 22, Movie 24) might mark specific locations in which actin routes either end or connect to each other. Both could result in a steric barrier or a detachment of the motor protein leading to a temporary stop of motion. Upon reattachment or reorientation of the motor proteins, the motion could be continued. In addition, differential entering and leaving of the cellular routes could be explained by a tightly interconnected actin net providing several options for the organelle to be transported. However, those kinds of targeted movements would need tight regulation and addressing in the cell. The fact that during this work all plastids are labeled, disregarding their differentiation and function, the data obtained from this study do not allow for speculations about any address signals that are linked to the plastids' function.

4.5 Stromule dynamics and their involvement in the plastidal motion

Stromules are characterized as a common feature of plastids which are very dynamic (Hanson & Hines, 2018; Kwok & Hanson, 2004b; Natesan et al., 2005). The results of this study underline both statements (Figure 28, Figure 29, Figure 31, Video 9, 14). Although differences in the number of stromules were observed between conditions and replicates (Figure 28), many plastids displayed a minimum of one stromule. Although the stromule function up to now is not elucidated, the amount of stromules formed during this study points out their physiological relevance of them for the root plastids. Since no further label was introduced to highlight potential interaction sites of stromules, this work only gives the basis for speculation about the function of the excrescences in the cellular context. Other studies that described the organellar colocalization with stromules at chloroplasts (Köhler and Hanson 2000; E. Y. Kwok and Hanson 2004; M. Schattat et al. 2011a) highlighted the potential interaction sites stromules provide. However, this matter should not be addressed too much at this point. The conditions applied for light sheet microscopy of the roots in this study were chosen to achieve a temporal resolution sufficient for the analysis of objects moving in a velocity range of about 7 µm/sec. These conditions also suited the analysis of the stromule dynamics. Prior studies regarding stromule dynamics (Jessica L. Erickson et al. 2018; Sampath Kumar et al. 2018) were solely performed on chloroplasts. Since the movement mechanism of chloroplasts differs greatly from the root plastid dynamics, (Schmidt Von Braun and Schleiff 2008, Figure 22) one can speculate if the dynamics observed at stromules induced at the chloroplast membrane are related to the dynamics displayed at root plastid stromules. The dynamics of chloroplast stromules were described to be associated with microtubules (Erickson et al., 2018; Kumar et al., 2018). In two different studies, microtubules-related and unrelated movement of stromules was not measured with more than 0.5 µm/sec. These velocities fit the microtubule-related movement speed of kinesins (Yamada et al. 2017), but did not fit the stromule dynamics measured at root plastids in this study with up to 3 µm/sec (Figure 31 C, D, Movie 9, 14). As previously stated, these movement speeds cannot be mediated by any identified kinesin of *Arabidopsis* (Yamada et al., 2017b), therefore the velocity of root plastid stromules is either mediated by the actin-myosin machinery, or by a passive cytoplasmic stream. The motions of plastids were not linearly aligned to each other (Movie 1) and therefore, a solely passive regulation of the stromule movement by a cytoplasmic stream seems highly unlikely. The active or semiactive transport mechanism by an actin motor protein attached to either the stromule tip or another organelle, which is associated with the stromule tip, is more in favor of these dynamics. Considering the proposed organellar interaction of stromules (Köhler & Hanson, 2000; Kwok & Hanson, 2004b; M. Schattat et al., 2011) both systems seem plausible. The similarity of the elongation and retraction dynamics of stromules (Figure 31 D, C) hints at an active role in both directions of the stromule dynamic. In contrast, the observed rubber band motions of stromules (Movie 15) greatly support the hypothesis that stromule tips are actively transported and pulled back by the physical force of the membrane upon losing halt. Since both findings do not exclude each other, both mechanisms are feasible.

4.6 The variety of the plastidal motions and the contributions of stromules

The results of the automated tracking analysis showed that root plastids possess a variety of different movement patterns (Figure 24). Like at other organelles (Vick and Nebenführ 2012), a mix of stop-and-go, directed- as well as undirected- and no motion was observed. The manual analysis of the image data (Figure 25-Figure 27) displayed similar results. Besides directed movement, stromules seem to have a big influence on the movement patterns that were carried out by the plastids. The directed movement of plastids (Figure 26) was solely carried out by plastids without stromules. In contrast, plastids with stromules seemed to be more restricted to cellular localization (Movie 1-8) and lose the ability for directed movement. The general movement of plastids with stromules can be characterized as diverse without an underlying pattern or a big movement radius. Either the stromule or the plastid body seemed to be anchored to a cellular component restricting the movement abilities of the whole organelle (Movie 14-20). However, a versatile and dynamic interplay between stromules and the plastid body was brought out in several ways and marked root plastid stromules as very dynamic structures (Figure 31-Figure 35 Movie 1, 14-20). The maximal velocity of elongation and retraction (Figure 31 C, D) is close to the velocity of directed plastid movement in most datasets (Figure 26 C). Those similarities allow for the assumption that the stromule dynamics can compensate for the loss of directed movement of the anchored plastid body. In addition, the plastid body was able to relocate in the cell by either moving through the stromule or by being retracted by a stromule (Figure 35). The mechanisms of those events could be mediated either by the force of the membrane that pulls the plastid or by an external force pulling the body. The frequency of those stromule-mediated interplays, observed between the stromule and plastid body (Figure 31 B, Figure 35 B), hints at a specific function in the cellular context of those motions. The ability of the plastids to form stromules of up to 60 µm (Movie 9) and the frequency with that long stromules were observed (Figure 28, Figure 29) give the plastid body a great potential for relocation in the cell upon a specific stimulus. However, the range of these motions is limited by the stromule length. Although no correlation between stromule length and plastid size was made in this study, the general impression prevailed that the size of the stromule was determined by the size of the plastid and thereby by the amount of potential membrane available for tubulation. The reverse motion in which an anchored stromule was elongated by a moving plastid body was also observed several times (Figure 34), although less frequent than individual stromule elongation. The velocities of those moving plastid bodies were drastically reduced in comparison to the plastids that displayed directed movement, leading to the assumption that a different mechanism is responsible for those movements. It also supports the hypothesis that plastids with stromules are locally bound in comparison to plastids without stromules. The attachment to another moving organelle could mediate these kinds of movements. Observations of a co-motion of plastids attached to another organelle were made during this work (Figure 27, Movie 21), demonstrating that this concept could be an underlying force.

The diversity throughout the plastidal movement that was observed in this work could well be ascribed to the diverse differentiation of plastids. Although differentiation between plastids could not be made here, the versatile movement patterns of plastids including their stromules hint at specific functions in the cellular context. Stromules seem to fulfill key aspects in the mediation of the plastidal dynamics and the positioning of the plastid in the cell.

4.7 The influence of stress conditions on the plastidal motion

The mechanisms and functions of root plastid motion cannot be compared to the well-understood light-induced movements of chloroplasts (compare 1.2.3 with Figure 21, Figure 24, Figure 26) and experimental data is lacking so far. To fill the lack of data, different stress treatments were executed with the established plastid tracking workflow. Classic abiotic stresses like heat, cold, salinity, and drought were approached to be implemented, but due to the restrictions dictated by the microscopic setup, especially heat, and cold stress were not realizable. However, salinity and drought stress were carried out as representatives of abiotic stress situations. Besides, a sucrose depletion condition was included, demonstrating the influence of the subtraction of easy, accessible energy on the plastid behavior. To generate an overview of how the different conditions affected the plant on a cellular level, the cell size and number, as well as the plastid number per cell and cell volume were determined (Figure 23). Salt stress led to a swelling of cells (Movie 3), whereas sucrose depletion led to a slight decrease in cell size. Cell swelling upon continuous salt stress has been reported previously (Li et al., 2014). The increase in cell size is a byproduct of a shortened elongation of root cells in response to salt stress and is mediated in the elongation zone induced by changes in cell wall formation and cytoskeletal reorganization (J. Liu et al., 2021). As a result, swelling of the root cells occurs upon continuous salt stress. This morphology indicates that the plants have faced long-term salinity stress and maybe have already adapted to the conditions. The decrease in cell size in sucrose depletion conditions could be a consequence of the decreased amounts of energy the plants could utilize, leading to a general decrease in growth. In contrast, the number of plastids per cell showed significant differences but equalized upon normalizing the plastid number to the cell volume. Little is known about the regulation of organelle numbers in cells (Cole, 2016), especially for plastids. The regulation of the plastid number in dependence on the cell size highlights the severe tasks plastids must cover in the cellular context for the maintenance of the cell's functions.

In terms of dynamics, salt stress did not affect the movement of the plastid body during the automated (Figure 24), as well as the manual analysis (Figure 26-Figure 35) compared to control conditions. The number and size of stromules however is slightly decreased (Figure 28-Figure 29), being a result of potential lipid damage induced by the continuous salt stress (Gong, 2021; van Zelm et al., 2020). Stromules are dependent on the excess membrane of the organelle (Bahrami & Hummer, 2017). Decreasing the amount of envelope could lead to decreased stromule dynamics. Consequently, the amount of stromule-related movement was also slightly decreased compared to control conditions (Figure 30- Figure 35). The fact that the overall plastid dynamic did not show great differences from the control condition leads to the assumption that either salt stress did not affect the dynamics of plastids, or the plant already adapted to the stress conditions and reached a homeostatic level again. Maybe effects displayed by the treatment must be observed in earlier stages of the stress response.

Drought stress had a more severe effect on the plastidal motion. Overall, the plastidal dynamics were drastically reduced in comparison to control conditions (Figure 24-Figure 35). Similar to salt stress conditions, the number of stromules (Figure 28) and therefore stromule mediated dynamics, in general, were drastically reduced compared to control conditions (Figure 30-Figure 35). Since drought and salt stress share a broad range of cellular defense mechanisms (Zhu, 2002), similar mechanisms could lead to a decreased number and size of stromules. In addition, a general reduction of plant growth was often

described during drought stress (Ahluwalia et al., 2021), which could affect the plastidal dynamic. The plant must focus its energy on the stress response and less energy is available for organellar transport mediated by motor proteins.

Sucrose depletion nearly led to abolishment of plastidal dynamics on all levels (Figure 24-Figure 35). These results highlight the energy dependence of organellar transport. Irrespective whether the molecular mechanism that drives plastidal motion is driven by cytoplasmic streaming or direct attachment of motor proteins, both are mediated by motor proteins that act in dependence of ATP (Nebenführ & Dixit, 2018). Since also cell size was decreased (Figure 23), the reduction of sucrose could lead to a general reduction in growth compared to all other conditions. Similar effects were observed, but not quantified during the growth of the plants. The gradual reduction of plastidal motion compared with the drastic reduction during sucrose depletion could hint to a general linkage of organellar transport and plant growth. Similarly, impairments of cytoplasmic streaming have been reported to restrict plant growth (Tominaga et al., 2013). The lack of easy energy could lead to a downregulation of general transport mechanisms resulting in reduced plant growth.

Stromule dynamics and plastid body dynamics seem to follow a trend throughout all conditions (Figure 24, Figure 26, Figure 31). This trend is also visible in the comparison of the number of stromules (Figure 28 B) with the general plastid dynamics (Figure 25-Figure 35). For stromule formation, the plastid needs an excess amount of membrane (Bahrami & Hummer, 2017; Erickson & Schattat, 2018), which could be limited due to lipid destruction by stress treatments. In this case, low amounts of stromules would correlate with low amounts of detectable stromule dynamics. Also, as previously discussed, the dynamics of plastids are most likely mediated by the active interaction of plastids with motor proteins (4.4). The results in this work strengthen the assumption that stromule dynamics could be mediated by the actin-myosin machinery (Figure 31, 4.5). In this case, the dynamic of stromules and the general plastidal movement would be connected by the same driving force. If the underlying transport system for stromules and plastids is affected by stress treatments, the observed trend of both during this study could be explained.

4.8 Stromule formation and dynamics are regulated independently by different factors

One key aim of this study was the generation of more information about the underlying mechanisms of stromule formation. The image data acquired via light sheet-based fluorescence microscopy of the *Arabidopsis* root gave phenomenal insights into the dynamic nature of stromules (Figure 28, Figure 29, Figure 31, Movie 1, 9, 14, 15). It also showed that stromules are very stable elements over a long period (Movie 1, 13). Considering that organelles need excess membrane and a positive membrane-to-volume ratio to be able to form tubular structures (Bahrami & Hummer, 2017), it is likely that stromule formation and stability at root plastids are favored by the composition and amount of their membranes. Contrary to this, it was shown in recent findings that stromules can be induced *in vitro* by the addition of a cellular extract (Ho & Theg, 2016). As stated in the publication, stromules can be induced *in vitro* at isolated chloroplasts by the addition of a concentrated cellular leaf extract (Figure 36). Stromule formation is more

commonly known to happen at root plastids than at green chloroplasts (Köhler & Hanson, 2000). However, the fact that stromules can be introduced by the addition of a cellular extract favors the hypothesis that an excess amount of membrane is not enough to force stromule formation and that other cellular factors are involved in their regulation. This study followed the initial idea of the *in vitro* assay (Figure 36). In addition, concentrated root extract was also tested for stromule-inducing capacities and was demonstrated to be more potent than extract generated from leaves (Figure 37, Figure 38). Since root extract induced stromules at green chloroplasts, these findings favor a general principle in terms of stromule induction, rather than a specific concept relying on specific structures present in differentiated plastid types. Also, it shows that factors required for stromule formation are more abundant in roots than they are in leaves. With the aim for later mass spectrometric analysis, the root extract was favored for this analysis. *In vitro* stromule induction was shown to be protein-mediated in different experiments (Figure 38, Figure 40) with the protein concentration directly influencing the number of formed stromules (Figure 38). Other cellular factors like cytoskeletal fragments or nuclei that are often described to co-localize with stromules did not show any effect on the stromule induction (Figure 39, Figure 40). Altogether, those findings lead to the assumption that those factors are not needed for the mechanisms of basic stromule formation. In addition, stromule formation was not influenced by the reduction of the chloroplast's outer envelope proteins (Figure 41). Although Thermolysin treatment was performed as desired at the analyzed envelope proteins (Figure 41 B), some outer envelope proteins could remain unaffected by the treatment. However, those findings favor cytosolic proteins that undergo a protein-lipid interaction with the outer envelope membrane, thereby inducing the formation of stromules. No movement was observed at stromules induced *in vitro*. These findings indicate that the stromule dynamic is mediated by external forces, like myosin motors. In addition, the length of stromules formed *in vitro* was very restricted, compared to the ones observed *in vivo* during light sheet-based fluorescence microscopy (Figure 36, Figure 29). Considering that the formation of a tubular shape at a spheroid organelle needs to overcome a specific energy barrier to form (Bahrami & Hummer, 2017), the results on isolated chloroplasts favor a protein that binds to the outer envelope lipids, delivering the stabilizing structure for tubules to form. Lacking external forces that pull the stromules *in vitro*, the formation of tubular structures was a process of several minutes. *In vivo,* the stromule elongation was a process of seconds, suggesting that *in vitro* stromule formation is driven by diffusion forces of the membrane upon the introduction of a stable origin point. The dynamics of stromule kinks and branches were analyzed at the image sets gathered by light sheet-based fluorescence microscopy (Figure 33, Movie 16-18). Stromule kinks turned out to be relatively stable structures. Also, new stromule branches emerged preferably at a kink (Movie 16-18) that was characterized by a 120 ° angle (Figure 32). Those angles have been previously reported (M. Schattat et al., 2011). Modeling approaches have shown that the Y-formation of membranes need an external force to be created, but once introduced to the membrane they remain somewhat stable structures (Maike Jung, 2021). The 120 ° angle in between this Y-formation is preferred and contributes to the stability, whereas no structure of higher orders is energetically favorable (Maike Jung, 2021). Since 120 ° angles were stable structures even without the formation of a third stromule branch (Figure 29, Figure 30, Figure 33, Movie 16-18) proteins interacting with lipids of the outer envelopes providing stromule origin structures could be involved in the maintenance of the 120 ° angles. For movement of the stromule origin points as observed in this study (Figure 33, Movie 16-18), motor proteins could either be associated at the protein complex and drag it into another position, or forces from overly stretched membranes could lead the

whole complex to move with the bound membrane elements through the membrane. The stromule origin point would be moved passively through the plastid membrane by these forces. The stabilizing structure would thereby regulate the stromule motion since the amount of usable membrane is the key factor in the stromule dynamic. A mechanism that signals for stromule formation is not explained by all of this. However, for a targeted formation and aimed motion of the protrusions, a molecular addressing is needed, and future experiments need to tackle these questions.

4.9 Fractionation and LC-MS analysis led to possible factors involved in stromule formation

The fact that concentrated cell extract can induce stromules *in vitro* is an excellent starting point for an analysis of cellular factors potentially involved in stromule formation. Since the data presented in this work led to the assumption that a specific protein factor is likely to bind to lipids of the outer envelope, leading to *in vitro* stromule formation (Figure 41), some limits were set for the search criteria. For a mass spectrometric analysis, a fractionation method was desired, eliminating a great portion of potential protein candidates in the extract, while maintaining the factors responsible for stromule formation. The feedback of the fractionation was given by the stromule induction of fractions harboring the wanted factors in the *in vitro* assay. Since stromule formation was dependent on the concentration of the desired factor, high protein amounts needed to be generated during the establishment of the workflow. Since the proteins needed to be fractionated at native conditions, this limited the potential usable method pool. A combination of a linear sucrose gradient coupled with anion exchange chromatography was able to maintain the factor through several operation steps (Figure 45). The initial linear sucrose gradient was able to eliminate a great portion of the overall protein content by keeping the desired factor in the top fractions with the lowest sucrose content (Figure 42). As indicated by the gel pictures (Figure 42 B), the overall proteins in this fraction are not bigger than 60 kDa in molecular weight. This is contrary to previous findings proposing that a factor or a complex with 100 kDa or more is responsible for the induction of stromules *in vitro* (Ho & Theg, 2016). This statement arose from the fact that the authors concentrated their cell extract with Amicon filter units with a cutoff of 100 kDa. Those filter units make use of a molecular mesh that corresponds to the cutoff. A mesh can easily be plugged, which could be an explanation for the divergence in those findings. The authors could probably have measured a mixture of several proteins smaller than 100 kDa maintained by the plugged filter unit. During anion exchange chromatography, the factor spread throughout several elution fractions, as well as the flowthrough, which led to the assumption that it did not bind to the column (Figure 43). However, since the wanted factor was present in the flowthrough fraction which excluded a very high amount of other proteins, both methods were coupled (Figure 44-Figure 46), with the result of a drastic decrease in overall proteins present in the flowthrough fraction of the anion exchange chromatography. One fraction surely harboring the wanted factor, two fractions potentially harboring it and a fourth fraction which was shown not to include the desired factors were chosen to be analyzed via LC-MS (Figure 45). The workflow was implemented with a protein extract of *Pisum sativum.* Any attempts to implement the workflow with protein extract of *Arabidopsis thaliana* failed to deliver any results in the *in vitro* assay. Therefore, the final workflow was transferred on cell extract generated from *Arabidopsis* roots. The similarity of protein content in the final elution fractions of

both organisms (Figure 45, Figure 46) was taken as proof that the protein distribution is comparable between the two plant species. However, the stromule-inducing capacities of the *Arabidopsis* extract were never demonstrated. However, detected hits throughout the fractions were analyzed (Figure 47). In total, the mass spectrometric analysis of those fractions harbored 251 protein candidates. No protein candidate was found, which is known to induce tubulation at any membrane. In the application of prior generated knowledge (Figure 41), protein candidates with potential lipid interaction, and functions during vesiculation, as well as protein candidates with unknown functions were highlighted as potential candidates responsible for stromule induction. This analysis left 54 potential candidates, responsible for stromule induction *in vitro*. At this point, one could only speculate about the candidate that mediates tubulation at the membrane. Two identified protein candidates have potential functions in sterol binding (At2g16005, At1g45015, Table 4, Table 5). The envelope of plastids harbors very few sterols with a proportion of 7 µg/mg protein (Block et al., 2007). However, it has been shown that the capacity for a membrane to bend is highly dependent on the presence of sterols during vesicle formation (Anderson et al., 2021). They lower the energetic barrier that is necessary for the membrane to bend. The recruitment of sterols by a protein structure thereby mediating the membrane deformation could lead to tubulation of the membrane. One protein with a potential lipid transfer function is also included in the analysis (At2g33470, Table 4). Membranes can be formed by local variations in the geometry of lipids (McMahon & Boucrot, 2015). A factor that recruits inverted conical lipids to the outer leaflet of the outer envelope could mediate tubulation. Various other factors involved in vesicle formation were identified (Table 3-Table 5). Those proteins are known to interact with the membrane and induce a form of curvature to the membrane. Most of these protein candidates were assigned with distinct functions in vesiculation and were therefore less likely to induce stromule formation. However, the concentration of a factor that is known to initiate membrane curvature or vesiculation could lead to unspecific membrane binding and in the following the induction of stromules. At last, most identified proteins were of unknown function. Since up to now no distinct protein is known to mediate stromule formation, all those proteins could be tested in future studies. Follow-up experiments are necessary to elucidate if any of the identified factors can induce stromules *in vitro* and *in vivo*.

5 Conclusion and outlook

Organelles provide distinct reaction compartments that are utilized by cellular machinery to carry out a variety of different functions. Since many functions of organelles are interconnected with each other, the different compartments must communicate and interact with each other for the exchange of metabolites. Repositioning of organelles to create membrane contact sites for organelle-organelle interaction is crucial for proper cell function. How the repositioning of organelles is facilitated by the cell is still not clear. This work aimed to establish an automated approach, for the tracking of root organelles of *Arabidopsis thaliana* in 4D. As model organelles, root plastids were chosen, since not much is known about their movement in the cell. Their movement was analyzed in detail and the angle between movement vectors of organelles was used to classify characteristic movement patterns that were observed and previously described at other organelles. Those movement patterns were shown to be linked to specific movement velocities of the plastids. Using the established tracking pipeline, it was possible to analyze high amounts of datasets in a semi-automatic way, but unfortunately, the automatically generated results did not represent the cellular situation and needed manual correction. The structural variety of plastids was the main aspect that interfered with the automated analysis leaving space for improvements. For complex structures like those of root plastids, the utilization of deep learning- or an artificial intelligence approach could be useful for distinct segmentation of differently shaped organelles like the ER or plastids with stromules. Mainly spherical organelles like peroxisomes should not be affected by the automated approach established in this work. Besides optimization of the automated setup, future approaches should include differently labeled organelles to carry out interaction studies, which could give insights in the cellular regulation of plastidal movement. The analysis of singularly labeled organelles allows for a much deeper characterization since the temporal resolution is lower and more distinct movement patterns can be recorded. In contrast, the value of information about the cellular functions and the functional context of those movements is limited. The established automated pipeline allows for the simultaneous analysis and visualization of several channels, giving a great perspective for future co-localization and interaction studies of organelles in 4D.

In parallel, a 3D approach aiming for additional characterization of the plastidal dynamics was carried out. The main aspects for this part of the work were the analysis and the characterization of plastidal movement patterns that could only be assumed by the automated approach and the potential contribution stromules deliver to the plastidal dynamics. This work demonstrated that plastidal motion is tightly regulated and that the regulation is dependent on the environmental conditions the plant faces. It also shows that plastidal motion is highly dependent on the level of energy available for the plant demonstrating a tight regulation of the organellar positioning in the cell. Plastidal dynamics are very versatile. Directed transport of plastids on distinct tracks that can clearly distinguish between distinct destinations of different plastids hints at a tight regulation of the plastidal movement and strong integration in the cellular systems. Findings presented in this work do not neglect the opportunities of potential involvement of cytoplasmic streaming in the plastidal movement, but most data hint at a regulated and directed force that drives the plastidal motion (Figure 48). Velocities measured during this study hint at an involvement of the actin-myosin machinery since other cellular components are not able to reach those paces in *Arabidopsis thaliana*. At sufficient energy levels, plastidal motion can reach

velocities that are equal to the maximum velocities measured for myosin XI members in *Arabidopsis* so far. Following those findings, this motion is most probably carried out by Myosin XI-2. More specific approaches like mutant studies of plants lacking the indicated motor protein are necessary to gather further insights into the molecular mechanisms that drive plastidal motion. Stromules are highly integrated into the plastidal dynamics and therefore are most probably a substantial mechanism of stationary plastids for the interaction with other cellular components. The difference in velocity measured for events with stromule involvement however implies that either the motion driving those events is delivered by another mechanism than directed plastid movement, or that mechanical force of the membrane, or the organelle size hinders the movement speed. Future research utilizing mutants harboring either mutations of single variants of the myosin XI family, like Myosin XI-2, or multiple affected proteins in combination with a comparable microscopic approach could give additional information about the molecular mechanisms that drive stromule and plastid dynamics. In addition, to investigate the cellular function of plastid dynamics, interaction studies with differently labeled organelles are highly recommended. The cellular functions of stromules are, up to date, not elucidated. The combination of stress treatment or targeted mutations of the actin-myosin machinery added to an interaction study could give a more holistic picture of the functions of the plastidal and the stromule dynamics.

In a third approach, the molecular basis for stromule formation was investigated. This work displayed that most likely a protein undergoing protein-lipid interaction with the outer envelope membrane is responsible for stromule formation (Figure 48 B). An LC-MS analysis discovered a variety of possible protein candidates that could mediate stromule formation. Future work needs to utilize easy genetic and molecular approaches like the protoplast system or overexpression of the identified candidates to verify the potential stromule-inducing capacity of any of those candidates. During this work, a fractionation pipeline for cellular extract was established, to enrich the factor mediating the *in vitro* stromule formation. This pipeline led to more than 50 potential candidates. To limit the number of candidates, future work needs to validate, and additional optimization of the fractionation pipeline could be carried out. The pipeline was established on high protein amounts delivered by *Pisum sativum*, whereas the final analysis was performed using *Arabidopsis thaliana* extract, giving a far lower quantity of proteins, which were implemented into the established process. Since both utilized fractionation methods came to good results, further optimization of the pipeline by either restructuring the order of methods or the implementation of additional fractions could further reduce the number of potential protein candidates. Different tissues could also be cross-examined. At least leaf extract is proven to induce stromules *in vitro*. Also, additional protein fractionation methods could be implemented, like fractionation based on the isoelectric point. However, the fractionation needs to be carried out at non-denaturing conditions, since the only reference for the presence of the wanted factor so far is the stromule induction assay, which is dependent on intact protein structure.

The combination of results gathered during the *in vitro* stromule induction and light sheet-based fluorescence microscopy data revealed that the formation of stromules is most likely delivered by a protein complex creating a structural origin point for stromules at the outer envelope, helping to overcome energetic barriers. The stromule dynamics however is most likely delivered by the actin-myosin machinery or other driving forces in the cell (Figure 48 B). The fact that the formation of stromules relies on the proportion of membrane to organelle volume in combination with those results hints at a tight regulation

of the stromule dynamic. Future research relies on the results of the analysis of potential interaction partners mediating stromule formation identified in this study. Targeted mutation of potential candidates in combination with a quantitative analysis of the amount and length of stromules as well as their dynamics could deliver a deeper understanding of the molecular mechanisms underlying stromule formation and dynamics.

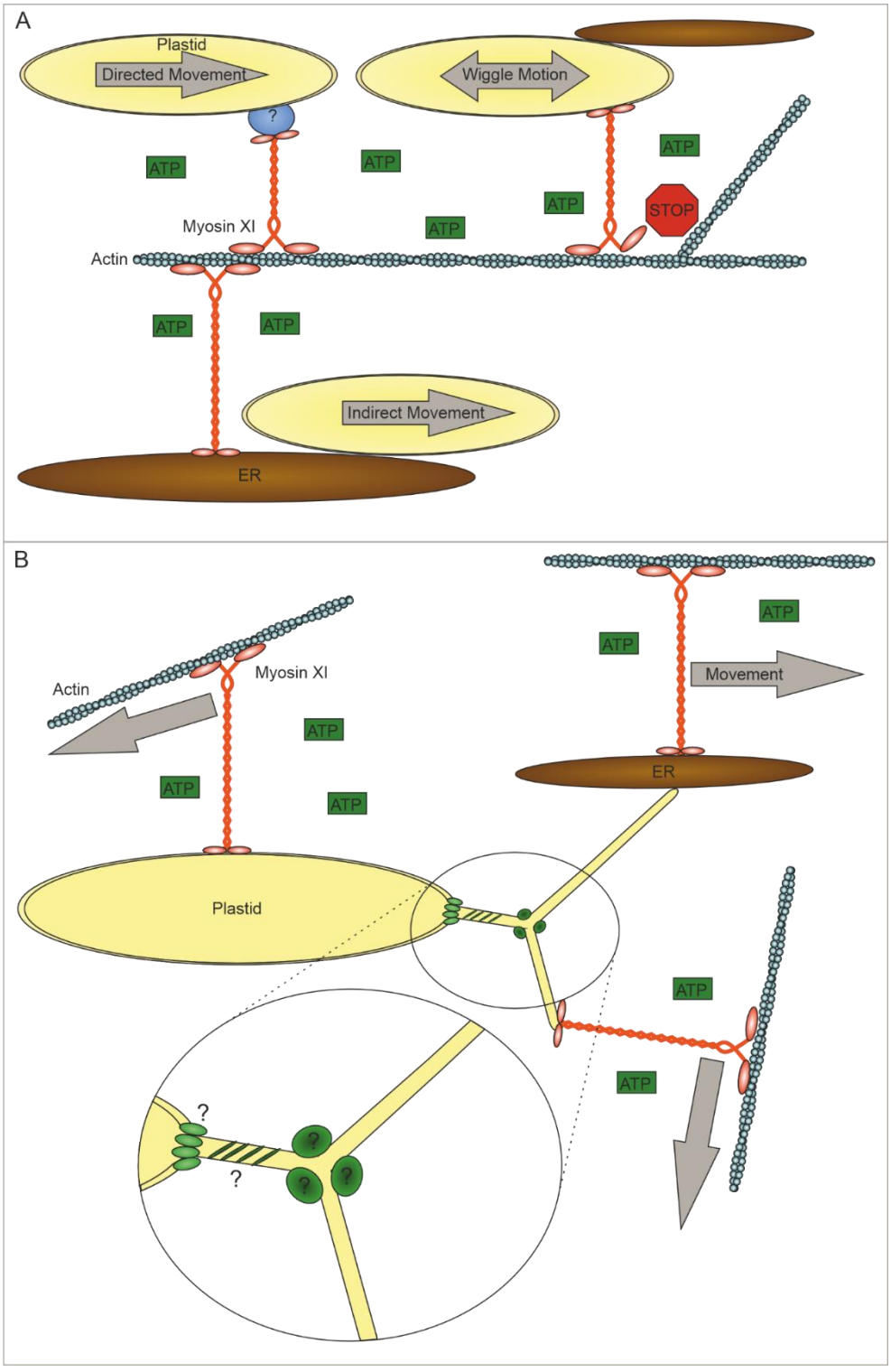

Figure 48 Schematic display of plastid movement and stromule formation in *Arabidopsis thaliana*. A) Root plastids are actively transported on actin filaments by myosin family XI members. The movement is ATP-dependent and is reduced at low energy conditions. Directed movement is carried out with either direct or indirect connection of myosin XI members to the outer envelope of the plastid. Additionally, directed movement can happen across a single actin filament that serves as a molecular highway. Wiggle motions can happen at interconnections of actin filaments when the motor proteins need to change tracks, upon dissociation of the motor protein from either the actin filament or the plastid, or at stops of the organelle to interact with other organelles. Besides the direct association of the motor protein to the plastid, plastids can be attached to other organelles, here represented by the ER, and get transported by the actin-myosin machinery. B) Schematic display of the *in vivo* stromule formation. Stromules are formed by external forces pulling the membrane and like plastidal movement dependent on the availability of ATP. The stromule tip is either connected to a member of myosin XI, which moves the tip directly across actin filaments, or the process is mediated by the attachment of stromules to other organelles, here represented by the ER. The third mechanism of stromule formation is the active transport of the plastid body across actin filaments, while the stromule tips are linked to stationary cellular elements. The stromule formation is guided by proteins mediating the formation of stromule origin points at the plastid body and stromule branches. The involved proteins are so far not known, but they interact with lipids of the outer envelope and mediate stromule formation by either stabilizing the stromule origin points or the tubular structure of the stromules.

6 References

Ahluwalia, O., Singh, P. C., & Bhatia, R. (2021). A review on drought stress in plants: Implications, mitigation and the role of plant growth promoting rhizobacteria. In *Resources, Environment and Sustainability* (Vol. 5). Elsevier B.V. https://doi.org/10.1016/j.resenv.2021.100032

Akkerman, M., Overdijk, E. J. R., Schel, J. H. N., Emons, A. M. C., & Ketelaar, T. (2011). Golgi body motility in the plant cell cortex correlates with actin cytoskeleton organization. *Plant and Cell Physiology*, *52*(10), 1844–1855. https://doi.org/10.1093/pcp/pcr122

Allen, N. S., & Allen, R. D. (1978). Cytoplasmic streaming in green plants. *Annual Review of Biophysics and Bioengineering*, *7*(1), 497–526. https://doi.org/10.1146/annurev.bb.07.060178.002433

Allen, R. D., & Allen, N. S. (1978). Cytoplasmic streaming in amoeboid movement. *Annual Review of Biophysics and Bioengineering*, *7*(1), 469–495. https://doi.org/10.1146/annurev.bb.07.060178.002345

Amodeo, A. A., & Skotheim, J. M. (2016). Cell-size control. *Cold Spring Harbor Perspectives in Biology*, *8*(4). https://doi.org/10.1101/cshperspect.a019083

Anderson, R. H., Sochacki, K. A., Vuppula, H., Scott, B. L., Bailey, E. M., Schultz, M. M., Kerkvliet, J. G., Taraska, J. W., Hoppe, A. D., & Francis, K. R. (2021). Sterols lower energetic barriers of membrane bending and fission necessary for efficient clathrin-mediated endocytosis. *Cell Reports*, *37*(7), 110008. https://doi.org/10.1016/j.celrep.2021.110008

Andersson, M. X., Goksör, M., & Sandelius, A. S. (2007). Optical manipulation reveals strong attracting forces at membrane contact sites between endoplasmic reticulum and chloroplasts. *Journal of Biological Chemistry*, *282*(2), 1170–1174. https://doi.org/10.1074/jbc.M608124200

Arimura, S.-I., Hirai, A., & Tsutsumi, N. (2001). Numerous and highly developed tubular projections from plastids observed in Tobacco epidermal cells. In *Plant Science* (Vol. 160). https//doi.org/10.1016/s0168-9452(00)00405-2.

Arnon, D. I. (1949). Copper Enzymes in Isolated Chloroplasts. Polyphenoloxidase in *Beta vulgaris*. *Plant Physiology*, *24*(1), 1–15. https://doi.org/10.1104/pp.24.1.1

Ausubel, F. M., Brent, R., Kingston, R. E., Moore, D. D., Seidman, J. G., Smith, J. A., & Struhler, K. (1987). *Current Protocols in Molecular Biology* (Vols. 1–4).

Avisar, D., Prokhnevsky, A. I., & Dolja, V. v. (2008). Class VIII Myosins Are Required for Plasmodesmatal Localization of a Closterovirus Hsp70 Homolog. *Journal of Virology*, *82*(6), 2836–2843. https://doi.org/10.1128/jvi.02246-07

Azevedo, R. A., Lancien, M., & Lea, P. J. (2006). The aspartic acid metabolic pathway, an exciting and essential pathway in plants. In *Amino Acids* (Vol. 30, Issue 2, pp. 143–162). https://doi.org/10.1007/s00726-005-0245-2

Bahrami, A. H., & Hummer, G. (2017). Formation and Stability of Lipid Membrane Nanotubes. *ACS Nano*, *11*(9), 9558–9565. https://doi.org/10.1021/acsnano.7b05542

Barton, K. A., Wozny, M. R., Mathur, N., Jaipargas, E. A., & Mathur, J. (2018). Chloroplast behaviour and interactions with other organelles in *Arabidopsis* thaliana pavement cells. *Journal of Cell Science*, *131*(2). https://doi.org/10.1242/jcs.202275

Bauwe, H., Hagemann, M., & Fernie, A. R. (2010). Photorespiration: players, partners and origin. In *Trends in Plant Science* (Vol. 15, Issue 6, pp. 330–336). https://doi.org/10.1016/j.tplants.2010.03.006

Berg, J. S., Powell, B. C., & Cheney, R. E. (2001). A Millennial Myosin Census. *Molecular Biology of the Cell*, *12*(4), 780–794. https://doi.org/10.1091/mbc.12.4.780

Bijalwan, P., Sharma, M., & Kaushik, P. (2022). Review of the Effects of Drought Stress on Plants: A Systematic Approach. *Preprints* https://doi.org/10.20944/preprints202202.0014.v1

Bionda, T., & Schleiff, E. (2010). Chloroplast isolation and *in vitro* protein import. *International Society of Endocytobiology Journal of Endocytobiosis and Cell Research Journal of Endocytobiosis and Cell Research*. 17-26.

Blanchoin, L., & Pollard, T. D. (2002). Hydrolysis of ATP by polymerized actin depends on the bound divalent cation but not profilin. *Biochemistry*, *41*(2), 597–602. https://doi.org/10.1021/bi011214b

Block, M. A., Douce, R., Joyard, J., & Rolland, N. (2007). Chloroplast envelope membranes: A dynamic interface between plastids and the cytosol. In *Photosynthesis Research* (Vol. 92, Issue 2, pp. 225–244). https://doi.org/10.1007/s11120-007-9195-8

Block, M. A., & Jouhet, J. (2015). Lipid trafficking at endoplasmic reticulum-chloroplast membrane contact sites. In *Current Opinion in Cell Biology* (Vol. 35, pp. 21–29). Elsevier Ltd. https://doi.org/10.1016/j.ceb.2015.03.004

Boevink, P., Oparka, K., Cruz, S. S., Martin, B., Betteridge, A., & Hawes, C. (1998). Stacks on tracks: the plant Golgi apparatus traffics on an actin/ER network. *The Plant Journal*, *15*(3), 441–447. https://doi.org/10.1046/j.1365-313X.1998.00208.x

Bostrom, T. E., & Walker, N. A. (1975). Intercellular Transport in Plants. *Journal of Experimental Botany*, *26*(6), 767–782. https://doi.org/10.1093/jxb/26.6.767

Botella, C., Sautron, E., Boudiere, L., Michaud, M., Dubots, E., Yamaryo-Botté, Y., Albrieux, C., Marechal, E., Block, M. A., & Jouhet, J. (2016). ALA10, a phospholipid flippase, controls FAD2/FAD3 desaturation of phosphatidylcholine in the ER and affects chloroplast lipid composition in *Arabidopsis thaliana*. *Plant Physiology*, *170*(3), 1300–1314. https://doi.org/10.1104/pp.15.01557

Boucrot, E., Pick, A., Çamdere, G., Liska, N., Evergren, E., McMahon, H. T., & Kozlov, M. M. (2012). Membrane fission is promoted by insertion of amphipathic helices and is restricted by crescent BAR domains. *Cell*, *149*(1), 124–136. https://doi.org/10.1016/j.cell.2012.01.047

Box, R., Andrews, M., & Raven, J. A. (1984). Intercellular Transport and Cytoplasmic Streaming in *Chara hispida*. *Journal of Experimental Botany*, *35*(7), 1016–1021. https://doi.org/10.1093/jxb/35.7.1016

Breuers, F. K. H., Bräutigam, A., Geimer, S., Welzel, U. Y., Stefano, G., Renna, L., Brandizzi, F., & Weber, A. P. M. (2012). Dynamic Remodeling of the Plastid Envelope Membranes – A Tool for Chloroplast Envelope *in vivo* Localizations. *Frontiers in Plant Science*, *3*(JAN). https://doi.org/10.3389/fpls.2012.00007

Brunkard, J. O., Runkel, A. M., & Zambryski, P. (2016). Visualizing stromule frequency with fluorescence microscopy. *Journal of Visualized Experiments*, *2016*(117). https://doi.org/10.3791/54692

Bublak, D. (2018). Unpublished Manuscript. Goehte University Frankfurt a.M. Department of molecular Biology of Plants

Cai, C., Henty-Ridilla, J. L., Szymanski, D. B., & Staoger, C. J. (2014). *Arabidopsis* myosin XI: A motor rules the tracks. *Plant Physiology*, *166*(3), 1359–1370. https://doi.org/10.1104/pp.114.244335

Campbell, N. A., & Reece, J. B. (2009). Biologie (Vol. 8). Pearson.

Cao, J., Li, X., & Lv, Y. (2017). Dynein light chain family genes in 15 plant species: Identification, evolution and expression profiles. *Plant Science*, *254*, 70–81. https://doi.org/10.1016/j.plantsci.2016.10.011

Caplan, J. L., Kumar, A. S., Park, E., Padmanabhan, M. S., Hoban, K., Modla, S., Czymmek, K., & Dinesh-Kumar, S. P. (2015). Chloroplast Stromules Function during Innate Immunity. *Developmental Cell*, *34*(1), 45–57. https://doi.org/10.1016/j.devcel.2015.05.011

Caplan, J. L., Mamillapalli, P., Burch-Smith, T. M., Czymmek, K., & Dinesh-Kumar, S. P. (2008). Chloroplastic Protein NRIP1 Mediates Innate Immune Receptor Recognition of a Viral Effector. *Cell*, *132*(3), 449–462. https://doi.org/10.1016/j.cell.2007.12.031

Caudron, N., Arnal, I., Buhler, E., Job, D., & Valiron, O. (2002). Microtubule nucleation from stable tubulin oligomers. *Journal of Biological Chemistry*, *277*(52), 50973–50979. https://doi.org/10.1074/jbc.M209753200

Chalfie, M., Tu, Y., Euskirchen, G., Ward, W. W., & Prasher, D. C. (1994). Green Fluorescent Protein as a Marker for Gene Expression. *Science*, *263*(5148), 802–805. https://doi.org/10.1126/science.8303295

Chapman, K. D., & Ohlrogge, J. B. (2012). Compartmentation of triacylglycerol accumulation in plants. In *Journal of Biological Chemistry* (Vol. 287, Issue 4, pp. 2288–2294). https://doi.org/10.1074/jbc.R111.290072

Chen, C., Marcus, A., Li, W., Hu, Y., Calzada, J.-P. V., Grossniklaus, U., Cyr, R. J., & Ma, H. (2002). The *Arabidopsis ATK1* gene is required for spindle morphogenesis in male meiosis. *Development*, *129*(10), 2401–2409. https://doi.org/10.1242/dev.129.10.2401

Cline, K., Werner-Washburne, M., Andrews, J., & Keegstra, K. (1984). Thermolysin Is a Suitable Protease for Probing the Surface of Intact Pea Chloroplasts. *Plant Physiology*, *75*(3), 675–678. https://doi.org/10.1104/pp.75.3.675

Cole, L. W. (2016). The evolution of per-cell organelle number. In *Frontiers in Cell and Developmental Biology* (Vol. 4, Issue AUG). Frontiers Media S.A. https://doi.org/10.3389/fcell.2016.00085

Collings, D. A., Harper, J. D. I., Marc, J., Overall, R. L., & Mullen, R. T. (2002). Life in the fast lane: Actin-based motility of plant peroxisomes. *Canadian Journal of Botany*, *80*(4), 430–441. https://doi.org/10.1139/b02-036

Cortese, J. D., Schwab, B., Frieden, C., & Elson, E. L. (1989). Actin polymerization induces a shape change in actin-containing vesicles. *Proceedings of the National Academy of Sciences*, *86*(15), 5773–5777. https://doi.org/10.1073/pnas.86.15.5773

Corti B. (1774). Osservazione Microscopische sulla Tremella e sulla Circulazione del Fluido in Una Planto Acquaguola. *Lucca, Italy: Appresso Giuseppe Rocchi*.

Cox, J., & Mann, M. (2008). MaxQuant enables high peptide identification rates, individualized p.p.b.-range mass accuracies and proteome-wide protein quantification. *Nature Biotechnology*, *26*(12), 1367–1372. https://doi.org/10.1038/nbt.1511

Crowell, E. F., Bischoff, V., Desprez, T., Rolland, A., Stierhof, Y. D., Schumacher, K., Gonneau, M., Höfte, H., & Vernhettes, S. (2009). Pausing of golgi bodies on microtubules regulates secretion of cellulose synthase complexes in *Arabidopsis*. *Plant Cell*, *21*(4), 1141–1154. https://doi.org/10.1105/tpc.108.065334

Cutler, S. R., Ehrhardt, D. W., Griffitts, J. S., & Somerville, C. R. (2000). Random GFP::cDNA fusions enable visualization of subcellular structures in cells of *Arabidopsis* at a high frequency. *Proceedings of the National Academy of Sciences*, *97*(7), 3718–3723. https://doi.org/10.1073/pnas.97.7.3718

Cutler, S. R., Rodriguez, P. L., Finkelstein, R. R., & Abrams, S. R. (2010). Abscisic acid: Emergence of a core signaling network. *Annual Review of Plant Biology*, *61*, 651–679. https://doi.org/10.1146/annurev-arplant-042809-112122

D. Requião, R., Fernandes, L., de Souza, H. J. A., Rossetto, S., Domitrovic, T., & Palhano, F. L. (2017). Protein charge distribution in proteomes and its impact on translation. *PLoS Computational Biology*, *13*(5). https://doi.org/10.1371/journal.pcbi.1005549

de La Cruz, E. M., Mandinova, A., Steinmetz, M. O., Stoffler, D., Aebi, U., & Pollard, T. D. (2000). Polymerization and structure of nucleotide-free actin filaments 1 1Edited by W. Baumeister. *Journal of Molecular Biology*, *295*(3), 517–526. https://doi.org/10.1006/jmbi.1999.3390

Dietz, K. J., Turkan, I., & Krieger-Liszkay, A. (2016). Redox- and reactive oxygen species-dependent signaling into and out of the photosynthesizing chloroplast. *Plant Physiology*, *171*(3), 1541–1550. https://doi.org/10.1104/pp.16.00375

Domanov, Y. A., & Kinnunen, P. K. J. (2006). Antimicrobial peptides temporins B and L induce formation of tubular lipid protrusions from supported phospholipid bilayers. *Biophysical Journal*, *91*(12), 4427–4439. https://doi.org/10.1529/biophysj.106.091702

Durand-Smet, P., Spelman, T. A., Meyerowitz, E. M., & Jönsson, H. (2020). Cytoskeletal organization in isolated plant cells under geometry control. *Proceedings of the National Academy of Sciences*, *117*(29), 17399–17408. https://doi.org/10.1073/pnas.2003184117

Eberhard, S., Finazzi, G., & Wollman, F. A. (2008). The dynamics of photosynthesis. In *Annual Review of Genetics* (Vol. 42, pp. 463–515). https://doi.org/10.1146/annurev.genet.42.110807.091452

Erickson, J. L., Adlung, N., Lampe, C., Bonas, U., & Schattat, M. H. (2018). The *Xanthomonas* effector XopL uncovers the role of microtubules in stromule extension and dynamics in *Nicotiana benthamiana*. *Plant Journal*, *93*(5), 856–870. https://doi.org/10.1111/tpj.13813

Erickson, J. L., Kantek, M., & Schattat, M. H. (2017). Plastid-Nucleus Distance Alters the Behavior of Stromules. *Frontiers in Plant Science*, *8*. https://doi.org/10.3389/fpls.2017.01135

Erickson, J. L., & Schattat, M. H. (2018). Shaping plastid stromules — principles of *in vitro* membrane tubulation applied *in planta*. In *Current Opinion in Plant Biology* (Vol. 46, pp. 48–54). Elsevier Ltd. https://doi.org/10.1016/j.pbi.2018.07.003

Farooq, M., A.Wahid, Kobayashi, N., Fujita, D., & Basra, S. M. A. (2009). Review article Plant drought stress : effects , mechanisms and management. *Agron. Sustain. Dev*, *29*, 185–212. https://doi.org/10.1051/agro:2008021

Ferro, M., Brugière, S., Salvi, D., Seigneurin-Berny, D., Court, M., Moyet, L., Ramus, C., Miras, S., Mellal, M., le Gall, S., Kieffer-Jaquinod, S., Bruley, C., Garin, J., Joyard, J., Masselon, C., & Rolland, N. (2010). AT_CHLORO, a comprehensive chloroplast proteome database with subplastidial localization and curated information on envelope proteins. *Molecular and Cellular Proteomics*, *9*(6), 1063–1084. https://doi.org/10.1074/mcp.M900325-MCP200

Frederick, S. E., Gruber, P. J., & Newcomb, E. H. (1975). Plant microbodies. *Protoplasma*, *84*(1–2), 1–29. https://doi.org/10.1007/BF02075940

Frelin, O., Agrimi, G., Laera, V. L., Castegna, A., Richardson, L. G. L., Mullen, R. T., Lerma-Ortiz, C., Palmieri, F., & Hanson, A. D. (2012). Identification of mitochondrial thiamin diphosphate carriers from *Arabidopsis* and maize. *Functional and Integrative Genomics*, *12*(2), 317–326. https://doi.org/10.1007/s10142-012-0273-4

Fujiwara, I., Vavylonis, D., & Pollard, T. D. (2007). Polymerization kinetics of ADP- and ADP-P_i-actin determined by fluorescence microscopy. *Proceedings of the National Academy of Sciences*, *104*(21), 8827–8832. https://doi.org/10.1073/pnas.0702510104

Fujiwara, M. T., Kojo, K. H., Kazama, Y., Sasaki, S., Abe, T., & Itoh, R. D. (2015). The *Arabidopsis* minE mutation causes new plastid and FtsZ1 localization phenotypes in the leaf epidermis. *Frontiers in Plant Science*, *6*(October). https://doi.org/10.3389/fpls.2015.00823

Fygenson, D. K., Marko, J. F., & Libchaber, A. (1997). Mechanics of Microtubule-Based Membrane Extension. *Physical Review Letters*, *79*(22), 4497–4500. https://doi.org/10.1103/PhysRevLett.79.4497

G. Senn. (1910). Die Gestalts- und Lageveränderung der Pflanzen-Chromatophoren. *Nature*, *83*(2105), 4–4. https://doi.org/10.1038/083004a0

Ganguly, S., Williams, L. S., Palacios, I. M., & Goldstein, R. E. (2012). Cytoplasmic streaming in *Drosophila* oocytes varies with kinesin activity and correlates with the microtubule cytoskeleton architecture. *Proceedings of the National Academy of Sciences*, *109*(38), 15109–15114. https://doi.org/10.1073/pnas.1203575109

Gao, H., Metz, J., Teanby, N. A., Ward, A. D., Botchway, S. W., Coles, B., Pollard, M. R., & Sparkes, I. (2016). *In vivo* quantification of peroxisome tethering to chloroplasts in tobacco epidermal cells using optical tweezers1. *Plant Physiology*, *170*(1), 263–272. https://doi.org/10.1104/pp.15.01529

Geitmann, A., & Nebenführ, A. (2015). Navigating the plant cell: Intracellular transport logistics in the green kingdom. In *Molecular Biology of the Cell* (Vol. 26, Issue 19, pp. 3373–3378). American Society for Cell Biology. https://doi.org/10.1091/mbc.E14-10-1482

Gittes, F., Mickey, B., Nettleton, J., & Howard, J. (1993). Flexural rigidity of microtubules and actin filaments measured from thermal fluctuations in shape. *Journal of Cell Biology*, *120*(4), 923–934. https://doi.org/10.1083/jcb.120.4.923

Goldstein, R. E., & van de Meent, J. W. (2015). A physical perspective on cytoplasmic streaming. *Interface Focus*, *5*(4). https://doi.org/10.1098/rsfs.2015.0030

Gong, Z. (2021). Plant abiotic stress: New insights into the factors that activate and modulate plant responses. In *Journal of Integrative Plant Biology* (Vol. 63, Issue 3, pp. 429–430). Blackwell Publishing Ltd. https://doi.org/10.1111/jipb.13079

Goodson, H. v., & Jonasson, E. M. (2018). Microtubules and microtubule-associated proteins. *Cold Spring Harbor Perspectives in Biology*, *10*(6). https://doi.org/10.1101/cshperspect.a022608

Goyer, A. (2010). Thiamine in plants: Aspects of its metabolism and functions. In *Phytochemistry* (Vol. 71, Issues 14–15, pp. 1615–1624). https://doi.org/10.1016/j.phytochem.2010.06.022

Gray, J. C., Hansen, M. R., Shaw, D. J., Graham, K., Dale, R., Smallman, P., Natesan, S. K. A., & Newell, C. A. (2012). Plastid stromules are induced by stress treatments acting through abscisic acid. *The Plant Journal*, *69*(3), 387–398. https://doi.org/10.1111/j.1365-313X.2011.04800.x

Green, M. R., & Sambrook, J. (2012). Molecular Cloning: A Labroratory Manual (4th Edition, Vols. 1, 2, 3). Cold Spring Harbor Laboratory Press.

Grierson, C., & Schiefelbein, J. (2002). Root Hairs. *The Arabidopsis Book*, *1*, e0060. https://doi.org/10.1199/tab.0060

Gu, Y., & Dong, X. (2015). Stromules: Signal Conduits for Plant Immunity. In *Developmental Cell* (Vol. 34, Issue 1, pp. 3–4). Cell Press. https://doi.org/10.1016/j.devcel.2015.06.018

Guirimand, G., Guihur, A., Perello, C., Phillips, M., Mahroug, S., Oudin, A., de Bernonville, T. D., Besseau, S., Lanoue, A., Giglioli-Guivarc'h, N., Papon, N., St-Pierre, B., Rodríguez-Concepcíon, M., Burlat, V., & Courdavault, V. (2020). Cellular and subcellular compartmentation of the 2C-methyl-D-erythritol 4-phosphate pathway in the madagascar periwinkle. *Plants*, *9*(4). https://doi.org/10.3390/plants9040462

Gunning, B. E. S. (2005). Plastid stromules: Video microscopy of their outgrowth, retraction, tensioning, anchoring, branching, bridging, and tip-shedding. *Protoplasma*, *225*(1–2), 33–42. https://doi.org/10.1007/s00709-004-0073-3

Hamada, T., Tominaga, M., Fukaya, T., Nakamura, M., Nakano, A., Watanabe, Y., Hashimoto, T., & Baskin, T. I. (2012). RNA Processing Bodies, Peroxisomes, Golgi Bodies, Mitochondria, and Endoplasmic Reticulum Tubule Junctions Frequently Pause at Cortical Microtubules. *Plant and Cell Physiology*, *53*(4), 699–708. https://doi.org/10.1093/pcp/pcs025

Hanson, M. R., & Hines, K. M. (2018). Stromules: Probing formation and function. In *Plant Physiology* (Vol. 176, Issue 1, pp. 128–137). American Society of Plant Biologists. https://doi.org/10.1104/pp.17.01287

Hanson, M. R., & Köhler, R. H. (2001). GFP imaging: methodology and application to investigate cellular compartmentation in plants. *Journal of Experimental Botany*, *52*(356), 529–539. https://doi.org/10.1093/jexbot/52.356.529

Hanson, M. R., & Sattarzadeh, A. (2011). Stromules: Recent insights into a long neglected feature of plastid morphology and function. *Plant Physiology*, *155*(4), 1486–1492. https://doi.org/10.1104/pp.110.170852

Harwood, J. L. (1996). Recent advances in the biosynthesis of plant fatty acids. *Biochimica et Biophysica Acta (BBA) - Lipids and Lipid Metabolism*, *1301*(1–2), 7–56. https://doi.org/10.1016/0005-2760(95)00242-1

Haswell, E. S., & Meyerowitz, E. M. (2006). MscS-like proteins control plastid size and shape in *Arabidopsis thaliana*. *Current Biology*, *16*(1), 1–11. https://doi.org/10.1016/j.cub.2005.11.044

Hawkins, T., Mirigian, M., Selcuk Yasar, M., & Ross, J. L. (2010). Mechanics of microtubules. *Journal of Biomechanics*, *43*(1), 23–30. https://doi.org/10.1016/j.jbiomech.2009.09.005

He, M., He, C. Q., & Ding, N. Z. (2018a). Abiotic stresses: General defenses of land plants and chances for engineering multistress tolerance. *Frontiers in Plant Science*, *871*(December), 1–18. https://doi.org/10.3389/fpls.2018.01771

He, M., He, C. Q., & Ding, N. Z. (2018b). Abiotic stresses: General defenses of land plants and chances for engineering multistress tolerance. In *Frontiers in Plant Science* (Vol. 871). Frontiers Media S.A. https://doi.org/10.3389/fpls.2018.01771

Higa, T., Suetsugu, N., Kong, S. G., & Wada, M. (2014). Actin-dependent plastid movement is required for motive force generation in directional nuclear movement in plants. *Proceedings of the National Academy of Sciences of the United States of America*, *111*(11), 4327–4331. https://doi.org/10.1073/pnas.1317902111

Higa, T., Suetsugu, N., & Wada, M. (2014). Plant nuclear photorelocation movement. *Journal of Experimental Botany*, *65*(11), 2873–2881. https://doi.org/10.1093/jxb/ert414

Higashi-Fujime, S., Ishikawa, R., Iwasawa, H., Kagami, O., Kurimoto, E., Kohama, K., & Hozumi, T. (1995). The fastest-actin-based motor protein from the green algae, *Chara*, and its distinct mode of interaction with actin. *FEBS Letters*, *375*(1–2), 151–154. https://doi.org/10.1016/0014-5793(95)01208-V

Ho, J., & Theg, S. M. (2016). The formation of stromules *in vitro* from chloroplasts isolated from *Nicotiana benthamiana*. *PLoS ONE*, *11*(2). https://doi.org/10.1371/journal.pone.0146489

Holzinger, A., Kwok, E. Y., & Hanson, M. R. (2008). Effects of *arc3*, *arc5* and *arc6* mutations on plastid morphology and stromule formation in green and nongreen tissues of *Arabidopsis thaliana*. *Photochemistry and Photobiology*, *84*(6), 1324–1335. https://doi.org/10.1111/j.1751-1097.2008.00437.x

Holzinger, A., Wasteneys, G. O., & Lütz, C. (2007). Investigating cytoskeletal function in chloroplast protrusion formation in the arctic-alpine plant *Oxyria digyna*. *Plant Biology*, *9*(3), 400–410. https://doi.org/10.1055/s-2006-924727

Hurlock, A. K., Roston, R. L., Wang, K., & Benning, C. (2014). Lipid trafficking in plant cells. In *Traffic* (Vol. 15, Issue 9, pp. 915–932). Blackwell Munksgaard. https://doi.org/10.1111/tra.12187

Hyman, A. A., Salser, S., Drechsel, D. N., Unwin, N., & Mitchison, T. J. (1992). Role of GTP hydrolysis in microtubule dynamics: information from a slowly hydrolyzable analogue, GMPCPP. *Molecular Biology of the Cell*, *3*(10), 1155–1167. https://doi.org/10.1091/mbc.3.10.1155

Iwabuchi, K., Minamino, R., & Takagi, S. (2010). Actin reorganization underlies phototropin-dependent positioning of nuclei in *Arabidopsis* leaf cells. *Plant Physiology*, *152*(3), 1309–1319. https://doi.org/10.1104/pp.109.149526

J.A. Böhm. (1856). Beiträge zur näheren Kenntnis des Chlorophylls. *Math.-Nat. Kl.*, *22*, 479–498.

Jarillo, J. A., Gabrys, H., Capel, J., Alonso, J., Cashmore, A. (2001). Phototropin-related NPL1 controls chloroplast relocation induced by blue light. Nature *410(6831)*, 952-954. https://doi.org/ 10.1038/35073622

Jedd, G., & Chua, N.-H. (2002). Visualization of Peroxisomes in Living Plant Cells Reveals Acto-Myosin-Dependent Cytoplasmic Streaming and Peroxisome Budding. *Plant and Cell Physiology*, *43*(4), 384–392. https://doi.org/10.1093/pcp/pcf045

Jégou, A., Niedermayer, T., Orbán, J., Didry, D., Lipowsky, R., Carlier, M. F., & Romet-Lemonne, G. (2011). Individual actin filaments in a microfluidic flow reveal the mechanism of ATP hydrolysis and give insight into the properties of profilin. *PLoS Biology*, *9*(9). https://doi.org/10.1371/journal.pbio.1001161

Jessen, D., Roth, C., Wiermer, M., & Fulda, M. (2015). Two activities of long-chain acyl-coenzyme a synthetase are involved in lipid trafficking between the endoplasmic reticulum and the plastid in *Arabidopsis*. *Plant Physiology*, *167*(2), 351–366. https://doi.org/10.1104/pp.114.250365

Jonsson, E., Yamada, M., Vale, R. D., & Goshima, G. (2015). Clustering of a kinesin-14 motor enables processive retrograde microtubule-based transport in plants. *Nature Plants*, *1*. https://doi.org/10.1038/nplants.2015.87

Jordan, D. B., Bacot, K. O., Carlson, T. J., Kessel, M., & Viitanen, P. v. (1999). Plant Riboflavin Biosynthesis. *Journal of Biological Chemistry*, *274*(31), 22114–22121. https://doi.org/10.1074/jbc.274.31.22114

Joshi, H. J., Hirsch-Hoffmann, M., Baerenfaller, K., Gruissem, W., Baginsky, S., Schmidt, R., Schulze, W. X., Sun, Q., van Wijk, K. J., Egelhofer, V., Wienkoop, S., Weckwerth, W., Bruley, C., Rolland, N., Toyoda, T., Nakagami, H., Jones, A. M., Briggs, S. P., Castleden, I. Heazlewood, J. L. (2011). MASCP gator: An aggregation portal for the visualization of *Arabidopsis* proteomics data. *Plant Physiology*, *155*(1), 259–270. https://doi.org/10.1104/pp.110.168195

Jouhet, J., Maréchal, E., Baldan, B., Bligny, R., Joyard, J., & Block, M. A. (2004). Phosphate deprivation induces transfer of DGDG galactolipid from chloroplast to mitochondria. *Journal of Cell Biology*, *167*(5), 863–874. https://doi.org/10.1083/jcb.200407022

Jouhet, J., Maréchal, E., Bligny, R., Joyard, J., & Block, M. A. (2003). Transient increase of phosphatidylcholine in plant cells in response to phosphate deprivation. *FEBS Letters*, *544*(1–3), 63–68. https://doi.org/10.1016/S0014-5793(03)00477-0

Joyard, J., Ferro, M., Masselon, C., Seigneurin-Berny, D., Salvi, D., Garin, J., & Rolland, N. (2009). Chloroplast proteomics and the compartmentation of plastidial isoprenoid biosynthetic pathways. In *Molecular Plant* (Vol. 2, Issue 6, pp. 1154–1180). Oxford University Press. https://doi.org/10.1093/mp/ssp088

Joyard, J., Ferro, M., Masselon, C., Seigneurin-Berny, D., Salvi, D., Garin, J., & Rolland, N. (2010). Chloroplast proteomics highlights the subcellular compartmentation of lipid metabolism. In *Progress in Lipid Research* (Vol. 49, Issue 2, pp. 128–158). https://doi.org/10.1016/j.plipres.2009.10.003

Kabsch, W., Mannherz, H. G., Suck, D., Pai, E. F., & Holmes, K. C. (1990). Atomic structure of the actin: DNase I complex. *Nature*, *347*(6288), 37–44. https://doi.org/10.1038/347037a0

Kagawa, T., Sakai, T., Suetsugu, N., Oikawa, K., Ishiguro, S., Kato, T., Tabata, S., Okada, K., & Wada, M. (2001). *Arabidopsis* NPL1: A phototropin homolog controlling the chloroplast high-light avoidance response. *Science*, *291*(5511), 2138–2141. https://doi.org/10.1126/science.291.5511.2138

Kamiya, N., & Kuroda, K. (1956). Velocity Distribution of the Protoplasmic Streaming in *Nitella* Cells. *Shokubutsugaku Zasshi*, *69*(822), 544–554. https://doi.org/10.15281/jplantres1887.69.544

Kantsler, V., Segre, E., & Steinberg, V. (2008). Critical dynamics of vesicle stretching transition in elongational flow. *Physical Review Letters*, *101*(4). https://doi.org/10.1103/PhysRevLett.101.048101

Keller, P. J., Schmidt, A. D., Santella, A., Khairy, K., Bao, Z., Wittbrodt, J., & Stelzer, E. H. K. (2010). Fast, high-contrast imaging of animal development with scanned light sheet-based structured-illumination microscopy. *Nature Methods*, *7*(8), 637–642. https://doi.org/10.1038/nmeth.1476

Kimura, M., & Kagawa, T. (2009). Blue Light-induced Chloroplast Avoidance and Phototropic Responses Exhibit Distinct Dose Dependency of Phototropin2 in *Arabidopsis thaliana*. *Photochemistry and Photobiology*, *85*(5), 1260–1264. https://doi.org/10.1111/j.1751-1097.2009.00564.x

Kinkema, M., & Schiefelbein, J. (1994). A Myosin from a Higher Plant has Structural Similarities to Class V Myosins. *Journal of Molecular Biology*, *239*(4), 591–597. https://doi.org/10.1006/jmbi.1994.1400

Kleffmann, T., Russenberger, D., von Zychlinski, A., Christopher, W., Sjölander, K., Gruissem, W., & Baginsky, S. (2004). The *Arabidopsis thaliana* chloroplast proteome reveals pathway abundance and novel protein functions. *Current Biology*, *14*(5), 354–362. https://doi.org/10.1016/j.cub.2004.02.039

Köhler, R. H., Cao, J., Zipfel, W. R., Webb, W. W., & Hanson, M. R. (1997). Exchange of Protein Molecules Through Connections Between Higher Plant Plastids. *Science*, *276*(5321), 2039–2042. https://doi.org/10.1126/science.276.5321.2039

Köhler, R. H., & Hanson, M. R. (2000). Plastid tubules of higher plants are tissue-specific and developmentally regulated. *Journal of Cell Science*, *113*(1), 81–89. https://doi.org/10.1242/jcs.113.1.81

Kollman, J. M., Merdes, A., Mourey, L., & Agard, D. A. (2011). Microtubule nucleation by γ-tubulin complexes. In *Nature Reviews Molecular Cell Biology* (Vol. 12, Issue 11, pp. 709–721). https://doi.org/10.1038/nrm3209

Kong, S. G., & Wada, M. (2014). Recent advances in understanding the molecular mechanism of chloroplast photorelocation movement. In *Biochimica et Biophysica Acta - Bioenergetics* (Vol. 1837, Issue 4, pp. 522–530). Elsevier B.V. https://doi.org/10.1016/j.bbabio.2013.12.004

Korn, E. D., Carlier, M.-F., & Pantaloni, D. (1987). Actin Polymerization and ATP Hydrolysis. *Science*, *238*(4827), 638–644. https://doi.org/10.1126/science.3672117

Kumar, A. S., Park, E., Nedo, A., Alqarni, A., Ren, L., Hoban, K., Modla, S., McDonald, J. H., Kambhamettu, C., Dinesh-Kumar, S. P., & Caplan, J. L. (2018). Stromule extension along microtubules coordinated with actin-mediated anchoring guides perinuclear chloroplast movement during innate immunity. *ELife*, *7*. https://doi.org/10.7554/eLife.23625

Kwok, E. Y., & Hanson, M. R. (2003). Microfilaments and microtubules control the morphology and movement of non-green plastids and stromules in *Nicotiana tabacum*. *Plant Journal*, *35*(1), 16–26. https://doi.org/10.1046/j.1365-313X.2003.01777.x

Kwok, E. Y., & Hanson, M. R. (2004a). *In vivo* analysis of interactions between GFP-labeled microfilaments and plastid stromules. *BMC Plant Biology*, *4*, 2. https://doi.org/10.1186/1471-2229-4-2

Kwok, E. Y., & Hanson, M. R. (2004b). Stromules and the dynamic nature of plastid morphology. *Journal of Microscopy*, *214*(2), 124–137. https://doi.org/10.1111/j.0022-2720.2004.01317.x

Laemmli, U. K. (1970). Cleavage of Structural Proteins during the Assembly of the Head of Bacteriophage T4. *Nature*, *227*(5259), 680–685. https://doi.org/10.1038/227680a0

Langeveld, S. M. J., van Wijk, R., Stuurman, N., Kijne, J. W., & de Pater, S. (2000). B-type granule containing protrusions and interconnections between amyloplasts in developing wheat endosperm revealed by transmission electron microscopy and GFP expression. *Journal of Experimental Botany*, *51*(349), 1357–1361. https://doi.org/10.1093/jexbot/51.349.1357

Lawrence, C. J., Dawe, R. K., Christie, K. R., Cleveland, D. W., Dawson, S. C., Endow, S. A., Goldstein, L. S. B., Goodson, H. v., Hirokawa, N., Howard, J., Malmberg, R. L., McIntosh, J. R., Miki, H., Mitchison, T. J., Okada, Y., Reddy, A. S. N., Saxton, W. M., Schliwa, M., Scholey, J. M., Wordeman, L. (2004). A standardized kinesin nomenclature. In *Journal of Cell Biology* (Vol. 167, Issue 1, pp. 19–22). https://doi.org/10.1083/jcb.200408113

Lee, Y. R. J., & Liu, B. (2004). Cytoskeletal motors in *Arabidopsis*. Sixty-one kinesins and seventeen myosins. In *Plant Physiology* (Vol. 136, Issue 4, pp. 3877–3883). American Society of Plant Biologists. https://doi.org/10.1104/pp.104.052621

Lee, Y.-R. J., Giang, H. M., & Liu, B. (2001). A Novel Plant Kinesin-Related Protein Specifically Associates with the Phragmoplast Organelles. *The Plant Cell*, *13*(11), 2427–2439. https://doi.org/10.1105/tpc.010225

Li, H., Yan, S., Zhao, L., Tan, J., Zhang, Q., Gao, F., Wang, P., Hou, H., & Li, L. (2014). Histone acetylation associated up-regulation of the cell wall related genes is involved in salt stress induced maize root swelling. *BMC Plant Biology*, *14*(1). https://doi.org/10.1186/1471-2229-14-105

Lian, N., Wang, X., Jing, Y., & Lin, J. (2021). Regulation of cytoskeleton-associated protein activities: Linking cellular signals to plant cytoskeletal function. In *Journal of Integrative Plant Biology* (Vol. 63, Issue 1, pp. 241–250). Blackwell Publishing Ltd. https://doi.org/10.1111/jipb.13046

Liu, J., Zhang, W., Long, S., & Zhao, C. (2021). Maintenance of cell wall integrity under high salinity. In *International Journal of Molecular Sciences* (Vol. 22, Issue 6). MDPI AG. https://doi.org/10.3390/ijms22063260

Liu, S. G., Zhu, D. Z., Chen, G. H., Gao, X. Q., & Zhang, X. S. (2012). Disrupted actin dynamics trigger an increment in the reactive oxygen species levels in the *Arabidopsis* root under salt stress. *Plant Cell Reports*, *31*(7), 1219–1226. https://doi.org/10.1007/s00299-012-1242-z

Logan, D. C., Scott, I., & Tobin, A. K. (2004). ADL2a, like ADL2b, is involved in the control of higher plant mitochondrial morphology. *Journal of Experimental Botany*, *55*(397), 783–785. https://doi.org/10.1093/jxb/erh073

Luthe, D. S. (1983). A simple technique for the preparation and storage of sucrose gradients. *Analytical Biochemistry*, *135*(1), 230–232. https://doi.org/10.1016/0003-2697(83)90755-8

Lütz, C., & Engel, L. (2007). Changes in chloroplast ultrastructure in some high-alpine plants: Adaptation to metabolic demands and climate? *Protoplasma*, *231*(3–4), 183–192. https://doi.org/10.1007/s00709-007-0249-8

Machettira, A. B., Groß, L. E., Tillmann, B., Weis, B. L., Englich, G., Sommer, M. S., Königer, M., & Schleiff, E. (2012). Protein-induced modulation of chloroplast membrane morphology. *Frontiers in Plant Science*, *2*(Jan). https://doi.org/10.3389/fpls.2011.00118

Madison, S. L., Buchanan, M. L., Glass, J. D., McClain, T. F., Park, E., & Nebenführ, A. (2015). Class XI myosins move specific organelles in pollen tubes and are required for normal fertility and pollen tube growth in *Arabidopsis*. *Plant Physiology*, *169*(3), 1946–1960. https://doi.org/10.1104/pp.15.01161

Maike Jung. (2021). Modeling Membrane Dynamics on the Level of Organelles. PhD Thesis, Johannes Gutenberg Universität.

Marcus, A. I., Li, W., Ma, H., & Cyr, R. J. (2003). A Kinesin Mutant with an Atypical Bipolar Spindle Undergoes Normal Mitosis. *Molecular Biology of the Cell*, *14*, 1717–1726. https://doi.org/10.1091/mbc.E02-09

Mathur, J., & Chua, N.-H. (2000). Microtubule Stabilization Leads to Growth Reorientation in *Arabidopsis* Trichomes. *The Plant Cell*, *12*(4), 465–477. https://doi.org/10.1105/tpc.12.4.465

Mathur, J., Mathur, N., & Hülskamp, M. (2002). Simultaneous visualization of Peroxisomes and cytoskeletal elements reveals actin and not microtubule-based peroxisome motility in plants. *Plant Physiology*, *128*(3), 1031–1045. https://doi.org/10.1104/pp.011018

McAinsh, M. R., & Pittman, J. K. (2009). Shaping the calcium signature. In *New Phytologist* (Vol. 181, Issue 2, pp. 275–294). https://doi.org/10.1111/j.1469-8137.2008.02682.x

McLean, B., Whatley, J. M., & Juniper, B. E. (1988). Continuity of chloroplast and endoplasmic reticulum membranes in *Chara* and *Equisetum*. *New Phytologist*, *109*(1), 59–65. https://doi.org/10.1111/j.1469-8137.1988.tb00219.x

McMahon, H. T., & Boucrot, E. (2015). Membrane curvature at a glance. *Journal of Cell Science*, *128*(6), 1065–1070. https://doi.org/10.1242/jcs.114454

Mehrshahi, P., Stefano, G., Andaloro, J. M., Brandizzi, F., Froehlich, J. E., & DellaPenna, D. (2013). Transorganellar complementation redefines the biochemical continuity of endoplasmic reticulum and chloroplasts. *Proceedings of the National Academy of Sciences of the United States of America*, *110*(29), 12126–12131. https://doi.org/10.1073/pnas.1306331110

Mendrinna, A., & Persson, S. (2015). Root hair growth: It's a one way street. *F1000Prime Reports*, *7*. https://doi.org/10.12703/P7-23

Menon, V. v., Inamdar, M. M., & Sain, A. (2021). Cytoplasmic streaming in *C. elegans*: Forces that drive oogenesis. *EPL*, *135*(2). https://doi.org/10.1209/0295-5075/135/24003

Michaud, M., Gros, V., Tardif, M., Brugière, S., Ferro, M., Prinz, W. A., Toulmay, A., Mathur, J., Wozny, M., Falconet, D., Maréchal, E., Block, M. A., & Jouhet, J. (2016). AtMic60 is Involved in Plant Mitochondria Lipid Trafficking and is Part of a Large Complex. *Current Biology*, *26*(5), 627–639. https://doi.org/10.1016/j.cub.2016.01.011

Mim, C., & Unger, V. M. (2012). Membrane curvature and its generation by BAR proteins. In *Trends in Biochemical Sciences* (Vol. 37, Issue 12, pp. 526–533). https://doi.org/10.1016/j.tibs.2012.09.001

Morita, M. T. (2010). Directional gravity sensing in gravitropism. *Annual Review of Plant Biology*, *61*, 705–720. https://doi.org/10.1146/annurev.arplant.043008.092042

Mueller-Schuessele, S. J., & Michaud, M. (2018). Plastid transient and stable interactions with other cell compartments. In *Methods in Molecular Biology* (Vol. 1829, pp. 87–109). Humana Press Inc. https://doi.org/10.1007/978-1-4939-8654-5_6

Mühlhausen, S., & Kollmar, M. (2013). Whole genome duplication events in plant evolution reconstructed and predicted using myosin motor proteins. *BMC Evolutionary Biology*, *13*(1). https://doi.org/10.1186/1471-2148-13-202

Mullineaux, P. M., Exposito-Rodriguez, M., Laissue, P. P., Smirnoff, N., & Park, E. (2020). Spatial chloroplast-to-nucleus signalling involving plastid–nuclear complexes and stromules. In *Philosophical Transactions of the Royal Society B: Biological Sciences* (Vol. 375, Issue 1801). Royal Society Publishing. https://doi.org/10.1098/rstb.2019.0405

Muralla, R., Sweeney, C., Stepansky, A., Leustek, T., & Meinke, D. (2007). Genetic dissection of histidine biosynthesis in *Arabidopsis*. *Plant Physiology*, *144*(2), 890–903. https://doi.org/10.1104/pp.107.096511

Murashige, T., & Skoog, F. (1962). A Revised Medium for Rapid Growth and Bio Assays with Tobacco Tissue Cultures. *Physiologia Plantarum*, *15*(3). https://doi.org/10.1111/j.1399-3054.1962.tb08052.x

Nakamura, Y. (2013). Phosphate starvation and membrane lipid remodeling in seed plants. In *Progress in Lipid Research* (Vol. 52, Issue 1, pp. 43–50). https://doi.org/10.1016/j.plipres.2012.07.002

Nakashima, K., Yamaguchi-Shinozaki, K., & Shinozaki, K. (2014). The transcriptional regulatory network in the drought response and its crosstalk in abiotic stress responses including drought, cold, and heat. In *Frontiers in Plant Science* (Vol. 5, Issue MAY). Frontiers Research Foundation. https://doi.org/10.3389/fpls.2014.00170

Natesan, S. K. A., Sullivan, J. A., & Gray, J. C. (2005). Stromules: A characteristic cell-specific feature of plastid morphology. In *Journal of Experimental Botany* (Vol. 56, Issue 413, pp. 787–797). https://doi.org/10.1093/jxb/eri088

Natesan, S. K. A., Sullivan, J. A., & Gray, J. C. (2009). Myosin XI is required for actin-associated movement of plastid stromules. *Molecular Plant*, *2*(6), 1262–1272. https://doi.org/10.1093/mp/ssp078

Nebenführ, A., & Dixit, R. (2018). Kinesins and Myosins: Molecular Motors that Coordinate Cellular Functions in Plants. In *Annual Review of Plant Biology* (Vol. 69, pp. 329–361). Annual Reviews Inc. https://doi.org/10.1146/annurev-arplant-042817-040024

Nebenführ, A., Gallagher, L. A., Dunahay, T. G., Frohlick, J. A., Mazurkiewicz, A. M., Meehl, J. B., & Staehelin, L. A. (1999). Stop-and-Go Movements of Plant Golgi Stacks Are Mediated by the Acto-Myosin System. *Plant Physiology*, *121*(4), 1127–1141. https://doi.org/10.1104/pp.121.4.1127

Nesterenko, M. v., Tilley, M., & Upton, S. J. (1994). A simple modification of Blum's silver stain method allows for 30 minute detection of proteins in polyacrylamide gels. *Journal of Biochemical and Biophysical Methods*, *28*(3), 239–242. https://doi.org/10.1016/0165-022X(94)90020-5

Nishihama, R., Soyano, T., Ishikawa, M., Araki, S., Tanaka, H., Asada, T., Irie, K., Ito, M., Terada, M., Banno, H., Yamazaki, Y., & Machida, Y. (2002). Expansion of the Cell Plate in Plant Cytokinesis Requires a Kinesin-like Protein/MAPKKK Complex. *Cell*, *109*(1), 87–99. https://doi.org/10.1016/S0092-8674(02)00691-8

Nogales, E., Downing, K. H., Amos, L. A., & Löwe, J. (1998). Tubulin and FtsZ form a distinct family of GTPases. *Nature Structural Biology*, *5*(6), 451–458. https://doi.org/10.1038/nsb0698-451

Noguchi, K., & Yoshida, K. (2008). Interaction between photosynthesis and respiration in illuminated leaves. *Mitochondrion*, *8*(1), 87–99. https://doi.org/10.1016/j.mito.2007.09.003

Oikawa, K., Kasahara, M., Kiyosue, T., Kagawa, T., Suetsugu, N., Takahashi, F., Kanegae, T., Niwa, Y., Kadota, A., & Wada, M. (2003). Chloroplast Unusual Positioning1 Is Essential for Proper Chloroplast Positioning. *Plant Cell*, *15*(12), 2805–2815. https://doi.org/10.1105/tpc.016428

Oikawa, K., Matsunaga, S., Mano, S., Kondo, M., Yamada, K., Hayashi, M., Kagawa, T., Kadota, A., Sakamoto, W., Higashi, S., Watanabe, M., Mitsui, T., Shigemasa, A., Iino, T., Hosokawa, Y., & Nishimura, M. (2015). Physical interaction between peroxisomes and chloroplasts elucidated by in situ laser analysis. *Nature Plants*, *1*. https://doi.org/10.1038/nplants.2015.35

Oikawa, K., Yamasato, A., Kong, S.-G., Kasahara, M., Nakai, M., Takahashi, F., Ogura, Y., Kagawa, T., & Wada, M. (2008). Chloroplast Outer Envelope Protein CHUP1 Is Essential for Chloroplast Anchorage to the Plasma Membrane and Chloroplast Movement. *Plant Physiology*, *148*(2), 829–842. https://doi.org/10.1104/pp.108.123075

Palm, D., Simm, S., Darm, K., Weis, B. L., Ruprecht, M., Schleiff, E., & Scharf, C. (2016). Proteome distribution between nucleoplasm and nucleolus and its relation to ribosome biogenesis in *Arabidopsis thaliana*. *RNA Biology*, *13*(4), 441–454. https://doi.org/10.1080/15476286.2016.1154252

Pan, R., Lee, Y.-R. J., & Liu, B. (2004). Localization of two homologous *Arabidopsis* kinesin-related proteins in the phragmoplast. *Planta*, *220*(1), 156–164. https://doi.org/10.1007/s00425-004-1324-4

Park, H. J., Kim, W. Y., & Yun, D. J. (2016). A new insight of salt stress signaling in plant. In *Molecules and Cells* (Vol. 39, Issue 6, pp. 447–459). Korean Society for Molecular and Cellular Biology. https://doi.org/10.14348/molcells.2016.0083

Peremyslov, V. v., Prokhnevsky, A. I., Avisar, D., & Dolja, V. v. (2008). Two class XI myosins function in organelle trafficking and root hair development in *Arabidopsis*. *Plant Physiology*, *146*(3), 1109–1116. https://doi.org/10.1104/pp.107.113654

Peremyslov, V. v., Prokhnevsky, A. I., & Dolja, V. v. (2010). Class XI myosins are required for development, cell expansion, and F-actin organization in *Arabidopsis*. *Plant Cell*, *22*(6), 1883–1897. https://doi.org/10.1105/tpc.110.076315

Pérez-Sancho, J., Tilsner, J., Samuels, A. L., Botella, M. A., Bayer, E. M., & Rosado, A. (2016). Stitching Organelles: Organization and Function of Specialized Membrane Contact Sites in Plants. In *Trends in Cell Biology* (Vol. 26, Issue 9, pp. 705–717). Elsevier Ltd. https://doi.org/10.1016/j.tcb.2016.05.007

Perico, C., & Sparkes, I. (2018). Plant organelle dynamics: cytoskeletal control and membrane contact sites. In *New Phytologist* (Vol. 220, Issue 2, pp. 381–394). Blackwell Publishing Ltd. https://doi.org/10.1111/nph.15365

Pickard, W. F. (1974). Hydrodynamic aspects of protoplasmic streaming in *Chara braunii*. *Protoplasma*, *82*(4), 321–339. https://doi.org/10.1007/BF01275727

Pieuchot, L., Lai, J., Loh, R. A., Leong, F. Y., Chiam, K. H., Stajich, J., & Jedd, G. (2015). Cellular Subcompartments through Cytoplasmic Streaming. *Developmental Cell*, *34*(4), 410–420. https://doi.org/10.1016/j.devcel.2015.07.017

Pollard, T. D. (1986). Rate constants for the reactions of ATP- and ADP-actin with the ends of actin filaments. *Journal of Cell Biology*, *103*(6), 2747–2754. https://doi.org/10.1083/jcb.103.6.2747

Pollard, T. D. (2016). Actin and actin-binding proteins. *Cold Spring Harbor Perspectives in Biology*, *8*(8). https://doi.org/10.1101/cshperspect.a018226

Popov, N., Schmitt, M., Schulzeck, S., & Matthies, H. (1975). Reliable micromethod for determination of the protein content in tissue homogenates. *Acta Biologica et Medica Germanica*, *34*(9), 1441–1446. http://www.ncbi.nlm.nih.gov/pubmed/1221733

Prestele, J., Hierl, G., Scherling, C., Hetkamp, S., Schwechheimer, C., Isono, E., Weckwerth, W., Wanner, G., & Gietl, C. (2010). Different functions of the C3HC4 zinc RING finger peroxins PEX10, PEX2, and PEX12 in peroxisome formation and matrix protein import. *Proceedings of the National Academy of Sciences of the United States of America*, *107*(33), 14915–14920. https://doi.org/10.1073/pnas.1009174107

Preuss, M. L., Delmer, D. P., & Liu, B. (2003). The cotton kinesin-like calmodulin-binding protein associates with cortical microtubules in cotton fibers. *Plant Physiology*, *132*(1), 154–160. https://doi.org/10.1104/pp.103.020339

Preuss, M. L., Kovar, D. R., Lee, Y. R. J., Staiger, C. J., Delmer, D. P., & Liu, B. (2004). A plant-specific kinesin binds to actin microfilaments and interacts with cortical microtubules in cotton fibers. *Plant Physiology*, *136*(4), 3945–3955. https://doi.org/10.1104/pp.104.052340

Prinz, W. A. (2014). Bridging the gap: Membrane contact sites in signaling, metabolism, and organelle dynamics. In *Journal of Cell Biology* (Vol. 205, Issue 6, pp. 759–769). Rockefeller University Press. https://doi.org/10.1083/jcb.201401126

Prokhnevsky, A. I., Peremyslov, V. v., & Dolja, V. v. (2008). Overlapping functions of the four class XI myosins in *Arabidopsis* growth, root hair elongation, and organelle motility. *Proceedings of the National Academy of Sciences*, *105*(50), 19744–19749. https://doi.org/10.1073/pnas.0810730105

Pyke, K. A., & Howells, C. A. (2002). Plastid and stromule morphogenesis in tomato. *Annals of Botany*, *90*(5), 559–566. https://doi.org/10.1093/aob/mcf235

Qian, D., & Xiang, Y. (2019). Actin cytoskeleton as actor in upstream and downstream of calcium signaling in plant cells. In *International Journal of Molecular Sciences* (Vol. 20, Issue 6). MDPI AG. https://doi.org/10.3390/ijms20061403

Rao, Y., & Haucke, V. (2011). Membrane shaping by the Bin/amphiphysin/Rvs (BAR) domain protein superfamily. In *Cellular and Molecular Life Sciences* (Vol. 68, Issue 24, pp. 3983–3993). https://doi.org/10.1007/s00018-011-0768-5

Reddy, A. S., & Day, I. S. (2001a). Analysis of the myosins encoded in the recently completed *Arabidopsis* thaliana genome sequence. *Genome Biology 2.* Research0023.1. https://doi.org/10.1186/gb-2001-2-7-research0024

Reddy, A. S., & Day, I. S. (2001b). Kinesins in the *Arabidopsis* genome: A comparative analysis among eukaryotes. *BMC Genomics*, *2*(1), 2. https://doi.org/10.1186/1471-2164-2-2

Rehm, H., & Letzel, T. (2016). Der Experimentator: Proteinbiochemie/Proteomics. Springer Berlin Heidelberg. https://doi.org/10.1007/978-3-662-48851-5

Reichelt, S., Knight, A. E., Hodge, T. P., Baluska, F., Samaj, J., Volkmann, D., & Kendrick-Jones, J. (1999). Characterization of the unconventional myosin VIII in plant cells and its localization at the post-cytokinetic cell wall. *The Plant Journal*, *19*(5), 555–567. https://doi.org/10.1046/j.1365-313X.1999.00553.x

Renaudin, S., & Capdepon, M. (1977). Association of the endoplasmic reticulum and the plastids in Tozzia alpina L. scale leaves. *Journal of Ultrastructure Research*, *61*(3), 303–308. https://doi.org/10.1016/S0022-5320(77)80055-5

Reumann, S., & Bartel, B. (2016). Plant peroxisomes: recent discoveries in functional complexity, organelle homeostasis, and morphological dynamics. In *Current Opinion in Plant Biology* (Vol. 34, pp. 17–26). Elsevier Ltd. https://doi.org/10.1016/j.pbi.2016.07.008

Richardson, D. N., Simmons, M. P., & Reddy, A. S. N. (2006). Comprehensive comparative analysis of kinesins in photosynthetic eukaryotes. In *BMC Genomics* (Vol. 7). https://doi.org/10.1186/1471-2164-7-18

Rippert, P., Puyaubert, J., Grisollet, D., Derrier, L., & Matringe, M. (2009). Tyrosine and phenylalanine are synthesized within the plastids in *Arabidopsis*. *Plant Physiology*, *149*(3), 1251–1260. https://doi.org/10.1104/pp.108.130070

Rolland, N., Bouchnak, I., Moyet, L., Salvi, D., & Kuntz, M. (2018). The main functions of plastids. In *Methods in Molecular Biology* (Vol. 1829, pp. 73–85). Humana Press Inc. https://doi.org/10.1007/978-1-4939-8654-5_5

Rolland, N., Curien, G., Finazzi, G., Kuntz, M., Maréchal, E., Matringe, M., Ravanel, S., & Seigneurin-Berny, D. (2012). The biosynthetic capacities of the plastids and integration between cytoplasmic and chloroplast processes. In *Annual Review of Genetics* (Vol. 46, pp. 233–264). https://doi.org/10.1146/annurev-genet-110410-132544

Sack, F. D., Suyemoto, M. M., & Leopold, A. C. (1984). Kinetics of amyloplast sedimentation in gravistimulated maize coleoptiles. *Planta*, *161*, 459–464. https://doi.org/https://doi.org/10.1007/BF00394578

Sack, F. D., Suyemoto, M. M., & Leopold, A. C. (1986). Amyloplast Sedimentation and Organelle Saltation in Living Corn Columella Cells. *American Journal of Botany*, *73*(12), 1692. https://doi.org/10.2307/2444235

Saito, C., Morita, M. T., Kato, T., & Tasaka, M. (2005). Amyloplasts and vacuolar membrane dynamics in the living graviperceptive cell of the *Arabidopsis* inflorescence stem. *Plant Cell*, *17*(2), 548–558. https://doi.org/10.1105/tpc.104.026138

Sattarzadeh, A., Franzen, R., & Schmelzer, E. (2008). The *Arabidopsis* class VIII myosin ATM2 is involved in endocytosis. *Cell Motility and the Cytoskeleton*, *65*(6), 457–468. https://doi.org/10.1002/cm.20271

Schattat, M., Barton, K., Baudisch, B., Klösgen, R. B., & Mathur, J. (2011). Plastid stromule branching coincides with contiguous endoplasmic reticulum dynamics. *Plant Physiology*, *155*(4), 1667–1677. https://doi.org/10.1104/pp.110.170480

Schattat, M. H., & Klösgen, R. B. (2011). Induction of stromule formation by extracellular sucrose and glucose in epidermal leaf tissue of *Arabidopsis thaliana*. *BMC Plant Biology*, *11*. https://doi.org/10.1186/1471-2229-11-115

Schindelin, J., Arganda-Carreras, I., Frise, E., Kaynig, V., Longair, M., Pietzsch, T., Preibisch, S., Rueden, C., Saalfeld, S., Schmid, B., Tinevez, J.-Y., White, D. J., Hartenstein, V., Eliceiri, K., Tomancak, P., & Cardona, A. (2012). Fiji: an open-source platform for biological-image analysis. *Nature Methods*, *9*(7), 676–682. https://doi.org/10.1038/nmeth.2019

Schleiff, E., Soll, J., Küchler, M., Kühlbrandt, W., & Harrer, R. (2003). Characterization of the translocon of the outer envelope of chloroplasts. *Journal of Cell Biology*, *160*(4), 541–551. https://doi.org/10.1083/jcb.200210060

Schmidt Von Braun, S., & Schleiff, E. (2008). The chloroplast outer membrane protein CHUP1 interacts with actin and profilin. *Planta*, *227*(5), 1151–1159. https://doi.org/10.1007/s00425-007-0688-7

Schumann, U., Prestele, J., O'Geen, H., Brueggeman, R., Wanner, G., & Gietl, C. (2007). Requirement of the C_3HC_4 zinc RING finger of the *Arabidopsis PEX10* for photorespiration and leaf peroxisome contact with chloroplasts. *Proceedings of the National Academy of Sciences*, *104*(3), 1069–1074. https://doi.org/10.1073/pnas.0610402104

Schweiger, H. G. (1969). Cell Biology of *Acetabularia* (pp. 1–36). https://doi.org/10.1007/978-3-642-46169-9_1

Shimmen, T., & Yokota, E. (1994). *Physiological and Biochemical Aspects of Cytoplasmic Streaming* (pp. 97–139). https://doi.org/10.1016/S0074-7696(08)62097-5

Shumilina, J., Kusnetsova, A., Tsarev, A., Janse van Rensburg, H. C., Medvedev, S., Demidchik, V., van den Ende, W., & Frolov, A. (2019). Glycation of plant proteins: Regulatory roles and interplay with sugar signalling? *International Journal of Molecular Sciences*, *20*(9). https://doi.org/10.3390/ijms20092366

Soll, J., & Schleiff, E. (2004). Protein import into chloroplasts. In *Nature Reviews Molecular Cell Biology* (Vol. 5, Issue 3, pp. 198–208). https://doi.org/10.1038/nrm1333

Plomer, S., Schneider, G. (2022) Untitled manuscript in work. Department of Applied Mathematical Statistics, Institute for Mathematics Facility Gaby Schneider. Goethe Universität Frankfurt a.M.

Sommer, M. S., Daum, B., Gross, L. E., Weis, B. L. M., Mirus, O., Abram, L., Maier, U.-G., Kühlbrandt, W., & Schleiff, E. (2011). Chloroplast Omp85 proteins change orientation during evolution. *Proceedings of the National Academy of Sciences*, *108*(33), 13841–13846. https://doi.org/10.1073/pnas.1108626108

Stachowiak, J. C., Hayden, C. C., & Sasaki, D. Y. (2010). Steric confinement of proteins on lipid membranes can drive curvature and tubulation. *Proceedings of the National Academy of Sciences*, *107*(17), 7781–7786. https://doi.org/10.1073/pnas.0913306107

Stelzer, E. H. K. (2014). Light-sheet fluorescence microscopy for quantitative biology. *Nature Methods*, *12*(1), 23–26. https://doi.org/10.1038/nmeth.3219

Stepansky, A., & Leustek, T. (2006). Histidine biosynthesis in plants. In *Amino Acids* (Vol. 30, Issue 2, pp. 127–142). https://doi.org/10.1007/s00726-005-0247-0

Strompen, G., el Kasmi, F., Richter, S., Lukowitz, W., Assaad, F. F., Jürgens, G., & Mayer, U. (2002). The *Arabidopsis* HINKEL Gene Encodes a Kinesin-Related Protein Involved in Cytokinesis and Is Expressed in a Cell Cycle-Dependent Manner. *Current Biology*, *12*(2), 153–158. https://doi.org/10.1016/S0960-9822(01)00655-8

Suetsugu, N., Higa, T., Gotoh, E., & Wada, M. (2016). Light-induced movements of chloroplasts and nuclei are regulated in both cp-actin-filament-dependent and -independent manners in *Arabidopsis thaliana*. *PLoS ONE*, *11*(6). https://doi.org/10.1371/journal.pone.0157429

Suetsugu, N., Higa, T., Kong, S. G., & Wada, M. (2015). PLASTID MOVEMENT IMPAIRED1 and PLASTID MOVEMENT IMPAIRED1-RELATED1 mediate photorelocation movements of both chloroplasts and nuclei. *Plant Physiology*, *169*(2), 1155–1167. https://doi.org/10.1104/pp.15.00214

Suetsugu, N., & Wada, M. (2012). Chloroplast Photorelocation Movement: A Sophisticated Strategy for Chloroplasts to Perform Efficient Photosynthesis. In *Advances in Photosynthesis - Fundamental Aspects*. InTech. https://doi.org/10.5772/26838

Sui, H., & Downing, K. H. (2010). Structural basis of interprotofilament interaction and lateral deformation of microtubules. *Structure*, *18*(8), 1022–1031. https://doi.org/10.1016/j.str.2010.05.010

Svenn, G. (1908). *Die Gestalt- und Längenveränderung der Pflanzen Chromatophoren*. Wilhelm Engelmann.

Sweitzer, S. M., & Hinshaw, J. E. (1998). Dynamin Undergoes a GTP-Dependent Conformational Change Causing Vesiculation. *Cell*, *93*(6), 1021–1029. https://doi.org/10.1016/S0092-8674(00)81207-6

Tamura, K., Iwabuchi, K., Fukao, Y., Kondo, M., Okamoto, K., Ueda, H., Nishimura, M., & Hara-Nishimura, I. (2013). Myosin XI-i links the nuclear membrane to the cytoskeleton to control nuclear movement and shape in *Arabidopsis*. *Current Biology*, *23*(18), 1776–1781. https://doi.org/10.1016/j.cub.2013.07.035

Tirlapur, U. K., Dahse, I., Reiss, B., Meurer, J., & Oelmüller, R. (1999). Characterization of the activity of a plastid-targeted green fluorescent protein in *Arabidopsis*. *European Journal of Cell Biology*, *78*(4), 233–240. https://doi.org/10.1016/S0171-9335(99)80056-9

Tominaga, M. (2003). Higher plant myosin XI moves processively on actin with 35 nm steps at high velocity. *The EMBO Journal*, *22*(6), 1263–1272. https://doi.org/10.1093/emboj/cdg130

Tominaga, M., Kimura, A., Yokota, E., Haraguchi, T., Shimmen, T., Yamamoto, K., Nakano, A., & Ito, K. (2013). Cytoplasmic Streaming Velocity as a Plant Size Determinant. *Developmental Cell*, *27*(3), 345–352. https://doi.org/10.1016/j.devcel.2013.10.005

Tyanova, S., Temu, T., Sinitcyn, P., Carlson, A., Hein, M. Y., Geiger, T., Mann, M., & Cox, J. (2016). The Perseus computational platform for comprehensive analysis of (prote)omics data. In *Nature Methods* (Vol. 13, Issue 9, pp. 731–740). Nature Publishing Group. https://doi.org/10.1038/nmeth.3901

Ueda, H., Yokota, E., Kutsuna, N., Shimada, T., Tamura, K., Shimmen, T., Hasezawa, S., Dolja, V. v., & Hara-Nishimuraa, I. (2010). Myosin-dependent endoplasmic reticulum motility and F-actin organization in plant cells. *Proceedings of the National Academy of Sciences of the United States of America*, *107*(15), 6894–6899. https://doi.org/10.1073/pnas.0911482107

Vale, R. D. (2003). The Molecular Motor Toolbox for Intracellular Transport. *Cell*, *112*(4), 467–480. https://doi.org/10.1016/S0092-8674(03)00111-9

van Gestel, K., Köhler, R. H., & Verbelen, J. (2002). Plant mitochondria move on F-actin, but their positioning in the cortical cytoplasm depends on both F-actin and microtubules. *Journal of Experimental Botany*, *53*(369), 659–667. https://doi.org/10.1093/jexbot/53.369.659

van Zelm, E., Zhang, Y., & Testerink, C. (2020). Salt Tolerance Mechanisms of Plants. *Annual Review of Plant Biology*, *71*(1), 403–433. https://doi.org/10.1146/annurev-arplant-050718-100005

Veley, K. M., Marshburn, S., Clure, C. E., & Haswell, E. S. (2012). Mechanosensitive channels protect plastids from hypoosmotic stress during normal plant growth. *Current Biology*, *22*(5), 408–413. https://doi.org/10.1016/j.cub.2012.01.027

Vick, J. K., & Nebenführ, A. (2012). Putting On The Breaks: Regulating Organelle Movements in Plant Cells. In *Journal of Integrative Plant Biology* (Vol. 54, Issue 11, pp. 868–874). https://doi.org/10.1111/j.1744-7909.2012.01180.x

von Wangenheim, D. (2014). Long-term observation of *Arabidopsis thaliana* root under close-to-natural conditions using Light Sheet-based Fluorescence Microscopy. PhD Thesis, Goethe Universität Frankfurt a.M.

Vulevic, B., & Correia, J. J. (1997). Thermodynamic and structural analysis of microtubule assembly: the role of GTP hydrolysis. *Biophysical Journal*, *72*(3), 1357–1375. https://doi.org/10.1016/S0006-3495(97)78782-4

Wada, M. (2018). Nuclear movement and positioning in plant cells. In *Seminars in Cell and Developmental Biology* (Vol. 82, pp. 17–24). Elsevier Ltd. https://doi.org/10.1016/j.semcdb.2017.10.001

Wada, M., & Kong, S. G. (2018). Actin-mediated movement of chloroplasts. In *Journal of Cell Science* (Vol. 131, Issue 2). Company of Biologists Ltd. https://doi.org/10.1242/jcs.210310

Wallace, R. A., Misulovin, Z., & Etkin, L. D. (1981). Full-grown oocytes from *Xenopus laevis* resume growth when placed in culture. *Proceedings of the National Academy of Sciences*, *78*(5), 3078–3082. https://doi.org/10.1073/pnas.78.5.3078

Waters, M. T., Fray, R. G., & Pyke, K. A. (2004). Stromule formation is dependent upon plastid size, plastid differentiation status and the density of plastids within the cell. *Plant Journal*, *39*(4), 655–667. https://doi.org/10.1111/j.1365-313X.2004.02164.x

Whatley, J. M., McLean, B., & Juniper, B. E. (1991). Continuity of chloroplast and endoplasmic reticulum membranes in *Phaseolus vulgaris*. *New Phytologist*, *117*(2), 209–217. https://doi.org/10.1111/j.1469-8137.1991.tb04901.x

Wightman, R., & Turner, S. R. (2008). The roles of the cytoskeleton during cellulose deposition at the secondary cell wall. *Plant Journal*, *54*(5), 794–805. https://doi.org/10.1111/j.1365-313X.2008.03444.x

Yamada, M., Tanaka-Takiguchi, Y., Hayashi, M., Nishina, M., & Goshima, G. (2017a). Multiple kinesin-14 family members drive microtubule minus end-directed transport in plant cells. *Journal of Cell Biology*, *216*(6), 1705–1714. https://doi.org/10.1083/jcb.201610065

Yamada, M., Tanaka-Takiguchi, Y., Hayashi, M., Nishina, M., & Goshima, G. (2017b). Multiple kinesin-14 family members drive microtubule minus end-directed transport in plant cells. *Journal of Cell Biology*, *216*(6), 1705–1714. https://doi.org/10.1083/jcb.201610065

Yoder, T. L., Zheng, H., Todd, P., & Staehelin, L. A. (2001). Amyloplast Sedimentation Dynamics in Maize Columella Cells Support a New Model for the Gravity-Sensing Apparatus of Roots. *Plant Physiology*, *125*(2), 1045–1060. https://doi.org/10.1104/pp.125.2.1045

Yokota, E., & Shimmen, T. (1994). Isolation and characterization of plant myosin from pollen tubes of lily. *Protoplasma*, *177*(3–4), 153–162. https://doi.org/10.1007/BF01378989

Yokota, E., Yukawa, C., Muto, S., Sonobe, S., & Shimmen, T. (1999). Biochemical and Immunocytochemical Characterization of Two Types of Myosins in Cultured Tobacco Bright Yellow-2 Cells. *Plant Physiology*, *121*(2), 525–534. https://doi.org/10.1104/pp.121.2.525

Yoon, H. S., Hackett, J. D., Ciniglia, C., Pinto, G., & Bhattacharya, D. (2004). A Molecular Timeline for the Origin of Photosynthetic Eukaryotes. *Molecular Biology and Evolution*, *21*(5), 809–818. https://doi.org/10.1093/molbev/msh075

Zawadzki, T., & Fensom, D. S. (1986). Transnodal Transport of ^{14}C in *Nitella flexilis*. *Journal of Experimental Botany*, *37*(9), 1341–1352. https://doi.org/10.1093/jxb/37.9.1341

Zhang, Q., Lin, F., Mao, T., Nie, J., Yan, M., Yuan, M., & Zhang, W. (2012). Phosphatidic acid regulates microtubule organization by interacting with map65-1 in response to salt stress in *Arabidopsis*. *Plant Cell*, *24*(11), 4555–4576. https://doi.org/10.1105/tpc.112.104182

Zhang, R., Alushin, G. M., Brown, A., & Nogales, E. (2015). Mechanistic origin of microtubule dynamic instability and its modulation by EB proteins. *Cell*, *162*(4), 849–859. https://doi.org/10.1016/j.cell.2015.07.012

Zhao, S., Zhang, Q., Liu, M., Zhou, H., Ma, C., & Wang, P. (2021). Regulation of plant responses to salt stress. In *International Journal of Molecular Sciences* (Vol. 22, Issue 9). MDPI AG. https://doi.org/10.3390/ijms22094609

Zhong, R., Burk, D. H., Morrison, W. H., & Ye, Z. H. (2002). A kinesin-like protein is essential for oriented deposition of cellulose microfibrils and cell wall strength. *Plant Cell*, *14*(12), 3101–3117. https://doi.org/10.1105/tpc.005801

Zhu, J. K. (2002). Salt and drought stress signal transduction in plants. In *Annual Review of Plant Biology* (Vol. 53, pp. 247–273). https://doi.org/10.1146/annurev.arplant.53.091401.143329

Zrenner, R., Stitt, M., Sonnewald, U., & Boldt, R. (2006). Pyrimidine and purine biosynthesis and degradation in plants. In *Annual Review of Plant Biology* (Vol. 57, pp. 805–836). https://doi.org/10.1146/annurev.arplant.57.032905.105421

Zybailov, B., Rutschow, H., Friso, G., Rudella, A., Emanuelsson, O., Sun, Q., & van Wijk, K. J. (2008). Sorting signals, N-terminal modifications and abundance of the chloroplast proteome. *PLoS ONE*, *3*(4). https://doi.org/10.1371/journal.pone.0001994

7 Supplemental material

Supplemental Table 1 All proteins identified in LC-MS analysis with a minimum of 2 hits in either flowthrough, flowthrough, and 0.1 M NaCl or flowthrough and 0.1 M and 0.2 M NaCl. Atg identifiers are displayed.

Flowthrough	Flowthrough + 0.1 M NaCl	Flowthrough + 0.1 M NaCl + 0.2 M NaCl
At1g76020	At1g26110	At2g04690
At2g04170	At5g13120	At3g07460
At4g17480	At4g21600	At5g20060
At4g00752	At1g74230	At5g01650
At5g04750	At1g63290	At4g34490
At4g27520	At1g53730	AT1G23130
At4g08280	At1g72230	At4g15410
At4g34150	At5g34850	At5g22770
At1g14930	At4g15093	At3g62560
At1g35260	At5g26280	At1g04750
At1g07040	At3g07810	At4g22150
At3g58550	At4g34180	At3g46060
At3g08030	At3g20390	At3g09900
At1g76160	At1g11580	At3g15970
At4g07820	At3g07390	At1g66240
At2g38870	At1g11890	At1g13280
At1g23900	At1g15750	At1g78870
At2g33470	At5g64570	At5g55730
At2g16005	At5g46230	At5g50920
At5g22360	At5g66170	At5g18100
At3g08530	At5g46750	At3g02540
At1g60070	At2g06050	At1g05260
At1g70530	At5g61030	At4g38220
At2g28470	At1g51850	At5g64350
At4g05200	At5g59680	At4g03080
At5g38550,At5g38540	At5g42850	At3g47590
At5g14030	At1g70520,	At2g02930
At4g28480	At5g44130	At2g17190
At3g21630	At3g11400	At3g16460
At1g56145	At4g17280	At4g13850
At1g47600	At2g25980	At3g12050
At1g29850	At4g25370	At5g11720
At1g64230	At1g70690	At3g53880

At1g79650	At5g18400	At1g56190
At3g15880	At2g27060	At3g10920
At3g11910	At4g22305	At1g14980
At3g26380	At4g15930	At2g37760
At3g14350	At3g44620	At5g20720
At1g09750	At5g64120	At2g44790
At2g34070	At1g55805,	At5g19550
At2g43590	At2g26210	At4g11650
At2g37550	At1g20220	At3g10850
At2g46740	At1g50320	At2g45470
At1g07930	At3g09260	
At3g63480	At3g09410	
At4g30270	At1g26380	
At5g41700	At4g10300	
At5g11520	At2g27060	
At5g46860, At4g17730	At2g36130	
At1g80490	At3g49120	
At3g25220	At1g58270	
At1g80670	At1g27530	
At3g59930, At5g33355	At1g03870	
At2g43510	At4g01900	
At1g54030	At4g26750	
At1g16190	At5g58060	
At4g17890	At2g18370	
At2g29960	At1g15340	
At4g21590	At5g16400	
At2g43535	At4g03520	
At4g25240	At1g01940	
At4g35890	At3g23750	
At1g52690	At3g16830	
At1g77710	At3g17840	
At5g45900	At3g18130	
At5g54580	At3g20370	
At5g53530	At2g25970	
At5g22410	At1g56580	
At5g06600	At1g27030	
At2g19500	At5g11150	
At5g07830	At1g45015	
At4g08780	At3g06050	
At4g08770	At5g06860	

At5g11340	At1g28200	
At3g15010	At5g09530	
At1g20760	At5g10560	
At1g17860	At5g10290	
At4g04020	At1g11860	
At1g21065	At1g51840	
At3g25290	At1g21090	
At1g21065	At2g19060	
At1g12040	At4g27960, At5g53300	
At5g14650	At5g15970	
At3g57260	At3g51030	
At4g05160	At3g12500	
At3g63190	At4g34110	
At3g50400	At4g19810	
At3g01910	At5g26330	
At5g61410	At2g38390	
At1g65680	At3g56070	
At2g27970,	At3g07570	
At2g21130	At1g73330	
At5g58710	At4g25130	
At4g12420	At3g52850	
At4g20860	At4g19720	
At4g23690	At4g32150	
At4g11290	At2g44610	
At4g20840	At5g67360	
At4g37530	At2g27960	
At4g27520	At2g17120	
At1g14185	At2g33410	
At2g27730	At3g16430	
At2g38730	At2g16060	
At1g03220, At1g03230	At1g18080